THE UNIVERSITY *of* EDINBURGH

Vulnerability of white matter structure and function to chronic cerebral hypoperfusion and the effects of pharmacological modulation

Jamie McQueen BSc (Hons) MSc

Doctor of Philosophy

University of Edinburgh

2014

Table of Contents

Acknowledgments

I would like to begin by thanking my supervisor Prof. Karen Horsburgh without whom this work would not have been possible. Karen has supported me through the highs and lows of my Ph.D and for that I am very grateful. I would also like to thank Dr. Michell Reimer and Dr. Jill Fowler for all their help and encouragement over the years – it has been a pleasure working with you both. Finally I wish to thank my thesis committee Dr. Anna Williams, Prof. Peter Brophy and Dr. David Lyons for their contributions to my studies.

During the course of my Ph.D I have been lucky to work with a great group of people who cannot all be mentioned here but whose contributions – whether simply going for a cup of tea in a moment of need or having an in-depth discussion about my work – have helped me along the way. A special mention must go to Mercede Pannozzo, Dr. Gillian Scullion and Kanelina Karali with whom I have always been able to talk to about anything – my Ph.D experience would not have been the same without you guys! I would also like to thank Abi Herrmann for always being able to make me laugh no matter what the circumstances and for being such a lovely friend.

I also want to take this opportunity to thank my family for their continual support throughout my studies. In particular I would like to thank my mother Fiona who has always encouraged me to follow my dreams and to do my best – I would not be where I am now if it was not for you. I would also like to thank my sister Jo for being hilariously entertaining and always being able to cheer me up – our weekend baking days have helped me more than you will ever know. In addition a special thanks has to go to my gran Dorothy for her support and encouragement throughout my Ph.D and to my brother Kai for being such a great example of how to chill out! Finally, no words can truly express how grateful I am to my partner Stuart Niven for all his

support and encouragement throughout the course of my postgraduate (and undergraduate) studies – you are my rock and I could not have done this without you.

Whilst the majority of the work described in this thesis was carried out by myself, I would like to acknowledge the following people for their contributions as outlined below and in the appropriate thesis sections:

Dr. Philip Holland: For all surgeries (with the exception of one cohort described in Chapter 4, operated on by Dr. Catherine Gliddon) and for running electrophysiology experiments and subsequent data analysis.

Dr. Michell Reimer: For analysis of $Na_v1.6$ immunostaining in 3 day and 1 month cohorts (Chapter 3)

Mr Stephen Mitchell: For processing and cutting of tissue for electron microscopy studies (Chapters 3 and 4)

I would additionally like to thank Prof. Karen Horsburgh, and Dr. Jill Fowler and Dr. Philip Holland for their assistance with laser speckle contrast imaging and Dr. Gillian Scullion, Dr. Guiquan Chen and Kanelina Karali for their help with running the radial arm maze. Finally I would like to acknowledge the help of the BRR staff at 1 George Square and Little France (LF2) for their help with animal work.

Declaration

I declare that this thesis comprises my own original work and has not been submitted for any degree or professional qualification, with the exception of Figure 4.4 which was previously submitted for the award of MSc in Neuroscience by Research (2010). The work comprising this thesis was carried out by myself, except where acknowledged in the text. All sources of data and information have been specifically referenced.

Jamie McQueen

List of Figures

List of Tables

Abstract

The structural integrity of the white matter is required for neuronal communication within the brain which is essential for normal cognitive function. Post-mortem and clinical imaging studies of elderly individuals have demonstrated that white matter integrity is weakened with increasing age which is proposed to underlie age-related cognitive decline. Whilst the exact mechanisms are unknown it is thought that modest age-related reductions in cerebral blood flow, termed chronic cerebral hypoperfusion, may contribute to white matter disruption and impaired cognition with ageing. Investigating the effects of white matter integrity in humans is limited as it is difficult to definitively ascertain a cause and effect relationship. Indeed, elderly individuals with cerebral hypoperfusion often have co-existing disease such as hypertension thus the effects of hypoperfusion in isolation cannot be determined. This has led to the development of a mouse model of chronic cerebral hypoperfusion which provides the opportunity to directly assess whether cerebral hypoperfusion results in disruption to white matter and cognitive impairment. This is achieved by applying small wire coils around both common carotid arteries of the mouse resulting in a global reduction in cerebral blood flow. Importantly the extent of blood flow reduction is dependent on the internal diameter of the coils meaning that differing severities of hypoperfusion can be studied. Previous studies using this model have demonstrated diffuse white matter pathology in white matter tracts including the corpus callosum, internal capsule and optic tract following 1 month of hypoperfusion which is accompanied by impaired spatial working memory.

This thesis sought to test the hypothesis that chronic cerebral hypoperfusion would influence the structural integrity of nodal and paranodal domains of myelinated axons of the white matter and result in decreased numbers of oligodendroglial cells. It was additionally hypothesised that treatment with the anti-inflammatory and antioxidant drug dimethyl fumarate (DMF) would ameliorate structural and functional alterations to white matter following hypoperfusion.

Aim 1 – To determine the impact of chronic cerebral hypoperfusion on the structural integrity of nodal and paranodal domains of myelinated axons

The first aim of this thesis was to investigate the effects of chronic cerebral hypoperfusion on the structural integrity of nodal and paranodal domains of myelinated axons. This was addressed by examining key myelin and axonal proteins found at nodal, paranodal and internodal domains. This revealed significant alterations to the distribution of voltage-gated sodium ($Na_v1.6$) channels at nodes of Ranvier which were differentially altered in response to increasing durations of chronic cerebral hypoperfusion. Specifically an increase in the $Na_v1.6^+$ domain length was observed in the corpus callosum following 3 days ($p < 0.0001$) and 1 month ($p < 0.001$) of chronic cerebral hypoperfusion but was not significantly different from sham controls following 6 weeks of hypoperfusion ($p = 0.066$). A significant decrease in $Na_v1.6$ domain length was observed following 3 months of hypoperfusion ($p = 0.003$). Assessment of paranodal integrity was carried out by measuring nodal gap length and by ultrastructural analysis of paranodal domains. This revealed pronounced alterations to nodal gap length, loss of paranodal septate-

like junctions and abnormal morphology of paranodal loops. Furthermore this study revealed a significant loss of myelin associated glycoprotein, a key protein involved in the maintenance of axon-glial integrity, as early as 3 days following the onset of hypoperfusion. A further aim of this study was to examine potential mechanisms underlying the observed alterations to nodal and paranodal domains following cerebral hypoperfusion. It was hypothesised that increased inflammation and accumulation of mitochondria at nodes of Ranvier would be observed following hypoperfusion. The extent of inflammation was assessed by counting numbers of microglia which revealed no significant difference between groups following 3 days of hypoperfusion ($p = 0.425$) but a significant increase in microglial number was observed following 1 month of hypoperfusion ($p = 0.001$). In addition, assessment of mitochondrial distribution along myelinated axons revealed decreased numbers of nodes containing mitochondria following 6 weeks of hypoperfusion ($p = 0.03$) with no difference between groups observed following 3 months ($p = 0.742$). Taken together the results from this study provide evidence that chronic cerebral hypoperfusion results in dynamic alterations in the localisation of $Na_v1.6$ channels which are accompanied by disruption to paranodal domains and impaired axon-glial integrity. Furthermore microglial number does not appear to mediate nodal and paranodal disruption following 3 days but may contribute to ongoing pathology following 1 month of chronic cerebral hypoperfusion.

Aim 2 – To determine the effects of chronic cerebral hypoperfusion on oligodendroglial populations

The second aim of this thesis was to determine the effect of chronic cerebral hypoperfusion on numbers of mature oligodendrocytes and oligodendrocyte precursor cells (OPCs). This revealed a significant decrease in numbers of both populations following 3 days of cerebral hypoperfusion however following 1 month numbers of OPCs were restored and a significant increase in mature oligodendrocyte number was observed. Assessment of OPC proliferation demonstrated low numbers of proliferating cells but revealed that a proportion of newly generated cells had differentiated into mature oligodendrocytes. To determine a potential mechanism involved in OPC differentiation following cerebral hypoperfusion the expression of the GPR17 receptor was examined which has recently been reported to mediate OPC differentiation in response to injury. The results demonstrated decreased expression of GPR17 following 3 days of hypoperfusion ($p = 0.007$) with no difference between groups observed following 1 month ($p = 0.362$) indicating that this receptor is not involved in differentiation of OPCs following hypoperfusion. Taken together the results from this study show that mature oligodendrocytes and OPCs are lost early in response to hypoperfusion but that these cells recover over time, highlighting the regenerative capacity of the white matter following cerebral hypoperfusion.

Aim 3 – To investigate whether modulation of inflammation and oxidative stress could ameliorate alterations to white matter structure and function following severe chronic cerebral hypoperfusion

The third and final aim of this thesis was to determine whether treatment with the anti-inflammatory and antioxidant drug DMF could ameliorate structural and functional alterations to white matter following severe chronic cerebral hypoperfusion. This was achieved by examining myelin and axonal integrity in addition to numbers of oligodendrocytes and OPCs following 7 days of severe chronic cerebral hypoperfusion. This revealed that myelin integrity was significantly decreased in vehicle-treated hypoperfused animals as compared to shams ($p = 0.005$). However no differences in myelin integrity were observed between sham and hypoperfused mice treated with DMF ($p = 0.312$). In contrast to the previous study, numbers of oligodendrocytes and OPCs were not altered following severe hypoperfusion however DMF treatment led to significantly increased numbers of oligodendrocytes in sham animals ($p = 0.003$). Assessment of white matter function using electrophysiology revealed that the conduction velocity of myelinated axons was significantly increased in DMF-treated hypoperfused animals as compared to those treated with vehicle ($p = 0.04$). Taken together the results of this study demonstrate that modulation of inflammation and oxidative stress may improve structural and functional white matter alterations following chronic cerebral hypoperfusion.

Conclusions

The results presented in this thesis demonstrate that chronic cerebral hypoperfusion results in structural alterations to myelinated axons and to oligodendroglial populations within the white matter which are accompanied by impaired spatial working memory. Whilst previous studies using the model have reported that cerebral hypoperfusion results in diffuse white matter pathology, this study has highlighted the vulnerability of nodal and paranodal domains of myelinated axons as regions which are altered early in response to hypoperfusion. Furthermore, characterisation of oligodendroglial populations has revealed that these cells are replaced over time despite ongoing hypoperfusion which demonstrates the regenerative capacity of the white matter following cerebral hypoperfusion. Critically the results presented in this thesis demonstrate that treatment with DMF improved the function of myelinated axons in response to severe reductions in cerebral blood flow and thus may represent an appropriate therapeutic strategy for chronic cerebral hypoperfusion.

List of abbreviations

aCSF	Artificial cerebrospinal fluid
AD	Alzheimer's disease
ANOVA	Analysis of variance
APP	Amyloid precursor protein
ATP	Adenosine triphosphate
BCCAO	Bilateral common carotid artery occlusion
BrdU	5-bromo-2'-deoxyuridine
BSA	Bovine serum albumin
CAP	Compound action potential
Caspr	Contactin associated protein
CBF	Cerebral blood flow
CC1 (APC)	Anti-adenomatous polyposis coli protein
CNPase	2',3'-Cyclic-nucleotide 3'-phosphodiesterase
CNS	Central nervous system
DAPI	4',6-diamidino-2-phenylindole
DMF	Dimethyl fumarate
DTI	Diffusion tensor imaging
EAE	Experimental autoimmune encephalomyelitis
EdU	5-ethynyl-2'-deoxyuridine
EDTA	Ethylenediaminetetraacetic acid
GFAP	Glial fibrillary acidic protein
GFP	Green fluorescent protein
GPR17	G protein-coupled receptor 17
GSTπ	Glutathione S-transferase π
HCl	Hydrochloric acid
HO-1	Haem oxygenase 1
Iba1	Ionised calcium-binding adaptor molecule 1
K_v	Voltage-gated potassium channels
MAG	Myelin associated glycoprotein
MBP	Myelin basic protein
MCT1	Monocarboxylate transporter 1
MMF	Monomethyl fumarate
MRI	Magnetic resonance imaging
MS	Multiple sclerosis
Na_v	Voltage-gated sodium channels
Nfasc155	Neurofascin 155 kDa isoform
Nfasc186	Neurofascin 186 kDa isoform
NG2	Neuron-glial antigen 2
Nrf2	Nuclear factor erythroid 2-related factor 2

NQO1	NAD(P)H quinone oxidoreductase 1
O-2A cells	Oligodendrocyte-type 2 astrocyte progenitor cells
OPC	Oligodendrocyte precursor cell
PB	Phosphate buffer
PBS	Phosphate buffered saline
PBS-Tx	Phosphate buffered saline containing 0.1% TritonX-100
PCNA	Proliferating cell nuclear antigen
PDGFRα	Platelet-derived growth factor receptor α
PDGFRβ	Platelet-derived growth factor receptor β
PGC-1α	Proliferator-activated receptor-γ co-activator 1α
PFA	Paraformaldehyde
PLP	Proteolipid protein
PNS	Peripheral nervous system
ROI	Region of interest
TB	Tris buffer
TNFα	Tumour necrosis factor α

Chapter 1

Introduction

1. Introduction

The white matter of the brain is essential for neuronal communication and therefore plays a critical role in normal cognitive function. Post-mortem and magnetic resonance imaging (MRI) studies of elderly individuals have demonstrated that white matter integrity is weakened with increasing age which is thought to contribute to cognitive decline (Brant-Zawadzki et al., 1985; Awad et al., 1986a; Breteler et al., 1994a; de Leeuw et al., 2001). Whilst the exact mechanisms underlying white matter disruption with ageing are unknown it is thought that modest age-related decreases in cerebral blood flow, termed chronic cerebral hypoperfusion, may be an important factor (Brun and Englund, 1986; O'Sullivan et al., 2002; Fernando et al., 2006). Studying the effects of cerebral hypoperfusion on white matter integrity in human brain is limited as elderly individuals often have co-morbid disease such as hypertension making it difficult to directly ascertain a causal relationship. This has led to the development of animal models of chronic cerebral hypoperfusion which can be used to directly determine the effects of cerebral hypoperfusion, in isolation, on white matter integrity and cognition. The studies described in this thesis sought to determine the impact of cerebral hypoperfusion on white matter structure and function, and to elucidate possible underlying mechanisms using a mouse model.

1.1 White matter

The human brain consists of grey and white matter which both account for around 50% of total brain volume (Zhang and Sejnowski, 2000). The white matter consists primarily of myelinated axons and associated glial cells including oligodendrocytes, astrocytes and microglia (Figure 1.1). The white matter also contains blood vessels which are essential for the delivery of oxygen and glucose to resident cells.

1.1.1 Cellular components of white matter

The glial cells of the white matter each have specific roles in the maintenance of white matter integrity but signalling mechanisms exist between glial cell types and myelinated axons, forming part of a larger network in which each component is critical.

1.1.1.1 Oligodendrocytes

Oligodendrocytes are the most abundant cells within the white matter, comprising around 70% of the total cell population (Ling and Leblond, 1973). Oligodendrocytes extend processes composed of myelin which wrap around neighbouring axons providing an insulating myelin sheath (Figures 1.1A and 1.1B). It has been estimated that a single oligodendrocyte can myelinate between 30-50 segments on individual axons (Hildebrand et al., 1993; Rivers et al., 2008), which are termed internodes (outlined in Section 1.1.2.2). The process of myelination is tightly regulated and there is a close association between axonal calibre and the thickness of the

surrounding compact myelin sheath which is called the g-ratio. In rodents the optimal g-ratio (axonal diameter divided by total fibre diameter) is reported to be approximately 0.64-0.77 (Smith and Koles, 1970; Little and Heath, 1994; Chomiak and Hu, 2009).

In addition to myelin production, oligodendrocytes are also involved in the clustering of axonal ion channels (Kaplan et al., 1997; Dupree et al., 2004) and provide trophic and metabolic support to the axons they ensheath (Nave, 2010a; Lee et al., 2012). It has additionally been reported that oligodendrocytes can directly modulate the conduction velocity of the axons they myelinate (Yamazaki et al., 2007).

1.1.1.2 Oligodendrocyte precursor cells

Oligodendrocytes are derived from oligodendrocyte precursor cells (OPCs; Figures 1.1A and 1.1C) which are abundant during late embryonic and early postnatal development but persist in the adult brain (Nishiyama et al., 2002). OPCs represent an intermediary stage in the oligodendrocyte lineage and differentiate into pre-myelinating oligodendrocytes which then undergo further differentiation into mature myelinating oligodendrocytes (Figure 1.2; Nishiyama et al., 2009). It has been estimated that OPCs comprise around 8-9% of all cells within adult rat white matter (Dawson et al., 2003) and as such they are considered to be a major glial cell type (Peters, 2004). Furthermore, studies have revealed that OPCs are the most abundant proliferating cell type in both adult mouse (Dawson et al., 2003) and human (Geha et al., 2010) brains. OPCs were first described in the 1980s and were referred to as

oligodendrocyte-type 2 astrocyte (O-2A) progenitor cells based on *in vitro* studies demonstrating that they could generate both oligodendrocytes and astrocytes (Raff et al., 1983; Ffrench-Constant and Raff, 1986). A growing number of studies have since characterised the fate of these precursor cells *in vivo* and have revealed that these cells exclusively belong to the oligodendrocyte lineage (reviewed by Richardson et al., 2011) and thus are now referred to as OPCs. Phenotypically, OPCs are identified based on expression of the neuron-glial antigen 2 (NG2) protein (Stallcup and Beasley, 1987) and are therefore also termed 'NG2 cells'.

The finding that OPCs with the ability to proliferate and differentiate are present in the adult brain has important implications both for myelin remodelling in the normal brain and repair following injury. Indeed, a recent study has shown that OPC proliferation and differentiation in healthy adult mouse brain are tightly co-ordinated to maintain a constant cell density throughout life (Hughes et al., 2013). Furthermore, it has been demonstrated that in response to white matter injury such as demyelination and ischaemia, OPCs can proliferate and differentiate into mature oligodendrocytes thus replacing any cells which may have been lost as a result of the insult (Mandai et al., 1997; Keirstead et al., 1998). Additionally, it has been reported that OPCs possess a variety of receptors, and that a subset of OPCs can generate action potentials (Karadottir et al., 2008) suggesting that they may have critical roles in signalling.

1.1.1.2 Astrocytes

The second most abundant cells are astrocytes which comprise approximately 15-20% of cells within the white matter (Ling and Leblond, 1973). Astrocytes have many and varied roles including intercellular signalling and repair following injury. Astrocytes make direct contact with blood vessels within the white matter (Figures 1.1A and 1.1D) allowing regulation of local blood flow and modulation of energy supply and metabolism (reviewed by Sofroniew and Vinters, 2010). In the normal brain, astrocytes are usually 'resting' but upon CNS injury they can become activated which can have both beneficial and detrimental consequences (Sofroniew, 2009).

1.1.1.3 Microglia/macrophages

Microglia are the resident immune cells of the CNS (Figures 1.1A and 1.1E) and it is estimated that microglia comprise approximately 5% of all cells within the white matter (Lawson et al., 1990). Microglia are considered to be a subpopulation of macrophages however these populations of cells differ in that macrophages are found in organs throughout the body whereas microglia are only found in brain (reviewed by Saijo and Glass, 2011; Cronk and Kipnis, 2013). Despite this difference, both microglia and macrophages are observed in the brain and due to a lack of markers to distinguish microglial and macrophage populations these terms are often used interchangeably to describe a single population of cells (as is the case in this thesis).

Like astrocytes, microglia are normally found in a ‘resting’ state but can be rapidly activated in response to injury and disease. Resting microglia perform active surveillance of the local microenvironment allowing them to react rapidly to injury. Upon activation, microglia become phagocytic and release a battery of inflammatory mediators in addition to reactive oxygen species (Kreutzberg, 1996). Thus microglial activation is thought to exert both protective and damaging effects in the injured CNS.

1.1.1.5 Blood vessels

In addition to glial cells, the white matter also contains blood vessels which are essential for the delivery of oxygen and glucose to the cells of the white matter. Blood vessels are lined by endothelial cells which release a variety of mediators both to regulate local blood flow and to signal to glial cells (Faraci and Heistad, 1998; Park et al., 2003; Miyamoto et al., 2013a).

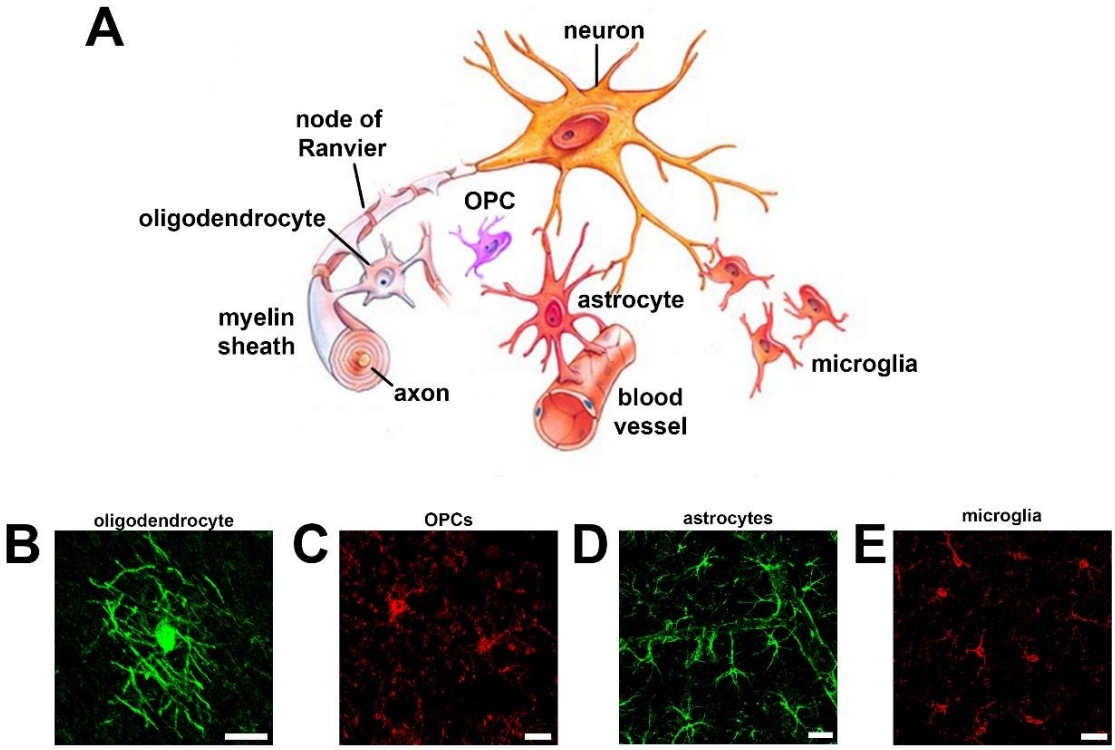

Figure 1.1: Cellular components of white matter. (**A**) The white matter consists of myelinated axons and associated glial cells including oligodendrocytes, astrocytes, microglia and oligodendrocyte precursor cells (OPCs). (**B-E**) Confocal images showing immunolabelled glial cells in mouse brain sections. (**B**) In this image a single oligodendrocyte can be seen forming internodal segments on multiple axons. (**C**) OPCs labelled using an anti-NG2 antibody. (**D**) In this image astrocyte processes can be seen outlining a blood vessel. (**E**) Resting microglia are shown in this image. Image A taken and adapted from The McGraw-Hill Company (www.mhhe.com). Image B was acquired at 40x magnification and images C-E were acquired at 20x. The following antibodies were used to label cells (B) myelin oligodendrocyte glycoprotein (MAG), (C) NG2, (D) glial fibrillary acidic protein (GFAP), and (E) ionised calcium-binding adaptor molecule 1 (Iba1). Scale bars = 20 µm.

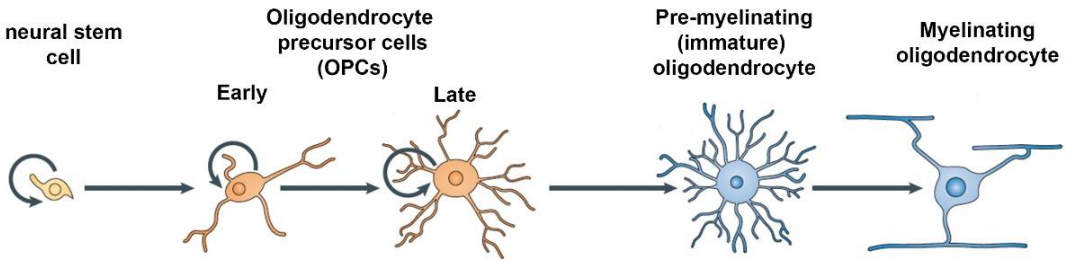

Figure 1.2: The oligodendrocyte lineage. Oligodendrocyte precursor cells are derived from multipotent neural stem cells during late embryonic and early postnatal development. OPCs persist in the adult brain and represent around ~9% of cells within the white matter. OPCs first differentiate into pre-myelinating oligodendrocytes which then further differentiate into mature myelinating oligodendrocytes. Image taken and adapted from Nishiyama et al (2009).

1.1.2 Structure and function of myelinated axons

1.1.2.1 Myelin

The presence of a myelin sheath around an axon is essential for fast and efficient axon potential conduction (outlined in Section 1.1.2.4). Myelin is comprised of approximately 70% lipids including phospholipids, glycolipids, cholesterol and glycosphingolipids which are commonly found in other cellular membranes (Baumann and Pham-Dinh, 2001). The lipid-rich composition of myelin gives the white matter its white appearance and provides myelin with its electrically insulating properties.

In addition to high lipid content, myelin is also composed of approximately 30% protein. The major myelin proteins are myelin basic protein (MBP) and proteolipid protein (PLP), which constitute 30% and 50% of total myelin protein respectively (Baumann and Pham-Dinh, 2001). Two other proteins, 2',3'-Cyclic-nucleotide 3'-phosphodiesterase (CNPase) and myelin-associated glycoprotein (MAG) are also present within the myelin sheath but represent minor proportions (4% and 1% respectively). Despite the relatively low proportion of MAG within the myelin sheath, this protein plays a key role in the maintenance of axon-glial connection (Li et al., 1998).

1.1.2.2 Domain structure of myelinated axons

Myelinated axons have a defined domain structure (Figure 1.3A). The regularly spaced, non-myelinated nodes of Ranvier are flanked either side by the paranodal domains where myelin forms its terminal loops. The paranodes are adjacent to the juxtaparanodes which in turn are found beside the internodal domains. Each domain is characterised by a unique protein architecture (Figure 1.3B) which is specialised to allow efficient axon potential propagation along the length of the axon.

1.1.2.3 Protein architecture of nodes, paranodes and juxtaparanodes

Nodes of Ranvier are non-myelinated regions of myelinated axons which are approximately 1 µm in length (in both human and rodent) and contain a high density of voltage-gated sodium (Na_v) channels (approximately 1000 channels per μm^2; (Waxman and Ritchie, 1993). The main sodium channel isoform present at adult nodes of Ranvier is $Na_v1.6$ (Caldwell et al., 2000) however $Na_v1.2$ has been demonstrated to be the predominant isoform during development (Kaplan et al., 2001). The high density clustering of $Na_v1.6$ channels is mediated by interactions with other nodal proteins, and through protein interactions at the paranodes (outlined below). At nodes of Ranvier $Na_v1.6$ channels are associated with Ankyrin G, a large protein which tethers the channels to the node through its interaction with the actin-binding protein βIV spectrin, which in turn anchors the complex to the axonal cytoskeleton (Figure 1.3B; Srinivasan et al., 1988). $Na_v1.6$ channels also interact with the cell adhesion molecule neurofascin 186 (Nfasc186) at nodes of Ranvier (Davis et al., 1996; Ratcliffe et al., 2001) which itself is associated with the

extracellular matrix (Figure 1.3B; Hedstrom et al., 2007). Thus the interactions between $Na_v1.6$ channels and other nodal proteins help to maintain the high density clustering of channels at nodes of Ranvier.

The nodes of Ranvier are flanked either side by the paranodes which are the primary sites of axon-glial connection in the CNS. At the paranodes, the axonal proteins contactin and contactin-associated protein (Caspr) form a trimeric complex with the myelin protein neurofascin 155 (Nfasc155; Figure 1.3B). Together these proteins form the paranodal septate-like junctions which act as physical barriers to prevent the diffusion of $Na_v1.6$ channels away from nodes of Ranvier. Studies using transgenic mice lacking Contactin (Boyle et al., 2001), Caspr (Bhat et al., 2001) and Nfasc155 (Pillai et al., 2009) have shown that each of these proteins is essential for the maintenance of paranodal septate-like junctions.

The juxtaparanodal domains are found adjacent to the paranodal domains (Figures 1.3A and 1.3B) and are characterised by a high density of voltage-gated potassium (K_v) channels, including $K_v1.1$ and $K_v1.2$ isoforms (Wang et al., 1993). Similar to $Na_v1.6$ channels at nodes of Ranvier, K_v channels are part of a larger protein complex including Caspr2 and TAG-1 (Poliak et al., 2003) however many components of the juxtaparanodal complex remain unidentified (Rasband, 2004). It is thought that the interaction between Caspr2 and TAG-1 plays an important role in restricting K_v channels to juxtaparanodes (Poliak and Peles, 2003) in addition to the paranodal septate-like junctions which prevent the diffusion of K_v channels from the

juxtaparanodes and into the neighbouring paranodes. The internodal domains of myelinated axons are found adjacent to juxtaparanodes and are the sites at which compact myelin is present. MAG is found within internodal myelin and plays an important role in maintenance of axon-glial connection through associations with axonal receptors including Nogo and sialoglycan receptor families (Schnaar and Lopez, 2009).

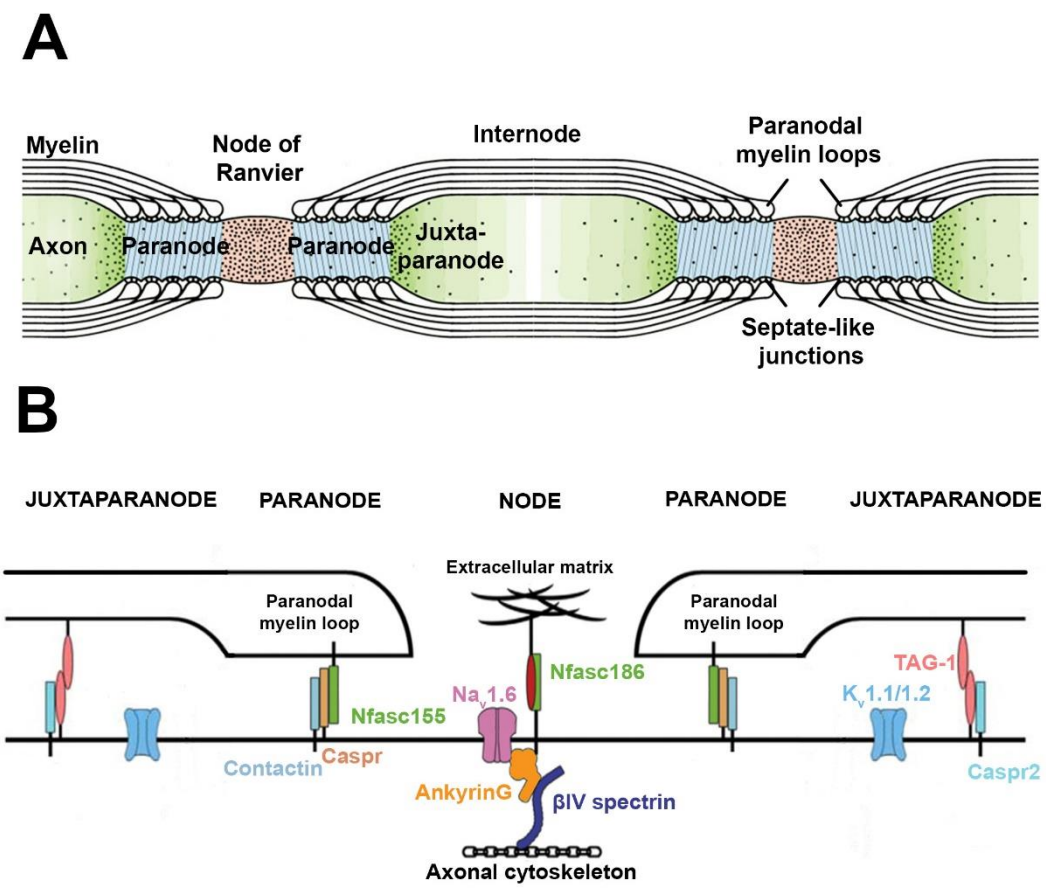

Figure 1.3 Myelinated axons consist of highly specialised domains. (**A**) Schematic diagram showing the domains of myelinated axons. Nodes of Ranvier are unmyelinated regions flanked either side by paranodal domains. The juxtaparanodes separate paranodal and internodal domains. (**B**) Nodes of Ranvier contain a high density of voltage-gated sodium channels ($Na_v1.6$) which are anchored to the cytoskeleton via interactions with Ankyrin G and βIV spectrin. Additionally, an association with Nfasc186 tethers these channels to the extracellular matrix. The paranodal septate-like junctions found either side of the nodes of Ranvier are formed by the trimeric protein complex between the glial protein Nfasc155 and the axonal proteins Caspr and Contactin. At juxtaparanodal domains, clusters of $K_v1.1$ and $K_v1.2$ channels are present in addition to TAG-1 and Caspr2 which are thought to play an important role in the localisation of K_v channels at juxtaparanodes. Images taken and adapted from Rosenbluth (2009) and Susuki (2013).

1.1.2.4 Action potential conduction along myelinated axons

The highly organised domain structure of myelinated axons and the presence of an intact myelin sheath are essential for saltatory conduction of action potentials along axons and are thus essential for neuronal communication within the brain. Saltatory conduction is the process by which action potentials are regenerated at nodes of Ranvier (Huxley and Stampfli, 1949; Hodgkin and Huxley, 1952) due to the fast influx of Na^+ ions through $Na_v1.6$ channels. The high density clustering of $Na_v1.6$ channels at nodes of Ranvier is essential for rapid Na^+ entry and subsequent axonal depolarisation. Additionally, the segregation of K_v channels at juxtaparanodal domains is thought to play an important role in repolarising the axonal membrane allowing the return to resting membrane potential (Waxman and Ritchie, 1993). The insulating myelin sheath around myelinated axons is also important for action potential conduction as it acts to prevent internodal current leakage and increase resistance (reviewed by Hartline and Colman, 2007). It has been estimated that myelination of axons can increase conduction velocity by up to 100x compared to values of non-myelinated axons (Nave, 2010a).

Measurement of action potential conduction along axons can be used to examine white matter function in experimental models and is assessed using electrophysiological approaches in brain slice preparations or teased nerve fibres. In such studies, the compound action potential (CAP) is typically measured which represents the combined action potential by all axons within the fibre bundle. This approach has been employed by numerous studies to determine the effects of white

matter disruption on action potential conduction. Such studies have demonstrated that disruption to the myelin sheath or to the localisation of $Na_v1.6$ channels at nodes of Ranvier can impair action potential conduction (McDonald and Sears, 1970; Ritter et al., 2013) and therefore may impact on cognition.

1.1.3 The impact of ageing on white matter integrity and cognition

The growing use of imaging techniques such as magnetic resonance imaging (MRI) in neurological research has helped advance our understanding of the role of white matter in the pathogenesis of brain disease but also during the normal ageing process. Early studies using T_2-weighted MRI revealed the presence of white matter 'lesions', appearing as areas of hyperintense signal, in periventricular and deep subcortical white matter of elderly individuals (Brant-Zawadzki et al., 1985; Awad et al., 1986b). Another study demonstrated that approximately 55% of individuals aged between 60 and 70 years old had white matter hyperintensities, the prevalence of which increased to 95% of subjects aged between 80 and 90 (de Leeuw et al., 2001). Additional studies have utilised diffusion tensor imaging (DTI) to visualise the directionality of white matter fibre tracts and have similarly reported age-related decreases in white matter integrity (Head et al., 2004; Bastin et al., 2009), with some studies demonstrating that this decline begins at approximately 40 years of age (Westlye et al., 2010; Lebel et al., 2012).

In addition to MRI, post-mortem studies have been carried out to study the pathological changes underlying white matter hyperintensities. These have revealed that areas of hyperintense signal correspond to areas in which there is a loss of myelinated fibres, myelin vacuolation and a marked increase in numbers of astrocytes and microglia (Awad et al., 1986a; Scarpelli et al., 1994; Simpson et al., 2007a). Furthermore a significant decrease in white matter volume has also been reported in aged brains as compared to younger brains in both humans (Tang et al., 1997) and primates (Peters and Sethares, 2002).

Importantly, parallel MRI and cognitive testing in the same individuals has shown a direct association between white matter lesions and poorer performance in cognitive tests of executive function (Breteler et al., 1994a; O'Sullivan et al., 2001) and memory recall (de Groot et al., 2000; O'Brien et al., 2002). It has been proposed that reduced myelin integrity in ageing results in 'disconnection' within the brain which subsequently leads to cognitive decline (O'Sullivan et al., 2001). It has similarly been hypothesised that this disconnection initially affects executive cognitive function and aspects of memory as these processes involve a high degree of signalling between neurons and therefore are more susceptible to impaired action potential propagation as a result of myelin disruption (Bartzokis et al., 2004). Importantly, longitudinal study in a large cohort of elderly individuals has demonstrated that periventricular white matter lesion volume can predict the rate of cognitive decline over a 7 year period (De Groot et al., 2002). Furthermore, periventricular white matter hyperintensities are also observed in individuals with Alzheimer's disease (AD) and are more extensive than observed in age-matched controls (Fazekas et al., 1987;

Scheltens et al., 1995; Barber et al., 1999), suggesting that white matter disruption may contribute both to 'normal' age-related cognitive decline and to clinical dementia. Taken together, the evidence from MRI and pathology studies demonstrate age-related alterations in white matter integrity which may underlie cognitive decline in ageing. The exact causes of white matter disruption in ageing are unknown but it is thought that reduced cerebral blood flow (CBF) may be an important contributing factor.

1.2 Blood supply to the brain and chronic cerebral hypoperfusion

1.2.1 Blood supply to the brain

Normal functioning of the brain requires a constant blood supply. In most mammals, including humans and rodents, the brain receives its blood supply primarily through the internal carotid arteries which supply the forebrain and the vertebral arteries which supply the hindbrain. These arteries enter the circle of Willis, a circular network of arteries which provides a uniform blood supply to the brain. This vascular network creates redundancies in the cerebral circulation such that perfusion remains constant in the event of blockage or stenosis of one of the arteries supplying or forming the circle of Willis. The integrity of the circle of Willis varies between species and individual strains of animals which can influence the ability of the brain to respond to perturbations in CBF (outlined in Section 1.2.3.2).

1.2.1.1 Blood supply to the white matter

The white matter receives its blood supply from deep penetrating arteries that run along the cortical surface and travel at right angles through the cortex into the subcortical white matter (Pantoni and Garcia, 1997; Nonaka et al., 2003). Microvessels branch from these penetrating arteries to form a three dimensional network supplying the white matter (Blinder et al., 2013). The periventricular white matter receives its blood supply from ventrofugal vessels arising from the base of the brain (Pantoni and Garcia, 1997). Anatomical studies have revealed that the vascular network supplying the white matter is less extensive than that of grey matter (Klein et al., 1986) and it has been estimated that capillary density is around one third to one quarter of that in the cortex (Klein et al., 1986; Nonaka et al., 2003). Similarly, MRI studies in humans have estimated that white matter CBF (~33.6 ml/min ± 11.5 per 100g) is approximately half of that of grey matter (~69.7 ml/min ± 29.7 per 100g Rempp et al., 1994). It has been proposed that this relatively low blood supply may render the white matter more susceptible to reductions in CBF (Pantoni and Garcia, 1997; Holland et al., 2008).

1.2.2 Cerebral energy metabolism

Although the brain accounts for only 2% of body weight, it is estimated to consume approximately 20% of total oxygen and 25% of total glucose (Edvinsson et al., 1993). This high requirement of oxygen and glucose is essential for the generation of adenosine triphosphate (ATP), the main energy substrate of all cells within the brain (reviewed by Sokoloff, 1992). ATP is required for maintaining cellular homeostasis

therefore any disruption to cerebral blood flow can alter the balance between ATP production and usage, resulting in disturbed cellular function or cell death. ATP is generated as a product of the oxidation of glucose to water and CO_2 through the sequential processes of glycolysis, which occurs in the cytosol, and the citric acid cycle and oxidative phosphorylation which occur within mitochondria. Together these processes yield approximately 30-36 molecules of ATP per molecule of glucose (reviewed by Magistretti and Allaman, 2013), the majority of which is generated from mitochondrial oxidative phosphorylation.

ATP can also be generated in the absence of oxygen as a result of anaerobic glycolysis however this process is inefficient, generating two molecules of both ATP and lactate per molecule of glucose (Magistretti and Allaman, 2013). Interestingly, a number of studies have revealed that the brain can utilise lactate as an alternative energy source in the absence of glucose. Electrophysiological study has demonstrated that the evoked synaptic response in rat hippocampal slices was not significantly different when supplied with lactate as compared to glucose (Schurr et al., 1988). In addition it has been shown that lactate released by astrocytes can be used as a neuronal energy substrate during times of increased energy demand (Pellerin and Magistretti, 1994; Magistretti and Pellerin, 1999; Tarczyluk et al., 2013). It is estimated that 1 molecule of lactate can generate approximately 15 molecules of ATP (Schurr, 2006). Thus while the brain preferentially utilises glucose as the main energy source it has the capability to use alternatives in the event of reduced glucose availability.

1.2.2.1 Energy metabolism in white matter

Given that white matter CBF is approximately 50% of that of grey matter it is not surprising that estimates of white matter oxygen and glucose consumption are similarly reported to be around half of grey matter values in both rodent (Sokoloff et al., 1977; Nishizaki et al., 1988) and human (Baron et al., 1984; Pantano et al., 1984). Despite this, myelinated axons and glial cells of the white matter are critically dependent on an uninterrupted supply of oxygen and glucose. Interestingly, electrophysiological assessment of adult rat optic nerve preparations has shown that whilst 60 minutes of glucose deprivation results in irreversible failure of the CAP (Wender et al., 2000), the CAP is maintained in the absence of glucose for between 30-40 minutes (Fern et al., 1998; Wender et al., 2000). Furthermore, the CAP is maintained for up to 15 minutes in the absence of both glucose and oxygen (Fern et al., 1998). Taken together these studies indicate that there are alternative energy stores within the white matter.

Within myelinated axons the vast majority of ATP is generated from axonal mitochondria which are dynamically transported along the length of the axon to areas of increased energy demand (reviewed by Hollenbeck and Saxton, 2005). Growing evidence indicates that in addition to axonal mitochondria, the energy requirements of myelinated axons may be met in part by metabolic support from myelinating oligodendrocytes (Nave, 2010b; Saab et al., 2013). This theory proposes that myelinating oligodendrocytes can metabolically support axons by the transfer of energy rich metabolites across the axonal membrane (Nave, 2010b). The presence of

the myelin sheath around an axon physically prevents axonal uptake of glucose from the extracellular environment (Nave, 2010a, b) therefore it has been postulated that oligodendrocyte metabolites such as lactate and pyruvate may be transferred to axons via 'channels' within non-compact myelin (Nave, 2010b; Saab et al., 2013). In support of this it has recently been demonstrated that the lactate transporter monocarboxylate transporter 1 (MCT1) is enriched along the myelin sheath and that loss of this transporter results in axonal damage (Lee et al., 2012). Furthermore, another recent study sought to determine the ability of myelinated axons to utilise oligodendrocyte-derived lactate and generated mutant mice in which oligodendrocyte mitochondria were disrupted and gradually lost the ability to generate ATP from oxidative phosphorylation (Funfschilling et al., 2012). In this model, oligodendrocytes were required to generate ATP through glycolysis leading to the production of lactate. Critically these mice did not exhibit any myelin or axonal pathology suggesting that both mature oligodendrocytes and myelinated axons could utilise lactate in the absence of glucose (Funfschilling et al., 2012). These recent findings confirm earlier studies which revealed that the rate of glycolytic metabolism is higher in white matter than grey matter (Morland et al., 2007) and that the CAP of optic nerve axons is unchanged when nerves are incubated in lactate as compared to glucose (Brown et al., 2001). It has additionally been reported that astrocytes also express MCT1 and that astrocyte-derived lactate can maintain the CAP in mouse optic nerve preparations, indicating a further energy source within the white matter (Tekkok et al., 2005). Taken together these studies demonstrate that in the absence of glucose, the energy requirements of oligodendrocytes and myelinated axons of the white matter can be maintained by the glycolytic production of ATP and lactate. This

is of particular importance for conditions in which CBF is reduced such as chronic cerebral hypoperfusion.

1.2.3 Chronic cerebral hypoperfusion

A common feature of ageing is a modest age-related reduction in CBF, termed chronic cerebral hypoperfusion. Studies have shown that from age 20 to 80 years, CBF is reduced by approximately 0.5% per year (Leenders et al., 1990; Scheel et al., 2000). This modest and chronic decrease in CBF with ageing should not be confused with ischaemic stroke which is a very acute and severe reduction (>70%) in CBF resulting in irreversible tissue damage with often debilitating consequences (Astrup et al., 1981; Baron, 2001).

1.2.3.1 The impact of cerebral hypoperfusion on white matter integrity and cognition

A growing number of studies have highlighted the association between chronic cerebral hypoperfusion and white matter disruption. Early MRI investigations revealed a strong correlation between white matter hyperintensities and cerebrovascular or cardiovascular disease (Awad et al., 1986b; Breteler et al., 1994b). Furthermore, post-mortem investigation of individuals with clinical dementia revealed areas of myelin pallor characterised by loss of myelinated axons and oligodendrocytes in addition to thickening of cerebral arterioles. This finding, together with a strong history of cardiovascular disease in many of the cases examined, led the authors to hypothesise that the disruption to white matter may be

due to hypoperfusion (Brun and Englund, 1986). This was later confirmed by parallel post-mortem MRI and pathology studies of ageing brains which revealed that periventricular white matter 'lesions' showed an increased expression of markers of hypoxia (Fernando et al., 2006) in addition to cerebrovascular pathology (Young et al., 2008). Additionally, a strong correlation between the presence of white matter hyperintensities and local blood flow has been reported (DeCarli et al., 1995; O'Sullivan et al., 2002). Furthermore it has been demonstrated that white matter hyperintensities often occur in regions in which blood flow is normally relatively lower compared to other white matter areas, namely the deep periventricular white matter (Holland et al., 2008). As indicated in Section 1.2.1.1, this low blood supply may render the periventricular white matter more susceptible to reductions in blood flow than other regions (Pantoni and Garcia, 1997; Holland et al., 2008).

Additional studies have reported an association between reduced CBF, increased white matter hyperintensity volume and poorer performance upon neuropsychological testing of executive function in elderly individuals (Appelman et al., 2010). Similarly it has been demonstrated that elderly individuals with dementia have lower CBF than age-matched controls (Ruitenberg et al., 2005). Taken together these studies indicate that chronic cerebral hypoperfusion may underlie white matter disruption and cognitive decline in ageing.

1.2.3.2 Animal models of chronic cerebral hypoperfusion

Investigating the effects of cerebral hypoperfusion on white matter integrity in human brain is limited as it is difficult to ascertain a cause and effect relationship through clinical imaging or post-mortem approaches. Indeed, many individuals with cerebral hypoperfusion often have co-existing disease states such as hypertension and diabetes mellitus and therefore it is difficult to study the effects of hypoperfusion on white matter integrity in isolation. This has led to the development of animal models which typically involve modulation of CBF through occlusion or stenosis of the common carotid arteries. The degree of hypoperfusion induced is dependent on the integrity of the circle of Willis which varies amongst species and strains (Figure 1.4).

1.2.3.2.1 Common carotid artery occlusion models

Many investigators studying cerebral hypoperfusion have utilised the bilateral common carotid artery occlusion (BCCAO) model in rat (Pulsinelli and Brierley, 1979). In this model both carotid arteries of Wistar or Sprague-Dawley rats are permanently occluded using nylon sutures, resulting in an approximate 60-70% decrease in CBF which recovers to around 50% of baseline within one month (reviewed by Farkas et al., 2007). Studies using this model have reported myelin disruption and vacuolation in the optic tract as early as 3 days after surgery with similar damage evident in the corpus callosum from 7 days (Wakita et al., 2002). This myelin pathology worsens over time such that disruption to other white matter regions such as the striatum is observed 4 weeks following surgery (Wakita et al.,

2002). In addition, increased numbers of activated microglia and astrocytes have been reported in this model after 2 weeks (Cho et al., 2006; Lee et al., 2006), and persist until over 4 months following surgery (Ohta et al., 1997). Behavioural assessment has revealed that these rats commit more revisiting errors in the 8-arm radial arm maze task than sham controls when assessed 3 days and 4 months following surgery (Ni et al., 1994). Similarly a significantly increased escape latency in the Morris water maze task has been reported as early as 7 days following surgery (Pappas et al., 1996). Whilst these mice exhibit characteristic features of human age-related white matter disruption (namely white matter damage, increased inflammation and cognitive decline) one limitation of this model is that due to the severity of the reduction in cerebral blood flow these animals often show pronounced ischaemic neuronal damage in the hippocampus (Farkas et al., 2004; Farkas et al., 2007). In addition, extensive damage to the optic nerve is also reported (Farkas et al., 2007) which may influence the ability of these animals to respond to visual cues during behavioural testing. The effects of decreased blood flow on white matter integrity and cognition can therefore not be studied in this model without the confounding presence of ischaemic neuronal damage.

Whilst the rat BCCAO model is useful for studying the effects of severe hypoperfusion, mouse models are advantageous as they can be easily genetically modified. Permanent BCCAO cannot be studied in mouse as many strains are unable to tolerate the procedure due to an incomplete circle of Willis (Figure 1.4; Barone et al., 1993; Fujii et al., 1997; Yang et al., 1997; Kitagawa et al., 1998). This is particularly true of the C57Bl/6J mouse which is the most commonly laboratory

mouse and is often used as a background strain for transgenic animals. These mice exhibit poorly developed or absent posterior communicating arteries which results in compromised collateral blood flow and a greater susceptibility to reductions in CBF (Figure 1.4; Yang et al., 1997; Kitagawa et al., 1998; Majid et al., 2000). A transient BCCAO model of global ischaemia, resulting in severe hypoperfusion, has been described in mouse through occlusion of the carotid arteries for 20 minutes (Yang et al., 1997). A disadvantage of this model however is that ischaemic neuronal damage is induced in the hippocampus (Yang et al., 1997), again confounding the study of hypoperfusion on white matter integrity. A model of permanent unilateral common carotid artery occlusion has more recently been described in mouse (Yoshizaki et al., 2008). In this model, occlusion of the right common carotid artery induces white matter rarefaction and loss of myelinated fibres in the corpus callosum together with an increase in microglial number and levels of pro-inflammatory cytokines following 1 month of hypoperfusion (Yoshizaki et al., 2008). These mice also exhibit impaired performance in object recognition tests (Yoshizaki et al., 2008) however this model is not widely used and therefore not well characterised.

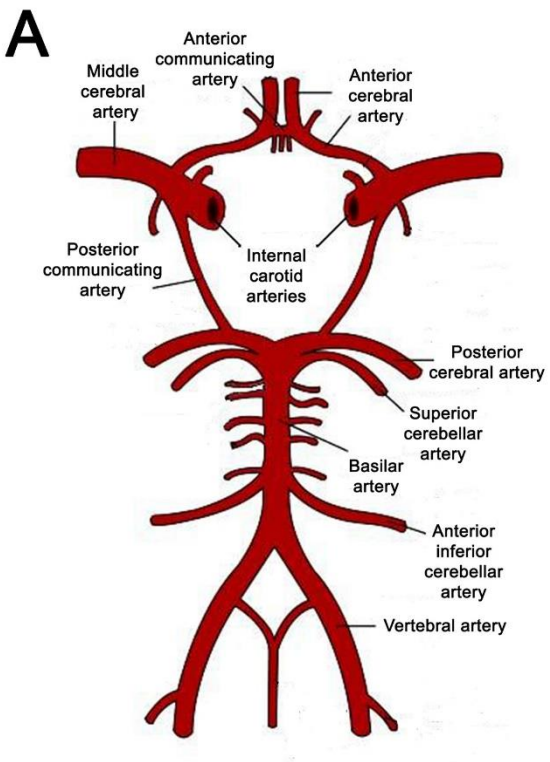

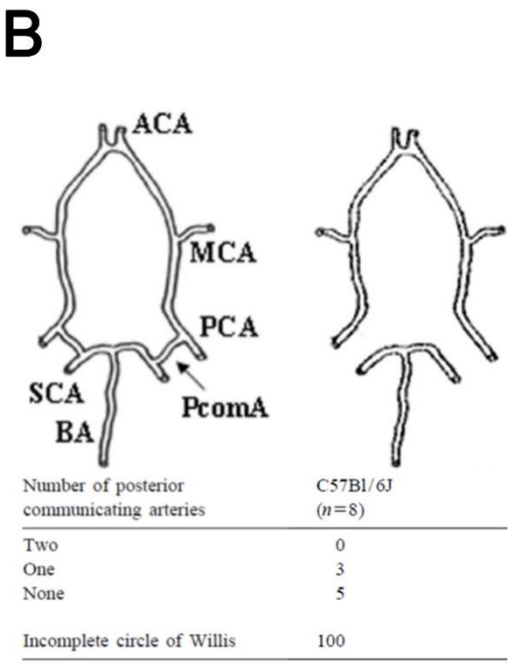

Number of posterior communicating arteries	C57Bl/6J (n=8)
Two	0
One	3
None	5
Incomplete circle of Willis	100

Figure 1.4: The anatomy of the Circle of Willis. (**A**) Schematic diagram showing the anatomy of the Circle of Willis. Blood is delivered to the forebrain via the internal carotid arteries and to the hindbrain via the vertebral arteries. The posterior communicating arteries connect these two supplies to provide collateral flow such that if there is a blockage or stenosis of one of the arteries supplying or forming the Circle of Willis, CBF will remain constant. (**B**) Schematic diagram showing the incomplete Circle of Willis in C57Bl/6J mice. This strain of mice typically have an absence of either one or both posterior communicating arteries (PComA) resulting in insufficient collateral flow and an increased vulnerability to reductions in CBF. ACA – anterior communicating artery, MCA – middle cerebral artery, PCA – posterior cerebral artery, BA – basilar artery, SCA – superior cerebellar artery. Image A taken and adapted from Wikipedia (www.wikipedia.org). Image B taken and adapted from Kelly et al. (2001).

1.2.3.2.2 Bilateral common carotid artery stenosis

Bilateral common carotid artery stenosis was first described as a model of cerebral hypoperfusion in gerbil (Kudo et al., 1990; Hattori et al., 1992). In this model, hypoperfusion is achieved through application of small wire coils to the carotid arteries resulting in stenosis (rather than complete occlusion) of the vessels and a reduction in CBF. A key advantage of this approach is that the level of hypoperfusion induced is dependent on the internal diameter of the microcoils which provides the opportunity to study the effects of increasing severity of hypoperfusion. Pathologically these animals exhibit widespread white matter rarefaction and increased astrocyte reactivity, together with ischaemic neuronal damage in the hippocampus and cortex from 1 week after surgery (Hattori et al., 1992). The extent of white and grey matter pathology induced in gerbil is a consequence of this species' incomplete circle of Willis which renders the brain highly vulnerable to reductions in CBF (Yoshizaki et al., 2008). These animals also display an impaired learning ability in the passive avoidance test after 6 weeks of hypoperfusion (Kudo et al., 1990).

Another bilateral carotid artery stenosis model has been developed using C57Bl/6J mice and similarly uses wire microcoils around the carotid arteries to reduce CBF (Shibata et al., 2004). The initial characterisation of the model studied the extent of white and grey matter pathology induced by microcoils of varying internal diameters (0.22mm, 0.20 mm, 0.18 mm and 0.16 mm). The authors reported that microcoils with an internal diameter of 0.18 mm reduced CBF by approximately 30% after 3

days which steadily recovered to around 15% of baseline values after one month (Shibata et al., 2004). Pathological assessment demonstrated diffuse white matter damage together with increased numbers of microglia and astrocytes evident from 14 days after surgery and persisting for up to 1 month (Shibata et al., 2004; Coltman et al., 2011). Critically, this white matter damage occurred in the absence of ischaemic neuronal damage. In contrast, mice in which hypoperfusion was induced using 0.16 mm diameter microcoils exhibited ischaemic neuronal damage in the cortex and hippocampus, together with cortical microinfarcts (Shibata et al., 2007). This highlights that the internal diameter of the microcoils can directly influence the extent of white and grey matter pathology, and indicates that the 0.18 mm microcoil is optimal for studying the effects of chronic cerebral hypoperfusion on white matter integrity. Furthermore, behavioural studies of mice fitted with 0.18 mm coils have demonstrated that hypoperfused mice commit significantly more revisiting errors that sham controls in the 8-arm radial arm maze assessment of spatial working memory (Shibata et al., 2007; Coltman et al., 2011). Thus this model provides the opportunity to study the effects of chronic cerebral hypoperfusion on white matter integrity and the downstream cognitive changes in the absence of ischaemic neuronal damage.

A modification of the bilateral carotid stenosis model has more recently been described (Miki et al., 2009). In this study the authors applied a 0.18 mm microcoil to the right carotid artery and a 0.16 mm microcoil to the left common carotid artery in order to induce a more severe reduction in CBF whilst limiting the excessive mortality (75%) associated with applying 0.16 mm microcoils to each carotid (Shibata et al, 2004). In this mixed coil model, blood flow is reported to decrease

initially to between 20 - 50% following six days which recovers to around 60% following 1 month. Pathologically these mice show myelin damage and glial activation following 1 month of cerebral hypoperfusion in addition to ischaemic neuronal damage, primarily in the hippocampus (Miki et al., 2009). Behavioural assessment using the Morris water maze has also demonstrated a significant increase in escape latency as compared to shams following 1 month of hypoperfusion (Miki et al., 2009). This modified model is therefore a useful tool to study the effects of more severe cerebral hypoperfusion.

1.2.4 Mechanisms of white matter damage following cerebral hypoperfusion

An understanding of the mechanisms underlying white matter disruption with hypoperfusion is essential for the development of future therapeutic strategies. Damage to myelinated axons and loss of oligodendrocytes is commonly observed in disease states such as cerebral ischaemia (Dewar et al., 2003) and multiple sclerosis (MS) (Lucchinetti et al., 2000). It has been demonstrated both *in vitro* and *in vivo* that oligodendrocytes are vulnerable to increased inflammation (Merrill and Scolding, 1999; Mabuchi et al., 2000) and oxidative stress (Bongarzone et al., 1995; Irving et al., 1997; Juurlink, 1997), both of which are features of chronic cerebral hypoperfusion.

1.2.4.1 Inflammation

White matter disruption associated with cerebral hypoperfusion in humans and in mouse models is accompanied by a pronounced inflammatory response. Post-mortem study of aged human brains has shown that periventricular white matter disruption is associated with a significant increase in microglial activation as compared to control brains (Simpson et al., 2007b). In addition, microarray analysis of white matter extracted from mice following 3 days of chronic cerebral hypoperfusion has revealed upregulation of several genes associated with inflammatory responses (Reimer et al., 2011). Furthermore, increased production of the pro-inflammatory cytokine tumour necrosis factor α (TNFα) has been shown in rat following 14 days of BCCAO (Lee et al., 2006) and in mouse following 30 days of chronic cerebral hypoperfusion (Washida et al., 2010). Colocalisation of macrophages and apoptotic oligodendrocytes has also been reported following focal cerebral ischaemia in rat, suggesting that cytokine release from nearby macrophages may directly lead to oligodendrocyte death (Mabuchi et al., 2000). Additionally administration of the microglial inhibitor minocycline to rats following BCCAO has been reported to significantly ameliorate myelin loss in the corpus callosum as compared to controls (Cho et al., 2006). Taken together these studies indicate that increased inflammation may contribute to white matter disruption following chronic cerebral hypoperfusion.

1.2.4.2 Oxidative stress

The vulnerability of myelinated axons and oligodendrocytes to severe reductions in oxygen and glucose is well documented both *in vitro* (Fern et al., 1998) and *in vivo*

using models of cerebral ischaemia (Pantoni et al., 1996; Dewar et al., 2003). As outlined in Section 1.2.2, cells require glucose and oxygen for the generation of ATP through mitochondrial oxidative phosphorylation. Reactive oxygen and nitrogen species are generated as bi-products of normal oxidative metabolism, and are scavenged by endogenous antioxidant enzymes (Yu, 1994). In conditions of decreased oxygen and glucose, axonal mitochondria are unable to meet the energy requirements to maintain ionic gradients, resulting in an influx of Ca^{2+} which itself causes damage to mitochondria resulting in a substantial release of reactive oxygen species (Brookes et al., 2004; Waxman, 2006). This increased free radical generation results in damaging lipid, protein and nucleic acid oxidation and can perpetuate the release of further free radical species (Finkel and Holbrook, 2000). Furthermore it has also been demonstrated that activated microglia can release nitric oxide and superoxide radicals (Colton and Gilbert, 1987; Block et al., 2007) highlighting a link between inflammation and oxidative stress.

It has been proposed that oligodendrocytes are particularly vulnerable to increased oxidative stress due to their high metabolic rate as compared to other cells (Hyden and Pigon, 1960) which is attributed to the high energy cost of myelin synthesis (McTigue and Tripathi, 2008), however this remains a contentious issue. In addition is has been demonstrated that oligodendrocytes and OPCs have a high iron content and low levels of the endogenous antioxidant enzyme glutathione (Connor and Menzies, 1996; Thorburne and Juurlink, 1996; Merrill and Scolding, 1999). Together these features of oligodendrocytes are thought to render them particularly vulnerable to oxidative stress (reviewed by Merrill and Scolding, 1999).

Studies in mouse have demonstrated increased oxidative stress within cerebral capillaries (Washida et al., 2010) and increased protein oxidation in white matter following 1 month of chronic cerebral hypoperfusion (Miyamoto et al., 2013b). In addition, increased lipid peroxidation and oxygen radicals have been demonstrated as early as 3 days following BCCAO in rat (Watanabe et al., 2006). Furthermore, an association between white matter hyperintensities and biochemical markers of oxidative stress has been reported in a recent human post-mortem study (Back et al., 2011). Critically, it has been demonstrated that oxidative stress results in decreased differentiation of OPCs (Miyamoto et al., 2013b) suggesting that in addition to the damaging effects on oligodendrocytes and myelin, oxidative stress may also impair white matter repair processes.

1.2.5 Mechanisms of white matter repair

A number of studies have identified key receptors and signalling pathways involved in the regulation of OPC proliferation and differentiation, and modulation of inflammation and oxidative stress which may provide the opportunity to modulate white matter disruption following hypoperfusion.

1.2.5.1 Modulation of OPC proliferation and differentiation

The ability of OPCs to proliferate and differentiate in response to white matter damage plays a critical role in white matter repair following injury. Increased NG2 immunoreactivity, indicative of increased numbers of OPCs, has been demonstrated

48 hours following focal cerebral ischaemia with restoration of numbers of mature oligodendrocytes observed following 7 days (McIver et al., 2010). Post-mortem study of aged human brains has shown increased numbers of remyelinating oligodendrocytes and the presence of OPCs in periventricular white matter (Simpson et al., 2007a). In addition, increased numbers of OPCs have been demonstrated in the brains of individuals with vascular dementia (Back et al., 2011). Furthermore microarray analysis of white matter from mice subject to 3 days of cerebral hypoperfusion has revealed significant upregulation of a number of genes involved in cell proliferation (Reimer et al., 2011). Taken together these studies indicate that OPCs may respond to reductions in cerebral blood flow in an attempt to ameliorate white matter damage.

Recent study has identified the G protein-coupled receptor 17 (GPR17) as a key modulator of OPC differentiation in response to injury such as ischaemia, spinal cord injury and cortical stab wound (Ciana et al., 2006; Lecca et al., 2008; Ceruti et al., 2009; Boda et al., 2011). Identified ligands of the GPR17 receptor include members of the cysteinyl leukotriene family of inflammatory mediators and uracil nucleotides which are both released in high concentrations following CNS injury (Ciana et al., 2006). GPR17 is expressed by a subset of OPCs and pre-myelinating oligodendrocytes and increased numbers of GPR17-expressing cells have been reported 24 hours following focal cerebral ischaemia (Lecca et al., 2008). Importantly, receptor activation has been demonstrated to increase OPC differentiation and thus may play an important role in oligodendrogenesis and white matter repair following injury (Boda et al., 2011; Fumagalli et al., 2011). It has been

hypothesised that receptor upregulation may also act as an early sensor of local damage and contribute to local white matter remodelling and repair (Lecca et al., 2008).

A number of other studies have identified additional mechanisms involved in the mediation of OPC proliferation and differentiation. For example, early studies identified that growth factors such as platelet derived growth factor (Raff et al., 1988), neurotrophin-3, and brain derived neurotrophic factor (McTigue et al., 1998) promote OPC proliferation and differentiation. In addition, it has been reported that the neurotransmitters ATP and glutamate inhibit OPC proliferation but stimulate differentiation (Yuan et al., 1998; Agresti et al., 2005; Cavaliere et al., 2012). This is of particular relevance to cerebral ischaemia as the severe and rapid depletion of oxygen and glucose results in decreased energy production and the release of these neurotransmitters in high (i.e. excitotoxic) concentrations (reviewed by Lo et al., 2003). It has recently been demonstrated in slice culture that decreasing glucose concentration dose-dependently influenced numbers of oligodendroglial cells and the extent of myelination, which were restored by application of lactate (Rinholm et al., 2011). It has also been reported that OPC proliferation is enhanced by the inflammatory mediator TNFα (Arnett et al., 2001). In addition, whilst oxidative stress inhibits OPC differentiation, a recent study has demonstrated that treatment with the antioxidant compound edaravone can restore the ability of OPCs to differentiate following chronic cerebral hypoperfusion in mouse (Miyamoto et al., 2013b). Thus OPC proliferation and differentiation can be modulated by several

mechanisms which may influence the ability of these cells to respond to chronic cerebral hypoperfusion.

1.2.5.2 Modulation of inflammation and oxidative stress

As indicated in Section 1.2.4.2, reactive oxygen and nitrogen species are generated as a consequence of normal cellular metabolism but cells are equipped with endogenous antioxidant defence mechanisms to prevent oxidative damage to DNA, proteins and lipids. One key mechanism by which cells mediate antioxidant responses occurs at the transcriptional level through activation of nuclear factor erythroid-derived 2-like 2 (Nrf2 or NFE2L2) transcription factor (Itoh et al., 1997; Kensler et al., 2007). This transcription factor is normally present within the cytoplasm of cells where it is inactive however in the presence of reactive oxygen species it translocates to the nucleus (Itoh et al., 1999) and increases the transcription of a battery of antioxidant and anti-inflammatory genes (reviewed by Kensler et al., 2007). In the CNS, Nrf2 is preferentially expressed by astrocytes (Vargas and Johnson, 2009) but has also been demonstrated in neurons (Ramsey et al., 2007; Linker et al., 2011; Dang et al., 2012), oligodendrocytes (Linker et al., 2011) and microglia (Dang et al., 2012) following injury.

The beneficial effects of Nrf2 activation in the brain have been demonstrated in mouse models of MS and focal cerebral ischaemia. It has been reported that pharmacological activation of Nrf2 with dimethyl fumarate (DMF) in the experimental autoimmune encephalomyelitis (EAE) model of MS results in

decreased numbers of macrophages and increased levels of the anti-inflammatory cytokine interleukin-10 (Schilling et al., 2006). Activation of Nrf2 has also been reported to decrease oxidative stress-mediated cell death, prevent myelin and axonal damage and improve clinical score following EAE (Linker et al., 2011). In support of this Nrf2 knockout mice display widespread myelin disruption and degeneration in addition to pronounced inflammation (Hubbs et al., 2007). Pharmacological activation of Nrf2 in mouse following focal cerebral ischaemia has been shown to significantly decrease hippocampal neuronal death and infarct size and improve neurological score (Son et al., 2010; Zhang et al., 2012). Furthermore, additional studies have demonstrated that brief (15 minute) hypoperfusion induced by middle cerebral artery occlusion in mouse activates Nrf2 target genes (Bell et al., 2011). This experimental paradigm is known to induce neuroprotective ischaemic preconditioning whereby a mild non-lethal stimulus can protect against subsequent ischaemic events (Stenzel-Poore et al., 2003). Thus a mild episode of reduced CBF can induce Nrf2-mediated antioxidant and anti-inflammatory signalling. Taken together these studies suggest that Nrf2 is important in the maintenance of white matter integrity and modulation of inflammation. Importantly these studies demonstrate that Nrf2 is activated in response to reduced CBF and indicate that pharmacological activation of Nrf2 may represent a valid therapeutic target for chronic cerebral hypoperfusion.

1.3 Summary

The presence of a myelin sheath around an axon together with the defined domain structure of myelinated axons is essential for efficient action potential conduction within the brain. Diffuse white matter disruption is observed in ageing brains and it is thought that chronic cerebral hypoperfusion may underlie these age-related white matter alterations and contribute to cognitive impairment. Previous studies using a mouse model of chronic cerebral hypoperfusion have demonstrated that 1 month of hypoperfusion results in diffuse white matter damage, increased microglial number and impaired spatial working memory. The studies described in this thesis sought to build upon these findings to further investigate the effects of chronic cerebral hypoperfusion on white matter structure and function. Specifically, the impact of chronic cerebral hypoperfusion on the domain structure of myelinated axons and on oligodendroglial populations was examined. A further aim was to identify potential mechanisms which may contribute to white matter disruption with cerebral hypoperfusion.

1.4 Thesis hypotheses and aims

It was hypothesised that that chronic cerebral hypoperfusion would disrupt the structural integrity of nodal and paranodal domains of myelinated axons and result in decreased numbers of oligodendrocytes and OPCs. It was additionally hypothesised that treatment with the anti-inflammatory and antioxidant drug DMF would ameliorate structural and functional alterations to white matter following severe hypoperfusion. The specific aims of the study were as follows:

1. To determine the impact of chronic cerebral hypoperfusion on the structural integrity of nodal and paranodal domains of myelinated axons and to identify potential underlying mechanisms. To investigate this, the distribution of nodal, paranodal and internodal proteins was examined in response to differing durations of chronic cerebral hypoperfusion.

2. To determine the effects of chronic cerebral hypoperfusion on oligodendroglial populations. This was assessed using markers of mature oligodendrocytes and OPCs in addition to markers of cellular proliferation. The expression of GPR17 was also assessed to determine whether this receptor was activated in response to chronic cerebral hypoperfusion.

3. To investigate whether modulation of inflammation and oxidative stress could ameliorate alterations to white matter structure and function following chronic cerebral hypoperfusion. To investigate this, the mixed coil model of severe cerebral hypoperfusion was employed and mice were administered the Nrf2-activating drug DMF. The extent of pathology to myelinated axons and oligodendroglial populations was examined to determine whether alleviation of inflammation and oxidative stress could prevent damage to white matter following chronic cerebral hypoperfusion.

Chapter 2

Materials and Methods

2. Materials and Methods

2.1 Animals

Adult male C57Bl/6J mice (25-30g, aged 3-5 months) were purchased from Charles River UK. All animals were housed on a 12 hour light/dark cycle and had access to food and water *ad libitum.* All experiments were conducted under a project and personal licence issued by the UK Home Office under the Animals (Scientific Procedures) Act 1986.

2.2 Surgery

Animals were anaesthetised with isoflurane (5% in oxygen) and the common carotid arteries exposed via a midline cervical incision. Anaesthesia was maintained at 1.5% via a face mask. Cerebral hypoperfusion was induced via bilateral common carotid artery stenosis (Figure 2.1; Shibata et al., 2004). Wire microcoils (0.18 or 0.16 mm internal diameter; Sawane Spring Co, Japan) were twined around the carotid arteries, just below the carotid bifurcation. A 30 minute recovery period was allowed between the application of the first and second coil. Sham animals underwent identical surgical procedures but were not fitted with microcoils. For 0.18 mm microcoil studies (Chapters 3 and 4) mice were fed on a soft food diet and monitored closely following surgery until termination. Animals fitted with a combination of 0.18 and 0.16 mm microcoils (Chapter 5) were fed on a soft food diet and closely monitored

for 7 days following surgery. Any animal showing poor recovery following surgery was culled. All surgeries were carried out by Dr Philip R Holland except for animals administered BrdU (Chapter 4) which were performed by Dr Catherine Gliddon.

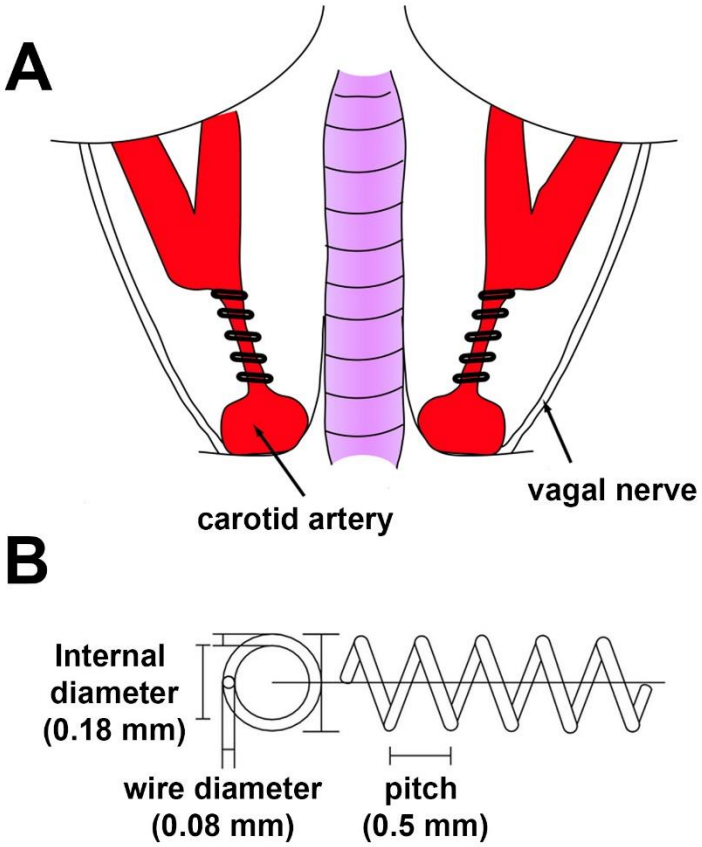

Figure 2.1: Chronic cerebral hypoperfusion is induced by bilateral common carotid artery stenosis. (**A**) Schematic diagram showing microcoil placement around the common carotid arteries just below the carotid bifurcation. (**B**) Schematic diagram showing the structural dimensions of microcoils. Figure adapted from Shibata et al. (2004) and Ihara and Tomimoto (2011).

2.3 Cerebral blood flow measurement

2.3.1 Principle of laser speckle contrast imaging

CBF measurements were carried out using laser speckle flowmetry. This technique exploits the fact that when an object is illuminated with a laser, it generates a speckle image on a connecting camera due to the scattered light travelling in different paths (Dunn et al., 2001). When the illuminated object contains moving components, e.g. red blood cells within a perfused tissue, the resulting speckle images change over time (Dunn et al., 2001). Analysis of the speckle pattern can be analysed to quantify motion within the area examined. This approach can therefore be used to accurately assess CBF in anaesthetised animals.

2.3.2 Acquisition of speckle sequences

Animals were anaesthetised with 5% isoflurane in oxygen for 80 seconds in an anaesthetic chamber. Animals were then transferred to a stereotaxic frame and their heads were fixed into position. Anaesthesia was maintained at 2-2.5% isoflurane via a nose cone. Body temperature was monitored and maintained at 37 °C. Where necessary, additional heat was provided to the mice via a heated mat. An incision was made down the midline of the head to expose the skull, and the skin overlying the skull was reflected. The skull was cleaned using warmed saline (37 ºC) and a cotton bud. Warmed KY gel (37 °C) was spread evenly over the skull to prevent drying out. A moorFLPI2 Speckle Contrast Imager (Moor Instruments, UK) connected to a laptop computer was positioned 20 cm from the brain. Images were

acquired using moorFLIP2 Measurement software (v1) at a resolution of 752 x 580 pixels and a frequency of 25 frames/second. Following stabilisation of CBF readings, a 2 minute CBF recording was carried out. Mice were then placed in an incubator at 28 °C for approximately 5-10 minutes until fully recovered. The mean time under anaesthesia per recording was approximately 10-15 minutes.

2.3.3 Analysis of speckle sequences

Following recording, speckle images were analysed using moorFLPI2 Review software (v4.0; Moor Instruments, UK). Regions of interest were placed on each hemisphere corresponding to approximately +1.7 mm to -4.36 mm from bregma and care was taken to avoid any artefacts on the skull. Mean perfusion measured over the 2 minute stable recording period was averaged across both hemispheres. Data were measured in arbitrary blood perfusion units and are expressed as the percentage change relative to baseline.

2.4 Radial arm maze

Spatial working memory was assessed using an 8-arm radial arm maze (Figure 2.2). The maze consists of an octagonal central platform with 8 arms (47 cm in length and 7 cm in width) leading from the central zone (Stoelting Europe, Ireland). Each arm had plexiglass walls (20 cm high) and a single food well was located at the distal end of each arm. The entrance to each arm from the central zone was blocked by doors which were remotely controlled from a PC using Any-Maze software (Stoelting

Europe, Ireland). A camera was fixed in position directly above the maze to monitor the movement of the animals and visual cues were placed around the room to aid spatial navigation.

The aim of the radial arm maze task is for the mice to retrieve a single food pellet from the end of each arm whilst remembering the arms they have already visited. The number of novel entries (i.e. visiting an arm that has not yet been visited) and the number of revisiting errors (i.e. re-entering an arm that has already been visited) were recorded by a remote operator observing via the PC.

2.4.1 Radial arm maze pre-training

Animals were food deprived for 7 days prior to radial arm maze testing in order to reduce body weight by approximately 10-15%. To maintain this weight reduction, animals were weighed daily and kept on a restricted diet until the end of testing.

To habituate the mice to the maze and to the task, two days of pre-training were carried out. On the first pre-training day, mice were placed in the central zone for 5 minutes and allowed to freely explore and consume food pellets that were scattered around the maze. On the second pre-training day, mice were placed in the central zone and food pellets were placed at the end of each arm. The door to one arm at a time was opened remotely using the PC and once the mice had entered the arm and

eaten a food pellet they were placed back in the central zone and the next door was opened. This was repeated until the mice had consumed a food pellet in each arm.

2.4.2 Radial arm maze testing

Radial arm maze testing was carried out for 16 consecutive days, with each animal undertaking one trial per day. The arms were baited with a single food pellet and at the start of the trial mice were placed in the central platform with all doors opened to allow them to make an arm choice. Following entry into the arm, the other 7 doors automatically closed. Once the animal left the arm it was held in the central zone for 5 seconds before all doors were once again opened allowing the animal to make another arm choice. The trial was completed when all 8 food pellets had been retrieved from each arm or a 25 minute period had elapsed. The number of novel arm entries within the first eight visits and the number of revisiting errors were recorded for each trial.

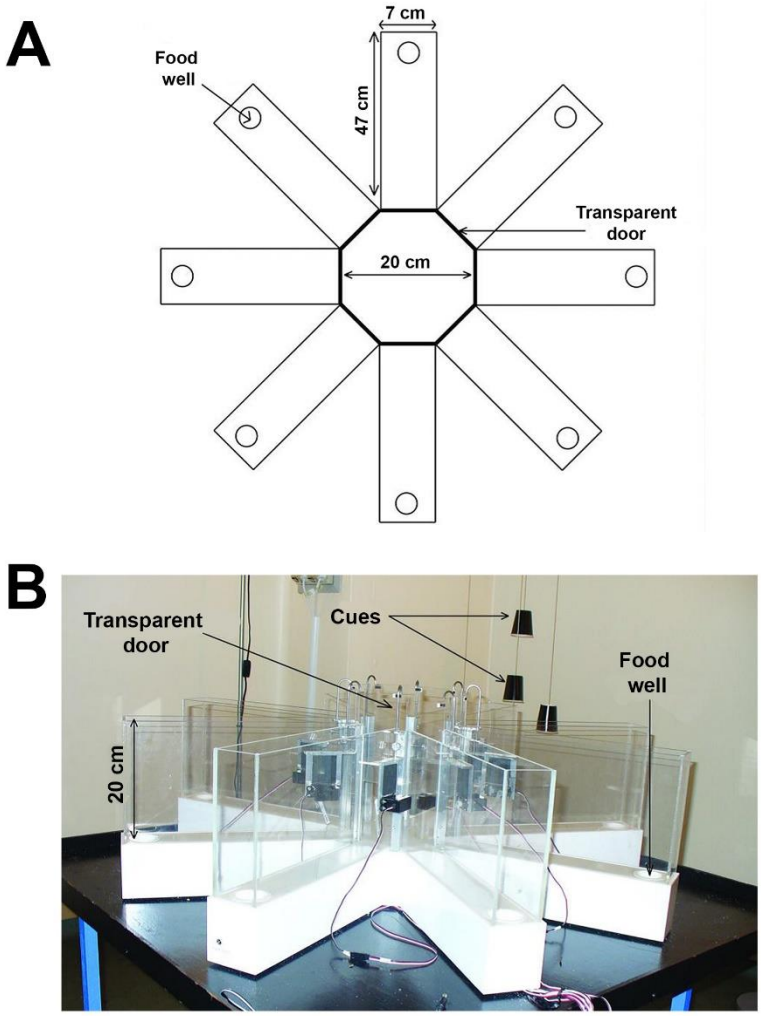

Figure 2.2 Assessment of spatial working memory using the radial arm maze. (**A**) Schematic diagram showing a top-down view of the radial arm maze including spatial dimensions. (**B**) Photograph showing the radial arm maze and the extra-maze cues. Image taken and adapted from Dr Aisling Spain, PhD thesis (2010).

2.5 Electrophysiology

All electrophysiology experiments and data analysis were carried out by Dr Philip R Holland.

2.5.1 Tissue preparation and slice cutting

Mice were terminated by cervical dislocation followed immediately by decapitation. Brains were then rapidly dissected, placed in a cell strainer and submerged in ice-cold oxygenated artificial cerebrospinal fluid (aCSF) (containing in mM: sucrose, 189; D-glucose, 10; $NaHCO_3$, 26; KCl, 3; $MgCl_2$, 5; $CaCl_2$, 0.1; NaH_2PO_4, 1.25) for 2-3 minutes. Brains were then removed from the sucrose-aCSF solution, placed on an ice-cold petri dish and the cerebellum removed using a blade. The brain was then affixed to a metal vibratome plate and placed in a bath of oxygenated ice-cold sucrose-aCSF. A single 400 µm coronal slice approximately -1.2 – -1.7 mm from bregma was cut using a vibratome (Zeiss, Germany). Slices were then transferred to a warmed incubation chamber (32-35 °C) containing oxygenated aCSF (containing in mM: D-Glucose, 10; $NaHCO_3$, 26; KCl, 5; $CaCl_2$, 2; NaCl, 124; NaH_2PO_4, 1.25; $MgSO_4$, 1.3). The incubation chamber was then allowed to return to room temperature for at least 1 hour prior to slice recording.

2.5.2 Slice recording

Slices were then transferred to the slice chamber and super-perfused with oxygenated aCSF (2-3 ml/minute) at room temperature. Recording electrodes were comprised of borosilicate glass capillaries filled with aCSF and a resistance of 1-5 MΩ. These were connected to Ag/AgCl wires and lowered into the appropriate location within the corpus callosum. A stimulating electrode was connected to a stimulus isolation unit (NL200 Digitimer) and lowered into the corpus callosum 2.5 mm from the recording electrode using a computer controlled micromanipulator (patchstar micromanuipulator, Scientifica). Constant current square wave pulses were delivered at 0.2 Hz for 8 sweeps and the average response of the final 4 sweeps were used for analysis. The data was digitised at 200 kHz, amplified at x100, low-pass filtered at 5 kHz and recorded using an Axopatch 200B and a PC running Clampex (v10.3) software (Molecular Devices LLC, USA). Analysis was conducted offline using Clampit v10.3.

2.5.3 Calculation of conduction velocity

Stimulating and recording electrodes were kept at a distance of 2.5 mm apart. The peak latency of the N1 and N2 components of the CAP were measured and conduction velocity calculated by dividing the distance (2.5 mm) by the latency of the response.

2.6 BrdU labelling

To determine the extent of proliferation following cerebral hypoperfusion mice were administered 5-bromo-2'-deoxyuridine (BrdU; Fluka, UK). BrdU was administered by intraperitoneal injection (35 mg/kg body weight, in phosphate buffered saline (PBS) twice daily for the first 3 days following surgery.

2.7 Administration of dimethyl fumarate

Dimethyl fumarate (DMF: $C_6H_8O_4$; Sigma, UK) was administered twice daily (at 8 am and 5pm) by oral gavage at 100 mg/kg body weight in 0.8% hydroxypropyl methylcellulose (hypromellose; Sigma, UK) vehicle as previously described (Scannevin et al., 2012). Control animals received vehicle only. Administration of DMF or vehicle began 24 hour prior to surgery.

2.8 Perfusion fixation and tissue processing for immunohistochemistry

2.8.1 Transcardial perfusion fixation

Animals were deeply anaesthetised using 5% isoflurane in oxygen. A midline incision was made and the diaphragm cut to expose the heart. A needle was inserted into the left ventricle and held in place using surgical clamp. Mice were perfused at a rate of 2 ml/min with 20 ml of 0.9% heparinised saline. A small incision was made in

the right atrium to allow blood to flow out. Mice were then perfused with 20 ml of 4% paraformaldehyde (PFA) in 0.1M phosphate buffer (PB, pH7.4)[1].

2.8.2 Tissue processing for vibratome sections

Following perfusion, the heads were removed and post-fixed in 4% PFA for 2 hours at room temperature. The brains were then removed from the skull and post-fixed in 4% PFA overnight at 4 °C. Brains were then transferred to PB and stored overnight at 4 °C. The brains were cut along the longitudinal fissure into hemi-brains and free-floating 50 µm sagittal sections were cut using a vibrating blade microtome (Zeiss, Germany.) Sections were stored in cryoprotective medium (30% glycerol and 30% ethylene glycol in PB) at -20 °C until required.

2.8.3 Tissue processing for cryostat sections

Following perfusion, the heads were removed and post-fixed in 4% PFA for 1 hour at room temperature. The brains were then carefully removed from the skull and post-fixed in 4% PFA for 24 hours at 4 °C. Brains were then transferred to 30% sucrose in phosphate buffered saline (PBS) and left for 48-72 hours until the brains sank to the

[1] As hypoperfused animals have microcoils around both common carotid arteries, there is a possibility that insufficient perfusion fixation may generate artefacts and potentially influence pathology. Studies within the group have shown that overnight post-fixation in 4% PFA significantly improves the quality of fixation and tissue preservation. It has been demonstrated that this post-fixation step ensures adequate fixation even in brains perfused only with saline. Furthermore, assessment of nodal length and nodal gap has shown similar differences between sham and hypoperfused mice in brains perfused with either saline or PFA followed by overnight post-fixation. Thus the presence of the overnight fixation step for all studies described in this thesis should improve fixation and eliminate potential perfusion artefacts between hypoperfused and sham mice.

bottom of the solution. Brains were then frozen in isopentane for 2 minutes at -42 °C and were stored at -20 °C. Brains were cut into 30 µm coronal sections using a cryostat (Bright Instruments, UK). Immediately following cutting sections were transferred into PB, mounted directly onto slides and air-dried overnight. Slide-mounted sections were stored at -20 ºC until required

2.9 Histology

2.9.1 FluoroMyelin staining

FluoroMyelin staining was used to assess myelin integrity following chronic cerebral hypoperfusion. Free-floating vibratome sections were given three 15 minute washes in PBS and two 15 minute washes in tris buffer (TB) to remove traces of cryoprotective medium. Sections were then mounted onto SuperFrost glass slides and left to air dry. Following rehydration in PBS, sections were incubated for one hour in FluoroMyelin at 1:200 in PBS. Sections were then given three 15 minute washes in PBS before being coverslipped using Vectashield Hardset mounting medium.

2.10 Immunohistochemistry

This technique is used to visualise proteins of interest and is routinely used to investigate tissue structure. It exploits the ability of antibodies to bind strongly to foreign proteins allowing their visualisation using microscopy. For all immunohistochemistry experiments the concentration of antibody was optimised by testing a range of dilutions. Negative controls, in which the addition of primary antibody was omitted, were run alongside experimental sections to determine the extent of non-specific staining.

2.10.1 Vibratome sections

Free-floating vibratome sections were given three 15 minute washes in PBS to remove traces of cryoprotective medium. Sections were then washed twice for 15 minutes in PBS containing 0.1% TritonX100 (PBS-Tx) prior to antigen retrieval (if required; see Section 2.10.3) Sections were then incubated for 1 hour at room temperature in 10% normal serum (optimised with or without 0.5-1% bovine serum albumin; BSA) to block non-specific binding. The blocking solution was then removed and sections were incubated in primary antibody (diluted in blocking solution) overnight at 4 °C. The following day sections were given three 15 minute washes in PBS and incubated in secondary antibody (in PBS) either overnight at 4°C or for 1 hour at room temperature. Sections were then given three 15 minute washes in PBS followed by two 10 minute washes in TB before being mounted onto slides. Sections were coverslipped using Vectashield HardSet mouning medium containing the nuclear stain 4',6-diamidino-2-phenylindole (DAPI). Primary and secondary antibodies are listed in Tables 2.1 and 2.2 respectively.

2.10.2 Cryostat sections

Cryostat sections were dehydrated through an increasing alcohol series as follows: 2 minutes in 70% ethanol, 2 minutes in 90% ethanol, and 5 minutes and 10 minutes in 100% ethanol. Sections were then immersed in xylene for 10 minutes before being rehydrated through a decreasing alcohol series as follows: 10 minutes and 5 minutes in 100% ethanol, 2 minutes in 90% ethanol and 2 minutes in 70% ethanol before being rinsed in running tap water for 2 minutes. Sections were then equilibrated in

PBS for 5 minutes before antigen retrieval (if required; see Section 2.10.3). Sections were then blocked using 20% normal serum (optimised with or without 1% BSA) for 2 hours at room temperature. Primary antibodies were made up in blocking solution and sections were incubated in primary antibody at 4 ºC overnight. The following day sections were given two 10 minute washes in PBS before incubation with secondary antibody (diluted in PBS) for 2 hours at room temperature. Following secondary antibody incubation, sections were given two 15 minute washes in PBS followed by a 10 minute wash in TB prior to air drying. Coverslips were mounted using Vectashield HardSet mounting medium with or without DAPI.

2.10.3 Antigen retrieval

Antigen retrieval was required to ensure optimal labelling with a subset of antibodies. Antigen retrieval was carried out using 10 mM citric acid (pH6), 2M hydrocholoric acid (HCl) or 1 mM tetrasodium ethylenediaminetetraacetic acid (EDTA; pH8) as shown in Table 2.3. Free-floating sections were placed in 24-well plates containing retrieval solution and placed in a water bath (Grant Instruments, UK). Slide-mounted sections were immersed in retrieval solution inside a heatproof container and placed inside a pressure cooker (A. Menarini Diagnostics Ltd, UK). Following antigen retrieval, sections were rinsed in PBS prior to blocking. Following HCl-mediated antigen retrieval, sections were rinsed in 0.1M sodium borate buffer ($Na_2B_4O_7$).

Table 2.1: Primary antibodies used in immunohistochemistry experiments

Antibody	Label	Species raised in	Clone	Source	Dilution
Ankyrin G	Ankyrin G	Rabbit	Polyclonal	Santa Cruz	1:50
APP	Amyloid precursor protein	Mouse	22C11	Millipore	1:200
BrdU	BrdU incorporating cells	Rat	BU1/75 (1CR1)	Abcam	1:200
Caspr	Caspr	Mouse	K65/35	Neuromab	1:50
CC1 (APC)	Mature oligodendrocytes	Mouse	Ab-7	Calbiochem	1:20
GFAP	$GFAP^+$ astrocytes	Rabbit	Polyclonal	Dako	1:1000
GPR17	GPR17 receptor	Rabbit	Polyclonal	Cayman Chemical	1:200
Iba1	$Iba1^+$ microglia	Goat	Polyclonal	Abcam	1:100
MAG	Myelin associated glycoprotein	Goat	Polyclonal	Santa Cruz	1:100
MBP	Myelin basic protein	Rat	12	Millipore	1:100
$Na_v1.6$	$Na_v1.6$ channels	Rabbit	Polyclonal	Millipore	1:100
NG2	$NG2^+$ OPCs	Rabbit	Polyclonal	Millipore	1:100
Olig2	Oligodendrocyte lineage cells	Mouse	211F1.1	Abcam	1:100
Olig2	Oligodendrocyte lineage cells	Rabbit	Polyclonal	Millipore	1:500
PCNA	$PCNA^+$ proliferating cells	Mouse	PC10	Abcam	1:500
PDGFRα	$PDGFR\alpha^+$ OPCs	Rat	APA5	BD Pharmingen	1:100
PDGFRβ	$PDGFR\beta^+$ pericytes	Goat	Polyclonal	R and D Systems	1:100
Porin (VDAC)	Mitochondrial inner membrane voltage-gated anion channels	Mouse	16G9E6BC4	Abcam	1:400

Table 2.2 Secondary antibodies used in immunohistochemistry experiments

Antibody	Species raised in	Source	Dilution
Anti-goat IgG Alexa Fluor 546	Donkey	Invitrogen	1:500
Anti-mouse IgG Alexa Fluor 488	Goat	Invitrogen	1:500
Anti-mouse IgG Alexa Fluor 488	Donkey	Jackson ImmunoResearch	1:200
Anti-mouse IgG1 Alexa Fluor 647	Goat	Invitrogen	1:500
Anti-mouse IgG2b Alexa Fluor 488	Goat	Invitrogen	1:500
Anti-mouse IgG DyLight 488	Donkey	Jackson ImmunoResearch	1:200
Anti-rabbit IgG Cy3	Donkey	Jackson ImmunoResearch	1:100
Anti-rabbit IgG Alexa Fluor 546	Goat	Invitrogen	1:500
Anti-rat IgG Alexa Fluor 647	Donkey	Jackson ImmunoResearch	1:200
Anti-rat IgG Cy3	Donkey	Jackson ImmunoResearch	1:100

Table 2.3 Antigen retrieval approaches used in immunohistochemistry experiments

Retrieval solution	Tissue	Temperature and duration	Appliance	Antibodies
10 mM citric acid	Slide-mounted vibratome sections	100 °C for 10 minutes	Antigen retrieval unit	MAG
10 mM citric acid	Free-floating vibratome sections	85 °C for 30 minutes	Water bath	PCNA
2M HCl	Free-floating vibratome sections	37 °C for 30 minutes	Water bath	BrdU
1 mM EDTA	Slide-mounted vibratome sections	100 °C for 10 minutes	Antigen retrieval unit	Porin
10 mM citric acid	Slide-mounted cryostat sections	100 °C for 10 minutes	Antigen retrieval unit	MAG, APP, CC1

2.11 Microscopy

2.11.1 Confocal laser scanning microscopy

Immunolabelled sections were imaged using confocal laser scanning microscopy (Axioskop LSM 510 or LSM710, Zeiss, Germany). Images were acquired using either 20x, 40x or 63x objectives at a 1024 x 1024 pixel resolution. For images obtained at 20x (numerical aperture 0.75) the field of view represented an area of 460 x 460 µm. For images acquired at 40x (numerical aperture 1.3) the field of view represented 212.5 x 212.5 µm. For images acquired using a 63x objective (numerical aperture 1.4), the correct Nyquist settings (3.1x zoom and 0.13 µm z-step) were used to allow image deconvolution. The corresponding field of view represented 43.5 x 43.5 µm. All images were acquired by the author who was blinded to surgical condition.

2.11.1.1 Image deconvolution

Images acquired using a 63x objective underwent image deconvolution using Huygens Professional deconvolution software (Scientific Volume Imaging, The Netherlands; v3.6).

2.11.2 Fluorescent microscopy

Images were acquired at 20x magnification using a Zeiss AX10 fluorescent microscope (Zeiss, Germany). Axiovision software (v4.8.1) was used to capture the

images at a resolution of 1388 x 1040 pixels. All images were acquired using constant exposure settings by the author who was blinded to surgical condition.

2.11.3 Regions of interest

Regions of interest for analysis of immunohistochemistry studies are shown in Figure 2.3.

2.12 Image analysis

Image analysis was carried out using ImageJ software (National Institutes of Health, USA; v1.42q).

2.12.1 Assessment of fluorescent intensity

For assessment of labelling intensity, all sections were imaged using identical gain and offset settings on the confocal microscope which ensured a common threshold was set across all images. To assess FluoroMyelin and MBP staining intensity, the corpus callosum was manually outlined and mean gray value was measured using ImageJ. For GPR17 labelling intensity, individual $GPR17^{+}$ cells were manually outlined and mean gray value was measured. All intensity measurements were carried out in duplicate and values averaged.

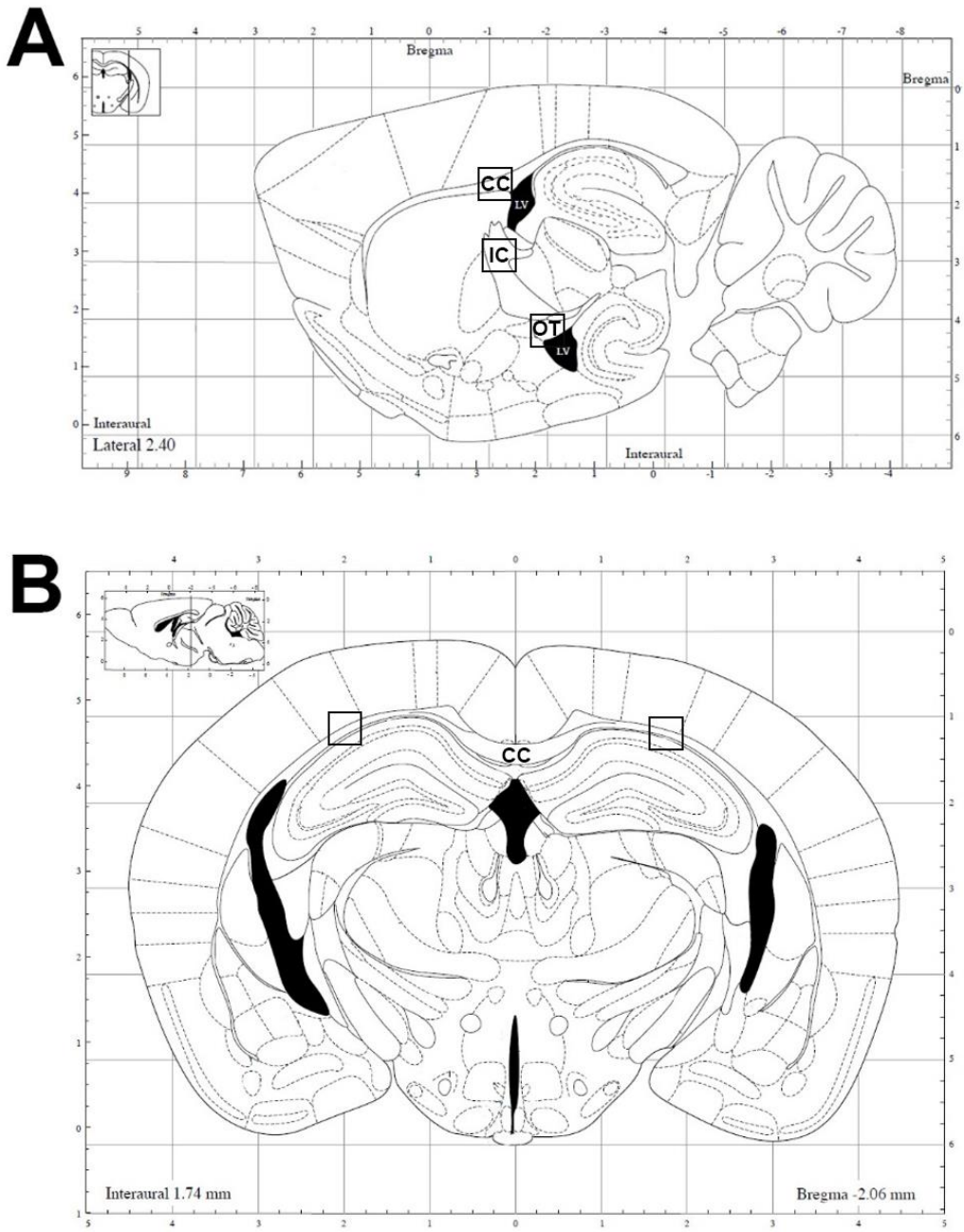

Figure 2.3: Regions of interest for immunohistochemistry studies. (**A**) For immunohistochemistry experiments described in Chapter 3, sagittal sections were used and images taken in the corpus callosum (CC), internal capsule (IC) and optic tract (OT). For studies outlined in Chapter 4 the corpus callosum was imaged above the lateral ventricle (LV) as indicated. (**B**) For immunohistochemistry studies described in Chapter 5, coronal sections were used and the corpus callosum imaged on each hemisphere as indicated. Images taken and adapted from Paxinos and Franklin (2001).

2.12.2 Assessment of density of staining

To assess the density (i.e. percentage area) of MAG, APP and MBP labelling, images were acquired using identical gain and offset settings on the confocal microscope, ensuring a common threshold. Images of MBP and MAG were subject to background subtraction (mean grey value of background + 3x standard deviation). A common threshold was set for images of APP labelling to ensure that APP^+ oligodendrocytes, microglia and astrocytes were excluded and that only APP^+ axonal bulbs were detected. For all density measurements, the corpus callosum was manually outlined and the percentage area of positive staining measured. All density measurements were carried out in duplicate across two days and values averaged.

2.12.3 Nodal domain length and nodal gap measurements

Nodal domain length and nodal gap were measured in deconvolved images using ImageJ. To eliminate sampling bias, the first 40 nodes which appeared whilst scrolling through the stack were selected for length measurement. Nodes were included on the basis of positive $Na_v1.6$ or Ankyrin G labelling delineated either side by positive Caspr staining of paranodal domains. For nodal gap measurements the distance between a pair of $Caspr^+$ paranodes was measured. Images were magnified 3x to ensure accurate measurement and lengths were manually measured using the line tool feature of ImageJ.

2.12.4 Assessment of porin localisation to nodal and paranodal domains

To assess porin localisation at nodal and paranodal domains following 6 weeks and 3 months of cerebral hypoperfusion, the 40 nodes that underwent $Na_v1.6$ length and nodal gap measurements were counted based on the presence of porin reactivity within nodes and paranodes.

2.12.5 Stereological counting

Nodes of Ranvier were manually identified on the basis of positive $Na_v1.6$ immunoreactivity and numbers of nodes were counted using the ImageJ Cell Counter plugin in a 43.5 x 43.5 x 5 µm image stack. To prevent over-counting, any nodes crossing the left and top boundaries of the image were excluded, whilst those crossing the right and lower boundaries of the image were included in the analysis.

For stereological cell counting, cells were identified based on expression of the immunolabel(s) of interest co-localised with the nuclear stain DAPI. Cells were manually identified and counted using the ImageJ Cell Counter plugin. The corpus callosum was manually outlined and cells crossing the left and top sides were included, but any cells crossing the right or bottom boundaries were not counted. Images from the top of the Z-stack were excluded from analysis whilst counts from the bottom image from the stack were included. Cell counts are expressed as the as the number of cells/0.01 mm^3.

2.13 Perfusion fixation and tissue processing for electron microscopy

2.13.1 Transcardial perfusion fixation

Animals were transcardially perfused with 20 ml of 0.9% heparinised saline followed by 20 ml of 5% glutaraldehyde and 4% paraformaldehyde in 0.1M PB. Perfusion was carried out manually and rapidly without the use of a perfusion pump. Following perfusion, the brains and optic nerves were removed and postfixed in the same fixative. Following 24 hours of post-fixation, a 1 mm thick section of brain (approximately 0 to -1 mm from bregma) was cut using a mouse brain matrix and the corpus callosum was manually dissected using a scalpel and a dissecting microscope. Corpus callosum and optic nerve samples were stored in fixative until processed.

2.13.2 Tissue processing

Optic nerve and corpus callosum samples were transferred into 3% glutaraldehyde in 0.1M sodium cacodylate buffer (pH 7.3) for 2 hours and then washed 3 times in the same buffer. Samples were then post-fixed in 1% osmium tetroxide in 0.1M sodium cacodylate. Following dehydration, sections were embedded in araldite resin. For corpus callosum samples, the corpus callosum was cut along the midline and 60 nm ultrathin transverse sections of corpus callosum were cut. Optic nerve sections were cut into 60 nm ultrathin longitudinal sections. All sections were cut using a Reichert OMU4 ultramicrotome (Leica Microsystems (UK) Ltd, UK) and stained in uranyl acetate and lead citrate. Tissue processing and cutting was carried out by Stephen Mitchell (University of Edinburgh, School of Biological Sciences).

2.14 Acquisition and analysis of electron micrographs

2.14.1 Acquisition of electron micrographs

Ultrathin sections were viewed using a Philips CM120 transmission electron microscope (FEI UK Ltd, UK) and images acquired using a Gatan CCD camera (Gatan, UK). Images of cross-sectional myelinated fibres of the corpus callosum were used to measure g-ratio and were acquired at 3500x. Longitudinal optic nerve sections were used to visualise paranodal domains and were imaged at 28000x. All images were acquired by the author who was blind to surgical condition.

2.14.2 G-ratio measurements

To quantify changes in myelin sheath thickness, a lined grid of 0.95 x 0.95 μm^2 was overlaid onto each image using Image J software (v1.42q). To eliminate selection bias, fibres were selected for analysis if their myelin sheath was intersected by a grid line. Using the freehand tool, the perimeters of each fibre and axon were manually traced and whole fibre area and axonal area measured. These values were used to calculate corresponding fibre and axonal diameters. To calculate g-ratio, axonal diameter was divided by whole fibre diameter. The mean number of fibres analysed were not significantly different between groups following either 3 days (sham- 355, hypoperfused- 300; $p = 0.427$) or 1 month (sham- 214, hypoperfused- 236 $p = 0.469$). Animal numbers for the 3 day cohort were n = 5 sham, 6 hypoperfused. Animal numbers for the 1 month cohort were n = 7 sham, 7 hypoperfused.

2.14.3 Assessment of paranodal disruption

The presence or absence of paranodal septate-like junctions and the morphology or paranodal myelin loops (normal or misfolded) were assessed by the author and Dr Michell Reimer who were blinded to surgical condition. Twelve individual paranodes were analysed per animal. Animal numbers were n = 3 sham, 3 hypoperfused.

2.15 Statistical analysis

Statistical analysis was carried out using GraphPad Prism 5 (GraphPad Software Inc, USA) or SPSS (v22, IBM Ltd, USA) software packages. Data are presented as the mean ± standard error of the mean. A probability (p) value of < 0.05 was considered to be statistically significant.

2.15.1 Cerebral blood flow data

CBF data in Chapter 4 were analysed using Student's *t*-test. CBF data in Chapter 5 were analysed using using a 2-way ANOVA. Student's *t*-test with Bonferroni correction for multiple comparisons was used post-hoc.

2.15.2 Radial arm maze

Radial arm maze data were analysed using a 2-way repeated measures ANOVA. Student's *t*-test with Bonferroni correction for multiple comparisons was used post-hoc.

2.15.3 Electrophysiology data

The peak latency of the action potential was measured for myelinated and unmyelinated fibres and calculated per animal. Student's *t*-test was used to compare groups.

2.15.4 Domain length and nodal gap measurements

The lengths of Nav1.6, Caspr and Ankyrin G domains and the nodal gap were plotted as cumulative frequency (%) and were analysed using a two-sample Kolgomorov-Smirnov test.

2.15.5 Stereological cell counts, intensity and density of staining

Analysis of cell counts, intensity of staining and density of staining described in Chapters 3 and 4 was carried out using Students *t*-test or Mann-Whitney U-test depending on parametric or non-parametric distribution. Analysis of cell counts and intensity of staining described in Chapter 5 was performed using a 2-way ANOVA

followed by Student's *t*-test with Bonferroni correction for multiple comparisons. A p value of < 0.01 was considered statistically significant.

2.15.6 Survival analysis

Analysis of survival in Chapter 5 was performed using Kaplan-Meier curves and corresponding data analysed using a log-rank (Mantel-Cox) test.

Chapter 3

The impact of chronic cerebral hypoperfusion on nodal and paranodal domains of myelinated axons

3.1 Introduction

The structural integrity of myelinated axons of the white matter is essential for efficient action potential conduction and normal cognitive function. Disruption to white matter and cognitive decline are commonly observed with ageing (Breteler et al., 1994a; Bartzokis et al., 2004) and it is thought that chronic cerebral hypoperfusion may underlie these structural and functional alterations (DeCarli et al., 1995; O'Sullivan et al., 2002; Holland et al., 2008; Appelman et al., 2010) however the underlying mechanisms are unknown.

Myelinated axons are comprised of nodal, paranodal, juxtaparanodal and internodal domains which are characterised by unique protein architectures. The high density clustering of $Na_v1.6$ channels at nodes of Ranvier is essential for saltatory conduction and is mediated by interactions with other nodal proteins and by the neighbouring paranodal septate-like junctions which act as physical barriers to prevent diffusion of $Na_v1.6$ channels away from the nodes. Disruption to proteins located at nodal or paranodal domains may therefore have important consequences for action potential conduction along myelinated axons. Importantly, paranodal disruption has been demonstrated to occur in ageing mice which show loss of paranodal septate-like junctions, 'piling' of paranodal myelin loops and diffusion of Caspr away from paranodal domains (Shepherd et al., 2012). Similarly, in aged primates, altered juxtaparanodal Kv localisation has been reported which is indicative of paranodal

disruption (Hinman et al., 2006). Furthermore, paranodal disruption and associated disruption to the localisation of $Na_v1.6$ channels at nodes of Ranvier has been reported in human MS tissue (Coman et al., 2006) and in mice subject to EAE (Howell et al., 2010). Taken together these studies indicate that nodal and paranodal domains of myelinated axons are vulnerable to injury and ageing, which may have important consequences for downstream cognitive function.

The mechanisms underlying nodal and paranodal disruption in ageing and in disease are unclear however a strong association between microglial activation and paranodal disruption has been reported in human post-mortem cases of MS and Parkinson's disease and in mice subject to EAE (Howell et al., 2010). Additional studies using Caspr knockout mice (Einheber et al., 2006; Garcia-Fresco et al., 2006) or mice expressing mutant Caspr (Sun et al., 2009) have demonstrated abnormal accumulation of mitochondria within swellings along myelinated axons suggesting that paranodal disruption results in impaired axonal transport of mitochondria. Given the importance of mitochondria in generating energy for myelinated axons, any disruption to mitochondrial transport may influence white matter integrity.

Previous studies using the mouse model of hypoperfusion have reported diffuse white matter pathology using histological (Shibata et al., 2004), immunohistochemical (Coltman et al., 2011) and MRI (Holland et al., 2011) approaches however a robust assessment of the effects of cerebral hypoperfusion on the domain structure of myelinated axons has not been undertaken. As intact nodal

and paranodal domains are required for action potential conduction along myelinated axons, alterations to these regions may contribute to the observed working memory deficit in these animals.

3.1.1 Study hypothesis and aims

It was hypothesised that chronic cerebral hypoperfusion would result in disruption to nodal and paranodal domains of myelinated axons. This was tested using immunohistochemistry against key proteins found at nodal, paranodal and internodal domains of myelinated axons and electron microscopy was used to examine paranodal integrity. A further aim was to investigate whether microglial activation may contribute to nodal and paranodal disruption and whether mitochondrial distribution along myelinated axons was altered following chronic cerebral hypoperfusion.

3.2 Methods

3.2.1 Animals and surgery

Male C57Bl/6J mice (aged 3-4 months old, 25-30g) underwent bilateral common carotid artery stenosis using 0.18 mm microcoils or sham surgery as previously described in Section 2.2. Group sizes for immunohistochemistry studies are listed in Table 3.1.

Additional cohorts of animals were used for electron microscopic analysis of paranodal integrity (n = 3 sham, 3 hypoperfused), measurement of cerebral blood flow (n = 8 sham, 6 hypoperfused) and assessment of spatial working memory (n = 12 sham, 12 hypoperfused) following hypoperfusion.

Table 3.1: Cohort sizes for immunohistochemistry studies

Cohort	Duration of hypoperfusion	Sham *n*	Hypoperfusion *n*
1	3 days	12	13
2a	1 month	9	9
2b	1 month	10	11
3	6 weeks	12	11
4	3 months	8	7

3.2.2 Radial arm maze

Radial arm maze assessment of spatial working memory was carried out as described in Section 2.4. Testing lasted for 16 consecutive days and began 3 weeks following surgery.

3.2.3 Perfusion/tissue processing for immunohistochemistry

At 3 days, 1 month, 6 weeks or 3 months post-surgery, mice were deeply anaesthetised with 5% isoflurane and transcardially perfused as described in Section 2.8.1. Following perfusion, the brains were processed and sagittal sections cut using a vibratome as described in Section 2.8.2.

3.2.4 FluoroMyelin labelling

FluoroMyelin labelling was carried out as described in Section 2.9.1

3.2.5 Immunohistochemistry

Immunohistochemistry was carried out as described in Section 2.10. Anti-MAG antibody was used to assess internodal axon-glial integrity and anti-Caspr, $Na_v1.6$, Ankyrin G antibodies were used to assess alterations in nodal and paranodal domains. Anti-Iba1 and anti-porin antibodies were used to assess numbers of microglia and mitochondrial localisation respectively.

3.2.6 Confocal laser scanning microscopy and image analysis

Immunolabelled 50 µm sections were imaged using confocal laser scanning microscopy as described in Section 2.11.1. Images were acquired in the corpus callosum, internal capsule and optic tract as shown in Figure 2.3A and were analysed as described in Section 2.11.2.

3.2.7 Perfusion/tissue processing for electron microscopy

Animals were transcardially perfused with 5% glutaraldehyde/4% paraformaldehyde 1 month after the onset of cerebral hypoperfusion as described in Section 2.13.1. Optic nerve samples were processed for electron microscopy as described in Section 2.13.2. Images were acquired at a magnification of 28000x.

3.2.8 Statistical analysis

$Na_v1.6$, Caspr, Ankyrin G and nodal gap measurements are plotted as cumulative frequency (%) and were analysed using a two-sample Kolgomorov-Smirnov test. Radial arm maze data was analysed using a 2-way repeated measures ANOVA. Student's *t*-test with Bonferroni correction for multiple comparisons was used post-hoc. All other measures were analysed using student's *t*-test or Mann-Whitney U-test depending on parametric or non-parametric distribution. A probability p value < 0.05 was considered to be statistically significant.

3.3 Results

3.3.1 Abnormal localisation of $Na_v1.6$ channels at nodes of Ranvier following chronic cerebral hypoperfusion

To test the hypothesis that chronic cerebral hypoperfusion would result in disruption to nodes of Ranvier, sections were stained for $Na_v1.6$ and the domain length of $Na_v1.6$ channel clusters was measured in the corpus callosum (Figure 3.1A). This revealed a significant increase in $Na_v1.6$ domain length following 3 days ($D = 0.1781$; $p < 0.0001$) and 1 month ($D = 0.2304$, $p < 0.0001$) of hypoperfusion as compared to shams (Figure 3.1B). This increase in $Na_v1.6$ domain length was similarly observed in the internal capsule and optic tract (Appendix A1.1). To determine the effects of longer term hypoperfusion, $Na_v1.6$ domain length was measured following 6 weeks and 3 months of chronic cerebral hypoperfusion (Figure 3.1C). This revealed that following 6 weeks of cerebral hypoperfusion, $Na_v1.6$ domain length was not significantly different between sham and hypoperfused animals ($D = 0.0854$; $p = 0.066$; Figure 3.1D). However, a significant decrease in $Na_v1.6$ domain length was observed in hypoperfused mice compared to shams ($D = 0.1446$; $p = 0.003$; Figure 3.1E). Taken together these results demonstrate dynamic alterations in $Na_v1.6$ localisation in response to chronic cerebral hypoperfusion. Data plotted as relative frequency are shown in Appendix A1.2.

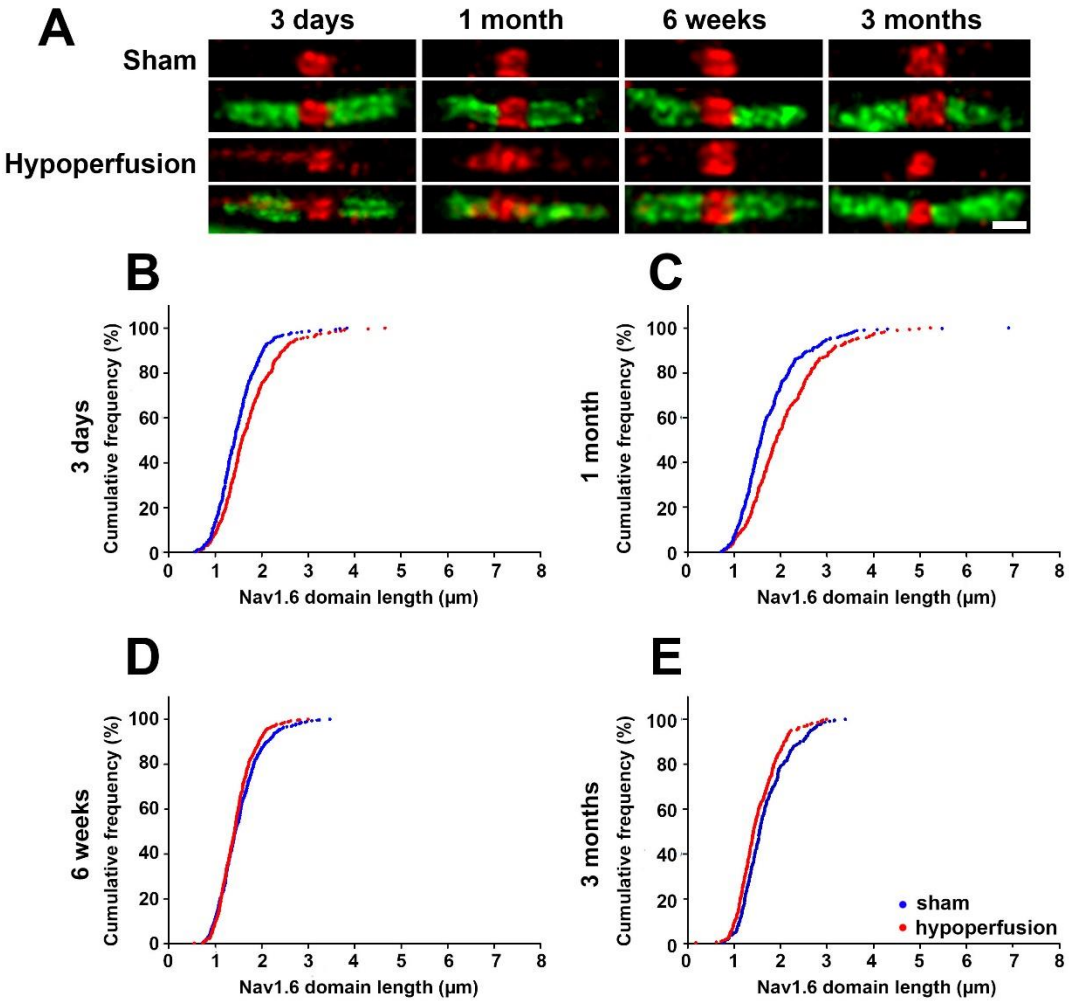

Figure 3.1: Dynamic changes in $Na_v1.6$ domain length with chronic cerebral hypoperfusion. (**A**) Representative confocal images showing $Na_v1.6$ labelled nodes of Ranvier (red) flanked either side by Caspr labelled paranodes (green) following 3 days, 1 month, 6 weeks and 3 months of chronic cerebral hypoperfusion. Scale bar = 1 µm. (**B**) $Na_v1.6$ domain length was significantly increased following 3 days ($p < 0.0001$) and (**C**) 1 month ($p < 0.0001$) of chronic cerebral hypoperfusion as compared to shams. (**D**) $Na_v1.6$ domain length was not significantly different between sham and hypoperfused mice following 6 weeks of hypoperfusion ($p = 0.0854$). (**E**) Following 3 months of hypoperfusion, $Na_v1.6$ domain length was significantly decreased as compared to shams ($p = 0.003$). $Na_v1.6$ domain length measurements following 3 days and 1 month of hypoperfusion were conducted by Dr Michell Reimer.

3.3.2 Numbers of nodes are unaltered following chronic cerebral hypoperfusion

To investigate whether chronic cerebral hypoperfusion altered numbers of nodes of Ranvier, numbers of $Na_v1.6^+$ nodes were counted in sections from 3 day, 1 month, 6 weeks and 3 month cohorts (Figure 3.2). This revealed that numbers of $Na_v1.6^+$ nodes were unchanged following chronic cerebral hypoperfusion (3 days $p = 0.931$; 1 month $p = 0.857$; 6 weeks $p = 0.665$; 3 months $p = 0.117$). Thus chronic cerebral hypoperfusion does not impact on numbers of nodes of Ranvier but instead alters the localisation of $Na_v1.6$ channels at nodes.

3.3.3 Ankyrin G distribution at nodes of Ranvier is unaltered following 3 days or 1 month of chronic cerebral hypoperfusion

$Na_v1.6$ channels at nodes of Ranvier are associated with Ankyrin G, which tethers the channels to the cytoskeleton through an interaction with βIV spectrin. To determine whether $Na_v1.6$ channel diffusion following 3 days and 1 month of hypoperfusion was accompanied by underlying alterations to Ankyrin G localisation, sections were labelled with Ankyrin G and domain lengths measured (Figure 3.3A). This revealed that Ankyrin G domain lengths were unchanged in the corpus callosum after 3 days ($D = 0.046$; $p = 0.818$; Figure 3.3B) and 1 month ($D = 0.057$; $p = 0.486$; Figure 3.3C) of chronic cerebral hypoperfusion. Therefore the diffusion of $Na_v1.6$ away from nodes of Ranvier in response to cerebral hypoperfusion occurs independently of Ankyrin G.

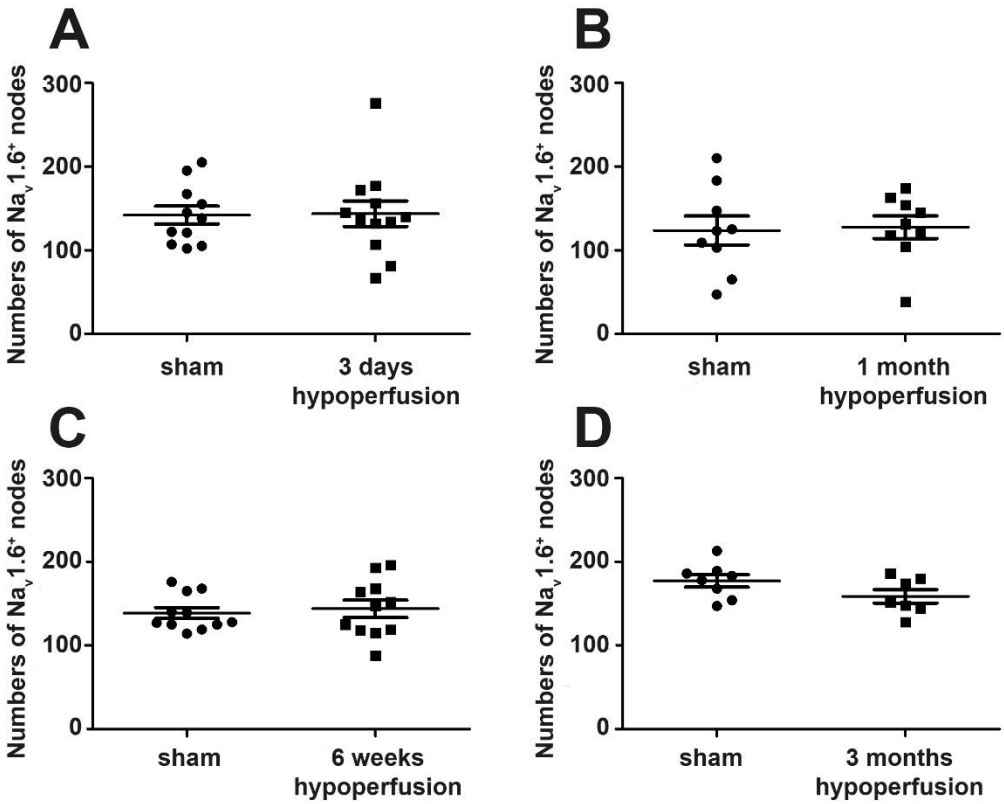

Figure 3.2: Numbers of nodes of Ranvier are unchanged following chronic cerebral hypoperfusion. (**A**) No significant differences in numbers of $Na_v1.6^+$ nodes of Ranvier was observed following 3 days ($p = 0.931$) or (**B**) 1 month ($p = 0.857$) of hypoperfusion. Similarly, numbers of nodes were unchanged following (**C**) 6 weeks ($p = 0.665$) and (**D**) 3 months ($p = 0.117$) of chronic cerebral hypoperfusion.

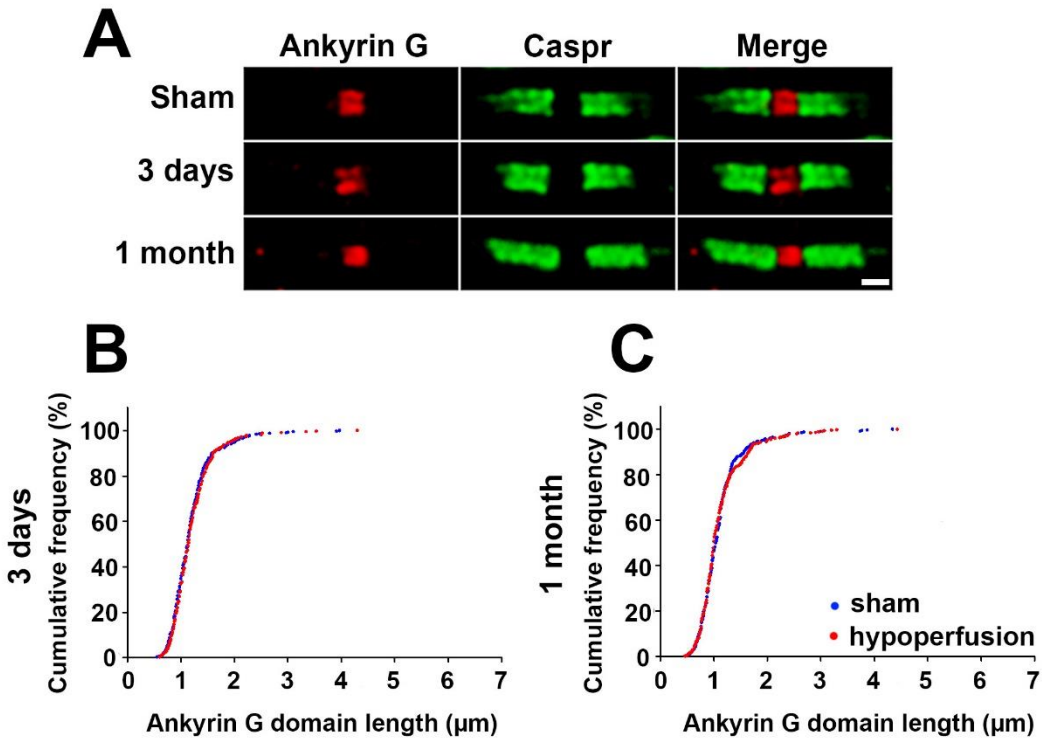

Figure 3.3: Ankyrin G domain length is unaltered following 3 days and 1 month of chronic cerebral hypoperfusion. (**A**) Representative images of Ankyrin G and Caspr labelling in the corpus callosum following 3 days and 1 month of hypoperfusion. Scale bar = 1 µm. (**B**) Ankyrin G domain length was unaltered in the corpus callosum following 3 days ($p = 0.818$) and (**C**) 1 month of hypoperfusion ($p = 0.486$).

3.3.4 Nodal gap is differentially altered in response to short and long term chronic cerebral hypoperfusion

Paranodal septate-like junctions are the main sites of axon-glial connection in the CNS and act as a physical barrier to prevent the diffusion of $Na_v1.6$ channels away from nodes of Ranvier. To determine whether the observed alterations in $Na_v1.6$ distribution following cerebral hypoperfusion were accompanied by disruption to paranodal domains, the 'nodal gap' (the internal space between a pair of adjacent paranodes; Figure 3.4A) was measured in the corpus callosum. Alterations in the length of the nodal gap have been reported to occur in animals with paranodal disruption (Thaxton et al., 2011; Ritter et al., 2013). In the current study, measurement of nodal gap length revealed a significant increase in length ($D = 0.136$; $p = 0.002$) after 3 days of hypoperfusion compared to sham-operated controls (Figure 3.4B). However, following 1 month of cerebral hypoperfusion, nodal gap was significantly decreased as compared to shams ($D = 0.1195$; $p = 0.005$; Figure 3.4C). These findings were confirmed in the internal capsule and optic tract (Appendix A1.3) and measurement of Caspr domain length revealed that alterations in nodal gap were not due to alterations in Caspr distribution (Appendix A1.4).

To determine the effects of longer term hypoperfusion nodal gap was also measured in the corpus callosum following 6 weeks and 3 months of hypoperfusion. This revealed a significant decrease in nodal gap following 6 weeks of hypoperfusion as compared to shams ($D = 0.1182$, $p = 0.003$; Figure 3.4D). Following 3 months of

hypoperfusion, nodal gap was not significantly different between groups ($D = 0.0722$, $p = 0.323$; Figure 3.4E).

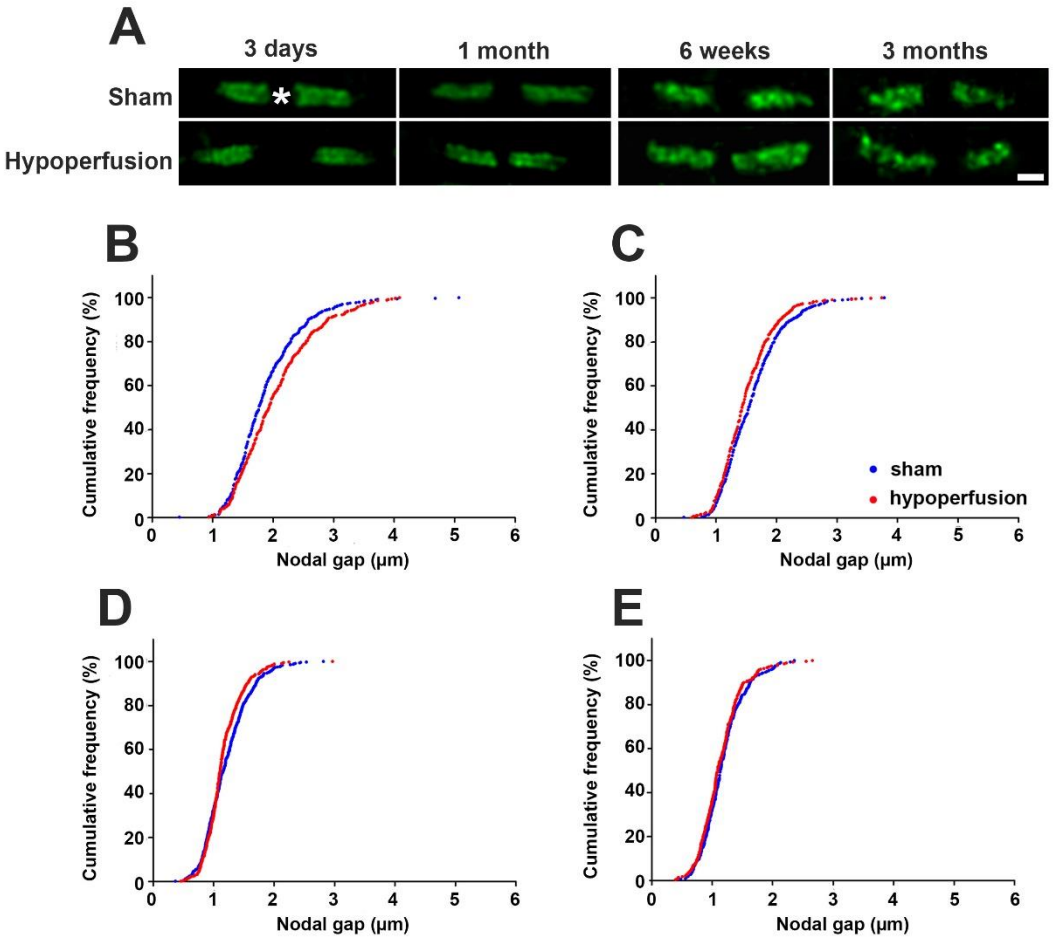

Figure 3.4: Nodal gap is differentially altered in response to increasing durations of chronic cerebral hypoperfusion. (**A**) Representative confocal images showing the nodal gap delineated by Caspr labelling following 3 days, 1 month, 6 weeks and 3 months of hypoperfusion. The nodal gap was defined as the internal distance between two Caspr^{+} paranodes and is indicated by the asterisk. Scale bar = 1 µm. (**B**) Nodal gap was significantly increased following 3 days of hypoperfusion as compared to shams ($p = 0.002$). (**C**) Following 1 month of hypoperfusion, a significant decrease in nodal gap was observed ($p = 0.005$). (**D**) A significant decrease in nodal gap was observed following 6 weeks of hypoperfusion as compared to shams ($p = 0.003$). (**E**) Following 3 months of hypoperfusion, nodal gap was not significantly different between groups ($p = 0.323$).

3.3.5 Paranodal septate-like junctions are disrupted following chronic cerebral hypoperfusion

To further investigate paranodal disruption following chronic cerebral hypoperfusion, ultrastructural analysis was undertaken in longitudinal sections of optic nerves of mice subjected to 1 month of cerebral hypoperfusion. Paranodal domains of myelinated axons were imaged and assessed for the presence or absence of paranodal septate-like junctions and whether or not paranodal myelin loops made contact with the underlying axon (Figures 3.5A-C). This revealed that intact paranodal junctions were observed in approximately 64 ± 7.35 % of shams compared to only 15 ± 7.64% in hypoperfused animals ($p = 0.009$; Figure 3.5D). Abnormal folding of paranodal loops was also observed. Observed abnormalities included paranodal loops which lacked contact with the axon, eversion of paranodal loops and the formation of double paranodal structures. Analysis revealed that abnormal paranodal loops were observed in 62.7 ± 13.9% of hypoperfused paranodes compared to 27.0 ± 3.1 % of paranodes in sham controls ($p = 0.03$; Figure 3.5E). Together these data show that 1 month of chronic cerebral hypoperfusion results in disruption to the paranodal domains of myelinated axons.

3.3.6 Hypoperfusion causes an impairment in internodal axon-glial integrity

In addition to their role in restricting $Na_v1.6$ channels to nodes of Ranvier, paranodes are the primary sites of axon-glial connection in the CNS. To further investigate the impact of chronic cerebral hypoperfusion on axon-glial integrity, the distribution of the internodal protein MAG was assessed. MAG is a key protein involved in the

maintenance of axon-glial connection at internodal domains and has been shown to be preferentially disrupted in hypoxic lesions (Aboul-Enein et al., 2003). To test whether MAG was altered following hypoperfusion, sections were stained and the percentage area occupied by MAG was measured (Figure 3.6A). This revealed a significant decrease in MAG density following 3 days ($p = 0.008$; Figure 3.6B) and 1 month ($p = 0.027$) of chronic cerebral hypoperfusion (Figure 3.6C). Additionally, MAG labelling appeared granular and discontinuous in hypoperfused mice as compared to shams. These data indicate that chronic cerebral hypoperfusion leads to disruption of axon-glial integrity at both paranodal and internodal domains.

3.3.7 No gross myelin changes following 3 days or 1 month of chronic cerebral hypoperfusion

The results of the current study indicate that chronic cerebral hypoperfusion results in rapid disruption to nodal and paranodal domains of myelinated axons and an impairment in axon-glial integrity. To assess whether hypoperfusion also led to disruption of compact myelin, FluoroMyelin staining was carried out and the intensity of staining was analysed (Figure 3.7A). This revealed no significant differences in staining intensity after 3 days ($p = 0.598$; Figure 3.7B) or 1 month of hypoperfusion ($p = 0.063$; Figure 3.7C). Thus cerebral hypoperfusion causes a specific impairment to axon-glial integrity in the absence of gross myelin changes.

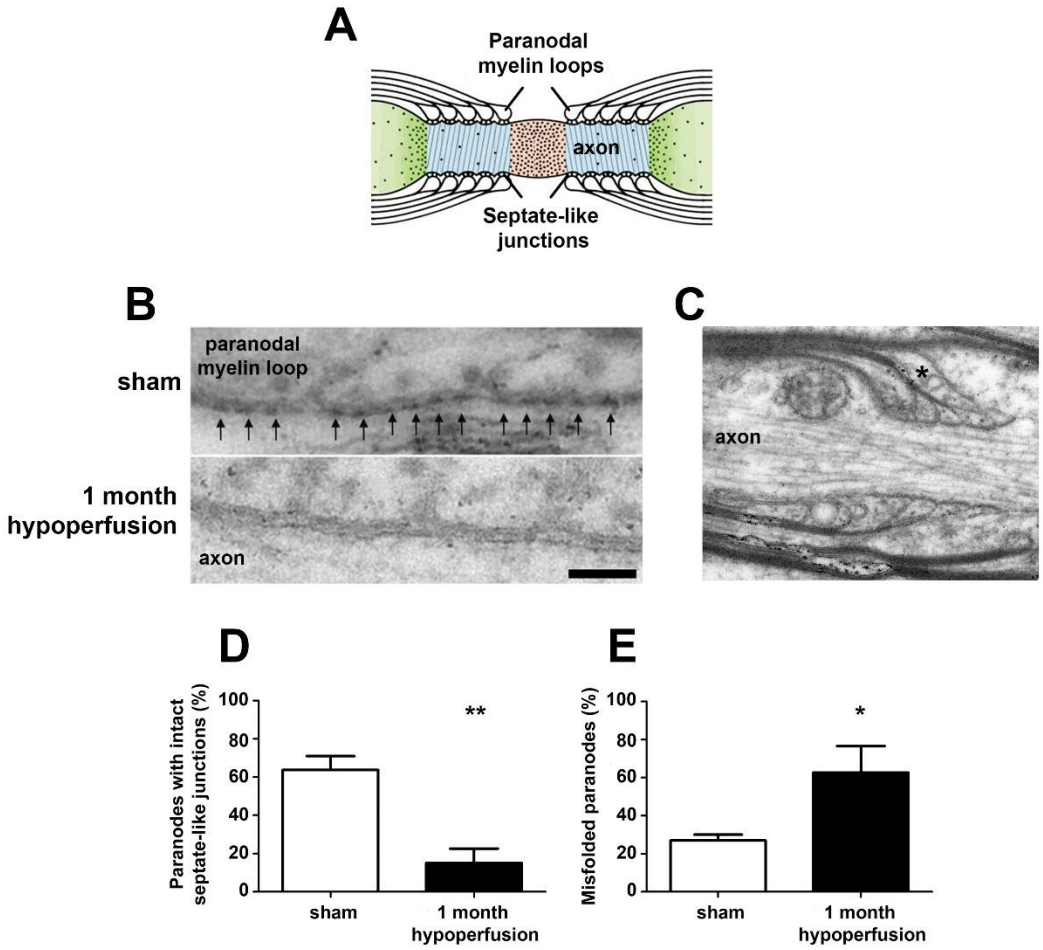

Figure 3.5: Chronic cerebral hypoperfusion results in paranodal disruption. (**A**) Schematic diagram showing the paranodal domains of myelinated axons and the septate-like junctions between the paranodal myelin loops and underlying axon. (**B**) Electron micrograph showing paranodal myelin loops making contact with the underlying axonal membrane. Paranodal septate-like junctions are visible between paranodal myelin and the underlying axon in the sham animal (indicated by arrows) but are absent in the hypoperfused animal. Scale bar = 0.1 µm. (**C**) Electron micrograph showing paranodal misfolding in the form of a double nodal structure. The asterisk indicates a paranodal loop which is not making contact with the underlying axon. (**D**) The percentage of paranodes with intact septate-like junctions was significantly decreased after 1 month of cerebral hypoperfusion compared to sham controls. (**E**) A significant increase in the number of misfolded paranodes was observed after 1 month of cerebral hypoperfusion relative to sham controls. *p = 0.03, ** p = 0.009 vs respective sham group.

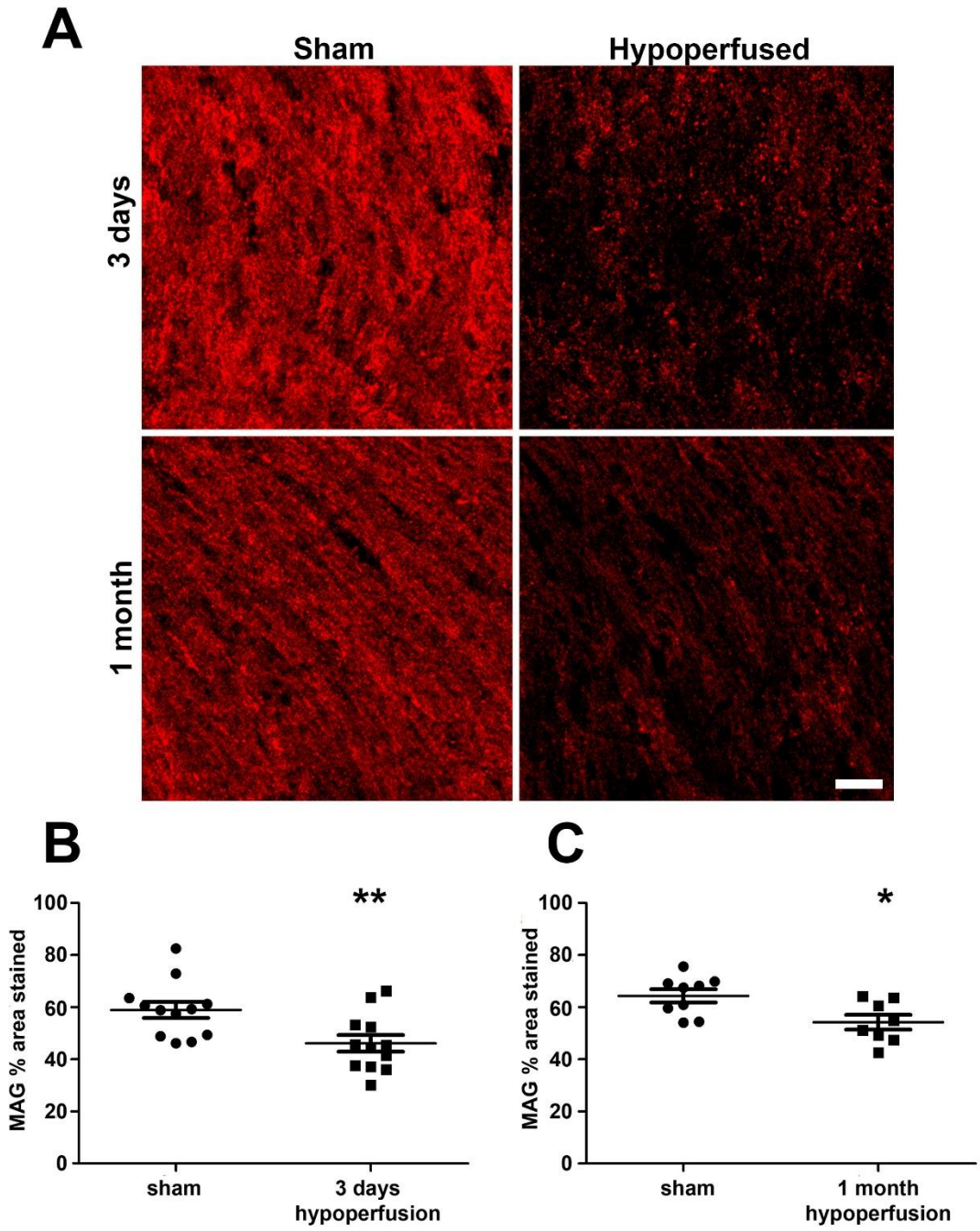

Figure 3.6: Myelin associated glycoprotein labelling is decreased following 3 days and 1 month of chronic cerebral hypoperfusion. (**A**) Representative confocal images showing MAG labelling in the corpus callosum after 3 days and 1 month of cerebral hypoperfusion. Scale bar = 20 µm. (**B**) The percentage area of MAG labelling was significantly decreased after 3 days of hypoperfusion as compared to sham controls. (**C**) Density of MAG labelling was similarly decreased following 1 month of hypoperfusion. * p = 0.027, ** p = 0.008 vs respective shams.

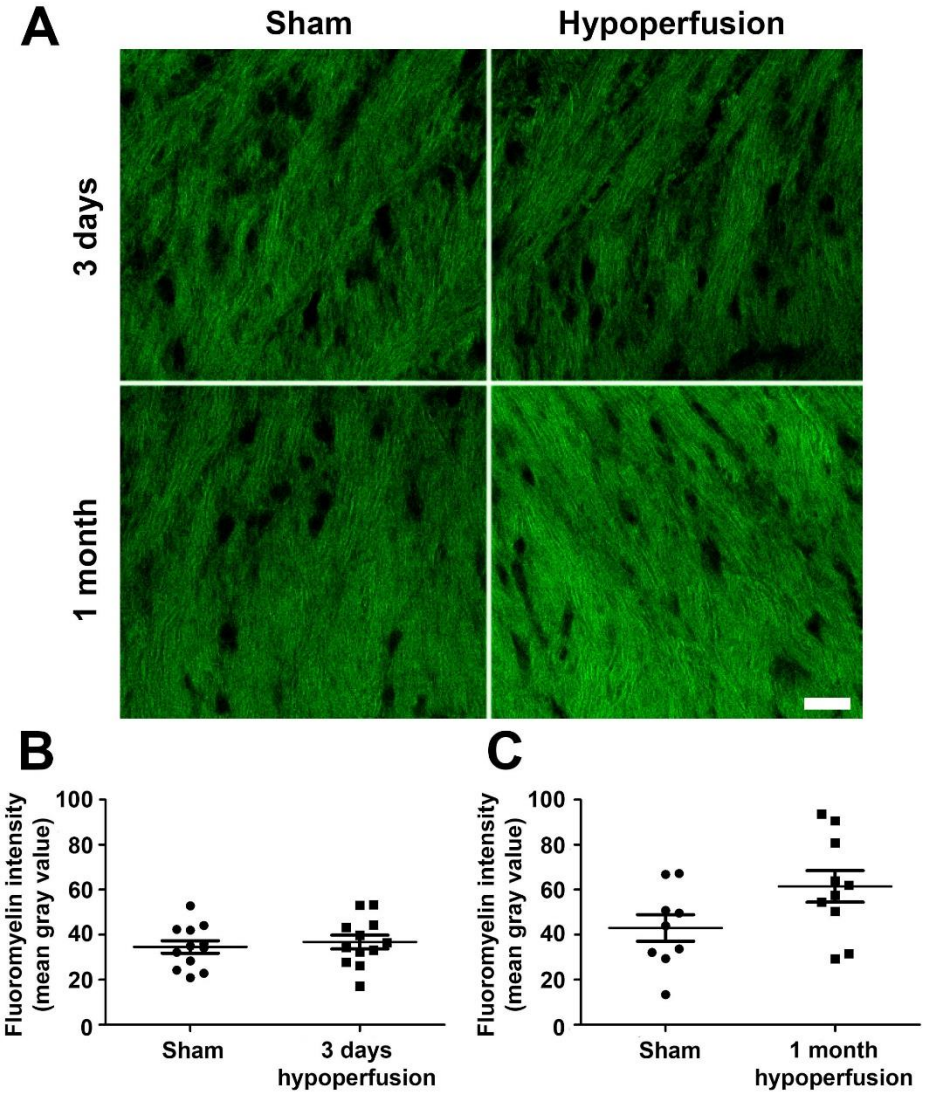

Figure 3.7: FluoroMyelin staining is unchanged with cerebral hypoperfusion. (**A**) Representative confocal images showing FluoroMyelin staining in the corpus callosum. Scale bar = 20 µm. (**B**) FluoroMyelin staining intensity was not significantly different between groups following either 3 days ($p = 0.598$) or (**C**) 1 month ($p = 0.063$) of chronic cerebral hypoperfusion.

3.3.8 Microglial number is increased following 1 month of chronic cerebral hypoperfusion

To determine whether microglial activation may contribute to paranodal disruption early in response to chronic cerebral hypoperfusion, sections were stained for the microglial marker Iba1 and numbers of $Iba1^+$ microglia counted in the corpus callosum following 3 days and 1 month of hypoperfusion (Figure 3.8A). This revealed that numbers of microglia were not significantly different between groups following 3 days of hypoperfusion ($p = 0.425$; Figure 3.8B). However following 1 month, a significant increase in microglial number was observed ($p = 0.001$; Figure 3.8C). Thus microglial number does not appear to mediate paranodal disruption following 3 days but may contribute to ongoing pathology following 1 month of hypoperfusion.

3.3.9 Altered mitochondrial localisation at nodes of Ranvier following chronic cerebral hypoperfusion

Previous studies in peripheral nerves have shown that paranodal disruption is associated with accumulation of mitochondria at nodes of Ranvier and paranodes (Einheber et al., 2006; Sun et al., 2009), indicating a defect in axonal transport of mitochondria. As axonal mitochondria are essential for energy generation within myelinated axons, impaired mitochondrial trafficking may influence white matter integrity. To investigate whether mitochondrial accumulation at nodes of Ranvier was observed following chronic cerebral hypoperfusion and to determine a potential mechanism mediating nodal and paranodal disruption following long term

hypoperfusion, sections were labelled with anti-$Na_v1.6$ and anti-Caspr antibodies together with an antibody against the mitochondrial membrane marker porin. Numbers of $Na_v1.6^+$ nodes and $Caspr^+$ paranodes with positive porin reactivity were then counted (Figure 3.9A). After 6 weeks of hypoperfusion, the percentage of nodes with porin reactivity was decreased in hypoperfused mice compared to sham controls ($p = 0.03$; Figure 3.9B). However following 3 months of cerebral hypoperfusion, no significant differences were observed between groups ($p = 0.742$; Figure 3.9C). No significant differences in porin localisation at paranodes were observed after either 6 weeks ($p = 0.07$; Figure 3.9D) or 3 months ($p = 0.694$; Figure 3.9E). Taken together these results indicate that paranodal disruption following long term chronic cerebral hypoperfusion is not associated with accumulation of mitochondria at nodal or paranodal regions.

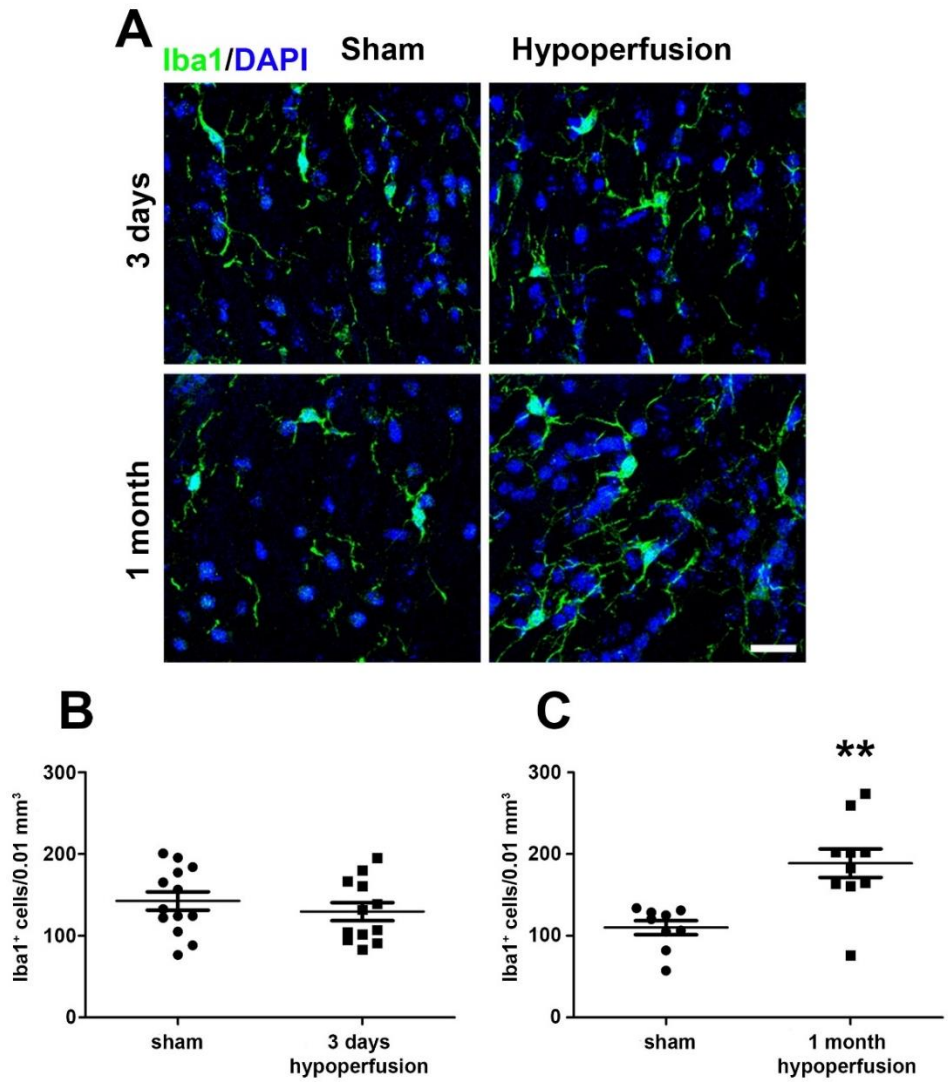

Figure 3.8: Numbers of microglia are unchanged following 3 days but are significantly increased after 1 month of chronic cerebral hypoperfusion. (**A**) Representative confocal images showing Iba^+ microglia in the corpus callosum following sham and hypoperfusion surgery. Scale bar = 20 µm. (**B**) No significant difference in number of microglia was observed between groups following 3 days of cerebral hypoperfusion ($p = 0.425$). (**C**) Following 1 month of hypoperfusion, a significant increase in microglial number was observed relative to sham controls. ** $p = 0.001$ vs sham.

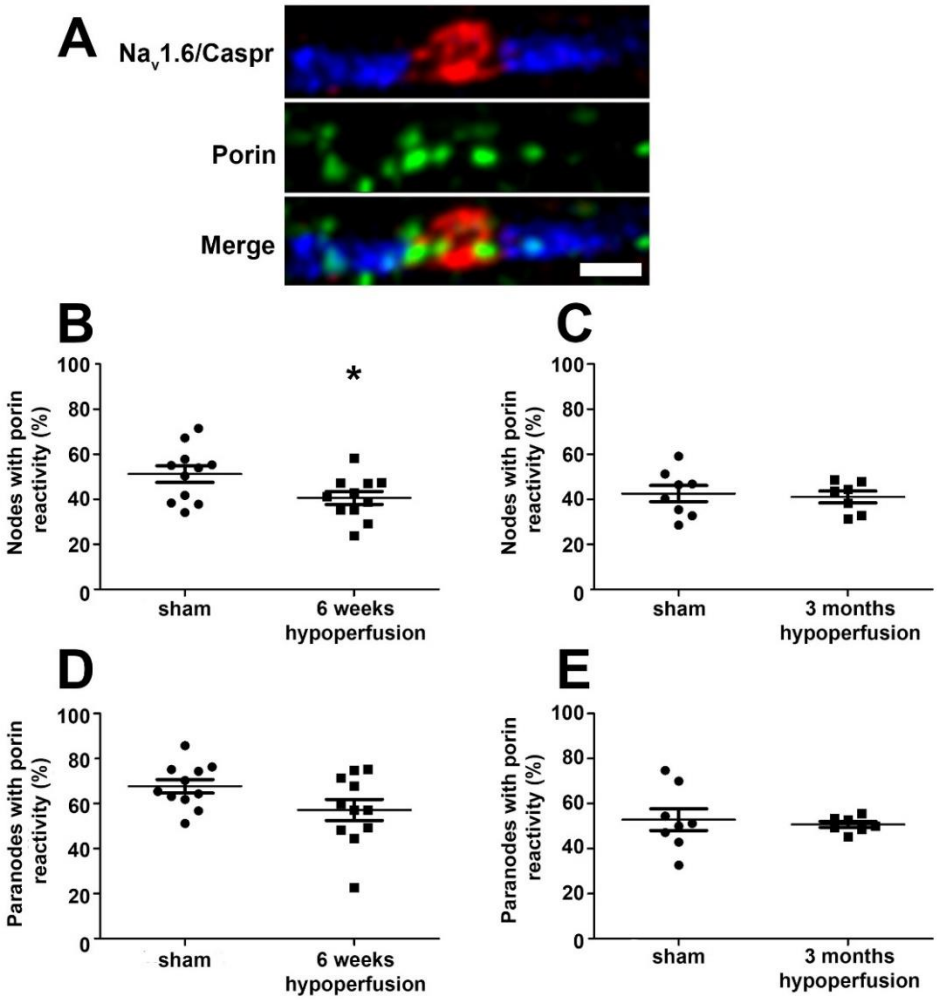

Figure 3.9: Decreased number of nodes with mitochondria following 6 weeks of chronic cerebral hypoperfusion. (**A**) Confocal image showing porin$^+$ mitochondria (green) present at a Na$_v$1.6$^+$ node of Ranvier (red) and Caspr$^+$ paranodes (blue). Scale bar = 1 µm. (**B**) A significant decrease in the numbers of nodes with porin reactivity was observed following 6 weeks of hypoperfusion as compared to shams ($p = 0.03$). (**C**) However no significant difference in numbers of nodes with porin reactivity was observed following 3 months of chronic cerebral hypoperfusion ($p = 0.742$). (**D**) No significant differences in numbers of paranodes with porin reactivity was observed between groups following 6 weeks ($p = 0.07$) or (**E**) 3 months ($p = 0.694$) of cerebral hypoperfusion. * $p = 0.03$ vs sham.

3.3.10 Chronic cerebral hypoperfusion impairs spatial working memory

Previous studies have demonstrated that in addition to diffuse white matter damage, chronic cerebral hypoperfusion causes an impairment in spatial working memory (Shibata et al., 2007; Coltman et al., 2011). To confirm this, spatial memory was assessed in a cohort of 1 month hypoperfused mice using the radial arm maze. Analysis of both parameters (number of novel entries and revisiting errors) revealed a significant effect of trial block ($p < 0.0001$) indicating that both groups had improved over time and successfully learned the task.

Hypoperfused animals made significantly fewer novel entries as compared to sham controls ($F_{(4.9,\ 147)} = 3.192$; $p = 0.011$; Figure 3.10A). In addition, the number of revisiting errors was significantly higher in hypoperfused mice ($F_{(1,\ 21)} = 7.274$; $p = 0.013$; Figure 3.10B). Total trial duration did not differ between groups (Appendix A1.5).

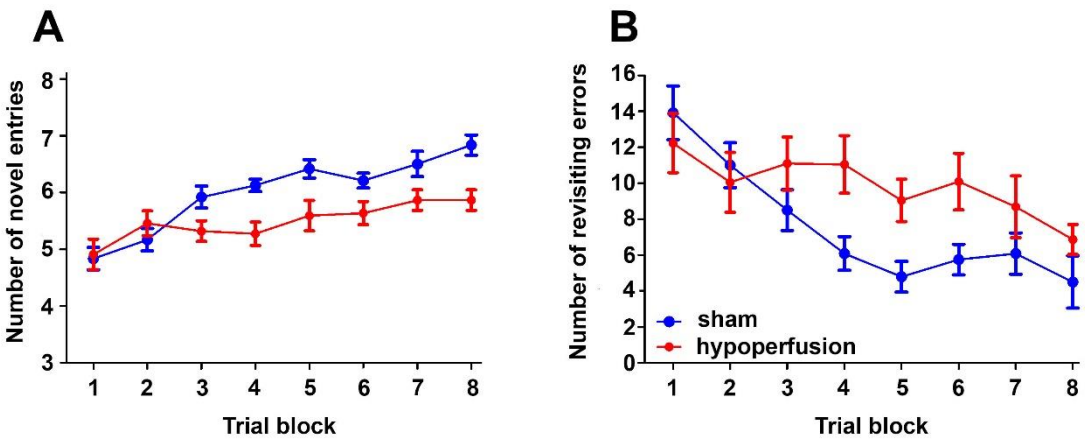

Figure 3.10 Spatial working memory is impaired in hypoperfused mice. (**A**) Hypoperfused mice made significantly fewer novel entries than sham control mice ($p = 0.011$). (**B**) Hypoperfused mice also made significantly more revisiting errors than sham controls ($p = 0.013$). A significant effect of trial block was observed indicating that both groups of mice improved over time, thus successfully learning the task ($p < 0.0001$).

3.4 Discussion

The current study sought to test the hypothesis that chronic cerebral hypoperfusion would lead to disruption of nodal and paranodal domains of myelinated axons. The results support the hypothesis and demonstrate that chronic cerebral hypoperfusion results in alterations to $Na_v1.6$ localisation at nodes of Ranvier, nodal gap length and loss of paranodal septate-like junctions. Furthermore this study unexpectedly revealed that alterations to $Na_v1.6$ distribution and nodal gap are dynamic and vary with increasing duration of chronic cerebral hypoperfusion. Importantly, chronic cerebral hypoperfusion also led to disruption of axon-glial integrity at internodal domains but no gross myelin pathology was observed following 3 days or 1 month of hypoperfusion. The results demonstrate increased numbers of microglia following 1 month of hypoperfusion and altered mitochondrial localisation following 6 weeks of hypoperfusion. Critically an impairment in spatial working memory was observed in mice subject to 1 month of chronic cerebral hypoperfusion indicating that alterations to nodal and paranodal domains of myelinated axons may have functional consequences.

3.4.1 Dynamic changes in the localisation of nodal and paranodal proteins

In the current study, paranodal disruption was observed following 3 days and 1 month of cerebral hypoperfusion resulting in diffusion of $Na_v1.6$ channels away from nodes of Ranvier into adjacent paranodal domains. Furthermore, alterations in $Na_v1.6$

domain length were highly dynamic and varied with increasing duration of hypoperfusion (summarised in Figure 3.11). Indeed despite increased $Na_v1.6$ domain length following 3 days and 1 month of hypoperfusion, no significant difference in domain length was observed following 6 weeks of hypoperfusion with a significant decrease observed following 3 months as compared to controls. The current study also demonstrated that $Na_v1.6$ domain length and nodal gap were differentially affected by hypoperfusion. Critically, following 1 month of hypoperfusion nodal gap was significantly decreased in hypoperfused animals while $Na_v1.6$ domain length was increased. One possible explanation is that this decrease in nodal gap may arise from the passive diffusion of Caspr along the axon as a result of the loss of its binding partner Nfasc155 as demonstrated by Reimer et al (2011). In support of this, a recent study using transgenic mice in which Nfasc155 is specifically ablated has shown that loss of Nfasc155 results in loss of paranodal localisation of Caspr (Pillai et al., 2009). On the other hand, it is equally possible that the decreased nodal gap at 1 month is associated with reformation of paranodal domains. Indeed in human MS studies, $Caspr^+$ and $Nfasc^+$ paranodes flanking $Na_v1.6^+$ nodes are observed in areas of remyelination suggesting that these proteins can re-cluster following injury to form nodal and paranodal domains (Coman et al., 2006; Howell et al., 2006). Additionally, the decrease in $Na_v1.6$ domain length following longer term hypoperfusion suggests that these channels are re-clustered to form nodes of Ranvier. To determine whether alterations in nodal gap are associated with reformation of paranodal domains, it would be pertinent to study Nfasc155 localisation following 6 weeks and 3 months of cerebral hypoperfusion to ascertain whether this protein reappears.

It should be noted that the alterations in $Na_v1.6$ domain length reported in the current study may be associated with alterations in number of $Na_v1.6$ channels. For example, it is unknown whether increased $Na_v1.6$ domain length following 3 days and 1 month of hypoperfusion is due to diffusion of existing channels along the axon or the result of increased numbers of $Na_v1.6$ channels recruited to the axonal membrane. Similarly, the decreased $Na_v1.6$ domain length following 3 months of hypoperfusion may be due to a loss of $Na_v1.6$ channels. This could be assessed in future studies by measuring the fluorescent intensity or volume occupied by $Na_v1.6$ staining.

Given that the highly organised domain structure of myelinated axons is essential for efficient action potential conduction, the observed disruption to axon-glial connection and alterations in the localisation of $Na_v1.6$ channels at nodes of Ranvier are likely to impair saltatory conduction along myelinated axons. In support of this, recent studies within the group have demonstrated that the conduction velocity of myelinated axons in the corpus callosum is significantly decreased following 6 weeks and 3 months of chronic cerebral hypoperfusion (Dr Philip R Holland, unpublished observations). Additional studies by other groups have also revealed that paranodal disruption and subsequent alterations in $Na_v1.6$ localisation and nodal gap negatively impact on conduction velocity (Bhat et al., 2001; Nie et al., 2006; Ritter et al., 2013). In the current study the observed alterations in $Na_v1.6$ localisation were subtle, with no differences in numbers of nodes between groups at any time point suggesting that hypoperfusion does not induce a widespread loss of nodes. Despite this, a recent mathematical modelling study has revealed that even modest paranodal disruption can significantly influence conduction velocity. By modelling subtle

alterations to paranodal resistance to mimic slight retraction of paranodal myelin and by increasing the theoretical nodal length from 0.65 µm to 1.95 µm, the authors demonstrated that conduction velocity was decreased up to 40% (Babbs and Shi, 2013). This is in keeping with the current study which showed that the mean $Na_V1.6$ domain length was 2.08 µm following 1 month of hypoperfusion, and indicates that the subtle alterations observed in this study may significantly influence conduction velocity. Taken together these studies highlight the importance of intact axon-glial integrity in the brain.

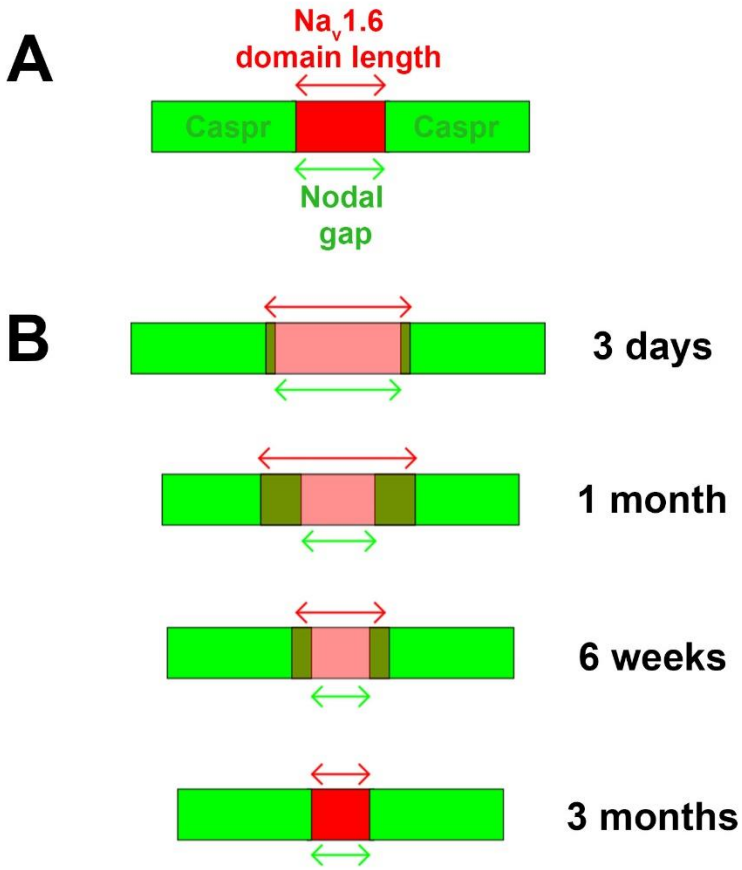

Figure 3.11: Dynamic alterations in Na$_v$1.6 localisation and nodal gap following chronic cerebral hypoperfusion. (**A**) In a normal myelinated axon, Na$_v$1.6 channels (red) are clustered at nodes of Ranvier which are flanked either side by Caspr$^+$ paranodes (green). Nodal and paranodal proteins are spatially segregated such that neighbouring domains do not show any overlap. In the current study, Na$_v$1.6 domain length (red arrows) and the internal space delineated by two Caspr$^+$ paranodes ('nodal gap'; green arrows) were measured. (**B**) Following 3 days of cerebral hypoperfusion, diffusion of Na$_v$1.6 channels away from nodes of Ranvier was observed, corresponding to a significant increase in Na$_v$1.6 domain length in addition to an increase in nodal gap. However following 1 month of cerebral hypoperfusion, Na$_v$1.6 domain length remained significantly increased but nodal gap was significantly decreased as compared to shams. Following 6 weeks of hypoperfusion, Na$_v$1.6 domain length was unchanged between groups but a significant decrease in nodal gap was observed. Finally, 3 months of chronic cerebral hypoperfusion resulted in a significant decrease in Na$_v$1.6 domain length whilst nodal gap was unchanged.

3.4.2 Rapid disruption to internodal axon-glial integrity following chronic cerebral hypoperfusion

This study has demonstrated that the density of MAG labelling was decreased following 3 days and 1 month of chronic cerebral hypoperfusion whilst FluoroMyelin staining was unchanged. This selective disruption to MAG is consistent with previous studies using the mouse model of hypoperfusion (Coltman et al., 2011; Reimer et al., 2011). Although MAG accounts for less than 1% of myelin protein composition it appears particularly vulnerable to decreased blood flow. Post-mortem study of hypoxic 'type III' MS lesions and ischaemic white matter lesions has shown that MAG is preferentially lost in both types of lesions whilst the compact myelin proteins MBP and PLP are unchanged (Aboul-Enein et al., 2003). A recent post-mortem investigation of individuals with small vessel disease and vascular dementia has shown decreased protein levels of MAG compared to controls (Barker et al., 2013). One possible reason for this selective vulnerability of MAG corresponds to its periaxonal localisation within the most distal oligodendrocyte processes (Aboul-Enein et al., 2003). An earlier study of anoxia in optic nerve preparations has demonstrated that terminal oligodendrocyte processes at paranodes are the first to be affected and that damage spreads from nodes of Ranvier outwards (Waxman et al., 1992). Consistent with this the periaxonal localisation of MAG suggests it will be one of the first internodal myelin proteins to be disrupted. It is important to note that MAG disruption indicates that the myelin sheath is detached or in the process of detaching from the axon however it is possible that despite this detachment, compact myelin remains intact hence the lack of apparent changes in FluoroMyelin or MBP (Reimer et al., 2011). Future studies are required to fully

characterise the axonal binding partners of MAG to determine whether these are also altered in response to chronic cerebral hypoperfusion. Furthermore it would also be pertinent to study MAG distribution following longer term hypoperfusion to determine whether this disruption to internodal axon-glial connection worsens with time or if there is any evidence of recovery.

The finding that MAG was preferentially disrupted in the absence of gross myelin disruption contrasts with earlier studies by another group using the mouse model of chronic cerebral hypoperfusion. These studies have demonstrated extensive myelin damage following 1 month of hypoperfusion (Fujita et al., 2010; Washida et al., 2010; Maki et al., 2011; Seo et al., 2013) which was not observed in the current study. These studies were carried out by another group in another institution and therefore one possible reason for the discrepancy in results may be due to subtle differences in surgical technique. Similarly, although both groups use C57/Bl6J mice from a commercial supplier, there may be slight strain differences based on the geographical location of the supplier. Given that C57Bl/6J mice are known to have an incomplete circle of Willis, any subtle differences in the cerebral architecture between commercial suppliers in different countries may have profound effects on the extent of pathology induced following chronic cerebral hypoperfusion. The different approaches used to visualise myelin may also partially contribute to the discrepancy between the current study and previous studies. The initial characterisation of the model used a Klüver-Barerra histological stain (also known as Luxol fast blue) to quantify myelin pathology which was assessed using a grading scale (Shibata et al., 2004). In the current study, sections were stained using the

lipophilic dye FluoroMyelin and the fluorescent intensity of the staining was measured. Whilst neither Luxol fast blue nor FluoroMyelin label specific myelin lipids, quantifying the intensity of staining is a more accurate way of assessing myelin integrity compared to a qualitative grading scale. In support of the current study it is important to note that previous studies within the Horsburgh group have consistently reported a lack of gross myelin pathology as assessed by MBP labelling and western blotting (Reimer et al., 2011; and unpublished observations) therefore the results of the current study are in keeping with previous results from the group.

3.4.3 Potential mechanisms involved in nodal and paranodal disruption following hypoperfusion

The exact mechanisms underlying paranodal disruption following cerebral hypoperfusion are unknown. Microarray analysis of white matter from mice subject to 3 days of chronic cerebral hypoperfusion has demonstrated significant upregulation of genes involved in inflammatory responses (Reimer et al., 2011) suggesting that inflammatory signalling cascades may be an important mediator of white matter disruption following hypoperfusion. In support of this, previous study in post-mortem MS tissue and in EAE mice has demonstrated a close association between paranodal disruption and microglial activation (Howell et al., 2010). Interestingly this study demonstrated that inhibition of microglial activation through administration of minocycline preserved paranodal structure (Howell et al., 2010) therefore modulation of inflammation may be an important therapeutic strategy to stabilise axon-glial connection. In the current study, numbers of microglia were not

significantly different between groups following 3 days of hypoperfusion but were significantly increased after 1 month. Given that axon-glial disruption is evident as early as 3 days following surgery it is unlikely that increased microglial number mediates early paranodal disruption following chronic cerebral hypoperfusion. Despite this, the evidence from microarray analysis indicates significant upregulation of inflammatory signalling at this time point thus a role for inflammation as a mediator of paranodal disruption cannot be excluded. Furthermore, there is growing evidence that microglia are highly dynamic cells and that phenotypically distinct pro-inflammatory (termed M1) and anti-inflammatory (M2) activation states exist within the greater microglial pool (Edwards et al., 2006; Mosser and Edwards, 2008). It has recently been demonstrated that the M1 or M2 phenotype can directly influence white matter damage following traumatic brain injury (Wang et al., 2013) or demyelination (Miron et al., 2013). The current study utilised the general microglial marker Iba1 to determine numbers of microglia following hypoperfusion but future studies should aim to characterise specific microglial phenotypes and to assess levels of pro-inflammatory mediators to fully clarify whether increased inflammation modulates paranodal disruption following chronic cerebral hypoperfusion.

In addition to inflammation, studies have demonstrated that myelinated axons are vulnerable to reductions in oxygen and glucose (Pantoni et al., 1996; Fern et al., 1998; Wender et al., 2000). Indeed given the extent of blood flow reduction reported in the mouse model of hypoperfusion (~30%; Shibata et al., 2004) it is likely that there is an energy deficit within the white matter following hypoperfusion. As outlined in Section 1.2.2.1, the energy demands of myelinated axons are met by

axonal mitochondria which are trafficked along axons. Previous studies in the peripheral nervous system (PNS) have demonstrated that mitochondria are preferentially localised to nodes of Ranvier and are thought to be recruited to this region in an activity-dependent manner (Zhang et al., 2010; Chiu, 2011). A recent study has additionally reported that in the CNS mitochondria preferentially localise to juxtaparanodal and internodal regions and that neuronal activity decreases mitochondrial motility in nodal and paranodal regions (Ohno et al., 2011). Indeed the presence of Na^+/K^+/ATPase pumps within internodal domains suggests that these regions have a high energy demand. These pumps require ATP to power the export of three Na^+ ions in exchange for two K^+ ions and thus play a key role in maintaining resting membrane potential (Waxman and Ritchie, 1993). Given the pronounced paranodal disruption and consequent altered distribution of $Na_v1.6$ at nodes of Ranvier observed in the current study it was hypothesised that the distribution of mitochondria along myelinated axons may also be disrupted in response to cerebral hypoperfusion. In support of this, accumulation of mitochondria within swellings in nodal and paranodal domains of peripheral nerves has been reported in Caspr knockout mice (Einheber et al., 2006) and in mice expressing mutant Caspr (Sun et al., 2009) demonstrating that disruption to paranodes can influence mitochondrial localisation. In the current study a significant decrease in the number of nodes containing mitochondria was observed after 6 weeks of hypoperfusion with no difference observed between groups following 3 months. Although speculative it is possible that disruption to $Na_v1.6$ channels following hypoperfusion results in increased Na^+ influx into the axon therefore increasing the energy demand of the internodal Na^+/K^+/ATPase pumps and the recruitment of mitochondria from nodes of

Ranvier into internodal domains. Alternatively it is possible that the decrease in mitochondrial localisation at nodes of Ranvier following 6 weeks of hypoperfusion is due to a loss of mitochondria which is restored by 3 months. One limitation of immunohistochemical approaches to study the localisation of mitochondria is that mitochondrial movement along axons is a dynamic process, which may not be readily detected at the end stage of animal experiments (Chiu, 2011). Transgenic mice in which mitochondria are fluorescently labelled have been developed (Misgeld et al., 2007) therefore future studies could conduct live imaging in slice preparations from such mice to determine whether modest reductions in oxygen and glucose influence the distribution of mitochondria along myelinated axons. Indeed these mice could also be subject to chronic cerebral hypoperfusion and *in vivo* mitochondrial dynamics studied using two-photon microscopy (Helmchen and Denk, 2005).

Mitochondria are transported along axons via microtubules and actin filaments of the cytoskeleton (Chang and Reynolds, 2006). Importantly, most nodal and paranodal proteins are also associated with the cytoskeleton either indirectly (in the case of $Na_v1.6$) or directly (e.g. βIV spectrin) and thus disruption to the underlying cytoskeleton may contribute to nodal and paranodal alterations following hypoperfusion. Ultrastructural analysis has revealed that paranodal junctions in CNS fibres are directly connected to cytoskeletal microtubules and neurofilaments and to axonal organelles through small filamentous connections (Ichimura and Ellisman, 1991; Nans et al., 2011). This direct association of paranodal junctions with the cytoskeleton further highlights the role of the paranodes in maintaining the domain organisation of myelinated axons. A study using Caspr knockout mice has

demonstrated axonal swellings close to paranodal domains which contain increased phosphorylated neurofilaments suggesting underlying deficits in axonal transport which may be caused by cytoskeletal disruption (Garcia-Fresco et al., 2006). However in the current study, altered localisation of $Na_v1.6$ channels was observed in the absence of altered Ankyrin G localisation suggesting an uncoupling of these two proteins rather than a generalised cytoskeletal disruption. To fully clarify whether disruption to the underlying cytoskeleton may mediate paranodal disruption following hypoperfusion it would be important for future study to investigate the effects of hypoperfusion on the distribution of cytoskeleton-associated proteins such as βIV spectrin. Interestingly, it has been demonstrated that MAG can modulate the spacing and phosphorylation of neurofilaments (Yin et al., 1998; Dashiell et al., 2002) which may alter axonal transport. Additionally MAG knockout mice exhibit paranodal disruption resulting in diffusion of juxtaparanodal K_v channels into neighbouring paranodes (Marcus et al., 2002). The rapid disruption to MAG following chronic cerebral hypoperfusion observed in the current study may therefore be directly associated with paranodal disruption.

3.4.4 Chronic cerebral hypoperfusion and impaired spatial working memory

A strong association between chronic cerebral hypoperfusion, white matter damage and cognitive decline has been demonstrated in imaging studies of elderly humans (DeCarli et al., 1995; Ruitenberg et al., 2005; Appelman et al., 2010). Age-related cognitive alterations in humans include decreases in processing speed and memory retrieval amongst others (reviewed by Deary et al., 2009). In the current study the 8-

arm radial arm maze was used to assess spatial working memory following chronic cerebral hypoperfusion in mice. The results revealed that hypoperfused animals made significantly more revisiting errors and fewer novel entries than sham controls, indicative of a deficit in spatial working memory. This finding is consistent with earlier studies in the model (Shibata et al., 2004; Coltman et al., 2011). Successful completion of the 8-arm radial arm maze task requires the mice to retrieve a food pellet from the end of each arm whilst remembering the arms they have previously visited. This task therefore requires significant memory flexibility as the animals need to constantly update their memory regarding the arms which they have visited and those which they have not. It is thought that the circuits involved in working memory tasks in rodents involve the hippocampus, prefrontal cortex, striatum and thalamus (Hodges, 1996; Floresco et al., 1997; Floresco et al., 1999). The diverse anatomical regions involved suggest that white matter pathways play a key role in transmission of information during memory encoding and retrieval therefore any disruption to white matter may significantly impair performance in the task. Indeed combined MRI and cognitive testing in humans has shown that ageing is associated with a slowing of memory retrieval and that this is correlated with decreased white matter integrity in the genu and splenium of the corpus callosum and frontal white matter in addition to other regions (Bucur et al., 2008).

The current study revealed that $Na_v1.6$ localisation to nodes of Ranvier was disrupted as early as 3 days following hypoperfusion and was accompanied by paranodal disruption and altered MAG labelling. Given the importance of both an intact myelin sheath and the high density $Na_v1.6$ clustering at nodes for efficient action potential

conduction it is likely that these observed alterations may contribute to the spatial working memory deficit following cerebral hypoperfusion. Indeed, a recent study within the group has demonstrated that the length of $Na_v1.6^+$ nodes of Ranvier is significantly decreased in aged mice and is correlated with poorer performance in radial arm maze testing (Miss Kanelina Karali, PhD thesis 2014). Critically the current study demonstrated that impaired axon-glial integrity and paranodal disruption occurred in the absence of widespread damage to compact myelin demonstrating that even subtle alterations to the structure of myelinated axons can have significant effects on functional capabilities.

3.4.5 Summary and conclusions

Previous studies have demonstrated that chronic cerebral hypoperfusion in mouse is associated with widespread and diffuse white matter damage (Shibata et al., 2004; Coltman et al., 2011). Critically the results presented in this chapter demonstrate the novel finding that chronic cerebral hypoperfusion results in paranodal disruption and diffusion of $Na_v1.6$ channels away from nodes of Ranvier. Furthermore impaired internodal axon-glial integrity was observed in the absence of gross myelin disruption. Importantly, this study has demonstrated that hypoperfused mice show decreased performance in the radial arm maze suggesting that relatively modest alterations to the domains of myelinated axons may have downstream cognitive consequences. In the next chapter the impact of chronic cerebral hypoperfusion on oligodendrocytes and OPCs will be examined to determine whether alterations in these populations of cells may contribute to white matter pathology in the model.

Chapter 4

The impact of chronic cerebral hypoperfusion on oligodendroglial populations

4.1 Introduction

The finding that chronic cerebral hypoperfusion resulted in disruption to the domain structure of myelin axons and impaired axon-glial integrity raised the question as to whether this may be driven by a deficit in myelinating oligodendrocytes. Indeed, post-mortem studies of MS cases have shown that injury to oligodendrocytes can result in a 'dying back' retraction of the most distal oligodendrocyte processes, resulting in impaired axon-glial connection and paranodal disruption (Ludwin and Johnson, 1981; Lassmann et al., 1997). In addition it has been estimated that a single oligodendrocyte can myelinate up to 50 internodal segments (Hildebrand et al., 1993; Rivers et al., 2008) therefore injury to individual oligodendrocytes may impact on multiple axons. Taken together, these studies suggest that oligodendrocyte health and/or number of oligodendrocytes may have important consequences for the structure of myelinated axons.

Previous studies have demonstrated that oligodendrocytes are particularly vulnerable to reductions in CBF. Loss of oligodendrocytes is observed as early as 24 hours following focal cerebral ischaemia in rats and mice (Pantoni et al., 1996; Valeriani et al., 2000; McIver et al., 2010) and has additionally been reported following 1 month of chronic cerebral hypoperfusion in mouse (Fujita et al., 2010; Washida et al., 2010; Maki et al., 2011), highlighting the vulnerability of these cells to even modest reductions in CBF. Despite this susceptibility of oligodendrocytes to decreased CBF

there is an abundance of evidence demonstrating that oligodendrocytes can be replaced through the proliferation and/or differentiation of OPCs (Tanaka et al., 2001; Tanaka et al., 2003). Restoration of mature oligodendrocyte number has been demonstrated as early as 7 days post-reperfusion in a study of focal cerebral ischaemia in mouse (McIver et al., 2010). Furthermore, increased numbers of remyelinating oligodendrocytes and the presence of OPCs has also been described in post-mortem study of aged human in regions of the brain where blood flow has been compromised (Simpson et al., 2007a). Additionally, increased numbers of OPCs have been demonstrated in post-mortem study of individuals with vascular cognitive impairment (Back et al., 2011) suggesting that OPCs may respond to reduced cerebral blood flow in an attempt to ameliorate white matter damage. Despite these studies demonstrating increased numbers of OPCs in response to severe reductions in CBF, the effects of modest reductions in CBF on OPC numbers is unknown.

A growing number of studies have investigated the mechanisms underlying OPC proliferation and differentiation in response to CNS injury. Several studies have identified the GPR17 receptor as a key modulator of OPC differentiation in response to insults such as ischaemia, spinal cord injury and cortical stab wound in mice (Ciana et al., 2006; Lecca et al., 2008; Ceruti et al., 2009; Boda et al., 2011) and more recently traumatic brain injury in humans (Franke et al., 2013). GPR17 is upregulated in response to injury and it is thought that receptor activation acts as a sensor of local damage (Lecca et al., 2008). Furthermore, GPR17 has been demonstrated to be expressed by subsets of OPCs and premyelinating oligodendrocytes and it has been shown that receptor activation promotes

differentiation of OPCs (Boda et al., 2011; Fumagalli et al., 2011). This receptor may therefore be an important mediator of white matter repair following injury and may represent an important therapeutic target for cerebral hypoperfusion.

4.1.1 Study hypothesis and aims

It was hypothesised that chronic cerebral hypoperfusion would result in loss of oligodendrocytes and OPCs. The specific aim of this study was to investigate oligodendrocyte and OPC pools in response to short term (3 days) and long term (1 month) hypoperfusion. A further aim was to characterise whether GPR17 receptor upregulation was observed in response to chronic cerebral hypoperfusion.

4.2 Methods

4.2.1 Animals and Surgery

Adult male C57Bl/6J mice (25-30g, age 3-4 months) underwent chronic cerebral hypoperfusion or sham surgery as described in Section 2.2. Group sizes for 3 day hypoperfusion studies were (1) n = 13 sham, 11 hypoperfused; and (2) n = 10 sham, 9 hypoperfused. For 1 month hypoperfusion studies group sizes were (3) n = 10 sham, 11 hypoperfused; and (4) n = 9 sham, 9 hypoperfused.

4.2.2 Laser speckle contrast imaging

Cerebral blood flow was measured using laser speckle contrast imaging though the intact skull as described in Section 2.3. Baseline readings were acquired 1 day prior to surgery with subsequent recordings made at 3 days and 28 days following surgery.

4.2.3 BrdU administration

Animals from cohort 3 were given intraperitoneal injections of the thymidine analogue 5-Bromo-2’-deoxyuridine (BrdU) as described in Section 2.6.

4.2.4 Perfusion and tissue processing for immunohistochemistry

At 3 days or 28 days (1 month) post-surgery, mice were deeply anaesthetised with 5% isoflurane and transcardially perfused as described in Section 2.8.1. Tissue was processed and cut into 50 µm thick sagittal sections using a vibratome as described in Section 2.8.2.

4.2.5 Immunohistochemistry

Immunohistochemistry was carried out as described in Section 2.10. Anti-CC1, NG2 and Olig2 antibodies were used to label oligodendroglia, anti-BrdU and PCNA antibodies were used to assess numbers of proliferating cells, and anti-GPR17 antibody was used to assess GPR17 expression.

4.2.6 Confocal microscopy and image analysis

Immunolabelled 50 µm sections were imaged using confocal laser scanning microscopy as described in Section 2.11.1. Images were acquired in the corpus callosum immediately adjacent to the lateral ventricle, as shown in Figure 2.3. Image analysis was carried out as described in Section 2.12.

4.2.7 Electron microscopy and g-ratio measurement

Animals were transcardially perfused and the corpus callosum manually dissected as described in Section 2.13.1. Tissue was processed and cut into 60 nm transverse sections as described in Section 2.13.2. Images of myelinated fibres were acquired at 3500x magnification and g-ratio was measured as described in Section 2.14.2.

4.2.8 Statistical analysis

Data were analysed using a two-tailed student's *t*-test or Mann-Whitney U-test depending on parametric or non-parametric distribution. A probability (p) value < 0.05 was considered to be statistically significant

4.3 Results

4.3.1 Loss of mature oligodendrocytes and OPCs following 3 days of cerebral hypoperfusion

At the outset of the study it was hypothesised that chronic cerebral hypoperfusion would lead to a loss of mature oligodendrocytes. To determine the effect of 3 days of hypoperfusion on mature oligodendrocyte populations, immunohistochemistry was carried out using an antibody against the adenomatous polyposis coli (CC1 or APC) protein and numbers of $CC1^+$ mature oligodendrocytes were counted in the corpus callosum (Figure 4.1A). This revealed a significant decrease in numbers of mature oligodendrocytes in hypoperfused mice as compared to sham controls ($p = 0.02$; Figure 4.1B). The specificity of CC1 as a marker of mature oligodendrocytes was confirmed through double labelling experiments with GFAP and NG2 (Appendix A2.1).

The impact of short term cerebral hypoperfusion on OPC populations was also assessed using anti-NG2 immunohistochemistry and counting numbers of $NG2^+$ cells in the corpus callosum. This revealed two distinct populations of $NG2^+$ OPCs: one group had circular bipolar reactivity around the nucleus and few processes (‘early OPCs’) whilst the other group of cells were intensely stained and processed (‘late OPCs’; Figure 4.1C). A significant decrease in numbers of early $NG2^+$ OPCs was observed ($p = 0.007$; Figure 4.1D) however numbers of late $NG2^+$ OPCs were

unchanged following 3 days of hypoperfusion ($p = 0.80$; Figure 4.1E). The specificity of NG2 as a marker of OPCs was confirmed through double labelling with PDGFRα and PDGFβ (Appendix A2.2; Nishiyama et al., 1996).

4.3.2 Increased numbers of mature oligodendrocytes and restoration of early OPC populations following 1 month of cerebral hypoperfusion

The impact of longer term (1 month) of chronic cerebral hypoperfusion on numbers of mature oligodendrocytes and OPCs in the corpus callosum was also assessed. This revealed that numbers of $CC1^+$ mature oligodendrocytes were significantly increased in hypoperfused animals as compared to shams ($p = 0.007$; Figures 4.2A and 4.2B). No significant difference in numbers of $NG2^+$ early OPCs ($p = 0.281$) or late OPCs ($p = 0.719$) was observed between groups following 1 month of chronic cerebral hypoperfusion (Figures 4.2C and 4.2D respectively).

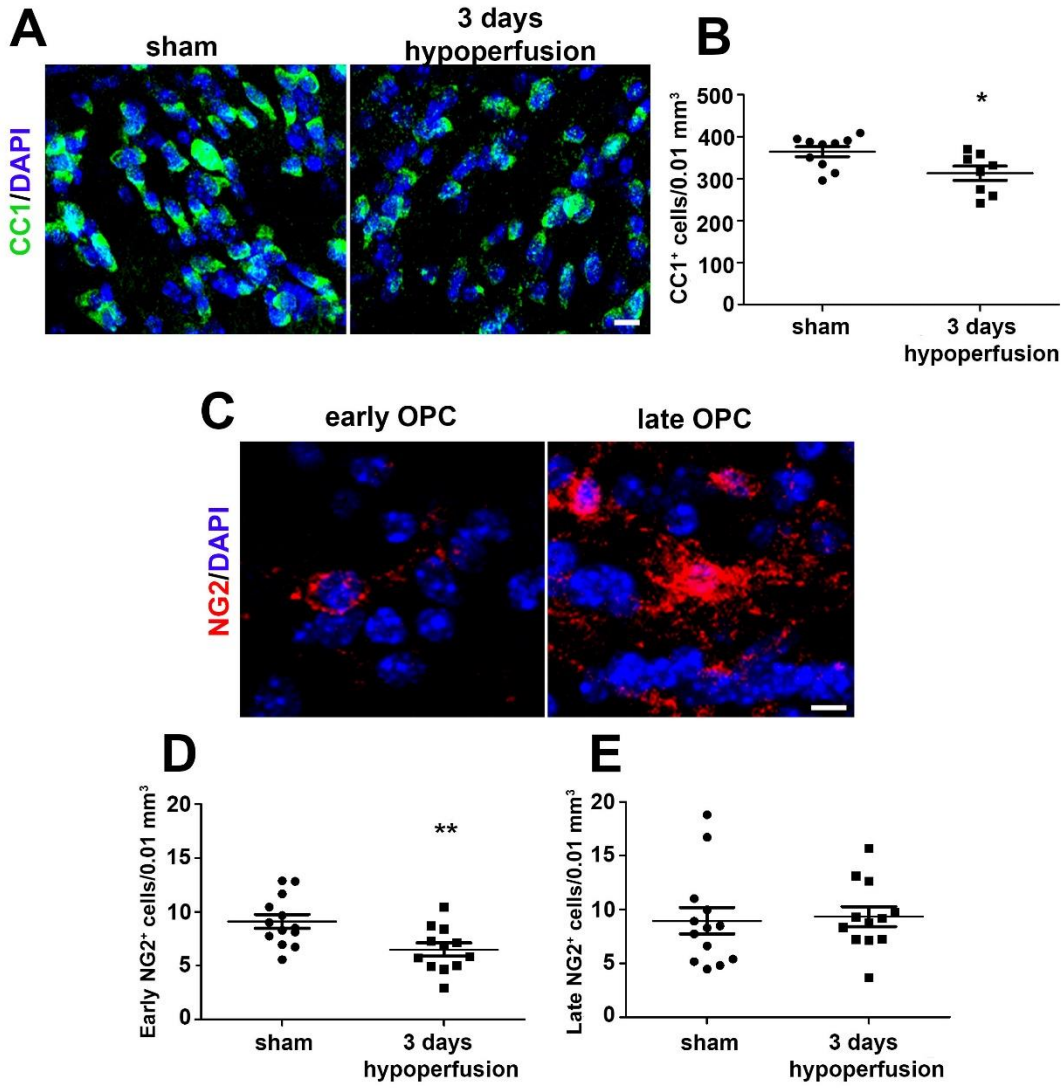

Figure 4.1: Decreased numbers of mature oligodendrocytes and OPCs following 3 days of cerebral hypoperfusion. (**A**) Representative confocal images showing CC1 labelling of mature oligodendrocyte cell bodies in the corpus callosum. Scale bar = 10 µm. (**B**) A significant decrease in the number of $CC1^+$ mature oligodendrocytes was observed after 3 days of cerebral hypoperfusion compared to sham controls ($p = 0.02$). (**C**) Representative confocal images showing morphology of early and late $NG2^+$ OPCs. Scale bar = 10 µm. (**D**) A significant decrease in the number of early $NG2^+$ OPCs was observed in the corpus callosum after 3 days of cerebral hypoperfusion ($p = 0.007$). (**E**) No significant difference in number of late $NG2^+$ OPCs was observed between groups following 3 days of cerebral hypoperfusion ($p = 0.80$). * $p = 0.02$, ** p 0.007 vs sham

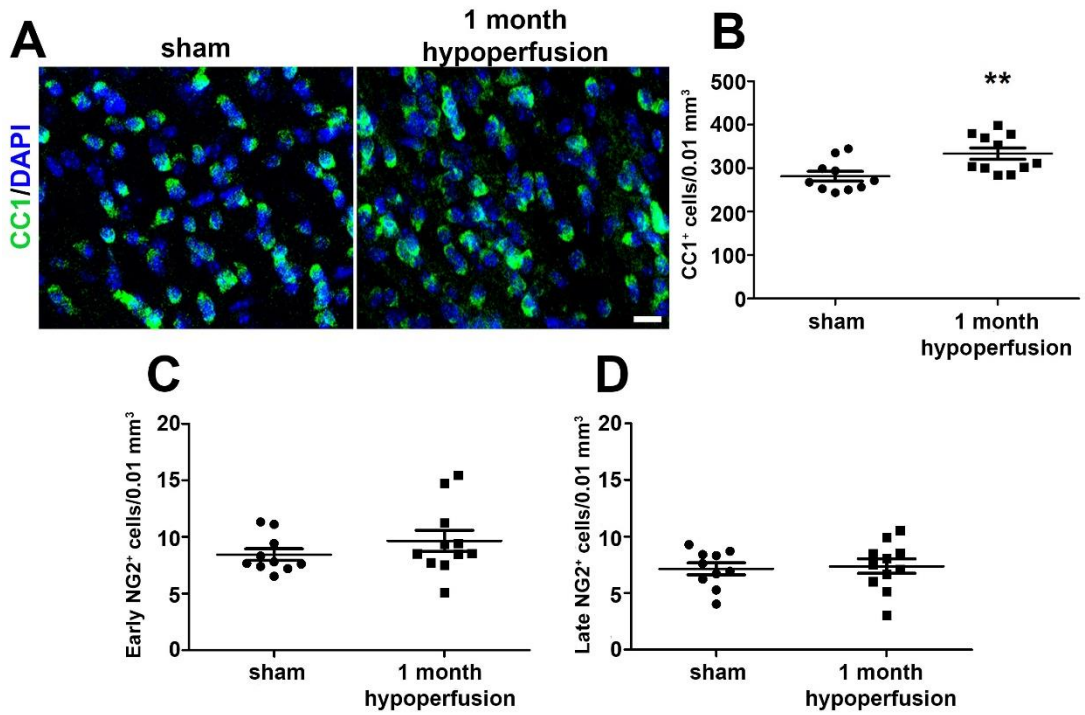

Figure 4.2: Increased numbers of mature oligodendrocytes and restoration of the early OPC pool following 1 month of chronic cerebral hypoperfusion. (**A**) Representative confocal images showing CC1 labelling of mature oligodendrocytes in the corpus callosum. Scale bar = 10 µm. (**B**) A significant increase in numbers of mature oligodendrocytes was observed in the corpus callosum following 1 month of cerebral hypoperfusion ($p = 0.007$). (**C**) Numbers of $NG2^+$ early OPCs were unchanged following 1 month of chronic cerebral hypoperfusion ($p = 0.281$). (**D**) Similarly, numbers of $NG2^+$ late OPCs were not different between groups following 1 month of hypoperfusion ($p = 0.719$). ** $p = 0.007$ vs sham

4.3.3 Altered proliferation of OPCs following 3 days and 1 month of chronic cerebral hypoperfusion

The unexpected finding of increased numbers of mature oligodendrocytes together with restored numbers of early OPCs following 1 month of hypoperfusion raised the question as to whether chronic cerebral hypoperfusion increased OPC proliferation. To test this and to determine the extent of proliferation following 3 days and 1 month of hypoperfusion, sections were labelled with proliferating cell nuclear antigen (PCNA) and numbers of positive cells counted in the corpus callosum (Figure 4.3A). This marker is acutely expressed by all cells during the S-phase of the cell cycle thus can be used to quantify numbers of proliferating cells. Cell counts revealed that total numbers of $PCNA^+$ cells were not significantly different between groups after 3 days ($p = 0.196$) or 1 month ($p = 0.564$) of hypoperfusion (Figures 4.3B and 4.3C respectively).

To specifically assess the extent of OPC proliferation, PCNA was used in combination with the oligodendroglial marker Olig2 and numbers of double labelled cells counted (Figure 4.3D). $PCNA^+/NG2^+$ double labelling could not be carried out due to the antibodies being raised in the same species. Whilst Olig2 is expressed throughout the oligodendrocyte lineage only OPCs have the ability to proliferate thus $PCNA^+/Olig2^+$ cells represent proliferating OPCs. Cell counts revealed that numbers of $PCNA^+/Olig2^+$ cells were significantly decreased after 3 days of hypoperfusion compared to sham controls ($p = 0.048$; Figure 4.3E). However, following 1 month of

cerebral hypoperfusion numbers of $PCNA^+/Olig2^+$ cells were not different between groups ($p = 0.264$; Figure 4.3F).

4.3.4 OPC differentiation following 1 month of chronic cerebral hypoperfusion

As PCNA is acutely expressed during the cell cycle, only cells actively proliferating at the time of termination will be labelled. This therefore represents a single 'snapshot' of proliferation. To further investigate the extent of proliferation following chronic cerebral hypoperfusion one cohort of animals received injections of the thymidine analogue BrdU which is incorporated into the DNA of proliferating cells and can be visualised using anti-BrdU immunohistochemistry. Importantly this approach allows cumulative labelling of proliferating cells during the period of BrdU administration and enables the phenotypic fate of proliferating cells to be determined. In the current study, animals received twice daily injections of BrdU for the first 3 days following surgery and were terminated following 1 month of hypoperfusion at which point numbers of $BrdU^+$ cells were counted. This revealed that $BrdU^+$ cells were present in 2 out of 9 of the sham control group and 5 out of 10 of the hypoperfused group although this difference did not reach statistical significance ($p = 0.157$; Figures 4.4A and 4.4B).

Finally, to assess whether newly generated $BrdU^+$ cells had differentiated into oligodendrocytes, $BrdU^+/CC1^+$ double labelling was carried out and numbers of double labelled cells were counted in the corpus callosum (Figure 4.4C). This

revealed that $BrdU^+/CC1^+$ cells were present in 3 out of 10 (30%) of hypoperfused mice but were absent in sham controls, however this difference did not reach statistical significance ($p = 0.09$; Figure 4.4D). Together these results indicate that chronic cerebral hypoperfusion does not increase OPC proliferation but demonstrates that a subset of cells generated following surgery have differentiated into mature oligodendrocytes.

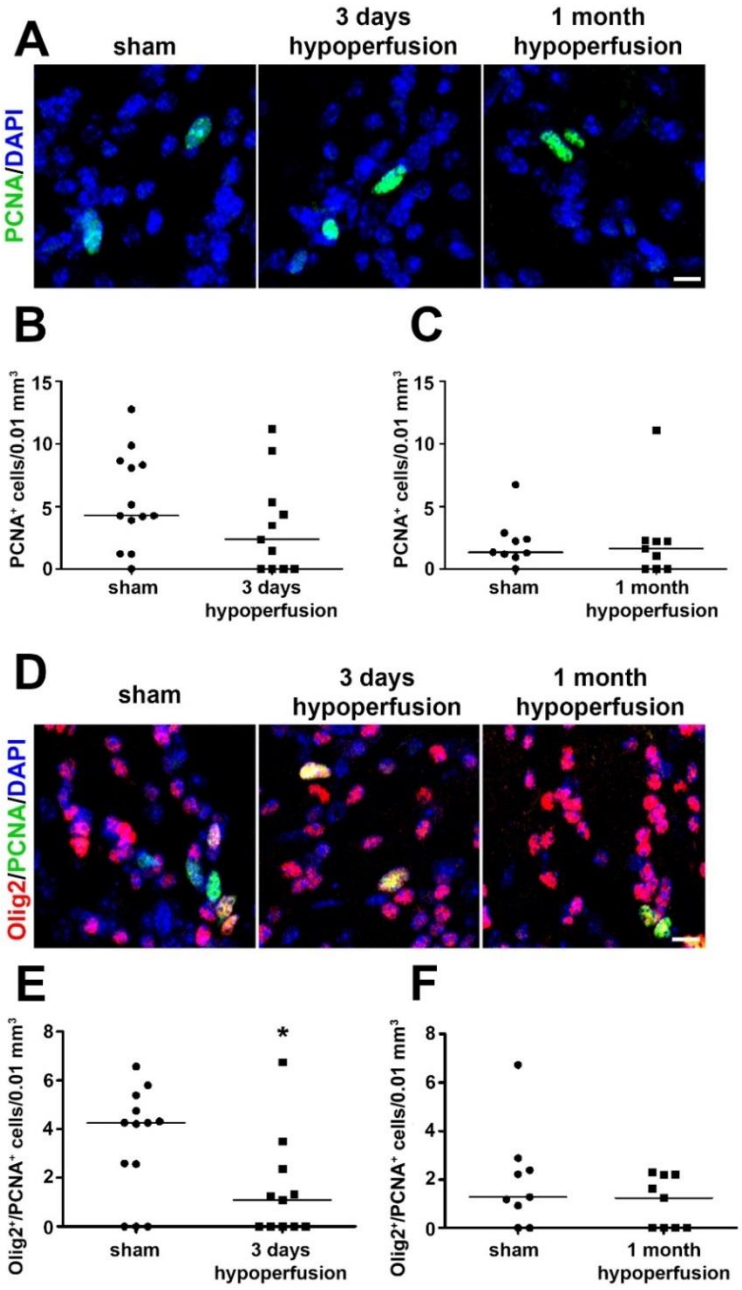

Figure 4.3: Low numbers of proliferating cells are observed in response to hypoperfusion. (**A**) Representative confocal images showing PCNA labelling in the corpus callosum. (**B**) No significant differences in numbers of $PCNA^+$ cells were observed between groups following 3 days ($p = 0.196$) or (**C**) 1 month ($p = 0.564$) of chronic cerebral hypoperfusion. (**D**) Representative confocal images showing Olig2/PCNA labelling of proliferating OPCs in the corpus callosum. (**E**) A significant decrease in numbers of $Olig2^+/PCNA^+$ cells was observed following 3 days of chronic cerebral hypoperfusion ($p = 0.048$). (**F**) Numbers of $Olig2^+/PCNA^+$ cells were not significantly different between groups following 1 month of cerebral hypoperfusion ($p = 0.264$). Scale bars = 10 µm. * $p = 0.048$ vs sham.

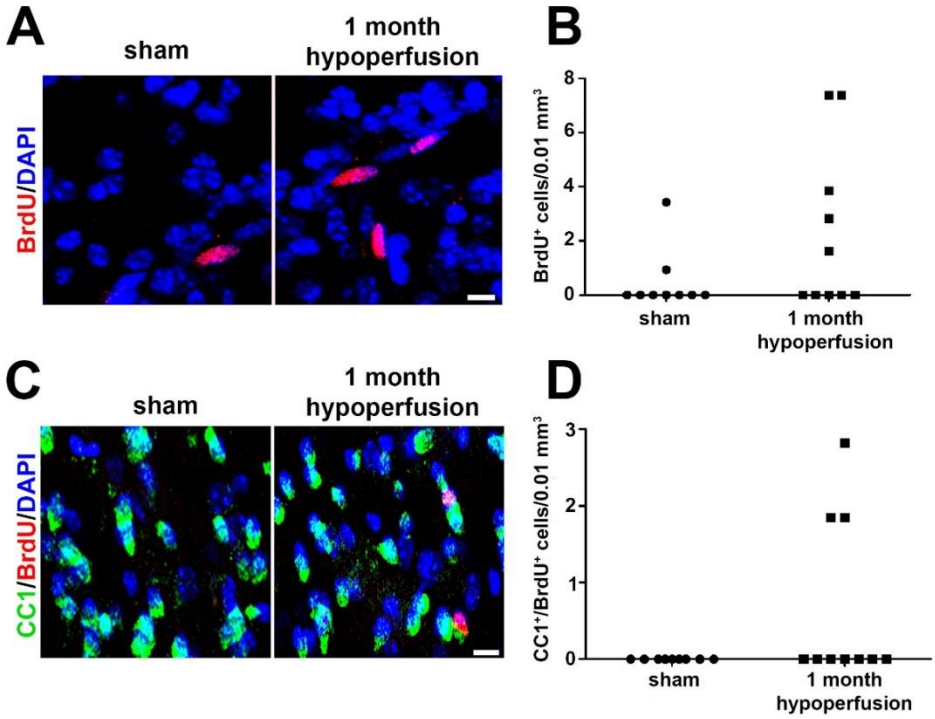

Figure 4.4: A proportion of newly generated cells differentiate into mature oligodendrocytes following 1 month of chronic cerebral hypoperfusion. (**A**) Representative confocal images showing $BrdU^+$ cells in the corpus callosum. (**B**) $BrdU^+$ cells were present in 2 out of 9 sham control animals and in 5 out of 10 hypoperfused animals but were not significantly different between groups ($p = 0.157$). (**C**) Representative confocal images showing $BrdU^+/CC1^+$ cells in the corpus callosum. (**D**) $CC1^+/BrdU^+$ double labelled cells were present in 3 out of 10 of the hypoperfused cohort but were completely absent from the sham control group. However as with numbers of $BrdU^+$ cells, this difference did not reach statistical significance ($p = 0.09$). Scale bars = 10 µm.

4.3.5 GPR17 expression is decreased in response to 3 days of chronic cerebral hypoperfusion

Recent studies have reported an emerging role for the GPR17 receptor in the regulation of OPC differentiation following cerebral ischaemia (Ciana et al., 2006; Lecca et al., 2008). To determine whether GPR17 activation was involved in differentiation of OPCs following chronic cerebral hypoperfusion, sections were stained for GPR17 (Figure 4.5A). GPR17/NG2 double labelling could not be carried out due to the antibodies being raised in the same species, therefore GPR17 expression within the oligodendrocyte lineage was determined using GPR17/Olig2 double labelling. This revealed that approximately 64% of $GPR17^{+}$ cells co-expressed Olig2 (Appendix A2.3) which is consistent with a previous report (Lecca et al., 2008).

Cell counts revealed that numbers of GPR17-expressing cells were not different between groups following 3 days ($p = 0.219$) or 1 month ($p = 0.172$) of chronic cerebral hypoperfusion (Figures 4.5B and 4.5C respectively). Despite no differences in numbers of GPR17 cells, a significant decrease in GPR17 receptor expression (as assessed by fluorescent intensity) was observed after 3 days of cerebral hypoperfusion ($p = 0.007$; Figure 4.5D). However following 1 month, GPR17 staining intensity was not different between groups ($p = 0.362$; Figure 4.5E).

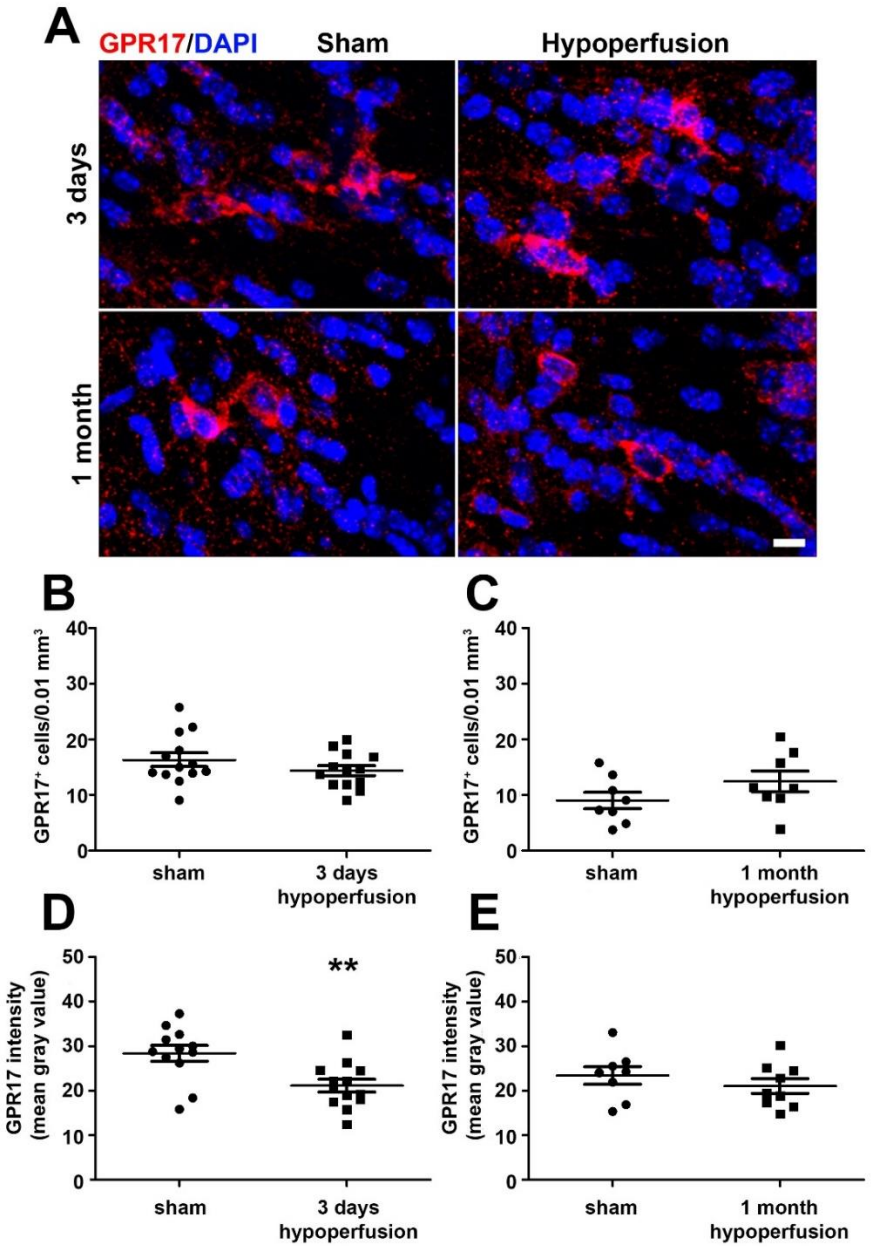

Figure 4.5: Decreased GPR17 staining intensity following 3 days of cerebral hypoperfusion. (**A**) Representative confocal images showing GPR17 labelling in the corpus callosum following 3 days and 1 month of chronic cerebral hypoperfusion. Scale bar = 10 µm. (**B**) Numbers of $GPR17^+$ cells were unchanged following 3 days ($p = 0.219$) and (**C**) 1 month ($p = 0.172$) of hypoperfusion. (**D**) The intensity of GPR17 staining was significantly decreased following 3 days of chronic cerebral hypoperfusion ($p = 0.007$). (**E**) Following 1 month of hypoperfusion, GPR17 staining intensity was not different between groups ($p = 0.362$). ** $p = 0.007$ vs sham

4.3.6 No difference in g-ratio of myelinated fibres following 3 days or 1 month of cerebral hypoperfusion

The current study revealed a significant decrease in mature oligodendrocyte number following 3 days of cerebral hypoperfusion with a significant increase in numbers of mature oligodendrocytes following 1 month. It has been estimated that a single oligodendrocyte can myelinate up to 50 individual internodes (Rivers et al., 2008) therefore the significant decrease and subsequent increase in oligodendrocyte number in response to cerebral hypoperfusion was predicted to influence the extent of myelination. Despite this, previous study revealed that chronic cerebral hypoperfusion resulted in a specific disruption to axon-glial connection in the absence of gross myelin changes (see Chapter 3; Reimer et al, 2011). To confirm previous findings and to further examine myelin structure following hypoperfusion, electron microscopy was carried out and the g-ratio (axonal diameter divided by fibre diameter) of myelinated axons was measured (Figure 4.6A). Analysis revealed no significant difference in g-ratio values between groups following 3 days ($p = 0.792$) or 1 month ($p = 0.692$) of hypoperfusion (Figure 4.6B). This finding is consistent with previous studies by the group demonstrating that the integrity of compact myelin is not altered following chronic cerebral hypoperfusion (see Chapter 3 and Reimer et al., 2011).

4.3.7 Cerebral blood flow is reduced in hypoperfused animals

Taken together the results from the current study demonstrate that mature oligodendrocytes and OPCs are lost early in response to cerebral hypoperfusion but that they are replaced over time resulting in increased numbers following 1 month of hypoperfusion as compared to shams. In addition compact myelin integrity following hypoperfusion is unchanged (Chapter 3; Reimer et al., 2011). These unexpected findings contrast with earlier studies using the model which report decreased numbers of mature oligodendrocytes together with myelin disruption (Fujita et al., 2010; Washida et al., 2010; Maki et al., 2011). One possible explanation for this discrepancy in findings may relate to the extent of CBF reduction induced following surgery, therefore laser speckle contrast imaging was used to assess CBF 24 hours prior to surgery (baseline), and at 3 days and 28 days following surgery (Figure 4.7A). This revealed that following 3 days of cerebral hypoperfusion, CBF was reduced to approximately 38% of sham levels ($p < 0.0001$; Figure 4.7B). After 28 days, CBF in hypoperfused animals had recovered slightly but was still approximately 20% lower than that observed in shams ($p = 0.002$; Figure 4.7C).

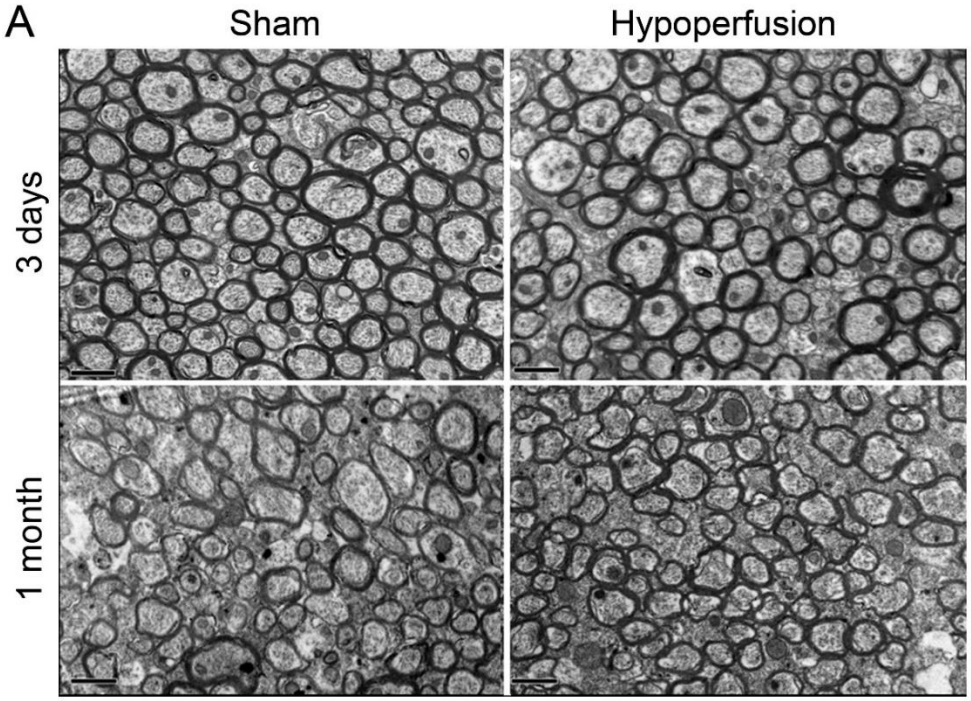

B

	Sham	Hypoperfusion
3 days	0.743 ± 0.005	0.746 ± 0.006
1 month	0.728 ± 0.002	0.725 ± 0.002

Figure 4.6: G-ratio is unchanged following 3 days and 1 month of chronic cerebral hypoperfusion. (**A**) Representative electron micrographs showing myelinated fibres in the corpus callosum following 3 days and 1 month of cerebral hypoperfusion. Scale bars = 1 µm. (**B**) G-ratio values were unchanged between sham and hypoperfused mice at both time points examined (3 days $p = 0.792$, 1 month $p = 0.962$).

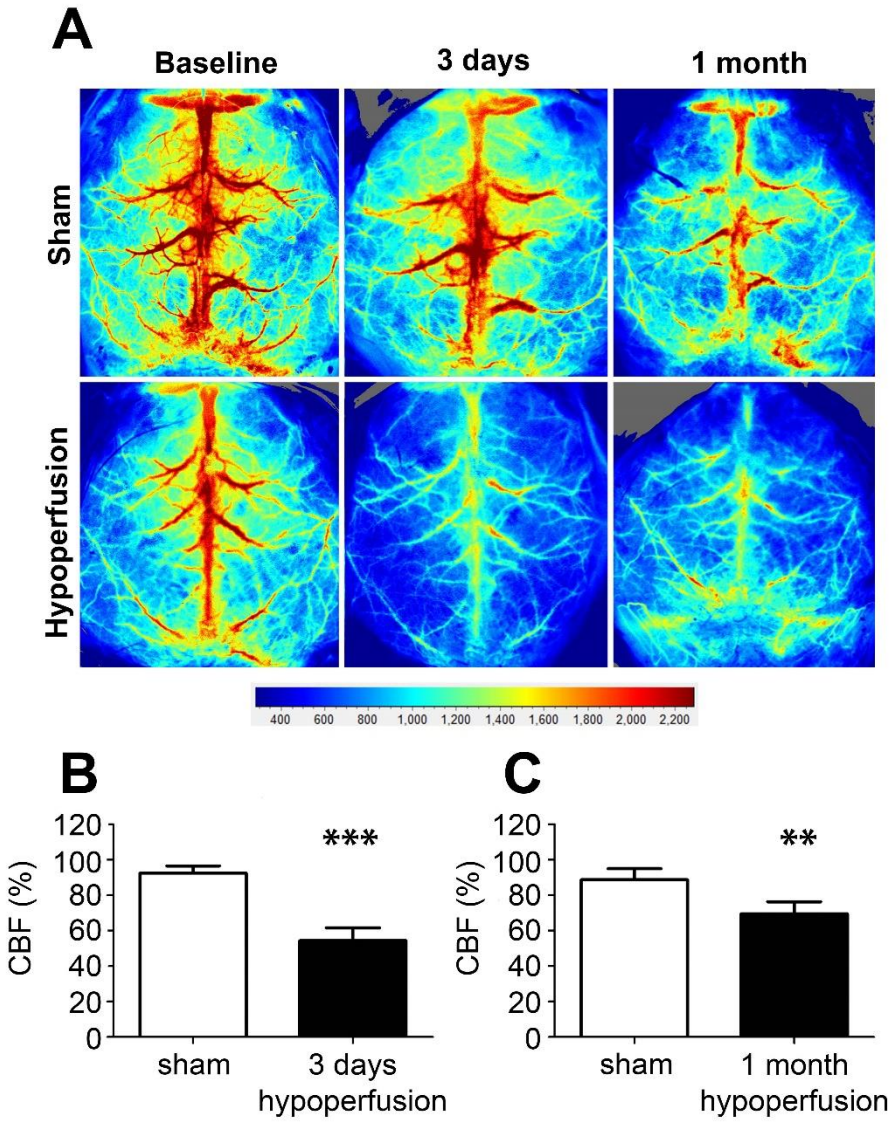

Figure 4.7: Cerebral blood flow is significantly reduced in hypoperfused animals. (**A**) Representative laser speckle images showing surface CBF through the intact skull at baseline, 3 days and 1 month after surgery. Images are the average of 100 frames acquired at 1 frame/second and are expressed in arbitrary perfusion units. (**B**) Following 3 days of hypoperfusion, CBF values were approximately 38% lower than those observed in sham animals (< 0.0001). (**C**) Following 28 days, there was a recovery in CBF such that values in hypoperfused animals were less than 20% of sham levels (p = 0.002) ** p = 0.002, *** p < 0.0001 vs sham

4.4 Discussion

At the outset of the study it was hypothesised that decreased numbers of oligodendrocyte and OPC pools would be observed following chronic cerebral hypoperfusion. However the results unexpectedly revealed that despite an initial loss of oligodendrocytes and OPCs early in response to hypoperfusion, these populations of cells recover over time resulting in increased numbers of mature oligodendrocytes and restoration of the OPC pool 1 month after surgery. Subsequent assessment of OPC proliferation demonstrated low numbers of proliferating cells but revealed that a subset of newly generated cells differentiated into mature oligodendrocytes however no significant difference was observed between sham and hypoperfused groups. In light of recent studies demonstrating a role for the GPR17 receptor in mediating OPC differentiation in response to cerebral ischaemia, the expression of GPR17 was examined. This revealed decreased expression of GPR17 following 3 days suggesting that this receptor was not involved in mediating the OPC response to cerebral hypoperfusion. Importantly the observed alterations to mature oligodendrocyte number did not influence the g-ratio of myelinated axons, confirming previous findings that chronic cerebral hypoperfusion does not lead to gross myelin disruption.

4.4.1 OPC proliferation and differentiation in response to hypoperfusion

The vulnerability of oligodendrocytes to severe reductions in CBF is well documented, with *in vivo* models of cerebral ischaemia demonstrating a loss of oligodendrocytes (Pantoni et al., 1996; Tanaka et al., 2003; McIver et al., 2010), occurring as early as 3 hours after reperfusion (Pantoni et al., 1996). Additionally, decreased numbers of oligodendrocytes have been reported following 1 month of chronic cerebral hypoperfusion in mouse (Fujita et al., 2010; Washida et al., 2010; Maki et al., 2011) suggesting that these cells are susceptible to even modest reductions in CBF. The current study sought to determine whether alterations to oligodendrocyte pools may explain previous findings of disruption to the domain structure of myelinated axons and impaired axon-glial connection following 3 days and 1 month of chronic cerebral hypoperfusion. Interestingly, this revealed increased numbers of mature oligodendrocytes and restoration of OPC populations following 1 month of chronic cerebral hypoperfusion raising the question of the source of these newly generated oligodendrocytes. The ability of OPCs to proliferate and differentiate in response to CNS injury is well characterised (Nait-Oumesmar et al., 1999; Levine et al., 2001) therefore it was hypothesised that increased proliferation and differentiation of OPCs was the likely mechanism underlying oligodendrogenesis in response to cerebral hypoperfusion. In support of this, upregulation of genes involved in proliferation has been demonstrated following 3 days of hypoperfusion (Reimer et al., 2011) and a very recent study has reported increased numbers of proliferating OPCs following 14 days of chronic cerebral hypoperfusion (Miyamoto et al., 2013c).

Immunohistochemical assessment of proliferation revealed numbers of $PCNA^+$ cells were unchanged between groups whilst numbers of $PCNA^+/Olig2^+$ OPCs were decreased following 3 days of hypoperfusion. Further assessment using BrdU which cumulatively labelled proliferating cells over the first 3 days following surgery revealed increased numbers of $BrdU^+$ cells in hypoperfused animals relative to shams however this was not statistically significant. Overall these data suggest there is not a significant upregulation of proliferation in the three day period following the onset of hypoperfusion. One possible explanation for these results is that the extent of proliferation has been underestimated in this study due to the methodological approaches used. It has been reported that the bioavailability of BrdU following systemic injection is 2 hours (Taupin, 2007) therefore in this study the total duration of BrdU incorporation per day was only 4 hours. This therefore represents a 'snapshot' of proliferation rather than a robust assessment. However, if mice had been given several BrdU injections per day this would be likely to cause considerable stress to the animals which itself may influence rates of proliferation (Gould et al., 1998). Additionally, BrdU is known to be toxic in high concentrations (Taupin, 2007) thus BrdU administration requires a fine balance between adequately labelling cells whilst avoiding toxicity. BrdU is commonly administered at doses of 50-100 mg/kg body weight without any adverse effects (Taupin, 2007). The dosing regimen used in this study (70 mg/kg body weight/day) is within this reported safe range therefore there is unlikely to be any BrdU-associated toxicity but it is likely that this approach has not been sufficient to label all proliferating cells. More recent studies are employing another thymidine analogue, EdU, as a superior alternative to BrdU (Chehrehasa et al., 2009; Young et al., 2013). Unlike BrdU, EdU labelling does not

require antigen retrieval and therefore is considered to be a more reliable marker of proliferation which may be important for future studies.

Whilst methodological approaches may explain the low numbers of proliferating cells observed in this study, it is also possible that the data are truly representative, i.e. hypoperfusion does not elicit a proliferative response at the time point studied. After 3 days of hypoperfusion, blood flow is reduced to around 62% and thus damage may still be evolving and alterations within the cellular microenvironment may impair the ability of cells to proliferate. As no intermediate time point was studied it is difficult to ascertain when, or if, a peak in proliferation occurs in response to cerebral hypoperfusion. A recent study has shown increased numbers of OPCs following 14 days of hypoperfusion (Miyamoto et al., 2013c) suggesting that proliferation may occur at a later time point than investigated in the current study. Indeed, in mice aged 2 months, the cell cycle time of OPCs in the corpus callosum is estimated to be approximately 10 days (Young et al., 2013) therefore it is perhaps unsurprising that low numbers of proliferating cells were observed following 3 days of hypoperfusion in the current study. An alternative explanation is that differentiation of existing OPCs may account for increased numbers of oligodendrocytes following 1 month of chronic cerebral hypoperfusion. In support of this, a study of focal cerebral ischaemia in rat has demonstrated regeneration of oligodendrocytes as early as 1 week post-reperfusion. The authors of this study reported low numbers of proliferating cells and concluded that increased oligodendrocyte number must be due to increased OPC differentiation rather than proliferation (McIver et al., 2010). Similarly, in the present study BrdU/CC1

labelling revealed that only a small number of newly generated cells differentiated into mature oligodendrocytes, however as indicated earlier the low numbers of cells labelled may be a technical limitation of BrdU labelling. Future studies should therefore employ a more robust assessment of OPC proliferation to fully address this.

4.4.2 Heterogeneity of $NG2^+$ OPCs

An interesting finding of the current study was the identification of two morphologically distinct types of cell with NG2 immunoreactivity, thought to correspond to early and late stage OPCs. Researchers within the field have hypothesised that two distinct populations of OPCs may exist: those which retain the ability to proliferate in response to injury and those which remain as post-mitotic OPCs (Dawson et al., 2000; Nishiyama et al., 2009). Indeed it is thought that $NG2^+$ OPCs with a simple, bipolar appearance are more likely to be true progenitor cells than their multi-processed counterparts, based on their morphological similarity to OPCs found during development (Horner et al., 2000; Reynolds et al., 2002; Watanabe et al., 2002). It has additionally been proposed that bipolar $NG2^+$ OPCs are more likely to be able to migrate to sites of injury in the adult CNS than multi-processed late stage OPCs (Watanabe et al., 2002). The current study revealed that numbers of early bipolar OPCs were decreased following 3 days of hypoperfusion whilst numbers of late OPCs were unchanged. If early OPCs are indeed the subset of cells with the ability to proliferate this may partly explain the low numbers of proliferating cells observed following 3 days of hypoperfusion. These findings

suggest that different subtypes exist within the OPC pool and may be differentially affected by cerebral hypoperfusion.

More recent studies have revealed that $NG2^+$ OPCs possess Na^+ channels and can generate action potentials (Karadottir et al., 2008) however there is disagreement within the literature as to whether all (De Biase et al., 2010) or subpopulations of NG2 cells (Karadottir et al., 2005) exert these physical properties. It has additionally been demonstrated that $NG2^+$ OPCs possess ionotropic NMDA, AMPA and kainate receptors (Bergles et al., 2000; Karadottir et al., 2008; De Biase et al., 2010) suggesting they may participate in intercellular signalling. $NG2^+$ cells have also been demonstrated to contact nodes of Ranvier (Butt et al., 1999), indicating that they may be able to respond to or influence neuronal activity (Levine et al., 2001). It has been argued that the molecular composition and corresponding functional characteristics of $NG2^+$ cells are not consistent with precursor cells again raising the question of whether subpopulations of cells exist within the larger $NG2^+$ cell pool. Additionally, differential receptor expression within $NG2^+$ populations may contribute to the vulnerability of early OPCs to cerebral hypoperfusion but future studies are required to fully elucidate differences in $NG2^+$ populations and their susceptibility to cerebral hypoperfusion.

4.4.3 Potential mechanisms underlying the OPC response to cerebral hypoperfusion

To investigate a potential mechanism underlying differentiation of OPCs following hypoperfusion, GPR17 labelling was carried out. GPR17 has recently been characterised as a receptor for cysteinyl-leukotrienes and uracil nucleotides which are released in high concentrations following ischaemic injury (Ciana et al., 2006; Lecca et al., 2008). Studies have shown that in response to ischaemia, GPR17 is upregulated and thus may act as a sensor of local damage (Ciana et al., 2006; Lecca et al., 2008). Critically, GPR17 is expressed by a subset of OPCs and pre-myelinating oligodendrocytes suggesting that receptor activation may be involved in the differentiation of OPCs in response to injury (Boda et al., 2011; Fumagalli et al., 2011). There is however conflicting evidence regarding the exact role of GPR17 in OPC differentiation. Whilst the majority of *in vitro* studies have demonstrated that activation of GPR17 promotes OPC differentiation, one study using GPR17 knockout and overexpressing mice has suggested that GPR17 activation inhibits OPC differentiation (Chen et al., 2009b) however the use of CNPase as a promoter of GPR17 expression in these studies has attracted some criticism. CNPase is expressed by mature oligodendrocytes thus it has been proposed that driving GPR17 expression in mature oligodendrocytes (rather than OPCs and immature oligodendrocytes which normally express GPR17) may have triggered apoptotic signalling cascades resulting in the conflicting evidence for the role of GPR17 in OPC differentiation (Ceruti et al., 2011).

In the current study, numbers of $GPR17^{+}$ cells were unchanged following either 3 days or 1 month of hypoperfusion but the labelling intensity was decreased in 3 day hypoperfused mice compared to controls. After 3 days of hypoperfusion, numbers of OPCs were decreased as compared to shams therefore was interesting to find that numbers of GPR17-expressing cells are unchanged at this time. It has been suggested that GPR17 is primarily expressed by immature pre-myelinating oligodendrocytes (Fumagalli et al., 2011) and therefore it is possible that cells at this stage of maturation are less susceptible to cerebral hypoperfusion that OPCs and mature oligodendrocytes. Another possibility is that surviving cells have upregulated GPR17 to compensate for the loss of other cells. A recent *in vitro* study using OPC cultures has demonstrated that GPR17-expressing cells are more sensitive to ATP-mediated cytotoxicity than non-expressing cells (Ceruti et al., 2011) however it remains to be determined whether this is also true *in vivo*. The downregulation of GPR17 expression following 3 days of hypoperfusion may therefore represent an attempt to limit ATP-mediated cell death or simply may be the result of low levels of its endogenous ligands. Taken together, the evidence regarding the role of GPR17 in OPC differentiation in response to injury is in many ways conflicting and future studies are required to fully clarify the function of this receptor.

The lack of evidence for involvement of GPR17 in mediating the OPC response to hypoperfusion suggests that other mechanisms may be involved. Previous studies have demonstrated that glutamate and ATP may play important roles in the regulation of OPC proliferation and differentiation. *In vitro* studies have demonstrated that glutamate inhibits OPC proliferation (Yuan et al., 1998) but

promotes OPC differentiation via NMDA receptor activation (Cavaliere et al., 2012). Similarly it has been demonstrated that ATP and related derivatives also inhibit proliferation whilst promoting OPC differentiation (Agresti et al., 2005). Thus glutamate and ATP mediated signalling following hypoperfusion may be acting to promote differentiation of existing OPCs.

4.4.4 Oligodendrocytes, myelin and axon-glial integrity

Although the current study revealed increased numbers of mature oligodendrocytes following one month of chronic cerebral hypoperfusion, it is not known whether these cells are myelinating or indeed capable of myelination. Mature oligodendrocytes were labelled using an antibody against the CC1 protein which labels oligodendrocyte cell bodies but not processes, and as a result cannot reliably distinguish between myelinating and non-myelinating oligodendrocytes. The results outlined in Chapter 3 demonstrate that axon-glial integrity is disrupted at this time point suggesting that these newly generated oligodendrocytes are not actively involved in myelin repair or remodelling. It is possible that these new oligodendrocytes are capable of myelinating but have not yet begun this process or that these cells are in some way deficient and unable to myelinate. A recent study investigating the effects of hyperoxia on developing white matter has demonstrated a rapid recovery of mature oligodendrocyte populations in the absence of increased levels of MBP and PLP proteins suggesting that these new oligodendrocytes are not myelinating (Ritter et al., 2013) however it remains to be determined whether this is also true in the adult brain. Two myelin proteins which are most vulnerable to

cerebral hypoperfusion are Nfasc155 (Reimer et al., 2011) and MAG (see Chapter 3 and Reimer et al., 2011), both of which are present within the most distal oligodendrocyte processes (Tait et al., 2000; Aboul-Enein et al., 2003). Future studies should investigate the localisation of Nfasc155 and MAG in response to long term hypoperfusion to determine whether these two proteins reappear over time, which would suggest that oligodendrocytes generated in response to hypoperfusion can contribute to white matter remodelling.

4.4.5 Extent of cerebral blood flow reduction following bilateral common carotid artery stenosis

The finding that numbers of mature oligodendrocytes were increased following 1 month of chronic cerebral hypoperfusion contrast with earlier studies using the model which show that numbers of mature oligodendrocytes remain significantly lower than shams following 1 month of hypoperfusion (Fujita et al., 2010; Washida et al., 2010; Maki et al., 2011; Seo et al., 2013). To test whether this discrepancy may be related to the extent of CBF reduction induced following surgery, CBF was measured following 3 days and 1 month of hypoperfusion. This revealed that following 3 days CBF was reduced by approximately 38% as compared to shams, recovering to around 20% by 1 month. These results are in keeping with previous studies in the model which show maximal decreases of approximately 25-37%, recovering to around 10-15% after 1 month (Shibata et al., 2004; Maki et al., 2011; Duan et al., 2012) therefore the differences between the findings presented in this thesis and findings by other groups are not due to differences in CBF.

Laser speckle contrast imaging is a widely used alternative to laser Doppler imaging. As with laser Doppler, a key advantage of laser speckle imaging is that measurements can be carried out non-invasively through the intact skull thus avoiding complications of possible surgical trauma (Ayata et al., 2004). Additionally this technique allows visualisation of the entire exposed cortical surface unlike cranial window preparations or laser Doppler which only allow measurement of CBF in a defined area. One drawback of laser speckle imaging is the penetration depth of approximately 500 µm to 1 mm (Dunn et al., 2001) which only allows measurement of CBF in the most superficial cortical vessels and thus does not necessarily reflect changes in the white matter. An additional disadvantage of laser speckle imaging is that CBF is measured in arbitrary units rather than absolute values therefore values need to be expressed relative to baseline and raw values cannot be compared between animals (Ayata et al., 2004). In the current study care was taken to prevent drying out of the skull however despite these efforts there were occasionally artefacts on the skull that prevented accurate measurement of perfusion within the affected area. Additionally, increased opacity of the skull was evident in the majority of animals by day 28 which is likely to influence CBF measurements. Indeed, CBF values for sham animals were reduced by approximately 11% from baseline following 28 days, which is most likely artifactual rather than a biological decrease in CBF. However despite these drawbacks, laser speckle contrast imaging is a useful tool to non-invasively assess longitudinal changes in CBF.

Another factor which may be important in understanding the differences between the findings of current study and other studies is the different approaches used to assess

oligodendrocyte number. Mature oligodendrocytes were identified in the current study using an antibody against the CC1 protein, a commonly used marker of mature oligodendrocytes (Ness et al., 2005) and double labelling experiments confirmed the specificity of this marker (Appendix A2). Assessment of oligodendrocyte numbers in other studies has been carried out using glutathione S-transferase π (GSTπ) which is also accepted as marker of mature oligodendrocytes however some studies have reported that GSTπ antibodies may additionally label astrocytes (Cammer and Zhang, 1993) and OPCs (Tamura et al., 2007). In addition, the current study used confocal laser scanning microscopy in thick tissue sections whereas other studies have used light microscopy in much thinner sections. The use of confocal microscopy allows a 3D picture of the staining to be acquired unlike conventional light microscopy which only depicts the staining on the surface of the section. Therefore stereological cell counts from a confocal z-stack are likely to be more representative than cell counts carried out using single plane images acquired at a light microscope. Furthermore, as outlined in Section 3.4.2, there may be subtle strain related differences in cerebrovascular integrity between C57Bl/6J mice from different suppliers in different countries which may affect the resulting pathology following chronic cerebral hypoperfusion and may explain the differences in findings between groups.

4.4.6 Summary and conclusions

The findings presented in this chapter demonstrate that mature oligodendrocytes and OPCs are initially lost following chronic cerebral hypoperfusion but that these populations of cells recover over time. Importantly the results suggest that differentiation of existing OPCs contributed to the increase in mature oligodendrocyte number observed following 1 month of hypoperfusion and that this is not associated with GPR17 upregulation. In support of previous findings, the g-ratio of myelinated axons (an index of the thickeness of the compact myelin sheath) was unchanged suggesting that although a loss of mature oligodendrocytes was observed in response to 3 days of hypoperfusion there was no downstream impact on compact myelin integrity. Despite this, the results presented in Chapter 3 demonstrate that axon-glial integrity remains disrupted following 1 month of hypoperfusion suggesting that although an increase in mature oligodendrocyte number was observed at this time, these cells may either be not yet myelinating or are incapble of myelination. In the next chapter the effects of modulation of inflammation and oxidative stress on myelin and axonal integrity and numbers of oligodendroglial cells will be examined to determine whether this may represent an appropriate therapeutic strategy for chronic cerebral hypoperfusion.

Chapter 5

The effects of dimethyl fumarate treatment on white matter structure and function following severe chronic cerebral hypoperfusion

5.1 Introduction

The results presented in this thesis demonstrate that chronic cerebral hypoperfusion results in disruption to nodal and paranodal domains of myelinated axons and alterations to oligodendrocyte pools, however the underlying mechanisms remain to be determined. Increased expression of inflammatory signalling cascades have been reported following 3 days of hypoperfusion (Reimer et al., 2011) and increased numbers of microglia are observed following 1 month (see Chapter 3; Shibata et al., 2004; Coltman et al., 2011) suggesting that increased inflammation may contribute to white matter damage following chronic cerebral hypoperfusion. Furthermore, recent studies have demonstrated that oxidative stress may also be an important mediator of white matter damage following hypoperfusion. Administration of the free radical scavenger edaravone has been shown to reduce myelin damage and restore numbers of oligodendrocytes following 1 month of chronic cerebral hypoperfusion in mice (Miyamoto et al., 2013b). In addition, an association between white matter hyperintensities and biochemical markers of oxidative stress has been reported in a human post-mortem study (Back et al., 2011). Taken together these studies indicate that increased inflammation and oxidative stress may contribute to white matter damage following chronic cerebral hypoperfusion.

A key mechanism by which cells mediate antioxidant and anti-inflammatory responses occurs at the transcriptional level through activation of Nrf2. A number of recent studies have demonstrated that pharmacological activation of Nrf2 using DMF

can exert powerful protective effects on white matter integrity. Specifically, DMF treatment has been demonstrated to decrease neuroinflammation (Schilling et al., 2006), ameliorate myelin and axonal pathology, protect against oxidative stress-mediated cell death and improve clinical score in mice subject to EAE (Linker et al., 2011). This has led to clinical trials involving DMF (BG-12; Fox et al., 2012; Gold et al., 2012) which revealed significantly improved disease outcome and neuroradiological measures of white matter integrity, resulting in its licencing as an MS treatment in the US. Importantly, in models of focal cerebral ischaemia treatment with alternative Nrf2-activating compounds has been demonstrated to significantly decrease infarct volume and improve neurological outcome following reperfusion (Shih et al., 2005; Son et al., 2010; Zhang et al., 2012). Taken together these studies suggest that DMF may exert beneficial effects on white matter structure and function following chronic cerebral hypoperfusion. This was examined in the current study using the mixed coil model of severe chronic cerebral hypoperfusion which was used to induce more pronounced white matter pathology (Miki et al., 2009).

5.1.1 Study hypothesis and aims

It was hypothesised that treatment with DMF would ameliorate structural and functional alterations to white matter following chronic cerebral hypoperfusion. The specific aims of the study were to characterise the effects of severe cerebral hypoperfusion on myelin and axonal integrity and oligodendroglial populations and to determine whether treatment with DMF ameliorated any observed changes. A

related aim was to use electrophysiology to assess functional alterations of myelinated axons in response to DMF treatment following severe hypoperfusion.

5.2 Methods

5.2.1 Animals and surgery

Adult male C57Bl/6J mice (~25 g, aged 3-4 months) underwent chronic cerebral hypoperfusion or sham surgery as described in Section 2.2. A 0.18 mm internal diameter microcoil was fitted to the left common carotid artery and a 0.16 mm microcoil fitted to the right common carotid artery (Miki et al., 2009). Mice were terminated 7 days following surgery.

Two cohorts of animals were used: cohort 1 to assess CBF and pathological alterations and cohort 2 to assess electrophysiological changes following hypoperfusion. Initial cohort sizes used in the study are shown in Table 5.1.

5.2.2 Administration of dimethyl fumarate

DMF was administered twice daily as described in Section 2.7.

Table 5.1: Initial group numbers for DMF study

	Sham		**Hypoperfusion**	
	Vehicle	DMF	Vehicle	DMF
Cohort 1	7	8	15	11
Cohort 2	-	-	16	13

5.2.3 Laser speckle contrast imaging and analysis

CBF was measured using laser speckle flowmetry as described in Section 2.3. Baseline recordings were acquired 2 days prior to surgery with subsequent recordings carried out at 1 day and 7 days following surgery.

5.2.4 Electrophysiology

Electrophysiology was carried out as described in Section 2.5.

5.2.5 Transcardial perfusion and tissue processing

Seven days following surgery animals from cohort 1 were deeply anaesthetised with 5% isoflurane and transcardially perfused as described in Section 2.8.1. Brains were then processed and cut into 30 µm coronal sections using a cryostat as described in Section 2.8.3.

5.2.6 Immunohistochemistry

Immunohistochemistry was carried out as described in Section 2.10.2. Anti-MBP and APP antibodies were used to assess myelin and axonal integrity. Anti-CC1 and NG2 antibodies were used to assess mature oligodendrocytes and OPCs respectively.

5.2.7 Confocal and fluorescent microscopy

All images were acquired at 20x magnification in the corpus callosum as shown in Figure 2.3B. Confocal microscopy was carried out as described in Section 2.11.1. Images of APP labelling were acquired using a Zeiss AX10 fluorescent microscope as described in Section 2.11.2.

5.2.8 Image analysis

Image analysis was carried out as described in Section 2.12. One image from each hemisphere was analysed and mean values calculated per animal.

5.2.9 Statistical analysis

Data were analysed using a 2-way ANOVA followed by Student's *t*-test with Bonferroni correction for multiple comparisons. Analysis of animal survival following surgery was performed using Kaplan-Meier curves and corresponding data analysed using a log-rank (Mantel-Cox) test. For electrophysiology data the peak latency of the response of myelinated and unmyelinated fibres was measured per animal and student's *t*-test was used to compare groups.

5.3 Results

5.3.1 Decreased MBP intensity following severe cerebral hypoperfusion in vehicle- treated mice but not in DMF-treated mice

Myelin disruption is consistently observed following severe reductions in CBF (Pantoni et al., 1996; Dewar et al., 2003). Importantly, DMF administration to mice subject to EAE has shown a protective effect of the drug on myelin integrity (Linker et al., 2011). Therefore to assess myelin integrity following severe hypoperfusion and to determine whether DMF treatment could ameliorate any observed changes, MBP labelling was carried out and the intensity of staining was measured (Figure 5.1A). Statistical analysis revealed that there was no significant effect of DMF treatment ($F_{(1, 33)} = 1.414$, $p = 0.243$, 2-way ANOVA) however an overall significant effect of surgery ($F_{(1, 33)} = 8.103$, $p = 0.008$, 2-way ANOVA) was observed between groups. Post-hoc *t*-tests showed a significant decrease in MBP labelling intensity in vehicle-treated hypoperfused animals as compared to shams ($p = 0.005$) with no difference in MBP labelling intensity between DMF-treated sham and hypoperfused groups ($p = 0.312$; Figure 5.1B). There was no significant difference between vehicle and DMF-treated sham groups ($p = 0.1775$).

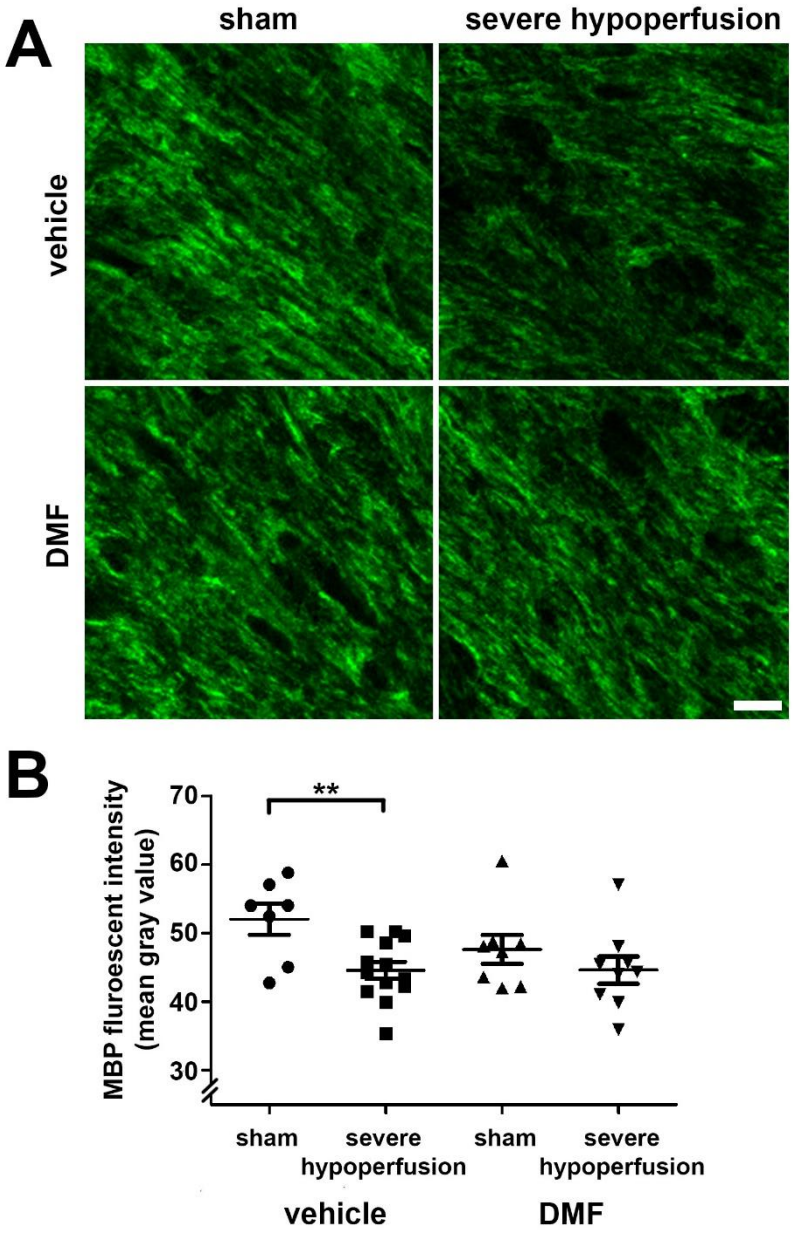

Figure 5.1: MBP intensity is decreased in vehicle-treated animals but not in DMF-treated animals following severe hypoperfusion. (**A**) Representative confocal images showing MBP labelling in the corpus callosum. Scale bar = 25 µm. (**B**) MBP labelling intensity was significantly decreased in vehicle-treated hypoperfused animals compared to respective shams ($p = 0.005$). No significant difference in MBP labelling intensity was observed between DMF-treated hypoperfused mice as compared to shams ($p = 0.312$). Despite apparent differences in the distribution of intensity values between vehicle-treated and DMF-treated sham animals, there was no significant difference between groups. ** $p = 0.005$ vs sham

5.3.2 Increased numbers of oligodendrocytes in DMF-treated sham animals

Previous study has demonstrated the vulnerability of mature oligodendrocytes to reduced CBF, with a significant decrease in mature oligodendrocytes observed following 3 days of modest cerebral hypoperfusion (see Chapter 4). To investigate the impact of severe cerebral hypoperfusion on mature oligodendrocyte populations and to determine whether observed changes in myelin integrity may be a consequence of reduced oligodendrocyte numbers, CC1 immunohistochemistry was carried out and numbers of $CC1^+$ mature oligodendrocytes in the corpus callosum were counted (Figure 5.2A). Analysis revealed an overall significant effect of DMF treatment on mature oligodendrocyte number ($F_{(1, 33)} = 9.699$, $p = 0.004$, 2-way ANOVA) but no effect of surgery ($F_{(1, 33)} = 2.488$, $p = 0.179$, 2-way ANOVA). Surprisingly, post-hoc *t*-tests revealed a significant increase in oligodendrocyte number in DMF-treated shams as compared to vehicle-treated animals ($p = 0.003$; Figure 5.2B). No significant differences were observed between vehicle-treated sham or hypoperfused animals, however numbers of oligodendrocytes were significantly increased in DMF-treated shams as compared to respective hypoperfused animals (Figure 5.2B). Therefore whilst no differences in mature oligodendrocyte number were observed following severe cerebral hypoperfusion, an increase in the number of mature oligodendrocytes was observed as a result of DMF treatment alone.

5.3.3 Numbers of oligodendrocyte precursor cells are unchanged following severe hypoperfusion

The vulnerability of OPCs to modest hypoperfusion has also been demonstrated previously (see Chapter 4) therefore to characterise the effect of severe hypoperfusion on OPC populations, NG2 labelling was carried out and numbers of $NG2^+$ OPCs were counted (Figure 5.3A). Unlike previous study (Chapter 4) $NG2^+$ cells could not be distinguished by early and late morphology due to the use of differently processed tissue. Statistical analysis revealed that numbers of OPCs were not altered with surgery ($F_{(1, 33)} = 0.071$, $p = 0.791$, 2-way ANOVA) or DMF-treatment (Figure 5.3B; $F_{(1, 33)} = 1.349$, $p = 0.254$). These data demonstrate that numbers of $NG2^+$ OPCs were not altered in response to severe hypoperfusion or DMF treatment.

5.3.4 Extent of axonal pathology following severe cerebral hypoperfusion is similar in vehicle and DMF-treated groups

The results from the current study revealed that myelin integrity in vehicle-treated animals was decreased following severe cerebral hypoperfusion as compared to sham controls but importantly this difference was not observed in DMF-treated animals. In addition to myelin pathology, axonal pathology has been reported in this model of severe cerebral hypoperfusion (Miki et al., 2009) therefore the extent of axonal pathology in vehicle and DMF-treated groups was assessed in the current study using amyloid precursor protein (APP) labelling (Figure 5.4A) and the density of staining measured. APP is normally transported along axons and is not detected in healthy

axons however following axonal damage, APP accumulation is observed in the form of APP^+ axonal bulbs (Cochran et al., 1991; Ohgami et al., 1992; Suenaga et al., 1994). Image analysis revealed that 2 out of 13 vehicle-treated animals and 4 out of 9 DMF-treated animals exhibited positive APP^+ labelling in the corpus callosum following severe chronic cerebral hypoperfusion. Statistical analysis revealed no significant effect of surgery ($F_{(1, 33)} = 4.110$, $p = 0.051$, 2-way ANOVA) or DMF-treatment ($F_{(1, 33)} = 1.751$, $p = 0.051$, 2-way ANOVA) on the extent of axonal pathology between groups (Figure 5.4B).

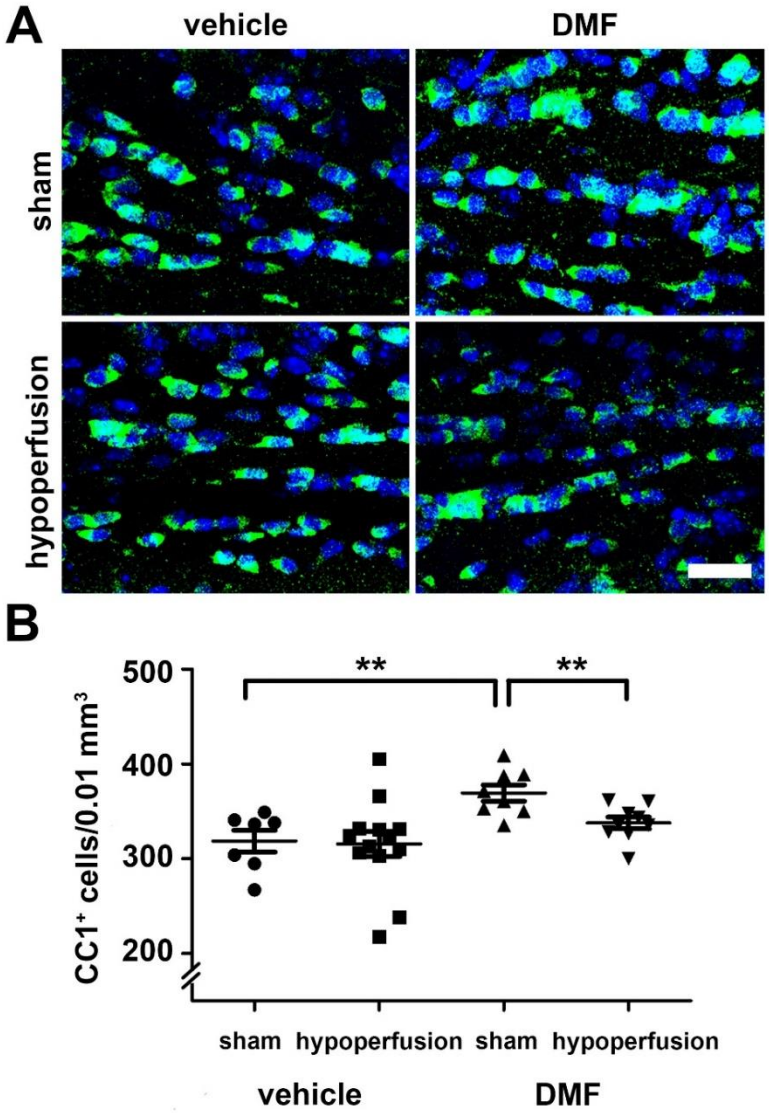

Figure 5.2: Increased numbers of mature oligodendrocytes in DMF-treated sham animals. (**A**) Representative confocal images showing $CC1^+$ mature oligodendrocytes in the corpus callosum. Scale bar = 20 µm. (**B**) No significant difference in mature oligodendrocyte number was observed between groups in vehicle-treated mice. However, DMF-treated sham animals had significantly higher numbers of mature oligodendrocytes than vehicle-treated shams and DMF-treated hypoperfused animals. ** p = 0.003 vs sham and p = 0.009 vs sham in vehicle-treated and DMF-treated groups respectively.

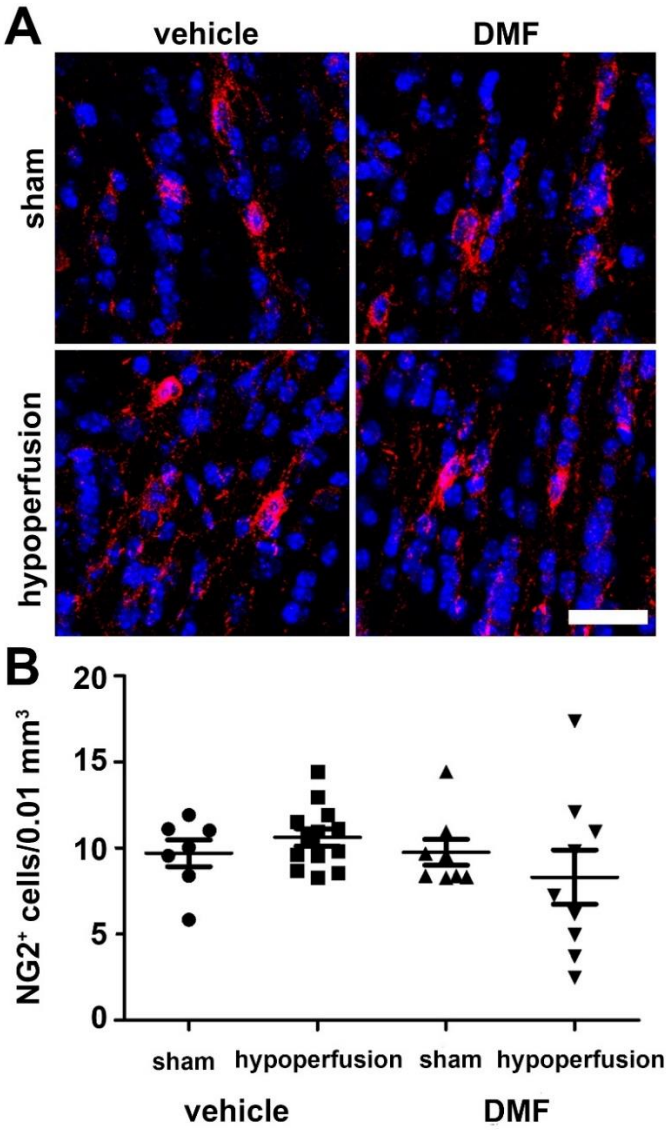

Figure 5.3: Numbers of OPCs are not altered by hypoperfusion or DMF treatment. (**A**) Representative confocal images showing $NG2^+$ OPCs in the corpus callosum. Scale bar = 20 µm. (**B**) Numbers of $NG2^+$ cells were not altered in response to severe cerebral hypoperfusion in either vehicle or DMF-treated groups.

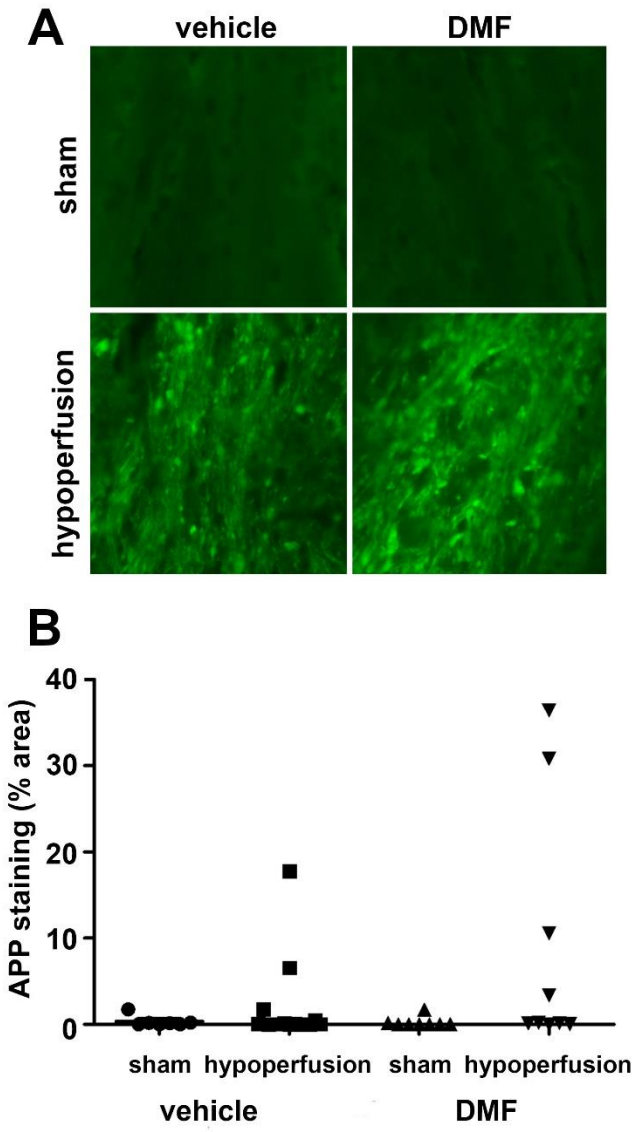

Figure 5.4 DMF does not influence the extent of axonal pathology following severe chronic cerebral hypoperfusion. (**A**) Representative images showing APP staining in the corpus callosum in sham and hypoperfused animals. APP^{+} axonal bulbs were present in a proportion of hypoperfused animals but were not observed in sham controls. Scale bar = 20 µm. (**B**) No significant difference in the percentage of APP labelling was observed following hypoperfusion between vehicle and DMF-treated groups.

5.3.5 Cerebral blood flow is reduced in hypoperfused mice but is not altered by DMF treatment

The finding that myelin integrity was not significantly different between DMF-treated sham and hypoperfused groups was indicative of a beneficial effect of DMF treatment. To exclude the possibility that the apparent beneficial effects of DMF treatment were due to DMF-mediated modulation of CBF, laser speckle contrast imaging was carried out.

Baseline CBF was measured 2 days prior to surgery and subsequent recordings were acquired at 1 day and 7 days after surgery (Figure 5.5A). This demonstrated that following 1 day of severe hypoperfusion CBF was reduced to approximately 47.6 ± 5.60% and 54.0 ± 5.63% of baseline values in vehicle and DMF-treated animals respectively. CBF in sham animals was approximately 110.8 ± 8.55% in the vehicle-treated group and 122.4 ± 5.90% in the DMF-treated group (Figure 5.5B). Statistical analysis revealed a significant effect of surgery ($F_{(1, 33)} = 222.6$, $p < 0.0001$) but no effect of DMF treatment ($F_{(1, 33)} = 0.041$, $p = 0.842$). Following 7 days of hypoperfusion, CBF values were approximately 44.1 ± 6.30% of baseline in vehicle-treated mice, whilst values for DMF-treated animals were similar at approximately 42.6 ± 5.71% of baseline (Figure 5.5C). CBF values for sham animals were 79.3 ± 5.40% and 89.8 ± 4.07% in vehicle and DMF-treated groups respectively. Statistical analysis again revealed a significant effect of surgery ($F_{(1, 33)} = 55.01$, $p < 0.0001$) but no effect of DMF treatment ($F_{(1, 33)} = 0.002$, $p = 0.969$). Individual data for each animal are shown in Appendix A3.1. Together these results demonstrate that CBF is

significantly decreased following 1 day and 7 days of chronic cerebral hypoperfusion as compared to shams however no differences were observed at any time point between vehicle and DMF-treated animals in either sham or hypoperfused groups, suggesting that DMF treatment does not alter cerebral blood flow.

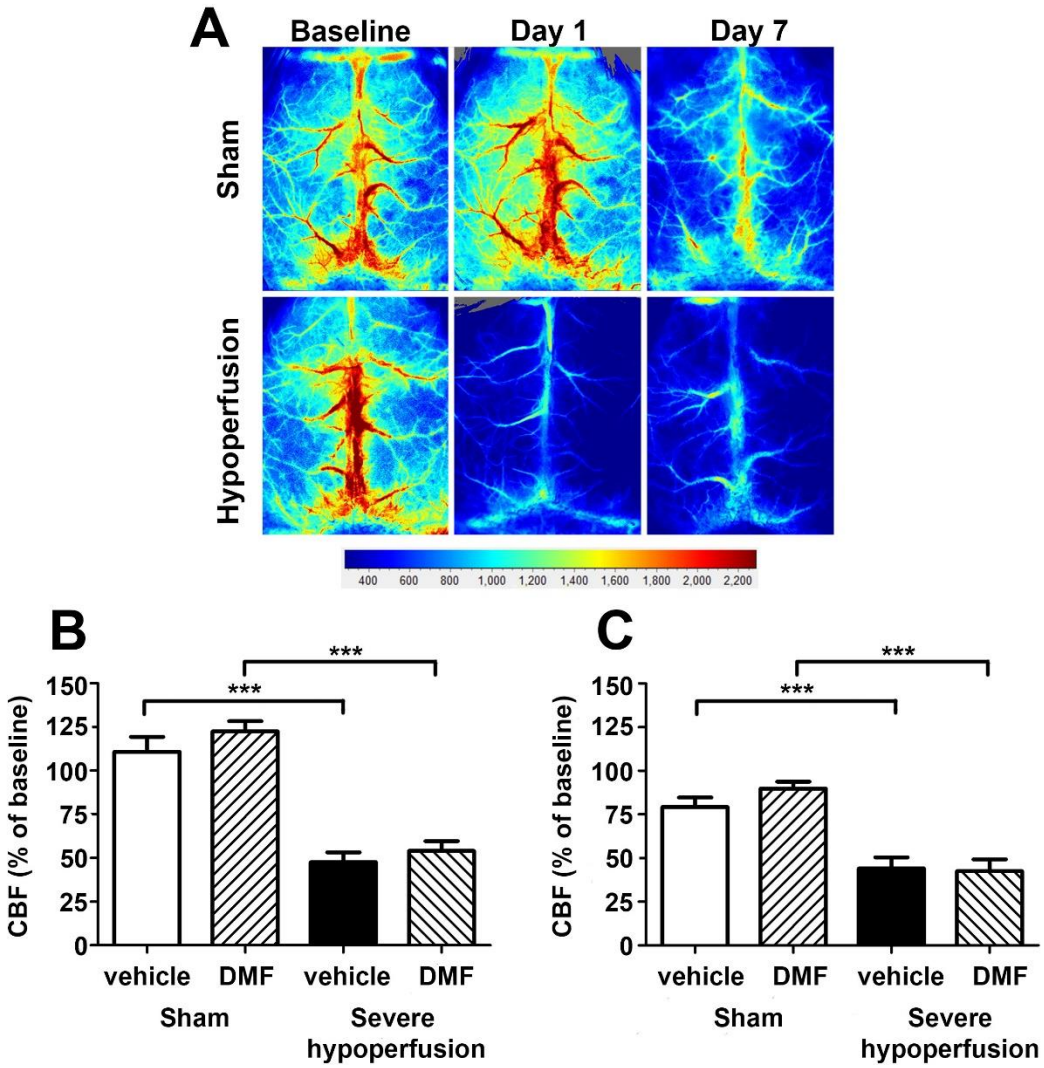

Figure 5.5: Cerebral blood flow is reduced in hypoperfused mice and is not altered by DMF treatment. (**A**) Representative laser speckle images showing cortical blood flow through the intact skull of sham and hypoperfused mice. (**B**) Following 1 day of severe hypoperfusion, CBF values were approximately 47.6 ± 5.60% and 54.0 ± 5.63% of baseline values in vehicle and DMF-treated animals respectively. In sham animals CBF was approximately 110.8 ± 8.55% in the vehicle-treated group and 122.4 ± 5.90% in the DMF-treated group. (**C**) Following 7 days of severe hypoperfusion, CBF values had decreased to around 44.1 ± 6.30% of baseline in vehicle-treated mice and to 42.6 ± 5.71% of baseline in DMF-treated mice. CBF values for sham animals were 79.3 ± 5.40% and 89.8 ± 4.07% in vehicle and DMF-treated groups respectively. *** $p < 0.0001$ vs respective sham controls

5.3.6 Conduction velocity of myelinated axons is improved in DMF-treated animals

To investigate whether DMF had a protective effect on the function of myelinated axons, electrophysiology in slice preparations was carried out and the conduction velocity was measured in the corpus callosum (Figure 5.6A). The peak latency of the initial N1 component followed by the slower N2 component of the CAP were measured, corresponding to myelinated and unmyelinated axons respectively (Figure 5.6B; Crawford et al., 2009) and conduction velocity was calculated by dividing the distance between electrodes (2.5 mm) by the latency of the response. Previous studies by the group have revealed a significant decrease in the conduction velocity of myelinated axons following severe hypoperfusion as compared to shams (Appendix A3.2). Therefore to determine the effects of DMF treatment electrophysiology experiments were restricted to hypoperfused animals only. This revealed that conduction velocity was significantly increased in DMF-treated compared to vehicle-treated mice ($p = 0.04$; Figure 5.6C). An increase in the conduction velocity of unmyelinated axons was also observed however this failed to reach statistical significance ($p = 0.054$; Figure 5.6D).

5.3.7 DMF treatment does not improve survival following severe chronic cerebral hypoperfusion

In light of the findings that DMF exerted beneficial effects on myelin integrity and conduction velocity, the survival rate of vehicle and DMF-treated animals was examined to determine whether DMF improved survival following severe hypoperfusion. Animals were closely monitored following surgery and those displaying a poor recovery were culled (Figure 5.7A). Survival rate in vehicle-treated hypoperfused mice was 80.6%, in line with previously reported findings (Miki et al., 2009). The survival rate of DMF-treated animals was approximately 87.5% (Figure 5.7B) however this difference between groups was not significantly different ($p = 0.458$, log-rank test).

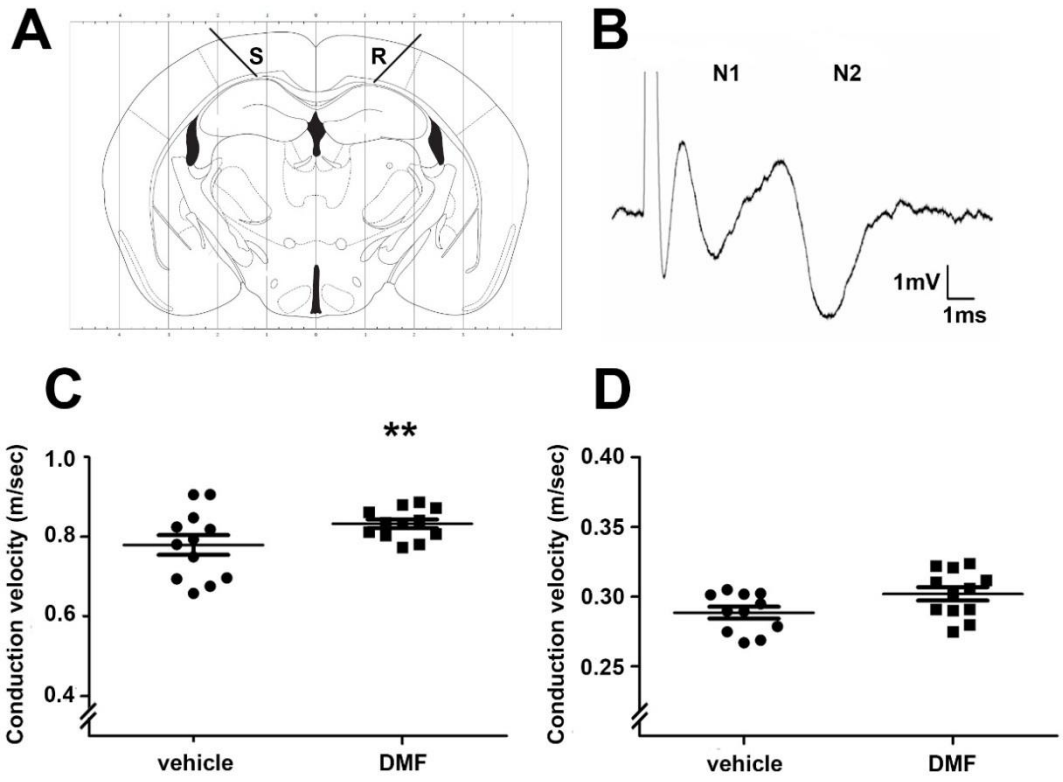

Figure 5.6: Increased conduction velocity in DMF-treated mice. (**A**) Schematic diagram showing the region of the corpus callosum in which conduction velocity was measured over a 2.5 mm distance. S = stimulating electrode, R = recording electrode. (**B**) Representative trace showing N1 and N2 components corresponding to myelinated and unmyelinated fibres respectively. (**C**) Conduction velocity of myelinated axons was significantly increased in DMF-treated mice as compared to vehicle-treated hypoperfused mice ($p = 0.04$). (**D**) Conduction velocity of unmyelinated axons was not significantly different between vehicle and DMF-treated groups following severe hypoperfusion ($p = 0.054$). Electrophysiological measures and analysis was carried out by Dr Philip Holland. Image A taken and adapted from Paxinos and Franklin (2001).

A

	Sham		Hypoperfusion	
	Vehicle	DMF	Vehicle	DMF
Cohort 1	**7**	**8**	**13** (2)	**9** (2)
Cohort 2	-	-	**12** (4)	**12** (1)

B

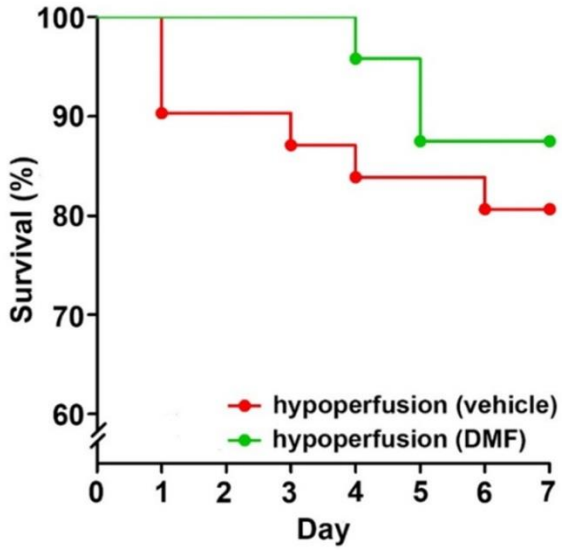

Figure 5.7: DMF treatment does not improve survival following surgery in DMF treated mice. (**A**) Animals were closely monitored following surgery and those displaying a poor recovery were culled. Final cohort sizes are shown in bold with numbers of animals culled in brackets. (**B**) Kaplan-Meier survival curve showing percentage survival in vehicle and DMF-treated mice following severe hypoperfusion. Survival in vehicle-treated animals was 80.6% compared to 87.5% in DMF-treated mice however this difference was not statistically significant ($p = 0.458$). Survival in both sham groups was 100%.

5.4 Discussion

It was hypothesised at the outset of the study that DMF treatment would improve the structure and function of myelinated axons following severe chronic cerebral hypoperfusion. The results indicated that myelin intensity (as assessed by MBP labelling) was significantly decreased in vehicle-treated hypoperfused mice as compared to shams, but that this difference was not observed between DMF-treated sham and hypoperfused groups indicative of a beneficial effect of DMF treatment on myelin integrity. In contrast, there was no effect of DMF treatment on axonal integrity following severe hypoperfusion. It was also hypothesised that severe hypoperfusion would lead to loss of oligodendrocytes and OPCs and that DMF treatment would ameliorate this. Surprisingly, no significant differences in numbers of mature oligodendrocytes and OPCs were observed following severe cerebral hypoperfusion in either vehicle or DMF-treated groups however DMF treatment in sham animals resulted in increased numbers of mature oligodendrocytes compared to vehicle-treated animals. This suggests that DMF, in the absence of cerebral hypoperfusion, may have a beneficial action on white matter. Finally, the conduction velocity of myelinated axons was assessed to determine whether the effects of DMF treatment on myelin integrity had a functional benefit. This revealed a significant increase in the conduction velocity of myelinated axons in DMF-treated mice as compared to the vehicle-treated groups.

5.4.1 DMF treatment in severe chronic cerebral hypoperfusion

Whilst increased inflammation (see Chapter 3; Shibata et al., 2004; Coltman et al., 2011) is observed following modest cerebral hypoperfusion, gross myelin and axonal damage are not observed (Reimer et al., 2011), therefore a modified version of the mouse hypoperfusion model (Miki et al., 2009) was used in the current study to induce more pronounced white matter pathology. Indeed, the results indicated a significant decrease in MBP labelling intensity following 1 week of severe hypoperfusion. Critically, MBP labelling was not significantly different between DMF-treated hypoperfused animals as compared to shams indicating a protective effect of DMF treatment on myelin integrity.

The beneficial effects of DMF have been primarily studied in the EAE model of MS which exploits the immune system to create autoimmunity to myelin resulting in a more gradual disease onset typically occurring approximately 10-14 days post injection (Pachner, 2011), however this can vary depending on the antigen used for EAE induction. Furthermore, two recent studies have shown beneficial effects of long term DMF administration in mouse models of Huntington's disease treated for 90 days (Ellrichmann et al., 2011) and in cuprizone-treated mice treated for up to 6 weeks (Moharregh-Khiabani et al., 2010). Given the beneficial effects of long-term DMF treatment in other disease models it would be important to study the effects of DMF in the modest cerebral hypoperfusion model to determine whether similar structural and functional effects are observed. Indeed, one study has reported that the working memory impairment in these animals persists following 6 months of cerebral hypoperfusion accompanied by ischaemic neuronal damage in the cortex

and hippocampus (Nishio et al., 2010). The protective effects of DMF treatment could therefore be assessed following long term modest hypoperfusion by assessing its effects on both pathology and working memory.

5.4.2 CBF reduction and pathology in the mixed-coil model of hypoperfusion

In chronic cerebral hypoperfusion studies, C57Bl/6J mice are preferentially used due to their strain-related incomplete circle of Willis. Compared to other strains, C57Bl/6J mice have an under-developed posterior communicating artery which impairs collateral flow within the circle of Willis (Yang et al., 1997; Kitagawa et al., 1998; Wellons et al., 2000; Kelly et al., 2001) and thus the brain is less able to compensate for alterations in CBF. A pilot study by the group (n = 6) revealed that 50% of C57Bl/6J mice had only one posterior communicating artery whilst the other 50% had neither posterior communicating arteries (Dr Robin Coltman, PhD thesis 2011). Whilst this compromised circle of Willis is useful for studying the effects of cerebral hypoperfusion, a disadvantage is that the difference in circle of Willis integrity between mice is an inherent source of variation. In the current study, the mixed-coil model was used to induce a more pronounced reduction in CBF however this showed a high degree of variability between animals, consistent with a previous report (Miki et al., 2009). Initial reductions in CBF 1 day after surgery varied from around 22 – 78% in vehicle treated animals and 18 – 93% in DMF-treated animals (see Appendix A3.1). Thus this high degree of variability in CBF is likely to have led to significant differences in the extent of pathology observed. Indeed a high degree of variability was observed in some measures, for example Figure 5.3B demonstrates

significant variability in numbers of $NG2^+$ OPCs in DMF-treated hypoperfused animals which may be masking potential effects of DMF. Future studies should therefore aim to assess the extent of pathology across a wider area of the corpus callosum or to increase cohort sizes in an attempt to reduce variability within groups.

In line with previous findings as reported by Miki et al (2009), pathological alterations were often more pronounced in the right hemisphere supplied by the 0.16 mm coil as compared to the left hemisphere, confirming that circle of Willis integrity is impaired in these animals. One technical limitation of the current study was that sections were placed in PB or cryoprotective medium before being mounted onto slides, thus making the definitive identification of left and right hemispheres impossible. Measurements were therefore carried out in both hemispheres and the mean of the values taken however this is likely to have masked any inter-hemispheric differences.

An associated limitation of the current study relates to the distribution of pathology in the mixed-coil model and the regions in which analysis was carried out. The extent of white matter pathology in this model varies depending on the anatomical region studied, with the most extensive damage reported to occur primarily in the striatum and the corpus callosum directly above it (approximately +1.1 mm from bregma) (Figure 5.8; Miki et al., 2009). In the current study, staining was analysed in the corpus callosum above the hippocampus (approximately -1.82 mm from bregma) as this is the approximate level that electophysiological testing in slice preparations was carried out. One disadvantage of this approach is that the white matter damage is

more modest at this level (Figure 5.8). Additionally, due to the severity of blood flow reduction in this model, focal areas of tissue damage and cell loss were observed but the exact locations of these 'lesions' varied between animals. Therefore insufficient sampling of the corpus callosum is likely to have been an issue for the current study. In addition, white matter damage is reported in other white matter regions including the anterior commissure and fimbria as well as white matter bundles of the striatum (Figure 5.8; Miki et al., 2009) therefore analysis within other white matter regions should be carried out in future studies using this model to fully characterise white matter alterations.

Additionally, the myelin and axonal markers used in the current study may not have been sensitive to subtle alterations in myelin and axonal integrity. Previous studies by the group have demonstrated that staining of MBP (Reimer et al., 2011) and FluoroMyelin (Figure 3.7) are unchanged following hypoperfusion but disruption to MAG is consistently observed (Figure 3.6; Coltman et al., 2011; Reimer et al., 2011) The current study demonstrated that the intensity and density of MBP labelling was reduced in vehicle-treated hypoperfused mice as compared to sham controls but was not different between DMF-treated sham and hypoperfused groups. This finding is suggestive of a protective effect of DMF on myelin integrity, consistent with the observed increase in the conduction velocity of myelinated axons. It would be pertinent for future studies to carry out a more robust assessment of myelin integrity in other white matter tracts and using additional markers including MAG which is known to be disrupted with cerebral hypoperfusion. Similarly, whilst APP is a useful marker of axonal damage, other markers may be more sensitive to underlying axonal

alterations. For example, there are a growing number of studies utilising markers of non-phosphorylated neurofilaments which can be indicative of underlying axonal stress (Trapp et al., 1998; Howell et al., 2010; Ritter et al., 2013). Therefore the use of additional axonal and myelin markers may reveal subtle beneficial effects of DMF that would not be detected through APP and MBP labelling.

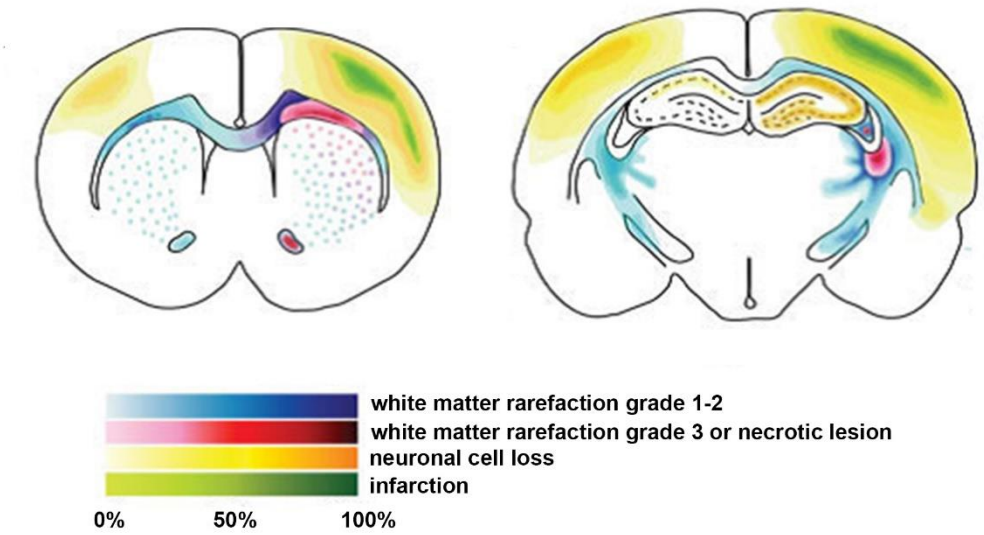

Figure 5.8: Distribution of white and grey matter pathology in the mixed coil model of chronic cerebral hypoperfusion. Schematic diagram showing the distribution of white and grey matter pathology following cerebral hypoperfusion. Severe white matter damage is observed in the corpus callosum above the striatum at approximately +1.1 mm from bregma. White matter disruption is less evident in the corpus callosum in sections corresponding to approximately -1.82 mm from bregma. Additional white matter tracts exhibiting white matter damage include fibre bundles of the striatum, the anterior commissure and fimbria. Image taken and adapted from Miki et al, 2009.

5.4.3 Functional benefit of DMF treatment

To determine the effects of DMF on the function of myelinated axons, electrophysiology was carried out and the conduction velocity of myelinated axons in the corpus callosum was measured. Importantly this revealed a significant increase in conduction velocity in DMF-treated animals as compared to the vehicle-treated group, indicative of a beneficial effect of DMF. Indeed pathological assessment revealed that myelin integrity was unchanged between DMF-treated sham and hypoperfused animals. Given the importance of the myelin sheath in efficient action potential conduction along axons it is likely that the increased conduction velocity in DMF-treated animals is due to preservation of myelin. Despite this, findings from previous studies (see Chapter 3; Reimer et al., 2011) demonstrate disruption to nodes of Ranvier and impaired axon-glial integrity as early as 3 days following modest chronic cerebral hypoperfusion whilst compact myelin is unaffected. It would therefore be important for future studies to determine the effects of severe hypoperfusion on axon-glial integrity and whether DMF restores any observed deficit.

In the current study the conduction velocity was measured by placing the stimulating and recording electrodes 1.25 mm either side of the midline corpus callosum (2.5 mm apart). This placement of electrodes was chosen due to the high density of aligned fibres in this region, ensuring strong CAP readings. Importantly the pathological analysis was carried out in the corpus callosum approximately 2 mm from the midline in each hemisphere (see Figure 2.3B). This again highlights that

greater sampling of the corpus callosum should be carried out to accurately assess pathological alterations in response to severe hypoperfusion.

5.4.4 DMF boosts oligodendrocyte number in healthy animals

In addition to investigating whether DMF could protect myelinated axons, a further aim of this study was to determine whether DMF influenced numbers of oligodendrocytes following cerebral hypoperfusion. Previous study in the modest hypoperfusion model (see Chapter 4) has shown loss of mature oligodendrocytes and OPCs following three days of hypoperfusion but demonstrates that these cells are restored within one month. In the current study it was hypothesised that oligodendrocyte loss would be observed following severe cerebral hypoperfusion and that DMF treatment would ameliorate this loss. Surprisingly, no significant differences in oligodendrocyte number were observed between vehicle-treated sham and hypoperfused animals. Possible reasons for this unexpected finding may relate to the region of the corpus callosum in which cells were counted, as outlined in Section 5.4.2. A surprising and interesting finding from this study however was that DMF-treated sham animals had higher numbers of oligodendrocytes than vehicle-treated shams indicating that in the absence of hypoperfusion, DMF may act to boost oligodendrocyte number. One possible explanation for this increased oligodendrocyte number in DMF-treated animals may be the result of increased differentiation of OPCs. A recent *in vitro* study using the Nrf2-activating compound CDDO has shown increased maturation of OPCs as compared to non-treated cultures (Pareek et al., 2011). Additionally, Nrf2 activation in human OPC cultures following

DMF treatment has been demonstrated suggesting that DMF may act directly on these cells (Scannevin et al., 2012). In the current study, numbers of OPCs were counted to determine whether increased OPC differentiation may have resulted in increased mature oligodendrocytes in DMF-treated shams. No significant differences in numbers of $NG2^+$ OPCs were observed between groups however this may be related to the time point studied. The cell cycle duration of OPCs in healthy adult mice aged 2 months is estimated to be approximately 10 days (Young et al., 2013). If cell cycle time is comparable in mice aged 4-5 months, and DMF treatment *in vivo* can enhance OPC differentiation as reported *in vitro* (Pareek et al., 2011), this may account for the increased numbers of mature oligodendrocytes following 1 month. However future studies would be required to clarify whether an OPC response is observed in this model and the temporal progression of any changes. Additionally, it is possible that increased numbers of oligodendrocytes may be due to differentiation of immature oligodendrocytes rather than OPCs however this again would need further clarification.

5.4.5 Biological properties of DMF

Despite being licenced for the treatment of MS, there is very little information regarding the pharmacokinetics and biological properties of DMF. DMF is also used in combination with monoethyl fumarate as an oral treatment for psoriasis (Rostami-Yazdi et al., 2010; Kees, 2013) and one study using this anti-psoriatic formulation in healthy individuals reported that DMF was not detectable in serum however a transient increase in its metabolite monomethyl fumarate (MMF) was observed,

indicating that DMF is rapidly metabolised to MMF (Litjens et al., 2004). Another study in individuals with psoriasis similarly reported undetectable levels of DMF in blood however the authors of this study hypothesised that a proportion of DMF may be rapidly metabolised to MMF in the intestine but that some may enter the blood where it is also converted to MMF (Rostami-Yazdi et al., 2010). Regardless of the exact mechanisms of absorption and metabolism, both studies in humans reported that the elimination half-life of MMF was approximately 40 minutes suggesting that this drug is rapidly cleared from the body (Litjens et al., 2004; Rostami-Yazdi et al., 2010). In the current study, DMF was suspended in a methocel (hypromellose) vehicle and administered twice daily by oral gavage. Methocel was used to control the rate of drug release and prevent rapid enzymatic degradation in the stomach (Li et al., 2005). However one clear limitation of the current study is that circulating levels of DMF and MMF were not assessed so the rate of release and half-life are unknown.

Importantly even if circulating levels of DMF and MMF had been assessed in the current study, this would not necessarily indicate whether DMF was transported to the brain. The efficacy of DMF has been tested in the cuprizone model of MS (Moharregh-Khiabani et al., 2010) and in mouse models of Huntington's disease (Ellrichmann et al., 2011), however as yet no study has examined DMF or MMF levels in brain tissue. It is unknown how effectively DMF or MMF can cross the blood brain barrier thus it is possible that very little of the administered dose reaches the brain. This could be easily assessed in an acute administration study using mass spectrometry to determine whether DMF or MMF is present in brain tissue.

5.4.6 Mechanism of action of DMF

In the current study DMF significantly improved the conduction velocity of myelinated axons following hypoperfusion in addition to boosting oligodendrocyte numbers in sham animals. Whilst it has been reported in previous studies that DMF exerts its protective effects via antioxidant and anti-inflammatory effects of Nrf2 activation (Ellrichmann et al., 2011; Linker et al., 2011; Scannevin et al., 2012), this was not confirmed in the current study. Quantitative assessment of Nrf2 target genes would be required to show whether administration of DMF was activating Nrf2 in the current study. Upregulation of the haem oxygenase 1 (HO-1) gene, an Nrf2 target gene, has been demonstrated following focal cerebral ischaemia (Zhang et al., 2012) and following 3 days of modest hypoperfusion (Dr Jill Fowler, unpublished observations). HO-1 is induced in response to increased oxidative stress and its upregulation is thought to confer cytoprotection both *in vitro* (Dwyer et al., 1995) and *in vivo* (Panahian et al., 1999). Therefore hypoperfusion alone may modulate Nrf2 target genes but future studies should clarify whether DMF can further modulate this gene expression. An additional Nrf2 target gene is NAD(P)H quinone oxidoreductase 1 (NQO1) which has been shown to be upregulated in response to oxygen-glucose deprivation *in vitro* (Soane et al., 2010) and thus may be important following hypoperfusion. Additionally, many other Nrf2-activating compounds are available which may exert more powerful effects than DMF however the safety profiles of these compounds are not as well characterised.

An increase in microglial number has been consistently reported in mouse studies of modest hypoperfusion (see Chapter 3; Shibata et al., 2004; Coltman et al., 2011)

whilst an increase in both microglial and astrocyte populations has been reported in the mixed-coil model (Miki et al., 2009). Given the anti-inflammatory role of DMF it would be critical for future studies to determine whether DMF can decrease the extent of inflammation following severe hypoperfusion. This could be achieved by assessing the levels of circulating inflammatory mediators in plasma from vehicle and DMF-treated animals in addition to immunohistochemistry to assess numbers of microglia and astrocytes. Indeed previous study has demonstrated that DMF decreases levels of circulating inflammatory mediators following EAE (Schilling et al., 2006) which may influence inflammation within the brain (Arvin et al., 1996).

The current study sought to determine the beneficial effects of DMF on myelinated axons and oligodendrocyte populations within the white matter, however DMF may exert additional protective effects in grey matter. Several studies using mouse models of Parkinson's disease (Chen et al., 2009a), motor neuron disease (Vargas et al., 2008), Huntington's disease (Ellrichmann et al., 2011), and MS (Linker et al., 2011) have shown that activation of Nrf2 is neuroprotective. Nrf2-mediated neuroprotection has also been described in models of focal ischaemia (Shih et al., 2005; Son et al., 2010; Zhang et al., 2012) suggesting that a similar protective effect may be observed following severe hypoperfusion. It is thought that the protective effect of Nrf2 activation is mediated indirectly through astrocytes rather than a direct effect on neurons (Calkins et al., 2009; Vargas and Johnson, 2009). Astrocyte-specific Nrf2 expression has been demonstrated to protect against neuronal death *in vitro* (Kraft et al., 2004) and more recently astrocyte-targeted overexpression of Nrf2 in mouse models of ALS significantly increased neuronal survival (Vargas et al.,

2008). Interestingly, recent studies have demonstrated Nrf2 activation in oligodendrocytes (Linker et al., 2011) and OPCs (Pareek et al., 2011) suggesting that Nrf2 may act on other glial cells. The exact role of Nrf2 activation in astrocytes and oligodendroglial cells should be investigated in future studies as these may be important for both grey and white matter protection.

5.4.7 Summary and conclusions

This study sought to determine whether treatment with the anti-inflammatory and antioxidant compound DMF could protect the structure and function of myelinated axons following severe chronic cerebral hypoperfusion. The results demonstrated that myelin integrity was not different between vehicle and DMF-treated hypoperfused mice. A significant decrease in myelin integrity was oberved between vehicle-treated hypoperfused mice as compared to shams, however there was no differnce between DMF-treated groups. Numbers of mature oligodendrocytes were not different between vehicle and DMF-treated hypoperfused mice however DMF treatment led to increased numbers of mature oligodendrocytes in sham animals as compared to vehicle-treated shams. In addition, increased conduction velocity was observed in hypoperfused DMF-treated animals as compared to vehicle-treated animals. Taken together the results of this study indicate that DMF may exert beneficial effects on white matter structure and function in response to reduced CBF and thus may represent an appropriate therapeutic strategy for chronic cerebral hypoperfusion.

Chapter 6

Discussion

6. Discussion

6.1 Summary

The findings presented in this thesis demonstrate the vulnerability of the white matter to chronic cerebral hypoperfusion. Specifically, cerebral hypoperfusion disrupts axon-glial integrity and the domain structure of myelinated axons which is likely to contribute to observed deficits in working memory. Additionally, cerebral hypoperfusion leads to a rapid loss of oligodendroglial cells which recover over time. Finally, treatment with DMF improved functional outcome following severe cerebral hypoperfusion suggesting that modulation of inflammation and oxidative stress may be important for the treatment of chronic cerebral hypoperfusion.

6.2 Alternative approaches to study the effects of cerebral hypoperfusion on white matter structure

The current study used wild-type C57Bl/6J mice and conventional immunohistochemistry and imaging techniques to investigate alterations in white matter structure following chronic cerebral hypoperfusion. However, a growing number of transgenic animals are available which may be advantageous to study myelinated axons and oligodendrocyte populations. For example, a recent study has described a novel transgenic mouse line in which existing myelin and newly generated myelin can be readily distinguished following injury (Powers et al., 2013).

This is achieved by using mice which express membrane targeted tomato fluorescent protein however following Cre-mediated recombination switches to express membrane bound green fluorescent protein (GFP). By injecting a retroviral vector expressing Cre recombinase driven by the NG2 promoter the authors were able to identify existing myelin and myelin generated as a result of OPC proliferation and differentiation based on expression of tomato or green fluorescent proteins respectively. This work has demonstrated that following spinal cord injury, GFP is first detected in $NG2^+$ OPCs but following differentiation of these cells GFP^+ mature oligodendrocytes and myelin sheaths are evident (Powers et al., 2013). Thus a similar approach could be employed to investigate differentiation of OPCs following chronic cerebral hypoperfusion and whether newly generated oligodendrocytes are functionally able to myelinate. Additionally, an MBP-GFP line has also been described which allows visualisation of mature oligodendrocytes and their processes (Chong et al., 2012) which could also be used in combination with a proliferation marker such as EdU to assess the extent of myelination by newly generated oligodendrocytes following hypoperfusion.

An alternative approach to transgenic modification is the labelling of oligodendrocytes using lentiviral injection of a fluorescent reporter. Lentiviral injection of MBP-GFP into the corpus callosum of mice has been described (McIver et al., 2005) and more recently utilised to study oligodendrocyte numbers and morphology following focal cerebral ischaemia (McIver et al., 2010). However disadvantages of this approach include the limited diffusion of the vector, resulting in labelling of oligodendrocytes in defined areas rather than globally throughout the

brain, and the transduction efficiency of the virus (McIver et al., 2005). Additionally, a growing number of studies are utilising recombination technology to track the phenotypic fate of OPCs during development and following injury. This involves using Cre-lox technology to drive the conditional expression of a fluorescent reporter driven by PDGFRα or NG2 promoters which label OPCs and their progeny (Rivers et al., 2008; Zhu et al., 2011; Young et al., 2013). A similar approach could be used to track the fate of OPCs following chronic cerebral hypoperfusion to fully characterise the OPC response.

One common limitation of the studies described in this thesis is the limited sampling of white matter which may not be representative of the brain as a whole. Additionally assessment of pathology in a small number of brain sections may not reveal pathological differences at different anatomical levels. However robust characterisation of pathology within different white matter tracts and at several anatomical levels would be expensive, labour intensive and slow. A novel approach to studying whole brain structure has recently been described which transforms mouse brains into optically transparent structures which do not require sectioning and thus whole brains can be labelled and imaged using conventional techniques (Chung et al., 2013). This technique therefore provides the opportunity to study regional differences within the brain which may be important in chronic cerebral hypoperfusion. Additionally, myelinated fibres could be labelled and followed along their entire length allowing a rigorous characterisation of the extent of paranodal disruption within particular pathways.

6.3 Alternative approaches to study the mechanisms underlying white matter disruption following chronic cerebral hypoperfusion

The studies described in this thesis attempted to characterise potential mechanisms involved in mediating axon-glial disruption and alterations to oligodendrocyte pools following chronic cerebral hypoperfusion. To build upon the findings of these studies, transgenic mouse lines could be used in future studies. For example, transgenic mice overexpressing MAG or Nfasc155 could be subject to chronic cerebral hypoperfusion to assess whether stabilising paranodal or internodal axon-glial connection could prevent white matter disruption and impaired cognition following hypoperfusion. A similar approach could be applied to GPR17 to determine the exact role, if any, of this receptor in mediating the OPC response to hypoperfusion.

The final study described in this thesis investigated the protective effects of Nrf2 activation on white matter structure following severe hypoperfusion. Previous studies in the EAE model of MS have demonstrated a poorer outcome in Nrf2 knockout mice subject to EAE than wild type counterparts (Schilling et al., 2006; Johnson et al., 2010). Chronic cerebral hypoperfusion could therefore be induced in Nrf2 knockouts to determine white matter damage and functional outcome were attenuated compared to shams. Additional studies have demonstrated that astrocyte-specific Nrf2 overexpression can increase neuronal survival in mouse models of Parkinson's disease (Gan et al., 2012) and motor neuron disease (Vargas et al., 2008), and following mitochondrial injury (Calkins et al., 2010). A similar approach

could be employed in the mouse model of hypoperfusion to investigate the role of astrocytes in the modulation of white matter damage. Alternatively, an oligodendrocyte-specific Nrf2 overexpressing mouse could be generated to determine whether protection of oligodendrocytes from inflammation and oxidative stress could prevent against oligodendrocyte loss and impaired axon-glial integrity following hypoperfusion.

6.4 Clinical relevance and potential therapeutic strategies

The mouse model of modest chronic cerebral hypoperfusion was designed to model age-related decreases in CBF and to determine the resulting effects on white matter integrity and cognition. Indeed CBF was shown to be approximately 38% lower than sham controls following 3 days of hypoperfusion recovering to around 19% by 28 days. In humans CBF is estimated to decrease by approximately 0.5% per year from age 20 to age 80 (Leenders et al., 1990; Scheel et al., 2000) therefore CBF values reported in mouse are within the predicted range of blood flow reduction over the course of an adult lifetime. The pathological findings in the current study are also consistent with studies of aged brains which show paranodal disruption (Hinman et al., 2006; Shepherd et al., 2012), increased numbers of oligodendrocytes (Simpson et al., 2007a; Lasiene et al., 2009) and increased inflammation (Conde and Streit, 2006; Simpson et al., 2007b). One limitation of the mouse model of cerebral hypoperfusion is that, although modest, the initial reduction in CBF is approximately 30-38% (Shibata et al., 2004; Washida et al., 2010; Maki et al., 2011; Duan et al., 2012) which does not mimic the gradual onset of hypoperfusion throughout the course of

an adult lifetime. A novel approach to studying cerebral hypoperfusion has been recently described in rat whereby stenosis of the carotid arteries is induced gradually using an ameroid constrictor device (Kitamura et al., 2012). This small device is placed around each common carotid artery and slowly absorbs water over approximately 3 days leading to swelling and subsequent constriction of the artery it surrounds. A similar approach could be applied to mice to more accurately mimic the onset of hypoperfusion. Despite this, the bilateral carotid artery stenosis model of hypoperfusion remains a clinically relevant and useful tool to study the effects of hypoperfusion on white matter and cognition.

Importantly, the studies described in this thesis investigated the effects of cerebral hypoperfusion in young animals (aged 3-5 months) which may not reflect the response in the ageing brain. A recent study has demonstrated that the extent of white matter disruption and working memory impairment induced by hypoperfusion is more severe in aged animals as compared to young, and importantly the endogenous OPC response to hypoperfusion is attenuated (Miyamoto et al., 2013c). These findings are supported by additional studies demonstrating increased white matter damage and inflammation following focal cerebral ischaemia in aged mice as compared to young mice (Rosenzweig and Carmichael, 2013) and a significant decrease in the cell cycle duration of OPCs in aged mice (Psachoulia et al., 2009; Young et al., 2013) which may impact on white matter repair. It would therefore be pertinent for future studies to distinguish the effects of cerebral hypoperfusion on myelinated axons and oligodendrocyte populations in aged animals as the underlying mechanisms driving pathology may be influenced by age. An alternative hypothesis

regarding the cause of white matter disruption and cognitive decline with ageing relates to OPC and oligodendrocyte population dynamics in the aged brain. It has been proposed that in the adult brain OPCs and oligodendrocytes may have a finite lifetime and that disruption to white matter with increasing age is the result of an inability of white matter repair mechanisms to match the rate of oligodendrogenesis with myelin loss (Richardson et al., 2011). This could be assessed by comparing the extent of white matter pathology in addition to CBF measurement in young and aged mice to determine whether there is evidence of white matter pathology between groups in the absence of significant decreases in CBF.

Although chronic cerebral hypoperfusion and subsequent age-related cognitive decline are features of the 'normal' ageing process, decreased cerebral blood flow is also observed in mild cognitive impairment (Hirao et al., 2005), vascular dementia (Kawamura et al., 1991) and Alzheimer's disease (AD; de la Torre, 1994). This raises the question of whether early pharmaceutical intervention may prevent the transition from subtle age-related changes in cognitive ability to end-stage AD. There is a growing body of research showing that the presence of vascular risk factors during mid-life can predispose to Alzheimer's disease in later life (Kivipelto et al., 2001) therefore this may represent a key time for pharmacological intervention. Indeed increased inflammation (Akiyama et al., 2000) and oxidative stress (Markesbery, 1997) are both features of AD and thus may represent key therapeutic targets for the treatment of cerebral hypoperfusion and subsequent cognitive decline in both aging and AD.

The beneficial effects of the anti-inflammatory and antioxidant Nrf2 activator DMF were examined in this thesis which demonstrated improved functional outcome following hypoperfusion as assessed by electrophysiology. Importantly this functional benefit was observed following severe hypoperfusion implying that even greater protective effects may be observed following mild cerebral hypoperfusion. Additional studies have demonstrated that long term dosing of DMF for 6 weeks to 3 months can improve disease progression in mouse models of MS (Moharregh-Khiabani et al., 2010) and Huntington's disease (Ellrichmann et al., 2011) respectively. This raises the question of whether long term DMF administration prior to and following hypoperfusion may exert greater protective effects on white matter than observed in this thesis. Additionally the current study revealed that 7 days of DMF treatment significantly increased numbers of mature oligodendrocytes in sham animals such that despite a decrease in oligodendrocyte number following hypoperfusion, values of DMF-treated hypoperfused animals were comparable to those of non-treated controls. This DMF-mediated increase in oligodendrocyte number over an extended period of time may help protect against white matter from the effects of cerebral hypoperfusion however future studies would be required to clarify this.

Although Nrf2 activation using DMF is a valid therapeutic approach for modulating inflammation and oxidative stress following cerebral hypoperfusion, alternative compounds exist which may be equally or more effective. For example, studies using the antibiotic drug minocycline have demonstrated improved white matter integrity and decreased inflammation following chronic cerebral hypoperfusion in rat (Cho et

al., 2006). Additionally, administration of minocycline has been demonstrated to decrease inflammation and protect against paranodal disruption in EAE (Howell et al., 2010). Similarly, treatment with the antioxidant drug edaravone has shown improved spatial memory and white matter integrity following chronic hypoperfusion in rat (Ueno et al., 2009) and treatment with idebenone has been shown to improve functional outcome and enhance cerebral metabolism following global ischaemia (Nagaoka et al., 1989). Indeed a growing number of studies have shown that cerebral metabolism can be boosted at the mitochondrial level through activation of proliferator-activated receptor-γ co-activator 1α (PGC-1α) which may improve antioxidant capacity and energy metabolism within the ageing brain (Austin and St-Pierre, 2012). Thus whilst a single drug approach is always preferable, a combination of different drugs may be required for the effective treatment of chronic cerebral hypoperfusion.

6.5 Conclusion

The results outlined in this thesis build on previous studies demonstrating the detrimental effects of chronic cerebral hypoperfusion on white matter integrity and working memory. Additionally, these findings reveal that treatment with DMF results in improved functional outcome following hypoperfusion suggesting that this may represent an important pharmacological target. Future studies should aim to fully characterise the mechanisms underlying white matter disruption following chronic cerebral hypoperfusion and whether intervention can prevent or halt these pathological processes. Given the increasing ageing population worldwide, there is a

growing need for therapeutic strategies aimed at improving cognitive function in ageing and dementia.

References

Aboul-Enein F, Rauschka H, Kornek B, Stadelmann C, Stefferl A, Bruck W, Lucchinetti C, Schmidbauer M, Jellinger K, Lassmann H (2003) Preferential loss of myelin-associated glycoprotein reflects hypoxia-like white matter damage in stroke and inflammatory brain diseases. J Neuropathol Exp Neurol 62:25-33.

Agresti C, Meomartini ME, Amadio S, Ambrosini E, Volonte C, Aloisi F, Visentin S (2005) ATP regulates oligodendrocyte progenitor migration, proliferation, and differentiation: involvement of metabotropic P2 receptors. Brain Res Brain Res Rev 48:157-165.

Akiyama H et al. (2000) Inflammation and Alzheimer's disease. Neurobiol Aging 21:383-421.

Appelman AP, van der Graaf Y, Vincken KL, Mali WP, Geerlings MI (2010) Combined effect of cerebral hypoperfusion and white matter lesions on executive functioning - The SMART-MR study. Dement Geriatr Cogn Disord 29:240-247.

Arnett HA, Mason J, Marino M, Suzuki K, Matsushima GK, Ting JP (2001) TNF alpha promotes proliferation of oligodendrocyte progenitors and remyelination. Nat Neurosci 4:1116-1122.

Arvin B, Neville LF, Barone FC, Feuerstein GZ (1996) The role of inflammation and cytokines in brain injury. Neurosci Biobehav Rev 20:445-452.

Astrup J, Siesjo BK, Symon L (1981) Thresholds in cerebral ischemia - the ischemic penumbra. Stroke 12:723-725.

Austin S, St-Pierre J (2012) PGC1alpha and mitochondrial metabolism--emerging concepts and relevance in ageing and neurodegenerative disorders. J Cell Sci 125:4963-4971.

Awad IA, Johnson PC, Spetzler RF, Hodak JA (1986a) Incidental subcortical lesions identified on magnetic resonance imaging in the elderly. II. Postmortem pathological correlations. Stroke 17:1090-1097.

Awad IA, Spetzler RF, Hodak JA, Awad CA, Carey R (1986b) Incidental subcortical lesions identified on magnetic resonance imaging in the elderly. I. Correlation with age and cerebrovascular risk factors. Stroke 17:1084-1089.

Ayata C, Dunn AK, Gursoy OY, Huang Z, Boas DA, Moskowitz MA (2004) Laser speckle flowmetry for the study of cerebrovascular physiology in normal and ischemic mouse cortex. J Cereb Blood Flow Metab 24:744-755.

Babbs CF, Shi R (2013) Subtle paranodal injury slows impulse conduction in a mathematical model of myelinated axons. PLoS One 8:e67767.

Back SA, Kroenke CD, Sherman LS, Lawrence G, Gong X, Taber EN, Sonnen JA, Larson EB, Montine TJ (2011) White matter lesions defined by diffusion tensor imaging in older adults. Ann Neurol 70:465-476.

Barber R, Scheltens P, Gholkar A, Ballard C, McKeith I, Ince P, Perry R, O'Brien J (1999) White matter lesions on magnetic resonance imaging in dementia with Lewy bodies, Alzheimer's disease, vascular dementia, and normal aging. J Neurol Neurosurg Psychiatry 67:66-72.

Barker R, Wellington D, Esiri MM, Love S (2013) Assessing white matter ischemic damage in dementia patients by measurement of myelin proteins. J Cereb Blood Flow Metab 33:1050-1057.

Baron JC (2001) Perfusion thresholds in human cerebral ischemia: historical perspective and therapeutic implications. Cerebrovasc Dis 11 Suppl 1:2-8.

Baron JC, Rougemont D, Soussaline F, Bustany P, Crouzel C, Bousser MG, Comar D (1984) Local interrelationships of cerebral oxygen consumption and glucose utilization in normal subjects and in ischemic stroke patients: a positron tomography study. J Cereb Blood Flow Metab 4:140-149.

Barone FC, Knudsen DJ, Nelson AH, Feuerstein GZ, Willette RN (1993) Mouse strain differences in susceptibility to cerebral ischemia are related to cerebral vascular anatomy. J Cereb Blood Flow Metab 13:683-692.

Bartzokis G, Sultzer D, Lu PH, Nuechterlein KH, Mintz J, Cummings JL (2004) Heterogeneous age-related breakdown of white matter structural integrity: implications for cortical "disconnection" in aging and Alzheimer's disease. Neurobiol Aging 25:843-851.

Bastin ME, Clayden JD, Pattie A, Gerrish IF, Wardlaw JM, Deary IJ (2009) Diffusion tensor and magnetization transfer MRI measurements of periventricular white matter hyperintensities in old age. Neurobiol Aging 30:125-136.

Baumann N, Pham-Dinh D (2001) Biology of oligodendrocyte and myelin in the mammalian central nervous system. Physiol Rev 81:871-927.

Bell KF, Fowler JH, Al-Mubarak B, Horsburgh K, Hardingham GE (2011) Activation of Nrf2-regulated glutathione pathway genes by ischemic preconditioning. Oxid Med Cell Longev 2011:689524.

Bergles DE, Roberts JD, Somogyi P, Jahr CE (2000) Glutamatergic synapses on oligodendrocyte precursor cells in the hippocampus. Nature 405:187-191.

Bhat MA, Rios JC, Lu Y, Garcia-Fresco GP, Ching W, St Martin M, Li J, Einheber S, Chesler M, Rosenbluth J, Salzer JL, Bellen HJ (2001) Axon-glia interactions and the domain organization of myelinated axons requires neurexin IV/Caspr/Paranodin. Neuron 30:369-383.

Blinder P, Tsai PS, Kaufhold JP, Knutsen PM, Suhl H, Kleinfeld D (2013) The cortical angiome: an interconnected vascular network with noncolumnar patterns of blood flow. Nat Neurosci 16:889-897.

Block ML, Zecca L, Hong JS (2007) Microglia-mediated neurotoxicity: uncovering the molecular mechanisms. Nat Rev Neurosci 8:57-69.

Boda E, Vigano F, Rosa P, Fumagalli M, Labat-Gest V, Tempia F, Abbracchio MP, Dimou L, Buffo A (2011) The GPR17 receptor in NG2 expressing cells: focus on in vivo cell maturation and participation in acute trauma and chronic damage. Glia 59:1958-1973.

Bongarzone ER, Pasquini JM, Soto EF (1995) Oxidative damage to proteins and lipids of CNS myelin produced by in vitro generated reactive oxygen species. J Neurosci Res 41:213-221.

Boyle ME, Berglund EO, Murai KK, Weber L, Peles E, Ranscht B (2001) Contactin orchestrates assembly of the septate-like junctions at the paranode in myelinated peripheral nerve. Neuron 30:385-397.

Brant-Zawadzki M, Fein G, Van Dyke C, Kiernan R, Davenport L, de Groot J (1985) MR imaging of the aging brain: patchy white-matter lesions and dementia. AJNR Am J Neuroradiol 6:675-682.

Breteler MM, van Amerongen NM, van Swieten JC, Claus JJ, Grobbee DE, van Gijn J, Hofman A, van Harskamp F (1994a) Cognitive correlates of ventricular enlargement and cerebral white matter lesions on magnetic resonance imaging. The Rotterdam Study. Stroke 25:1109-1115.

Breteler MM, van Swieten JC, Bots ML, Grobbee DE, Claus JJ, van den Hout JH, van Harskamp F, Tanghe HL, de Jong PT, van Gijn J, et al. (1994b) Cerebral white matter lesions, vascular risk factors, and cognitive function in a population-based study: the Rotterdam Study. Neurology 44:1246-1252.

Brookes PS, Yoon Y, Robotham JL, Anders MW, Sheu SS (2004) Calcium, ATP, and ROS: a mitochondrial love-hate triangle. Am J Physiol Cell Physiol 287:C817-833.

Brown AM, Wender R, Ransom BR (2001) Metabolic substrates other than glucose support axon function in central white matter. J Neurosci Res 66:839-843.

Brun A, Englund E (1986) A white matter disorder in dementia of the Alzheimer type: a pathoanatomical study. Ann Neurol 19:253-262.

Bucur B, Madden DJ, Spaniol J, Provenzale JM, Cabeza R, White LE, Huettel SA (2008) Age-related slowing of memory retrieval: contributions of perceptual speed and cerebral white matter integrity. Neurobiol Aging 29:1070-1079.

Butt AM, Duncan A, Hornby MF, Kirvell SL, Hunter A, Levine JM, Berry M (1999) Cells expressing the NG2 antigen contact nodes of Ranvier in adult CNS white matter. Glia 26:84-91.

Caldwell JH, Schaller KL, Lasher RS, Peles E, Levinson SR (2000) Sodium channel Na(v)1.6 is localized at nodes of ranvier, dendrites, and synapses. Proc Natl Acad Sci U S A 97:5616-5620.

Calkins MJ, Vargas MR, Johnson DA, Johnson JA (2010) Astrocyte-specific overexpression of Nrf2 protects striatal neurons from mitochondrial complex II inhibition. Toxicological sciences : an official journal of the Society of Toxicology 115:557-568.

Calkins MJ, Johnson DA, Townsend JA, Vargas MR, Dowell JA, Williamson TP, Kraft AD, Lee JM, Li J, Johnson JA (2009) The Nrf2/ARE pathway as a potential therapeutic target in neurodegenerative disease. Antioxid Redox Signal 11:497-508.

Cammer W, Zhang H (1993) Atypical localization of the oligodendrocytic isoform (PI) of glutathione-S-transferase in astrocytes during cuprizone intoxication. J Neurosci Res 36:183-190.

Cavaliere F, Urra O, Alberdi E, Matute C (2012) Oligodendrocyte differentiation from adult multipotent stem cells is modulated by glutamate. Cell Death Dis 3:e268.

Ceruti S, Villa G, Genovese T, Mazzon E, Longhi R, Rosa P, Bramanti P, Cuzzocrea S, Abbracchio MP (2009) The P2Y-like receptor GPR17 as a sensor of damage and a new potential target in spinal cord injury. Brain 132:2206-2218.

Ceruti S, Vigano F, Boda E, Ferrario S, Magni G, Boccazzi M, Rosa P, Buffo A, Abbracchio MP (2011) Expression of the new P2Y-like receptor GPR17

during oligodendrocyte precursor cell maturation regulates sensitivity to ATP-induced death. Glia 59:363-378.
Chang DT, Reynolds IJ (2006) Mitochondrial trafficking and morphology in healthy and injured neurons. Prog Neurobiol 80:241-268.
Chehrehasa F, Meedeniya AC, Dwyer P, Abrahamsen G, Mackay-Sim A (2009) EdU, a new thymidine analogue for labelling proliferating cells in the nervous system. Journal of neuroscience methods 177:122-130.
Chen PC, Vargas MR, Pani AK, Smeyne RJ, Johnson DA, Kan YW, Johnson JA (2009a) Nrf2-mediated neuroprotection in the MPTP mouse model of Parkinson's disease: Critical role for the astrocyte. Proc Natl Acad Sci U S A 106:2933-2938.
Chen Y, Wu H, Wang S, Koito H, Li J, Ye F, Hoang J, Escobar SS, Gow A, Arnett HA, Trapp BD, Karandikar NJ, Hsieh J, Lu QR (2009b) The oligodendrocyte-specific G protein-coupled receptor GPR17 is a cell-intrinsic timer of myelination. Nat Neurosci 12:1398-1406.
Chiu SY (2011) Matching mitochondria to metabolic needs at nodes of Ranvier. Neuroscientist 17:343-350.
Cho KO, La HO, Cho YJ, Sung KW, Kim SY (2006) Minocycline attenuates white matter damage in a rat model of chronic cerebral hypoperfusion. J Neurosci Res 83:285-291.
Chomiak T, Hu B (2009) What is the optimal value of the g-ratio for myelinated fibers in the rat CNS? A theoretical approach. PLoS One 4:e7754.
Chong SY, Rosenberg SS, Fancy SP, Zhao C, Shen YA, Hahn AT, McGee AW, Xu X, Zheng B, Zhang LI, Rowitch DH, Franklin RJ, Lu QR, Chan JR (2012) Neurite outgrowth inhibitor Nogo-A establishes spatial segregation and extent of oligodendrocyte myelination. Proc Natl Acad Sci U S A 109:1299-1304.
Chung K, Wallace J, Kim SY, Kalyanasundaram S, Andalman AS, Davidson TJ, Mirzabekov JJ, Zalocusky KA, Mattis J, Denisin AK, Pak S, Bernstein H, Ramakrishnan C, Grosenick L, Gradinaru V, Deisseroth K (2013) Structural and molecular interrogation of intact biological systems. Nature 497:332-337.
Ciana P, Fumagalli M, Trincavelli ML, Verderio C, Rosa P, Lecca D, Ferrario S, Parravicini C, Capra V, Gelosa P, Guerrini U, Belcredito S, Cimino M, Sironi L, Tremoli E, Rovati GE, Martini C, Abbracchio MP (2006) The orphan receptor GPR17 identified as a new dual uracil nucleotides/cysteinyl-leukotrienes receptor. EMBO J 25:4615-4627.
Cochran E, Bacci B, Chen Y, Patton A, Gambetti P, Autilio-Gambetti L (1991) Amyloid precursor protein and ubiquitin immunoreactivity in dystrophic axons is not unique to Alzheimer's disease. Am J Pathol 139:485-489.
Coltman R, Spain A, Tsenkina Y, Fowler JH, Smith J, Scullion G, Allerhand M, Scott F, Kalaria RN, Ihara M, Daumas S, Deary IJ, Wood E, McCulloch J, Horsburgh K (2011) Selective white matter pathology induces a specific impairment in spatial working memory. Neurobiol Aging 32:2324 e2327-2312.
Colton CA, Gilbert DL (1987) Production of superoxide anions by a CNS macrophage, the microglia. FEBS Lett 223:284-288.

Coman I, Aigrot MS, Seilhean D, Reynolds R, Girault JA, Zalc B, Lubetzki C (2006) Nodal, paranodal and juxtaparanodal axonal proteins during demyelination and remyelination in multiple sclerosis. Brain 129:3186-3195.

Conde JR, Streit WJ (2006) Microglia in the aging brain. J Neuropathol Exp Neurol 65:199-203.

Connor JR, Menzies SL (1996) Relationship of iron to oligodendrocytes and myelination. Glia 17:83-93.

Crawford DK, Mangiardi M, Tiwari-Woodruff SK (2009) Assaying the functional effects of demyelination and remyelination: revisiting field potential recordings. Journal of neuroscience methods 182:25-33.

Cronk JC, Kipnis J (2013) Microglia - the brain's busy bees. F1000Prime Rep 5:53.

Dang J, Brandenburg LO, Rosen C, Fragoulis A, Kipp M, Pufe T, Beyer C, Wruck CJ (2012) Nrf2 expression by neurons, astroglia, and microglia in the cerebral cortical penumbra of ischemic rats. J Mol Neurosci 46:578-584.

Dashiell SM, Tanner SL, Pant HC, Quarles RH (2002) Myelin-associated glycoprotein modulates expression and phosphorylation of neuronal cytoskeletal elements and their associated kinases. J Neurochem 81:1263-1272.

Davis JQ, Lambert S, Bennett V (1996) Molecular composition of the node of Ranvier: identification of ankyrin-binding cell adhesion molecules neurofascin (mucin+/third FNIII domain-) and NrCAM at nodal axon segments. J Cell Biol 135:1355-1367.

Dawson MR, Levine JM, Reynolds R (2000) NG2-expressing cells in the central nervous system: are they oligodendroglial progenitors? J Neurosci Res 61:471-479.

Dawson MR, Polito A, Levine JM, Reynolds R (2003) NG2-expressing glial progenitor cells: an abundant and widespread population of cycling cells in the adult rat CNS. Mol Cell Neurosci 24:476-488.

De Biase LM, Nishiyama A, Bergles DE (2010) Excitability and synaptic communication within the oligodendrocyte lineage. J Neurosci 30:3600-3611.

de Groot JC, de Leeuw FE, Oudkerk M, van Gijn J, Hofman A, Jolles J, Breteler MM (2000) Cerebral white matter lesions and cognitive function: the Rotterdam Scan Study. Ann Neurol 47:145-151.

De Groot JC, De Leeuw FE, Oudkerk M, Van Gijn J, Hofman A, Jolles J, Breteler MM (2002) Periventricular cerebral white matter lesions predict rate of cognitive decline. Ann Neurol 52:335-341.

de la Torre JC (1994) Impaired brain microcirculation may trigger Alzheimer's disease. Neurosci Biobehav Rev 18:397-401.

de Leeuw FE, de Groot JC, Achten E, Oudkerk M, Ramos LM, Heijboer R, Hofman A, Jolles J, van Gijn J, Breteler MM (2001) Prevalence of cerebral white matter lesions in elderly people: a population based magnetic resonance imaging study. The Rotterdam Scan Study. J Neurol Neurosurg Psychiatry 70:9-14.

Deary IJ, Corley J, Gow AJ, Harris SE, Houlihan LM, Marioni RE, Penke L, Rafnsson SB, Starr JM (2009) Age-associated cognitive decline. Br Med Bull 92:135-152.

DeCarli C, Murphy DG, Tranh M, Grady CL, Haxby JV, Gillette JA, Salerno JA, Gonzales-Aviles A, Horwitz B, Rapoport SI, et al. (1995) The effect of white

matter hyperintensity volume on brain structure, cognitive performance, and cerebral metabolism of glucose in 51 healthy adults. Neurology 45:2077-2084.
Dewar D, Underhill SM, Goldberg MP (2003) Oligodendrocytes and ischemic brain injury. J Cereb Blood Flow Metab 23:263-274.
Duan W, Ran H, Zhou Z, He Q, Zheng J (2012) Adenosine A2A receptor deficiency up-regulates cystatin F expression in white matter lesions induced by chronic cerebral hypoperfusion. PLoS One 7:e52566.
Dunn AK, Bolay H, Moskowitz MA, Boas DA (2001) Dynamic imaging of cerebral blood flow using laser speckle. J Cereb Blood Flow Metab 21:195-201.
Dupree JL, Mason JL, Marcus JR, Stull M, Levinson R, Matsushima GK, Popko B (2004) Oligodendrocytes assist in the maintenance of sodium channel clusters independent of the myelin sheath. Neuron Glia Biol 1:179-192.
Dwyer BE, Nishimura RN, Lu SY (1995) Differential expression of heme oxygenase-1 in cultured cortical neurons and astrocytes determined by the aid of a new heme oxygenase antibody. Response to oxidative stress. Brain Res Mol Brain Res 30:37-47.
Edvinsson L, MacKenzie ET, McCulloch J (1993) Cerebral blood flow and metabolism, First edition Edition. New York: Raven press.
Edwards JP, Zhang X, Frauwirth KA, Mosser DM (2006) Biochemical and functional characterization of three activated macrophage populations. J Leukoc Biol 80:1298-1307.
Einheber S, Bhat MA, Salzer JL (2006) Disrupted axo-glial junctions result in accumulation of abnormal mitochondria at nodes of ranvier. Neuron Glia Biol 2:165-174.
Ellrichmann G, Petrasch-Parwez E, Lee DH, Reick C, Arning L, Saft C, Gold R, Linker RA (2011) Efficacy of fumaric acid esters in the R6/2 and YAC128 models of Huntington's disease. PLoS One 6:e16172.
Faraci FM, Heistad DD (1998) Regulation of the cerebral circulation: role of endothelium and potassium channels. Physiol Rev 78:53-97.
Farkas E, Luiten PG, Bari F (2007) Permanent, bilateral common carotid artery occlusion in the rat: a model for chronic cerebral hypoperfusion-related neurodegenerative diseases. Brain Res Rev 54:162-180.
Farkas E, Donka G, de Vos RA, Mihaly A, Bari F, Luiten PG (2004) Experimental cerebral hypoperfusion induces white matter injury and microglial activation in the rat brain. Acta Neuropathol 108:57-64.
Fazekas F, Chawluk JB, Alavi A, Hurtig HI, Zimmerman RA (1987) MR signal abnormalities at 1.5 T in Alzheimer's dementia and normal aging. AJR Am J Roentgenol 149:351-356.
Fern R, Davis P, Waxman SG, Ransom BR (1998) Axon conduction and survival in CNS white matter during energy deprivation: a developmental study. J Neurophysiol 79:95-105.
Fernando MS, Simpson JE, Matthews F, Brayne C, Lewis CE, Barber R, Kalaria RN, Forster G, Esteves F, Wharton SB, Shaw PJ, O'Brien JT, Ince PG, Function MRCC, Ageing Neuropathology Study G (2006) White matter lesions in an unselected cohort of the elderly: molecular pathology suggests origin from chronic hypoperfusion injury. Stroke 37:1391-1398.

Ffrench-Constant C, Raff MC (1986) The oligodendrocyte-type-2 astrocyte cell lineage is specialized for myelination. Nature 323:335-338.
Finkel T, Holbrook NJ (2000) Oxidants, oxidative stress and the biology of ageing. Nature 408:239-247.
Floresco SB, Seamans JK, Phillips AG (1997) Selective roles for hippocampal, prefrontal cortical, and ventral striatal circuits in radial-arm maze tasks with or without a delay. J Neurosci 17:1880-1890.
Floresco SB, Braaksma DN, Phillips AG (1999) Thalamic-cortical-striatal circuitry subserves working memory during delayed responding on a radial arm maze. J Neurosci 19:11061-11071.
Fox RJ, Miller DH, Phillips JT, Hutchinson M, Havrdova E, Kita M, Yang M, Raghupathi K, Novas M, Sweetser MT, Viglietta V, Dawson KT (2012) Placebo-controlled phase 3 study of oral BG-12 or glatiramer in multiple sclerosis. The New England journal of medicine 367:1087-1097.
Franke H, Parravicini C, Lecca D, Zanier ER, Heine C, Bremicker K, Fumagalli M, Rosa P, Longhi L, Stocchetti N, De Simoni MG, Weber M, Abbracchio MP (2013) Changes of the GPR17 receptor, a new target for neurorepair, in neurons and glial cells in patients with traumatic brain injury. Purinergic Signal 9:451-462.
Fujii M, Hara H, Meng W, Vonsattel JP, Huang Z, Moskowitz MA (1997) Strain-related differences in susceptibility to transient forebrain ischemia in SV-129 and C57black/6 mice. Stroke 28:1805-1810; discussion 1811.
Fujita Y, Ihara M, Ushiki T, Hirai H, Kizaka-Kondoh S, Hiraoka M, Ito H, Takahashi R (2010) Early protective effect of bone marrow mononuclear cells against ischemic white matter damage through augmentation of cerebral blood flow. Stroke 41:2938-2943.
Fumagalli M, Daniele S, Lecca D, Lee PR, Parravicini C, Fields RD, Rosa P, Antonucci F, Verderio C, Trincavelli ML, Bramanti P, Martini C, Abbracchio MP (2011) Phenotypic changes, signaling pathway, and functional correlates of GPR17-expressing neural precursor cells during oligodendrocyte differentiation. J Biol Chem 286:10593-10604.
Funfschilling U, Supplie LM, Mahad D, Boretius S, Saab AS, Edgar J, Brinkmann BG, Kassmann CM, Tzvetanova ID, Mobius W, Diaz F, Meijer D, Suter U, Hamprecht B, Sereda MW, Moraes CT, Frahm J, Goebbels S, Nave KA (2012) Glycolytic oligodendrocytes maintain myelin and long-term axonal integrity. Nature 485:517-521.
Gan L, Vargas MR, Johnson DA, Johnson JA (2012) Astrocyte-specific overexpression of Nrf2 delays motor pathology and synuclein aggregation throughout the CNS in the alpha-synuclein mutant (A53T) mouse model. J Neurosci 32:17775-17787.
Garcia-Fresco GP, Sousa AD, Pillai AM, Moy SS, Crawley JN, Tessarollo L, Dupree JL, Bhat MA (2006) Disruption of axo-glial junctions causes cytoskeletal disorganization and degeneration of Purkinje neuron axons. Proc Natl Acad Sci U S A 103:5137-5142.
Geha S, Pallud J, Junier MP, Devaux B, Leonard N, Chassoux F, Chneiweiss H, Daumas-Duport C, Varlet P (2010) NG2+/Olig2+ cells are the major cycle-related cell population of the adult human normal brain. Brain Pathol 20:399-411.

Gold R, Kappos L, Arnold DL, Bar-Or A, Giovannoni G, Selmaj K, Tornatore C, Sweetser MT, Yang M, Sheikh SI, Dawson KT (2012) Placebo-controlled phase 3 study of oral BG-12 for relapsing multiple sclerosis. The New England journal of medicine 367:1098-1107.

Gould E, Tanapat P, McEwen BS, Flugge G, Fuchs E (1998) Proliferation of granule cell precursors in the dentate gyrus of adult monkeys is diminished by stress. Proc Natl Acad Sci U S A 95:3168-3171.

Hartline DK, Colman DR (2007) Rapid conduction and the evolution of giant axons and myelinated fibers. Curr Biol 17:R29-35.

Hattori H, Takeda M, Kudo T, Nishimura T, Hashimoto S (1992) Cumulative white matter changes in the gerbil brain under chronic cerebral hypoperfusion. Acta Neuropathol 84:437-442.

Head D, Buckner RL, Shimony JS, Williams LE, Akbudak E, Conturo TE, McAvoy M, Morris JC, Snyder AZ (2004) Differential vulnerability of anterior white matter in nondemented aging with minimal acceleration in dementia of the Alzheimer type: evidence from diffusion tensor imaging. Cereb Cortex 14:410-423.

Hedstrom KL, Xu X, Ogawa Y, Frischknecht R, Seidenbecher CI, Shrager P, Rasband MN (2007) Neurofascin assembles a specialized extracellular matrix at the axon initial segment. J Cell Biol 178:875-886.

Helmchen F, Denk W (2005) Deep tissue two-photon microscopy. Nat Methods 2:932-940.

Hildebrand C, Remahl S, Persson H, Bjartmar C (1993) Myelinated nerve fibres in the CNS. Prog Neurobiol 40:319-384.

Hinman JD, Peters A, Cabral H, Rosene DL, Hollander W, Rasband MN, Abraham CR (2006) Age-related molecular reorganization at the node of Ranvier. The Journal of comparative neurology 495:351-362.

Hirao K, Ohnishi T, Hirata Y, Yamashita F, Mori T, Moriguchi Y, Matsuda H, Nemoto K, Imabayashi E, Yamada M, Iwamoto T, Arima K, Asada T (2005) The prediction of rapid conversion to Alzheimer's disease in mild cognitive impairment using regional cerebral blood flow SPECT. Neuroimage 28:1014-1021.

Hodges H (1996) Maze procedures: the radial-arm and water maze compared. Brain Res Cogn Brain Res 3:167-181.

Hodgkin AL, Huxley AF (1952) A quantitative description of membrane current and its application to conduction and excitation in nerve. J Physiol 117:500-544.

Holland CM, Smith EE, Csapo I, Gurol ME, Brylka DA, Killiany RJ, Blacker D, Albert MS, Guttmann CR, Greenberg SM (2008) Spatial distribution of white-matter hyperintensities in Alzheimer disease, cerebral amyloid angiopathy, and healthy aging. Stroke 39:1127-1133.

Holland PR, Bastin ME, Jansen MA, Merrifield GD, Coltman RB, Scott F, Nowers H, Khallout K, Marshall I, Wardlaw JM, Deary IJ, McCulloch J, Horsburgh K (2011) MRI is a sensitive marker of subtle white matter pathology in hypoperfused mice. Neurobiol Aging 32:2325 e2321-2326.

Hollenbeck PJ, Saxton WM (2005) The axonal transport of mitochondria. J Cell Sci 118:5411-5419.

Horner PJ, Power AE, Kempermann G, Kuhn HG, Palmer TD, Winkler J, Thal LJ, Gage FH (2000) Proliferation and differentiation of progenitor cells throughout the intact adult rat spinal cord. J Neurosci 20:2218-2228.

Howell OW, Rundle JL, Garg A, Komada M, Brophy PJ, Reynolds R (2010) Activated microglia mediate axoglial disruption that contributes to axonal injury in multiple sclerosis. J Neuropathol Exp Neurol 69:1017-1033.

Howell OW, Palser A, Polito A, Melrose S, Zonta B, Scheiermann C, Vora AJ, Brophy PJ, Reynolds R (2006) Disruption of neurofascin localization reveals early changes preceding demyelination and remyelination in multiple sclerosis. Brain 129:3173-3185.

Hubbs AF, Benkovic SA, Miller DB, O'Callaghan JP, Battelli L, Schwegler-Berry D, Ma Q (2007) Vacuolar leukoencephalopathy with widespread astrogliosis in mice lacking transcription factor Nrf2. Am J Pathol 170:2068-2076.

Hughes EG, Kang SH, Fukaya M, Bergles DE (2013) Oligodendrocyte progenitors balance growth with self-repulsion to achieve homeostasis in the adult brain. Nat Neurosci 16:668-676.

Huxley AF, Stampfli R (1949) Evidence for saltatory conduction in peripheral myelinated nerve fibres. J Physiol 108:315-339.

Hyden H, Pigon A (1960) A cytophysiological study of the functional relationship between oliodendroglial cells and nerve cells of Deiters' nucleus. J Neurochem 6:57-72.

Ichimura T, Ellisman MH (1991) Three-dimensional fine structure of cytoskeletal-membrane interactions at nodes of Ranvier. J Neurocytol 20:667-681.

Ihara M, Tomimoto H (2011) Lessons from a mouse model characterizing features of vascular cognitive impairment with white matter changes. J Aging Res 2011:978761.

Irving EA, Yatsushiro K, McCulloch J, Dewar D (1997) Rapid alteration of tau in oligodendrocytes after focal ischemic injury in the rat: involvement of free radicals. J Cereb Blood Flow Metab 17:612-622.

Itoh K, Wakabayashi N, Katoh Y, Ishii T, Igarashi K, Engel JD, Yamamoto M (1999) Keap1 represses nuclear activation of antioxidant responsive elements by Nrf2 through binding to the amino-terminal Neh2 domain. Genes Dev 13:76-86.

Itoh K, Chiba T, Takahashi S, Ishii T, Igarashi K, Katoh Y, Oyake T, Hayashi N, Satoh K, Hatayama I, Yamamoto M, Nabeshima Y (1997) An Nrf2/small Maf heterodimer mediates the induction of phase II detoxifying enzyme genes through antioxidant response elements. Biochem Biophys Res Commun 236:313-322.

Johnson DA, Amirahmadi S, Ward C, Fabry Z, Johnson JA (2010) The absence of the pro-antioxidant transcription factor Nrf2 exacerbates experimental autoimmune encephalomyelitis. Toxicological sciences : an official journal of the Society of Toxicology 114:237-246.

Juurlink BH (1997) Response of glial cells to ischemia: roles of reactive oxygen species and glutathione. Neurosci Biobehav Rev 21:151-166.

Kaplan MR, Cho MH, Ullian EM, Isom LL, Levinson SR, Barres BA (2001) Differential control of clustering of the sodium channels Na(v)1.2 and Na(v)1.6 at developing CNS nodes of Ranvier. Neuron 30:105-119.

Kaplan MR, Meyer-Franke A, Lambert S, Bennett V, Duncan ID, Levinson SR, Barres BA (1997) Induction of sodium channel clustering by oligodendrocytes. Nature 386:724-728.

Karadottir R, Cavelier P, Bergersen LH, Attwell D (2005) NMDA receptors are expressed in oligodendrocytes and activated in ischaemia. Nature 438:1162-1166.

Karadottir R, Hamilton NB, Bakiri Y, Attwell D (2008) Spiking and nonspiking classes of oligodendrocyte precursor glia in CNS white matter. Nat Neurosci 11:450-456.

Kawamura J, Meyer JS, Terayama Y, Weathers S (1991) Leukoaraiosis correlates with cerebral hypoperfusion in vascular dementia. Stroke 22:609-614.

Kees F (2013) Dimethyl fumarate : a Janus-faced substance? Expert Opin Pharmacother 14:1559-1567.

Keirstead HS, Levine JM, Blakemore WF (1998) Response of the oligodendrocyte progenitor cell population (defined by NG2 labelling) to demyelination of the adult spinal cord. Glia 22:161-170.

Kelly S, McCulloch J, Horsburgh K (2001) Minimal ischaemic neuronal damage and HSP70 expression in MF1 strain mice following bilateral common carotid artery occlusion. Brain Res 914:185-195.

Kensler TW, Wakabayashi N, Biswal S (2007) Cell survival responses to environmental stresses via the Keap1-Nrf2-ARE pathway. Annu Rev Pharmacol Toxicol 47:89-116.

Kitagawa K, Matsumoto M, Yang G, Mabuchi T, Yagita Y, Hori M, Yanagihara T (1998) Cerebral ischemia after bilateral carotid artery occlusion and intraluminal suture occlusion in mice: evaluation of the patency of the posterior communicating artery. J Cereb Blood Flow Metab 18:570-579.

Kitamura A, Fujita Y, Oishi N, Kalaria RN, Washida K, Maki T, Okamoto Y, Hase Y, Yamada M, Takahashi J, Ito H, Tomimoto H, Fukuyama H, Takahashi R, Ihara M (2012) Selective white matter abnormalities in a novel rat model of vascular dementia. Neurobiol Aging 33:1012 e1025-1035.

Kivipelto M, Helkala EL, Laakso MP, Hanninen T, Hallikainen M, Alhainen K, Soininen H, Tuomilehto J, Nissinen A (2001) Midlife vascular risk factors and Alzheimer's disease in later life: longitudinal, population based study. BMJ 322:1447-1451.

Klein B, Kuschinsky W, Schrock H, Vetterlein F (1986) Interdependency of local capillary density, blood flow, and metabolism in rat brains. Am J Physiol 251:H1333-1340.

Kraft AD, Johnson DA, Johnson JA (2004) Nuclear factor E2-related factor 2-dependent antioxidant response element activation by tert-butylhydroquinone and sulforaphane occurring preferentially in astrocytes conditions neurons against oxidative insult. J Neurosci 24:1101-1112.

Kreutzberg GW (1996) Microglia: a sensor for pathological events in the CNS. Trends Neurosci 19:312-318.

Kudo T, Tada K, Takeda M, Nishimura T (1990) Learning impairment and microtubule-associated protein 2 decrease in gerbils under chronic cerebral hypoperfusion. Stroke 21:1205-1209.

Lasiene J, Matsui A, Sawa Y, Wong F, Horner PJ (2009) Age-related myelin dynamics revealed by increased oligodendrogenesis and short internodes. Aging Cell 8:201-213.

Lassmann H, Bartsch U, Montag D, Schachner M (1997) Dying-back oligodendrogliopathy: a late sequel of myelin-associated glycoprotein deficiency. Glia 19:104-110.

Lawson LJ, Perry VH, Dri P, Gordon S (1990) Heterogeneity in the distribution and morphology of microglia in the normal adult mouse brain. Neuroscience 39:151-170.

Lebel C, Gee M, Camicioli R, Wieler M, Martin W, Beaulieu C (2012) Diffusion tensor imaging of white matter tract evolution over the lifespan. Neuroimage 60:340-352.

Lecca D, Trincavelli ML, Gelosa P, Sironi L, Ciana P, Fumagalli M, Villa G, Verderio C, Grumelli C, Guerrini U, Tremoli E, Rosa P, Cuboni S, Martini C, Buffo A, Cimino M, Abbracchio MP (2008) The recently identified P2Y-like receptor GPR17 is a sensor of brain damage and a new target for brain repair. PLoS One 3:e3579.

Lee JH, Park SY, Shin YW, Hong KW, Kim CD, Sung SM, Kim KY, Lee WS (2006) Neuroprotection by cilostazol, a phosphodiesterase type 3 inhibitor, against apoptotic white matter changes in rat after chronic cerebral hypoperfusion. Brain Res 1082:182-191.

Lee Y, Morrison BM, Li Y, Lengacher S, Farah MH, Hoffman PN, Liu Y, Tsingalia A, Jin L, Zhang PW, Pellerin L, Magistretti PJ, Rothstein JD (2012) Oligodendroglia metabolically support axons and contribute to neurodegeneration. Nature 487:443-448.

Leenders KL, Perani D, Lammertsma AA, Heather JD, Buckingham P, Healy MJ, Gibbs JM, Wise RJ, Hatazawa J, Herold S, et al. (1990) Cerebral blood flow, blood volume and oxygen utilization. Normal values and effect of age. Brain 113 (Pt 1):27-47.

Levine JM, Reynolds R, Fawcett JW (2001) The oligodendrocyte precursor cell in health and disease. Trends Neurosci 24:39-47.

Li C, Trapp B, Ludwin S, Peterson A, Roder J (1998) Myelin associated glycoprotein modulates glia-axon contact in vivo. J Neurosci Res 51:210-217.

Li CL, Martini LG, Ford JL, Roberts M (2005) The use of hypromellose in oral drug delivery. J Pharm Pharmacol 57:533-546.

Ling EA, Leblond CP (1973) Investigation of glial cells in semithin sections. II. Variation with age in the numbers of the various glial cell types in rat cortex and corpus callosum. The Journal of comparative neurology 149:73-81.

Linker RA, Lee DH, Ryan S, van Dam AM, Conrad R, Bista P, Zeng W, Hronowsky X, Buko A, Chollate S, Ellrichmann G, Bruck W, Dawson K, Goelz S, Wiese S, Scannevin RH, Lukashev M, Gold R (2011) Fumaric acid esters exert neuroprotective effects in neuroinflammation via activation of the Nrf2 antioxidant pathway. Brain 134:678-692.

Litjens NH, Burggraaf J, van Strijen E, van Gulpen C, Mattie H, Schoemaker RC, van Dissel JT, Thio HB, Nibbering PH (2004) Pharmacokinetics of oral fumarates in healthy subjects. Br J Clin Pharmacol 58:429-432.

Little GJ, Heath JW (1994) Morphometric analysis of axons myelinated during adult life in the mouse superior cervical ganglion. J Anat 184 (Pt 2):387-398.

Lo EH, Dalkara T, Moskowitz MA (2003) Mechanisms, challenges and opportunities in stroke. Nat Rev Neurosci 4:399-415.
Lucchinetti C, Bruck W, Parisi J, Scheithauer B, Rodriguez M, Lassmann H (2000) Heterogeneity of multiple sclerosis lesions: implications for the pathogenesis of demyelination. Ann Neurol 47:707-717.
Ludwin SK, Johnson ES (1981) Evidence for a "dying-back" gliopathy in demyelinating disease. Ann Neurol 9:301-305.
Mabuchi T, Kitagawa K, Ohtsuki T, Kuwabara K, Yagita Y, Yanagihara T, Hori M, Matsumoto M (2000) Contribution of microglia/macrophages to expansion of infarction and response of oligodendrocytes after focal cerebral ischemia in rats. Stroke 31:1735-1743.
Magistretti PJ, Pellerin L (1999) Cellular mechanisms of brain energy metabolism and their relevance to functional brain imaging. Philos Trans R Soc Lond B Biol Sci 354:1155-1163.
Magistretti PJ, Allaman I (2013) Brain Energy Metabolism. New York: Springer.
Majid A, He YY, Gidday JM, Kaplan SS, Gonzales ER, Park TS, Fenstermacher JD, Wei L, Choi DW, Hsu CY (2000) Differences in vulnerability to permanent focal cerebral ischemia among 3 common mouse strains. Stroke 31:2707-2714.
Maki T, Ihara M, Fujita Y, Nambu T, Miyashita K, Yamada M, Washida K, Nishio K, Ito H, Harada H, Yokoi H, Arai H, Itoh H, Nakao K, Takahashi R, Tomimoto H (2011) Angiogenic and vasoprotective effects of adrenomedullin on prevention of cognitive decline after chronic cerebral hypoperfusion in mice. Stroke 42:1122-1128.
Mandai K, Matsumoto M, Kitagawa K, Matsushita K, Ohtsuki T, Mabuchi T, Colman DR, Kamada T, Yanagihara T (1997) Ischemic damage and subsequent proliferation of oligodendrocytes in focal cerebral ischemia. Neuroscience 77:849-861.
Marcus J, Dupree JL, Popko B (2002) Myelin-associated glycoprotein and myelin galactolipids stabilize developing axo-glial interactions. J Cell Biol 156:567-577.
Markesbery WR (1997) Oxidative stress hypothesis in Alzheimer's disease. Free Radic Biol Med 23:134-147.
McDonald WI, Sears TA (1970) The effects of experimental demyelination on conduction in the central nervous system. Brain 93:583-598.
McIver SR, Lee CS, Lee JM, Green SH, Sands MS, Snider BJ, Goldberg MP (2005) Lentiviral transduction of murine oligodendrocytes in vivo. J Neurosci Res 82:397-403.
McIver SR, Muccigrosso M, Gonzales ER, Lee JM, Roberts MS, Sands MS, Goldberg MP (2010) Oligodendrocyte degeneration and recovery after focal cerebral ischemia. Neuroscience 169:1364-1375.
McTigue DM, Tripathi RB (2008) The life, death, and replacement of oligodendrocytes in the adult CNS. J Neurochem 107:1-19.
McTigue DM, Horner PJ, Stokes BT, Gage FH (1998) Neurotrophin-3 and brain-derived neurotrophic factor induce oligodendrocyte proliferation and myelination of regenerating axons in the contused adult rat spinal cord. J Neurosci 18:5354-5365.

Merrill JE, Scolding NJ (1999) Mechanisms of damage to myelin and oligodendrocytes and their relevance to disease. Neuropathol Appl Neurobiol 25:435-458.

Miki K, Ishibashi S, Sun L, Xu H, Ohashi W, Kuroiwa T, Mizusawa H (2009) Intensity of chronic cerebral hypoperfusion determines white/gray matter injury and cognitive/motor dysfunction in mice. J Neurosci Res 87:1270-1281.

Miron VE, Boyd A, Zhao JW, Yuen TJ, Ruckh JM, Shadrach JL, van Wijngaarden P, Wagers AJ, Williams A, Franklin RJ, ffrench-Constant C (2013) M2 microglia and macrophages drive oligodendrocyte differentiation during CNS remyelination. Nat Neurosci 16:1211-1218.

Misgeld T, Kerschensteiner M, Bareyre FM, Burgess RW, Lichtman JW (2007) Imaging axonal transport of mitochondria in vivo. Nat Methods 4:559-561.

Miyamoto N, Pham LD, Seo JH, Kim KW, Lo EH, Arai K (2013a) Crosstalk between cerebral endothelium and oligodendrocyte. Cell Mol Life Sci 711055-66:1055-1066.

Miyamoto N, Maki T, Pham LD, Hayakawa K, Seo JH, Mandeville ET, Mandeville JB, Kim KW, Lo EH, Arai K (2013b) Oxidative Stress Interferes With White Matter Renewal After Prolonged Cerebral Hypoperfusion in Mice. Stroke 44:3516-3352.

Miyamoto N, Pham LD, Hayakawa K, Matsuzaki T, Seo JH, Magnain C, Ayata C, Kim KW, Boas D, Lo EH, Arai K (2013c) Age-Related Decline in Oligodendrogenesis Retards White Matter Repair in Mice. Stroke 44:2573-2578.

Moharregh-Khiabani D, Blank A, Skripuletz T, Miller E, Kotsiari A, Gudi V, Stangel M (2010) Effects of fumaric acids on cuprizone induced central nervous system de- and remyelination in the mouse. PLoS One 5:e11769.

Morland C, Henjum S, Iversen EG, Skrede KK, Hassel B (2007) Evidence for a higher glycolytic than oxidative metabolic activity in white matter of rat brain. Neurochem Int 50:703-709.

Mosser DM, Edwards JP (2008) Exploring the full spectrum of macrophage activation. Nat Rev Immunol 8:958-969.

Nagaoka A, Suno M, Shibota M, Kakihana M (1989) Effects of idebenone on neurological deficits, local cerebral blood flow, and energy metabolism in rats with experimental cerebral ischemia. Arch Gerontol Geriatr 8:193-202.

Nait-Oumesmar B, Decker L, Lachapelle F, Avellana-Adalid V, Bachelin C, Baron-Van Evercooren A (1999) Progenitor cells of the adult mouse subventricular zone proliferate, migrate and differentiate into oligodendrocytes after demyelination. Eur J Neurosci 11:4357-4366.

Nans A, Einheber S, Salzer JL, Stokes DL (2011) Electron tomography of paranodal septate-like junctions and the associated axonal and glial cytoskeletons in the central nervous system. J Neurosci Res 89:310-319.

Nave KA (2010a) Myelination and support of axonal integrity by glia. Nature 468:244-252.

Nave KA (2010b) Myelination and the trophic support of long axons. Nat Rev Neurosci 11:275-283.

Ness JK, Valentino M, McIver SR, Goldberg MP (2005) Identification of oligodendrocytes in experimental disease models. Glia 50:321-328.

Ni J, Ohta H, Matsumoto K, Watanabe H (1994) Progressive cognitive impairment following chronic cerebral hypoperfusion induced by permanent occlusion of bilateral carotid arteries in rats. Brain Res 653:231-236.

Nie DY, Ma QH, Law JW, Chia CP, Dhingra NK, Shimoda Y, Yang WL, Gong N, Chen QW, Xu G, Hu QD, Chow PK, Ng YK, Ling EA, Watanabe K, Xu TL, Habib AA, Schachner M, Xiao ZC (2006) Oligodendrocytes regulate formation of nodes of Ranvier via the recognition molecule OMgp. Neuron Glia Biol 2:151-164.

Nishio K, Ihara M, Yamasaki N, Kalaria RN, Maki T, Fujita Y, Ito H, Oishi N, Fukuyama H, Miyakawa T, Takahashi R, Tomimoto H (2010) A mouse model characterizing features of vascular dementia with hippocampal atrophy. Stroke 41:1278-1284.

Nishiyama A, Watanabe M, Yang Z, Bu J (2002) Identity, distribution, and development of polydendrocytes: NG2-expressing glial cells. J Neurocytol 31:437-455.

Nishiyama A, Komitova M, Suzuki R, Zhu X (2009) Polydendrocytes (NG2 cells): multifunctional cells with lineage plasticity. Nat Rev Neurosci 10:9-22.

Nishiyama A, Lin XH, Giese N, Heldin CH, Stallcup WB (1996) Co-localization of NG2 proteoglycan and PDGF alpha-receptor on O2A progenitor cells in the developing rat brain. J Neurosci Res 43:299-314.

Nishizaki T, Yamauchi R, Tanimoto M, Okada Y (1988) Effects of temperature on the oxygen consumption in thin slices from different brain regions. Neurosci Lett 86:301-305.

Nonaka H, Akima M, Hatori T, Nagayama T, Zhang Z, Ihara F (2003) The microvasculature of the cerebral white matter: arteries of the subcortical white matter. J Neuropathol Exp Neurol 62:154-161.

O'Brien JT, Wiseman R, Burton EJ, Barber B, Wesnes K, Saxby B, Ford GA (2002) Cognitive associations of subcortical white matter lesions in older people. Ann N Y Acad Sci 977:436-444.

O'Sullivan M, Jones DK, Summers PE, Morris RG, Williams SC, Markus HS (2001) Evidence for cortical "disconnection" as a mechanism of age-related cognitive decline. Neurology 57:632-638.

O'Sullivan M, Lythgoe DJ, Pereira AC, Summers PE, Jarosz JM, Williams SC, Markus HS (2002) Patterns of cerebral blood flow reduction in patients with ischemic leukoaraiosis. Neurology 59:321-326.

Ohgami T, Kitamoto T, Tateishi J (1992) Alzheimer's amyloid precursor protein accumulates within axonal swellings in human brain lesions. Neurosci Lett 136:75-78.

Ohno N, Kidd GJ, Mahad D, Kiryu-Seo S, Avishai A, Komuro H, Trapp BD (2011) Myelination and axonal electrical activity modulate the distribution and motility of mitochondria at CNS nodes of Ranvier. J Neurosci 31:7249-7258.

Ohta H, Nishikawa H, Kimura H, Anayama H, Miyamoto M (1997) Chronic cerebral hypoperfusion by permanent internal carotid ligation produces learning impairment without brain damage in rats. Neuroscience 79:1039-1050.

Pachner AR (2011) Experimental models of multiple sclerosis. Curr Opin Neurol 24:291-299.

Panahian N, Yoshiura M, Maines MD (1999) Overexpression of heme oxygenase-1 is neuroprotective in a model of permanent middle cerebral artery occlusion in transgenic mice. J Neurochem 72:1187-1203.

Pantano P, Baron JC, Lebrun-Grandie P, Duquesnoy N, Bousser MG, Comar D (1984) Regional cerebral blood flow and oxygen consumption in human aging. Stroke 15:635-641.

Pantoni L, Garcia JH (1997) Pathogenesis of leukoaraiosis: a review. Stroke 28:652-659.

Pantoni L, Garcia JH, Gutierrez JA (1996) Cerebral white matter is highly vulnerable to ischemia. Stroke 27:1641-1646; discussion 1647.

Pappas BA, de la Torre JC, Davidson CM, Keyes MT, Fortin T (1996) Chronic reduction of cerebral blood flow in the adult rat: late-emerging CA1 cell loss and memory dysfunction. Brain Res 708:50-58.

Pareek TK, Belkadi A, Kesavapany S, Zaremba A, Loh SL, Bai L, Cohen ML, Meyer C, Liby KT, Miller RH, Sporn MB, Letterio JJ (2011) Triterpenoid modulation of IL-17 and Nrf-2 expression ameliorates neuroinflammation and promotes remyelination in autoimmune encephalomyelitis. Scientific reports 1:201.

Park JA, Choi KS, Kim SY, Kim KW (2003) Coordinated interaction of the vascular and nervous systems: from molecule- to cell-based approaches. Biochem Biophys Res Commun 311:247-253.

Paxinos G, Franklin KBJ (2001) The Mouse Brain in Stereotaxic Coordinates: Academic Press.

Pellerin L, Magistretti PJ (1994) Glutamate uptake into astrocytes stimulates aerobic glycolysis: a mechanism coupling neuronal activity to glucose utilization. Proc Natl Acad Sci U S A 91:10625-10629.

Peters A (2004) A fourth type of neuroglial cell in the adult central nervous system. J Neurocytol 33:345-357.

Peters A, Sethares C (2002) Aging and the myelinated fibers in prefrontal cortex and corpus callosum of the monkey. The Journal of comparative neurology 442:277-291.

Pillai AM, Thaxton C, Pribisko AL, Cheng JG, Dupree JL, Bhat MA (2009) Spatiotemporal ablation of myelinating glia-specific neurofascin (Nfasc NF155) in mice reveals gradual loss of paranodal axoglial junctions and concomitant disorganization of axonal domains. J Neurosci Res 87:1773-1793.

Poliak S, Peles E (2003) The local differentiation of myelinated axons at nodes of Ranvier. Nat Rev Neurosci 4:968-980.

Poliak S, Salomon D, Elhanany H, Sabanay H, Kiernan B, Pevny L, Stewart CL, Xu X, Chiu SY, Shrager P, Furley AJ, Peles E (2003) Juxtaparanodal clustering of Shaker-like K+ channels in myelinated axons depends on Caspr2 and TAG-1. J Cell Biol 162:1149-1160.

Powers BE, Sellers DL, Lovelett EA, Cheung W, Aalami SP, Zapertov N, Maris DO, Horner PJ (2013) Remyelination reporter reveals prolonged refinement of spontaneously regenerated myelin. Proc Natl Acad Sci U S A 110:4075-4080.

Psachoulia K, Jamen F, Young KM, Richardson WD (2009) Cell cycle dynamics of NG2 cells in the postnatal and ageing brain. Neuron Glia Biol 5:57-67.

Pulsinelli WA, Brierley JB (1979) A new model of bilateral hemispheric ischemia in the unanesthetized rat. Stroke 10:267-272.
Raff MC, Miller RH, Noble M (1983) A glial progenitor cell that develops in vitro into an astrocyte or an oligodendrocyte depending on culture medium. Nature 303:390-396.
Raff MC, Lillien LE, Richardson WD, Burne JF, Noble MD (1988) Platelet-derived growth factor from astrocytes drives the clock that times oligodendrocyte development in culture. Nature 333:562-565.
Ramsey CP, Glass CA, Montgomery MB, Lindl KA, Ritson GP, Chia LA, Hamilton RL, Chu CT, Jordan-Sciutto KL (2007) Expression of Nrf2 in neurodegenerative diseases. J Neuropathol Exp Neurol 66:75-85.
Rasband MN (2004) It's "juxta" potassium channel! J Neurosci Res 76:749-757.
Ratcliffe CF, Westenbroek RE, Curtis R, Catterall WA (2001) Sodium channel beta1 and beta3 subunits associate with neurofascin through their extracellular immunoglobulin-like domain. J Cell Biol 154:427-434.
Reimer MM, McQueen J, Searcy L, Scullion G, Zonta B, Desmazieres A, Holland PR, Smith J, Gliddon C, Wood ER, Herzyk P, Brophy PJ, McCulloch J, Horsburgh K (2011) Rapid disruption of axon-glial integrity in response to mild cerebral hypoperfusion. J Neurosci 31:18185-18194.
Rempp KA, Brix G, Wenz F, Becker CR, Guckel F, Lorenz WJ (1994) Quantification of regional cerebral blood flow and volume with dynamic susceptibility contrast-enhanced MR imaging. Radiology 193:637-641.
Reynolds R, Dawson M, Papadopoulos D, Polito A, Di Bello IC, Pham-Dinh D, Levine J (2002) The response of NG2-expressing oligodendrocyte progenitors to demyelination in MOG-EAE and MS. J Neurocytol 31:523-536.
Richardson WD, Young KM, Tripathi RB, McKenzie I (2011) NG2-glia as multipotent neural stem cells: fact or fantasy? Neuron 70:661-673.
Rinholm JE, Hamilton NB, Kessaris N, Richardson WD, Bergersen LH, Attwell D (2011) Regulation of oligodendrocyte development and myelination by glucose and lactate. J Neurosci 31:538-548.
Ritter J, Schmitz T, Chew LJ, Buhrer C, Mobius W, Zonouzi M, Gallo V (2013) Neonatal hyperoxia exposure disrupts axon-oligodendrocyte integrity in the subcortical white matter. J Neurosci 33:8990-9002.
Rivers LE, Young KM, Rizzi M, Jamen F, Psachoulia K, Wade A, Kessaris N, Richardson WD (2008) PDGFRA/NG2 glia generate myelinating oligodendrocytes and piriform projection neurons in adult mice. Nat Neurosci 11:1392-1401.
Rosenbluth J (2009) Multiple functions of the paranodal junction of myelinated nerve fibers. J Neurosci Res 87:3250-3258.
Rosenzweig S, Carmichael ST (2013) Age-Dependent Exacerbation of White Matter Stroke Outcomes: A Role for Oxidative Damage and Inflammatory Mediators. Stroke.
Rostami-Yazdi M, Clement B, Mrowietz U (2010) Pharmacokinetics of anti-psoriatic fumaric acid esters in psoriasis patients. Arch Dermatol Res 302:531-538.
Ruitenberg A, den Heijer T, Bakker SL, van Swieten JC, Koudstaal PJ, Hofman A, Breteler MM (2005) Cerebral hypoperfusion and clinical onset of dementia: the Rotterdam Study. Ann Neurol 57:789-794.

Saab AS, Tzvetanova ID, Nave KA (2013) The role of myelin and oligodendrocytes in axonal energy metabolism. Curr Opin Neurobiol 231065-72:1065-1072.
Saijo K, Glass CK (2011) Microglial cell origin and phenotypes in health and disease. Nat Rev Immunol 11:775-787.
Scannevin RH, Chollate S, Jung MY, Shackett M, Patel H, Bista P, Zeng W, Ryan S, Yamamoto M, Lukashev M, Rhodes KJ (2012) Fumarates promote cytoprotection of central nervous system cells against oxidative stress via the nuclear factor (erythroid-derived 2)-like 2 pathway. The Journal of pharmacology and experimental therapeutics 341:274-284.
Scarpelli M, Salvolini U, Diamanti L, Montironi R, Chiaromoni L, Maricotti M (1994) MRI and pathological examination of post-mortem brains: the problem of white matter high signal areas. Neuroradiology 36:393-398.
Scheel P, Ruge C, Petruch UR, Schoning M (2000) Color duplex measurement of cerebral blood flow volume in healthy adults. Stroke 31:147-150.
Scheltens P, Barkhof F, Leys D, Wolters EC, Ravid R, Kamphorst W (1995) Histopathologic correlates of white matter changes on MRI in Alzheimer's disease and normal aging. Neurology 45:883-888.
Schilling S, Goelz S, Linker R, Luehder F, Gold R (2006) Fumaric acid esters are effective in chronic experimental autoimmune encephalomyelitis and suppress macrophage infiltration. Clinical and experimental immunology 145:101-107.
Schnaar RL, Lopez PH (2009) Myelin-associated glycoprotein and its axonal receptors. J Neurosci Res 87:3267-3276.
Schurr A (2006) Lactate: the ultimate cerebral oxidative energy substrate? J Cereb Blood Flow Metab 26:142-152.
Schurr A, West CA, Rigor BM (1988) Lactate-supported synaptic function in the rat hippocampal slice preparation. Science 240:1326-1328.
Seo JH, Miyamoto N, Hayakawa K, Pham LD, Maki T, Ayata C, Kim KW, Lo EH, Arai K (2013) Oligodendrocyte precursors induce early blood-brain barrier opening after white matter injury. J Clin Invest 123:782-786.
Shepherd MN, Pomicter AD, Velazco CS, Henderson SC, Dupree JL (2012) Paranodal reorganization results in the depletion of transverse bands in the aged central nervous system. Neurobiol Aging 33:203 e213-224.
Shibata M, Ohtani R, Ihara M, Tomimoto H (2004) White matter lesions and glial activation in a novel mouse model of chronic cerebral hypoperfusion. Stroke 35:2598-2603.
Shibata M, Yamasaki N, Miyakawa T, Kalaria RN, Fujita Y, Ohtani R, Ihara M, Takahashi R, Tomimoto H (2007) Selective impairment of working memory in a mouse model of chronic cerebral hypoperfusion. Stroke 38:2826-2832.
Shih AY, Li P, Murphy TH (2005) A small-molecule-inducible Nrf2-mediated antioxidant response provides effective prophylaxis against cerebral ischemia in vivo. J Neurosci 25:10321-10335.
Simpson JE, Fernando MS, Clark L, Ince PG, Matthews F, Forster G, O'Brien JT, Barber R, Kalaria RN, Brayne C, Shaw PJ, Lewis CE, Wharton SB, Function MRCC, Ageing Neuropathology Study G (2007a) White matter lesions in an unselected cohort of the elderly: astrocytic, microglial and oligodendrocyte precursor cell responses. Neuropathol Appl Neurobiol 33:410-419.

Simpson JE, Ince PG, Higham CE, Gelsthorpe CH, Fernando MS, Matthews F, Forster G, O'Brien JT, Barber R, Kalaria RN, Brayne C, Shaw PJ, Stoeber K, Williams GH, Lewis CE, Wharton SB, Function MRCC, Ageing Neuropathology Study G (2007b) Microglial activation in white matter lesions and nonlesional white matter of ageing brains. Neuropathol Appl Neurobiol 33:670-683.

Smith RS, Koles ZJ (1970) Myelinated nerve fibers: computed effect of myelin thickness on conduction velocity. Am J Physiol 219:1256-1258.

Soane L, Li Dai W, Fiskum G, Bambrick LL (2010) Sulforaphane protects immature hippocampal neurons against death caused by exposure to hemin or to oxygen and glucose deprivation. J Neurosci Res 88:1355-1363.

Sofroniew MV (2009) Molecular dissection of reactive astrogliosis and glial scar formation. Trends Neurosci 32:638-647.

Sofroniew MV, Vinters HV (2010) Astrocytes: biology and pathology. Acta Neuropathol 119:7-35.

Sokoloff L (1992) The brain as a chemical machine. Prog Brain Res 94:19-33.

Sokoloff L, Reivich M, Kennedy C, Des Rosiers MH, Patlak CS, Pettigrew KD, Sakurada O, Shinohara M (1977) The [14C]deoxyglucose method for the measurement of local cerebral glucose utilization: theory, procedure, and normal values in the conscious and anesthetized albino rat. J Neurochem 28:897-916.

Son TG, Camandola S, Arumugam TV, Cutler RG, Telljohann RS, Mughal MR, Moore TA, Luo W, Yu QS, Johnson DA, Johnson JA, Greig NH, Mattson MP (2010) Plumbagin, a novel Nrf2/ARE activator, protects against cerebral ischemia. J Neurochem 112:1316-1326.

Srinivasan Y, Elmer L, Davis J, Bennett V, Angelides K (1988) Ankyrin and spectrin associate with voltage-dependent sodium channels in brain. Nature 333:177-180.

Stallcup WB, Beasley L (1987) Bipotential glial precursor cells of the optic nerve express the NG2 proteoglycan. J Neurosci 7:2737-2744.

Stenzel-Poore MP, Stevens SL, Xiong Z, Lessov NS, Harrington CA, Mori M, Meller R, Rosenzweig HL, Tobar E, Shaw TE, Chu X, Simon RP (2003) Effect of ischaemic preconditioning on genomic response to cerebral ischaemia: similarity to neuroprotective strategies in hibernation and hypoxia-tolerant states. Lancet 362:1028-1037.

Suenaga T, Ohnishi K, Nishimura M, Nakamura S, Akiguchi I, Kimura J (1994) Bundles of amyloid precursor protein-immunoreactive axons in human cerebrovascular white matter lesions. Acta Neuropathol 87:450-455.

Sun XY, Takagishi Y, Okabe E, Chishima Y, Kanou Y, Murase S, Mizumura K, Inaba M, Komatsu Y, Hayashi Y, Peles E, Oda S, Murata Y (2009) A novel Caspr mutation causes the shambling mouse phenotype by disrupting axoglial interactions of myelinated nerves. J Neuropathol Exp Neurol 68:1207-1218.

Susuki K (2013) Node of Ranvier disruption as a cause of neurological diseases. ASN Neuro.

Tait S, Gunn-Moore F, Collinson JM, Huang J, Lubetzki C, Pedraza L, Sherman DL, Colman DR, Brophy PJ (2000) An oligodendrocyte cell adhesion molecule at the site of assembly of the paranodal axo-glial junction. J Cell Biol 150:657-666.

Tamura Y, Kataoka Y, Cui Y, Takamori Y, Watanabe Y, Yamada H (2007) Intracellular translocation of glutathione S-transferase pi during oligodendrocyte differentiation in adult rat cerebral cortex in vivo. Neuroscience 148:535-540.

Tanaka K, Nogawa S, Suzuki S, Dembo T, Kosakai A (2003) Upregulation of oligodendrocyte progenitor cells associated with restoration of mature oligodendrocytes and myelination in peri-infarct area in the rat brain. Brain Res 989:172-179.

Tanaka K, Nogawa S, Ito D, Suzuki S, Dembo T, Kosakai A, Fukuuchi Y (2001) Activation of NG2-positive oligodendrocyte progenitor cells during post-ischemic reperfusion in the rat brain. Neuroreport 12:2169-2174.

Tang Y, Nyengaard JR, Pakkenberg B, Gundersen HJ (1997) Age-induced white matter changes in the human brain: a stereological investigation. Neurobiol Aging 18:609-615.

Tarczyluk MA, Nagel DA, O'Neil JD, Parri HR, Tse EH, Coleman MD, Hill EJ (2013) Functional astrocyte-neuron lactate shuttle in a human stem cell-derived neuronal network. J Cereb Blood Flow Metab 33:1386-1393.

Taupin P (2007) BrdU immunohistochemistry for studying adult neurogenesis: paradigms, pitfalls, limitations, and validation. Brain Res Rev 53:198-214.

Tekkok SB, Brown AM, Westenbroek R, Pellerin L, Ransom BR (2005) Transfer of glycogen-derived lactate from astrocytes to axons via specific monocarboxylate transporters supports mouse optic nerve activity. J Neurosci Res 81:644-652.

Thaxton C, Pillai AM, Pribisko AL, Dupree JL, Bhat MA (2011) Nodes of Ranvier act as barriers to restrict invasion of flanking paranodal domains in myelinated axons. Neuron 69:244-257.

Thorburne SK, Juurlink BH (1996) Low glutathione and high iron govern the susceptibility of oligodendroglial precursors to oxidative stress. J Neurochem 67:1014-1022.

Trapp BD, Peterson J, Ransohoff RM, Rudick R, Mork S, Bo L (1998) Axonal transection in the lesions of multiple sclerosis. The New England journal of medicine 338:278-285.

Ueno Y, Zhang N, Miyamoto N, Tanaka R, Hattori N, Urabe T (2009) Edaravone attenuates white matter lesions through endothelial protection in a rat chronic hypoperfusion model. Neuroscience 162:317-327.

Valeriani V, Dewar D, McCulloch J (2000) Quantitative assessment of ischemic pathology in axons, oligodendrocytes, and neurons: attenuation of damage after transient ischemia. J Cereb Blood Flow Metab 20:765-771.

Vargas MR, Johnson JA (2009) The Nrf2-ARE cytoprotective pathway in astrocytes. Expert reviews in molecular medicine 11:e17.

Vargas MR, Johnson DA, Sirkis DW, Messing A, Johnson JA (2008) Nrf2 activation in astrocytes protects against neurodegeneration in mouse models of familial amyotrophic lateral sclerosis. J Neurosci 28:13574-13581.

Wakita H, Tomimoto H, Akiguchi I, Matsuo A, Lin JX, Ihara M, McGeer PL (2002) Axonal damage and demyelination in the white matter after chronic cerebral hypoperfusion in the rat. Brain Res 924:63-70.

Wang G, Zhang J, Hu X, Zhang L, Mao L, Jiang X, Liou AK, Leak RK, Gao Y, Chen J (2013) Microglia/macrophage polarization dynamics in white matter after traumatic brain injury. J Cereb Blood Flow Metab.

Wang H, Kunkel DD, Martin TM, Schwartzkroin PA, Tempel BL (1993) Heteromultimeric K+ channels in terminal and juxtaparanodal regions of neurons. Nature 365:75-79.

Washida K, Ihara M, Nishio K, Fujita Y, Maki T, Yamada M, Takahashi J, Wu X, Kihara T, Ito H, Tomimoto H, Takahashi R (2010) Nonhypotensive dose of telmisartan attenuates cognitive impairment partially due to peroxisome proliferator-activated receptor-gamma activation in mice with chronic cerebral hypoperfusion. Stroke 41:1798-1806.

Watanabe M, Toyama Y, Nishiyama A (2002) Differentiation of proliferated NG2-positive glial progenitor cells in a remyelinating lesion. J Neurosci Res 69:826-836.

Watanabe T, Zhang N, Liu M, Tanaka R, Mizuno Y, Urabe T (2006) Cilostazol protects against brain white matter damage and cognitive impairment in a rat model of chronic cerebral hypoperfusion. Stroke 37:1539-1545.

Waxman SG (2006) Axonal conduction and injury in multiple sclerosis: the role of sodium channels. Nat Rev Neurosci 7:932-941.

Waxman SG, Ritchie JM (1993) Molecular dissection of the myelinated axon. Ann Neurol 33:121-136.

Waxman SG, Black JA, Stys PK, Ransom BR (1992) Ultrastructural concomitants of anoxic injury and early post-anoxic recovery in rat optic nerve. Brain Res 574:105-119.

Wellons JC, 3rd, Sheng H, Laskowitz DT, Burkhard Mackensen G, Pearlstein RD, Warner DS (2000) A comparison of strain-related susceptibility in two murine recovery models of global cerebral ischemia. Brain Res 868:14-21.

Wender R, Brown AM, Fern R, Swanson RA, Farrell K, Ransom BR (2000) Astrocytic glycogen influences axon function and survival during glucose deprivation in central white matter. J Neurosci 20:6804-6810.

Westlye LT, Walhovd KB, Dale AM, Bjornerud A, Due-Tonnessen P, Engvig A, Grydeland H, Tamnes CK, Ostby Y, Fjell AM (2010) Life-span changes of the human brain white matter: diffusion tensor imaging (DTI) and volumetry. Cereb Cortex 20:2055-2068.

Yamazaki Y, Hozumi Y, Kaneko K, Sugihara T, Fujii S, Goto K, Kato H (2007) Modulatory effects of oligodendrocytes on the conduction velocity of action potentials along axons in the alveus of the rat hippocampal CA1 region. Neuron Glia Biol 3:325-334.

Yang G, Kitagawa K, Matsushita K, Mabuchi T, Yagita Y, Yanagihara T, Matsumoto M (1997) C57BL/6 strain is most susceptible to cerebral ischemia following bilateral common carotid occlusion among seven mouse strains: selective neuronal death in the murine transient forebrain ischemia. Brain Res 752:209-218.

Yin X, Crawford TO, Griffin JW, Tu P, Lee VM, Li C, Roder J, Trapp BD (1998) Myelin-associated glycoprotein is a myelin signal that modulates the caliber of myelinated axons. J Neurosci 18:1953-1962.

Yoshizaki K, Adachi K, Kataoka S, Watanabe A, Tabira T, Takahashi K, Wakita H (2008) Chronic cerebral hypoperfusion induced by right unilateral common

carotid artery occlusion causes delayed white matter lesions and cognitive impairment in adult mice. Exp Neurol 210:585-591.
Young KM, Psachoulia K, Tripathi RB, Dunn SJ, Cossell L, Attwell D, Tohyama K, Richardson WD (2013) Oligodendrocyte dynamics in the healthy adult CNS: evidence for myelin remodeling. Neuron 77:873-885.
Young VG, Halliday GM, Kril JJ (2008) Neuropathologic correlates of white matter hyperintensities. Neurology 71:804-811.
Yu BP (1994) Cellular defenses against damage from reactive oxygen species. Physiol Rev 74:139-162.
Yuan X, Eisen AM, McBain CJ, Gallo V (1998) A role for glutamate and its receptors in the regulation of oligodendrocyte development in cerebellar tissue slices. Development 125:2901-2914.
Zhang CL, Ho PL, Kintner DB, Sun D, Chiu SY (2010) Activity-dependent regulation of mitochondrial motility by calcium and Na/K-ATPase at nodes of Ranvier of myelinated nerves. J Neurosci 30:3555-3566.
Zhang F, Wang S, Zhang M, Weng Z, Li P, Gan Y, Zhang L, Cao G, Gao Y, Leak RK, Sporn MB, Chen J (2012) Pharmacological induction of heme oxygenase-1 by a triterpenoid protects neurons against ischemic injury. Stroke 43:1390-1397.
Zhang K, Sejnowski TJ (2000) A universal scaling law between gray matter and white matter of cerebral cortex. Proc Natl Acad Sci U S A 97:5621-5626.
Zhu X, Hill RA, Dietrich D, Komitova M, Suzuki R, Nishiyama A (2011) Age-dependent fate and lineage restriction of single NG2 cells. Development 138:745-753.

Appendices

Appendix 1: Additional domain length and behavioural data for experiments described in Chapter 3

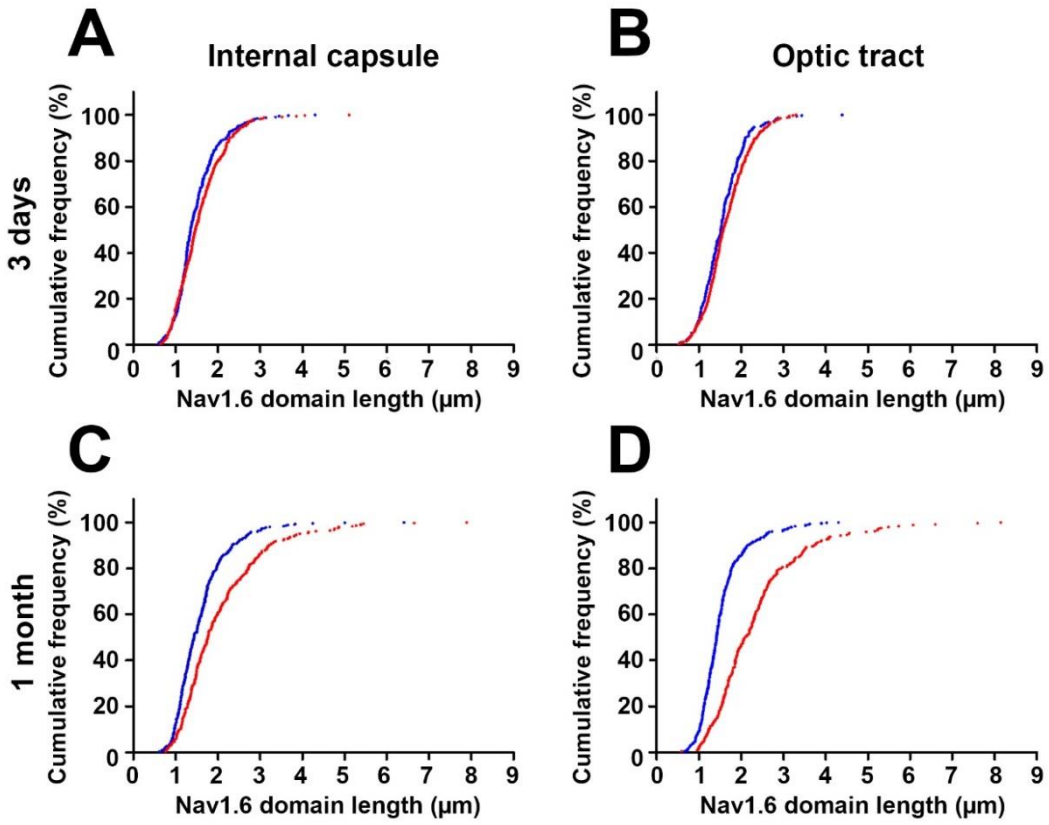

Figure A1.1 Nav1.6 domain length is increased in the internal capsule and optic tract following 3 days and 1 month of chronic cerebral hypoperfusion. (**A**) Following 3 days of chronic cerebral hypoperfusion, $Na_v1.6$ domain length was significantly increased in the internal capsule (D = 0.1125; p = 0.032). (**B**) $Na_v1.6$ domain length was not altered in the optic tract following 3 days of chronic cerebral hypoperfusion (D = 0.0987; p = 0.103). (**C**) Following 1 month of hypoperfusion, $Na_v1.6$ domain length was significantly decreased in the internal capsule (D = 0.2300; p < 0.0001) and (**D**) the optic tract (D = 0.4667, p < 0.0001).

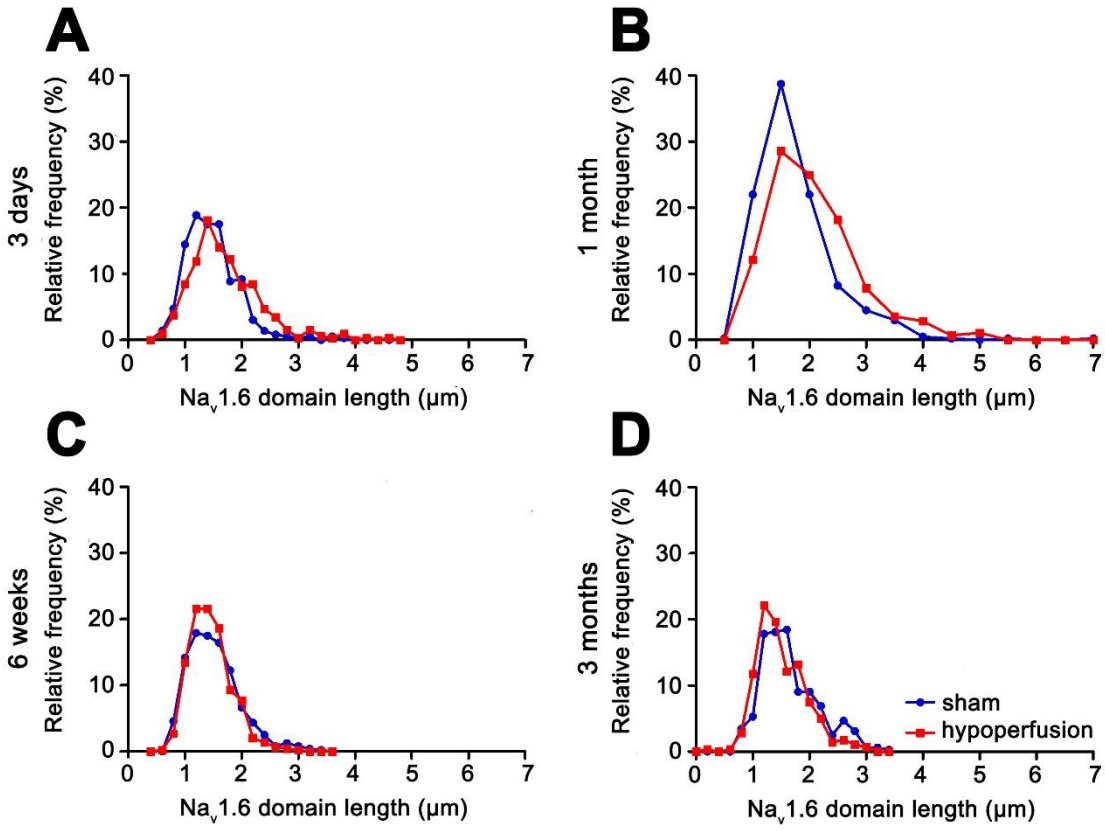

Figure A1.2: Na$_v$1.6 domain length measurements plotted as relative frequency. Relative frequency graphs showing the relative frequency of Na$_v$1.6 domain length measurements in response to (**A**) 3 days, (**B**) 1 month, (**C**) 6 weeks and (**D**) 3 months of chronic cerebral hypoperfusion.

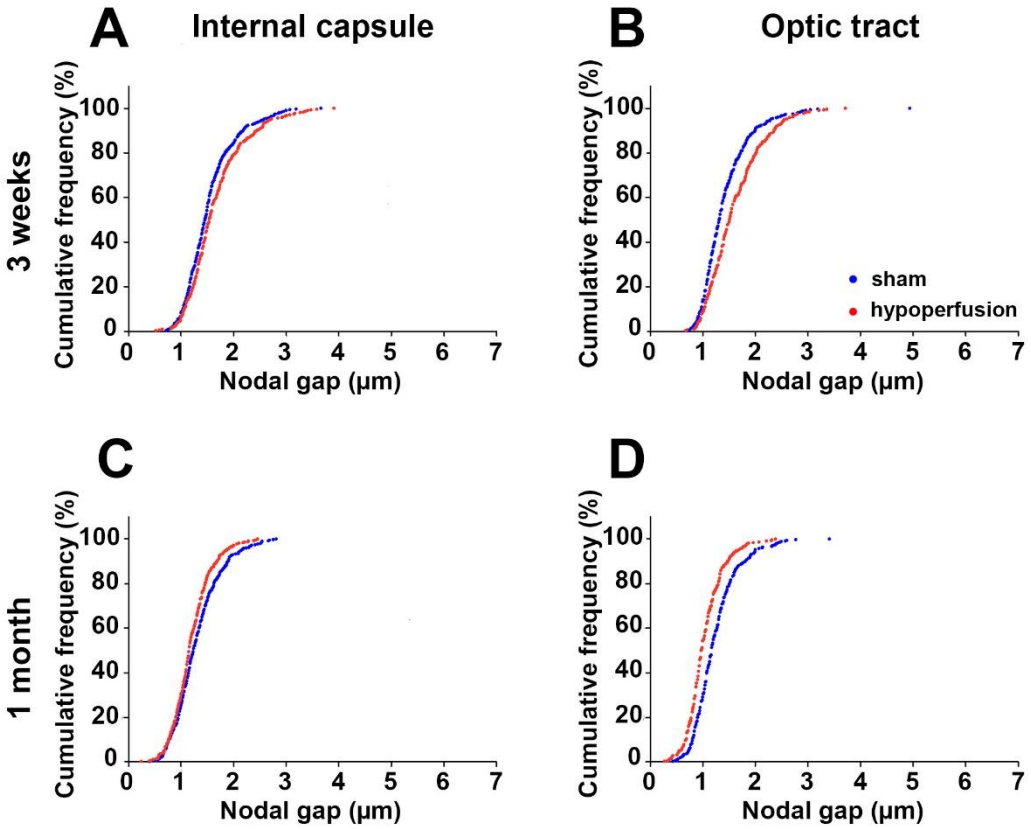

Figure A1.3 Nodal gap length in the internal capsule and optic tract is differentially altered with increasing duration of hypoperfusion. (**A**) Following 3 days of hypoperfusion, nodal gap length was significantly increased in the internal capsule (D = 0.1122; p = 0.026) and (**B**) the optic tract (D = 0.2017; p < 0.0001). (**C**) However following 1 month of hypoperfusion nodal gap length was significantly decreased as compared to shams in the internal capsule D = 0.3275, p 0.001) and (**D**) optic tract (D = 0.2017, p < 0.0001).

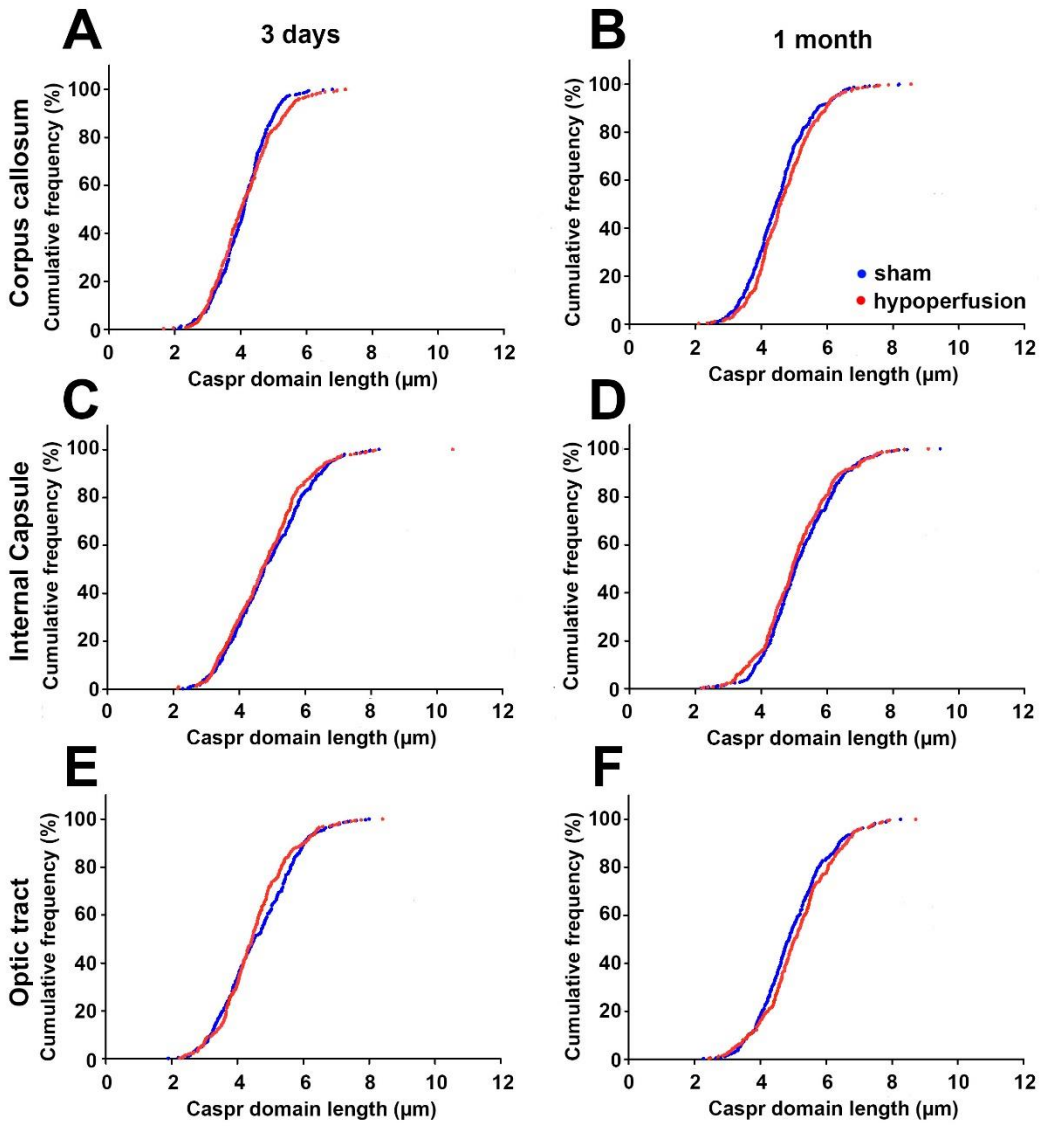

Figure A1.4 Caspr domain length is unchanged following 3 days and 1 month of chronic cerebral hypoperfusion. (A) Caspr domain length was not significantly different between groups in the corpus callosum following 3 days (D = 0.0797; p = 0.172) or (**B**) 1 month (D = 0.0898; p = 0.064) of hypoperfusion. (**C**) Caspr domain lengths in the internal capsule were also unchanged following 3 days (D = 0.0858; p = 0.157) or (**D**) 1 month (D = 0.0591; p = 0.446) of chronic cerebral hypoperfusion following 3 days of chronic cerebral hypoperfusion. (**E**) A significant decrease in Caspr length was observed in the optic tract following 3 days of hypoperfusion (D = 0.1104; p = 0.03) however (**F**) no significant difference was observed between groups following 1 month (D = 0.0872; p = 0.145).

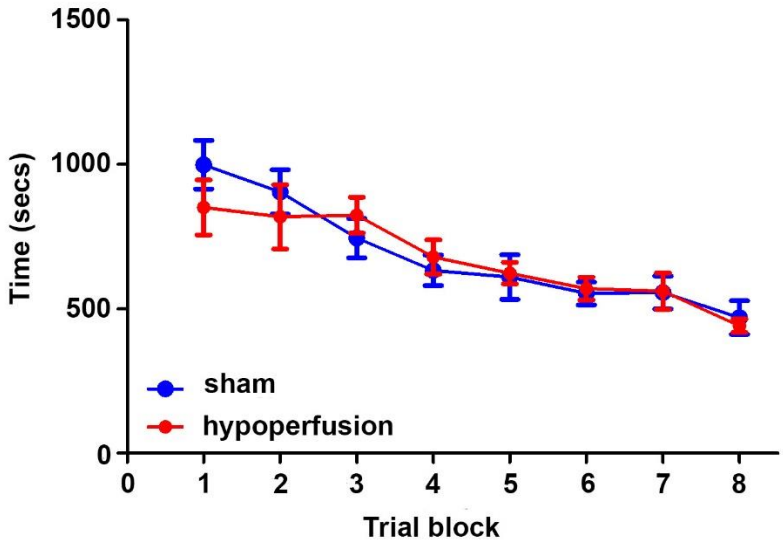

Figure A1.5: Trial duration in the radial arm maze was not different between groups. Analysis revealed a significant effect of trial block ($p < 0.0001$) indicating that trial duration for both groups decreased with increasing time, i.e. mice were performing the task faster each day. Trial duration was not significantly different between groups ($F_{(1, 37)} = 0.044$; $p = 0.836$)

Appendix 2: Confirmation of antibody specificity for oligodendroglial markers described in Chapter 4

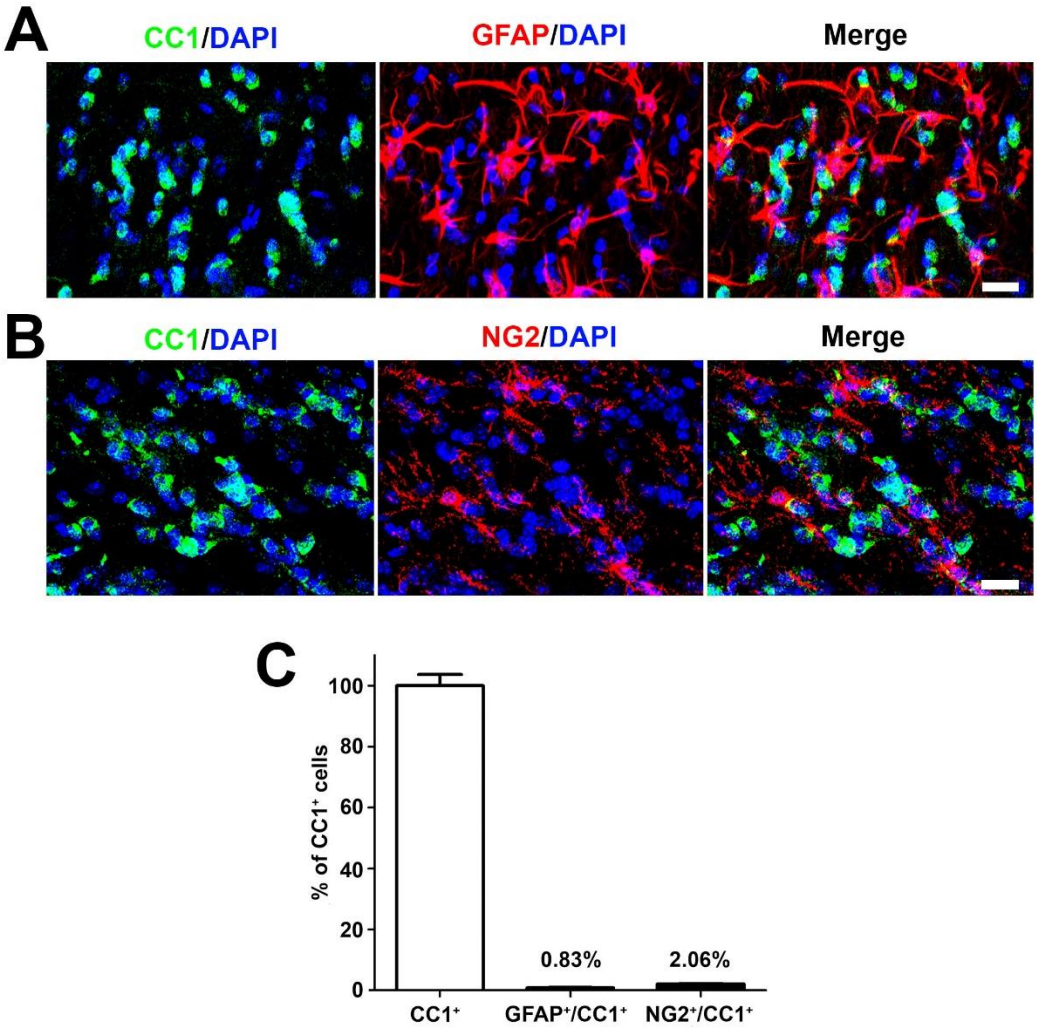

Figure A2.1: CC1 is a specific marker of mature oligodendrocytes. (**A**) Representative confocal images showing CC1 and GFAP and (**B**) CC1 and NG2 double labelling in the corpus callosum. Scale bars = 20 µm. (**C**) Cell counts of double labelled cells revealed only 0.83% of $CC1^+$ cells were also labelled with GFAP. Similarly only 2.06% of CC1+ cells were $CC1^+/NG2^+$. This small proportion of cells expressing both markers likely represents cells in the transition between OPCs and mature oligodendrocytes (Nishiyama et al., 2002).

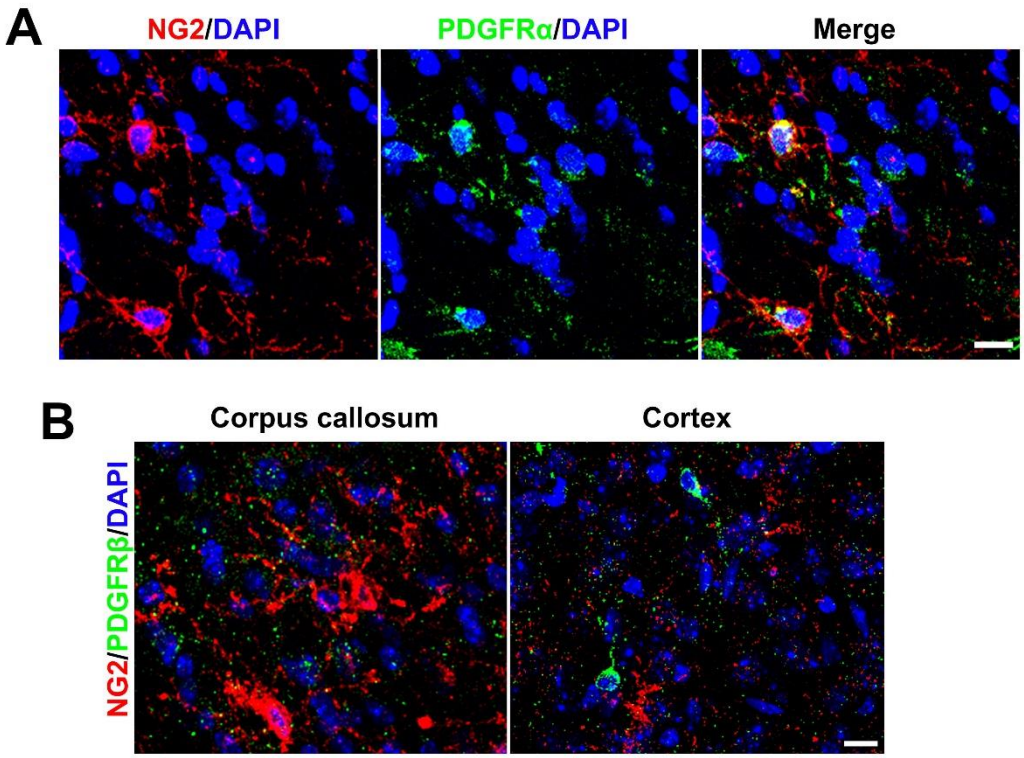

Figure A2.2: NG2 is a specific marker of OPCs. To confirm the specificity of NG2 as a marker of OPCs double labelling with another OPC marker, PDGFRα, was carried out (**A**). This revealed colocalisation of both OPC markers. (**B**) NG2 has also been descried as a marker of pericytes therefore to determine whether NG2 was labelling pericytes in addition to OPCs, double labelling with the pericyte marker PDGFRβ was carried out. This showed that both markers did not colocalise in either white or grey matter. Scale bars = 20 µm.

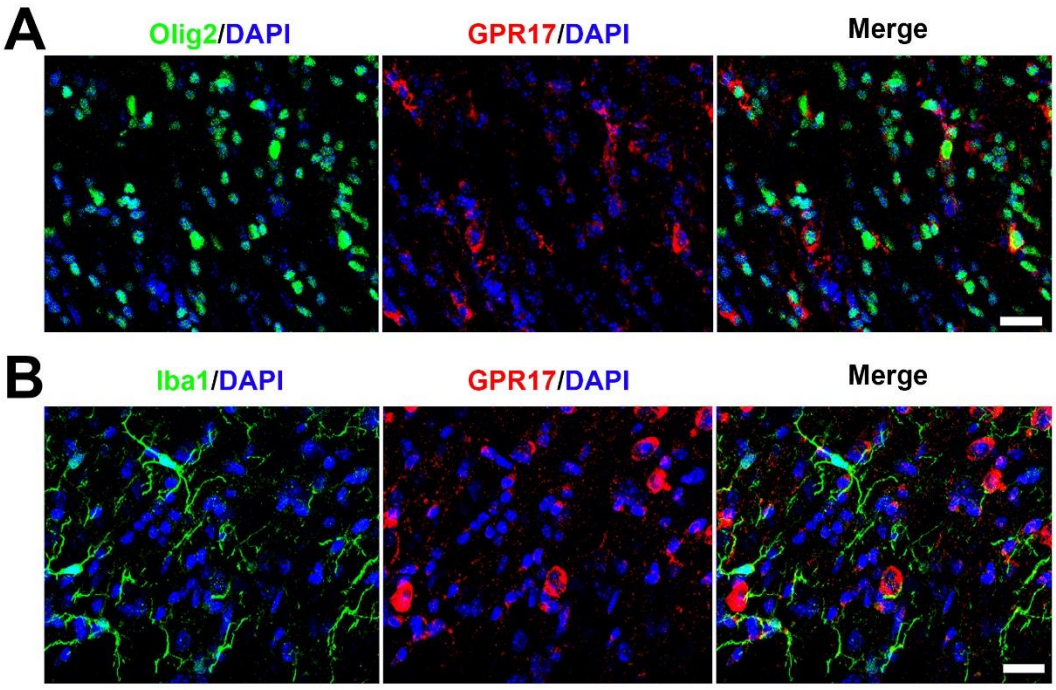

C

	% of double labelled cells
GPR17+/Olig2+	64.41 ± 3.33
GPR17+/Iba1+	8.29 ± 0.75

Figure A2.3: GPR17 is expressed by oligodendroglia and a small percentage of microglia. (**A**) Representative confocal images showing Olig2 and GPR17 and (**B**) Iba1 and GPR17 double labelling in the corpus callosum. Scale bars = 20 µm. (**C**) Cell counting revealed GPR17 was expressed by approximately 64% of $Olig2^+$ cells, whereas only 8% of microglia were $GPR17^+$.

Appendix **3: Additional blood flow and conduction velocity data for animals subject to severe cerebral hypoperfusion using the mixed-coil model**

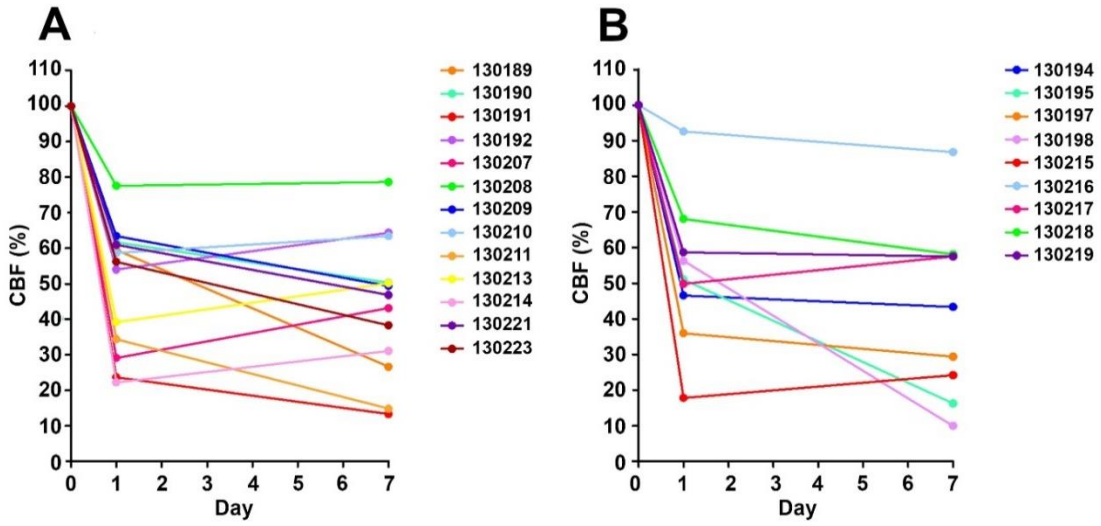

Figure A3.1: Variable response to severe cerebral hypoperfusion. Alterations in CBF are plotted individually for each animal. All values are expressed as a percentage relative to baseline values. (**A**) CBF values for vehicle-treated hypoperfused animals showed significant variability between animals. (**B**) CBF was similarly variable in DMF-treated animals following severe cerebral hypoperfusion.

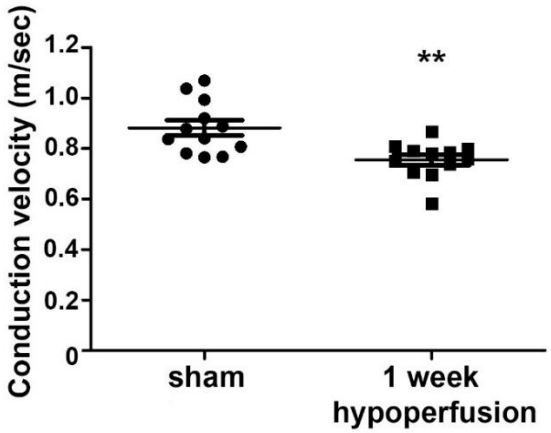

Figure A3.2: Conduction velocity of myelinated axons is significantly decreased following 1 week of hypoperfusion in the mixed coil model. Statistical analysis revealed a significant decrease in conduction velocity of hypoperfused animals as compared to shams (** p = 0.002). Data courtesy of Dr Philip Holland (unpublished).

Appendix 4: Publications

McQueen J, Reimer MM, Holland PR, Manso Y, McLaughlin M, Fowler JH, and Horsburgh K (2014) Restoration of oligodendrocyte pools in a mouse model of chronic cerebral hypoperfusion, *PLoS ONE* 9: e87227

Reimer M.M., **McQueen J**., Searcy L, Scullion G, Zonta B, Desmazieres A, Holland PR, Smith J, Gliddon C, Wood ER, Herzyk P, Brophy PJ, McCulloch, J and Horsburgh K (2011) Rapid disruption of axon-glial integrity in response to mild cerebral hypoperfusion, *J Neurosci* 31: 18185-18194.

OPEN ACCESS Freely available online

PLOS ONE

Restoration of Oligodendrocyte Pools in a Mouse Model of Chronic Cerebral Hypoperfusion

Jamie McQueen[1,2], Michell M. Reimer[1,2], Philip R. Holland[1,2], Yasmina Manso[1], Mark McLaughlin[3], Jill H. Fowler[1], Karen Horsburgh[1,2]*

1 Centre for Neuroregeneration, University of Edinburgh, Edinburgh, United Kingdom, **2** Centre for Cognitive Ageing and Cognitive Epidemiology, University of Edinburgh, Edinburgh, United Kingdom, **3** School of Veterinary Medicine, Division of Veterinary Biosciences, University of Glasgow, Glasgow, United Kingdom

Abstract

Chronic cerebral hypoperfusion, a sustained modest reduction in cerebral blood flow, is associated with damage to myelinated axons and cognitive decline with ageing. Oligodendrocytes (the myelin producing cells) and their precursor cells (OPCs) may be vulnerable to the effects of hypoperfusion and in some forms of injury OPCs have the potential to respond and repair damage by increased proliferation and differentiation. Using a mouse model of cerebral hypoperfusion we have characterised the acute and long term responses of oligodendrocytes and OPCs to hypoperfusion in the corpus callosum. Following 3 days of hypoperfusion, numbers of OPCs and mature oligodendrocytes were significantly decreased compared to controls. However following 1 month of hypoperfusion, the OPC pool was restored and increased numbers of oligodendrocytes were observed. Assessment of proliferation using PCNA showed no significant differences between groups at either time point but showed reduced numbers of proliferating oligodendroglia at 3 days consistent with the loss of OPCs. Cumulative BrdU labelling experiments revealed higher numbers of proliferating cells in hypoperfused animals compared to controls and showed a proportion of these newly generated cells had differentiated into oligodendrocytes in a subset of animals. Expression of GPR17, a receptor important for the regulation of OPC differentiation following injury, was decreased following short term hypoperfusion. Despite changes to oligodendrocyte numbers there were no changes to the myelin sheath as revealed by ultrastructural assessment and fluoromyelin however axon-glial integrity was disrupted after both 3 days and 1 month hypoperfusion. Taken together, our results demonstrate the initial vulnerability of oligodendroglial pools to modest reductions in blood flow and highlight the regenerative capacity of these cells.

Citation: McQueen J, Reimer MM, Holland PR, Manso Y, McLaughlin M, et al. (2014) Restoration of Oligodendrocyte Pools in a Mouse Model of Chronic Cerebral Hypoperfusion. PLoS ONE 9(2): e87227. doi:10.1371/journal.pone.0087227

Editor: Ken Arai, Massachusetts General Hospital/Harvard Medical School, United States of America

Received July 16, 2013; **Accepted** December 25, 2013; **Published** February 3, 2014

Funding: The funding of the Lifelong Health and Wellbeing Initiative (supported by the BBSRC, EPSRC, ESRC and MRC), The Disconnected Mind (supported by Age UK) and Alzheimer's Research UK (ARUK) is gratefully acknowledged. JHF is supported by a research fellowship from the Alzheimer's Society. Confocal imaging was performed at the IMPACT Imaging facility and at the Euan MacDonald Centre at the University of Edinburgh. The funders had no role in study design, data collection and analysis, decision to publish, or preparation of the manuscript.

Competing Interests: The authors have declared that no competing interests exist.

* E-mail: Karen.Horsburgh@ed.ac.uk

Introduction

Oligodendrocytes are the myelin producing cells of the CNS and are critical for maintaining and regulating the myelination of axons. Oligodendrocyte survival and the integrity of myelinated axons is essential for maintaining saltatory conduction, neuronal communication and normal cognitive function (for review see [1]). A single oligodendrocyte can myelinate up to 50 axonal segments [2] and thus damage to individual oligodendrocytes could have a major effect on myelination of axons and efficiency of the relay of information.

Oligodendroglia appear to be particularly vulnerable to blood flow reductions and in animal models of cerebral ischemia and severe hypoperfusion a marked loss of oligodendrocytes occurs rapidly in response to severe reductions in blood flow [3–6]. Additionally, *in vitro* models of hypoxia and oxygen-glucose deprivation, common pathways in cerebral ischaemia, have demonstrated the susceptibility of oligodendrocytes to these conditions [7,8] and it is now thought that damage to oligodendrocytes is mediated by oxidative stress, inflammation and excitotoxicity (for review see [9]). Indeed, damage to myelinated axons and oligodendrocytes is prominent in various conditions in which cerebral blood flow is compromised such as the ageing brain [10,11], Alzheimer's disease [12,13] and stroke [4,14] and may contribute to a functional impairment.

Despite the initial degeneration of oligodendrocytes following injury there is now evidence to indicate that oligodendrocyte precursor cells (OPCs) can proliferate and differentiate and as a result may serve to replenish the loss of damaged oligodendrocytes and potentially repair functional deficits. In neonatal models of hypoxic-ischaemic injury, cell proliferation is increased and new oligodendrocytes are generated up to several weeks after the initial injury [15]. In the adult brain there also appears to be an endogenous capacity to generate new oligodendrocytes in response to cerebral ischaemia. In models of focal cerebral ischaemia when either blood flow is restored with reperfusion or in the peri-infarct region where there is sufficient collateral flow, increased numbers of OPCs are detectable [6,16,17]. Interestingly, in aged human brain, increased numbers of oligodendrocytes and OPCs occur in areas adjacent to white matter disruption where blood flow is compromised [18] and increased numbers of oligodendrocytes have been demonstrated in cases of vascular cognitive impairment

[19]. Together these studies suggest that OPCs may respond to reduced cerebral blood flow in an attempt to ameliorate white matter damage.

There are a number of mechanisms that may regulate OPC proliferation and differentiation. Relevant to blood flow alterations both glutamate and ATP, the extracellular levels of which may be increased with reduced blood flow, have been shown to be important in regulating OPC proliferation and differentiation [20,21]. In addition, recent studies have identified a role for a G-coupled protein receptor, GPR17, as an important mediator of OPC differentiation and white matter repair [22,23]. GPR17 has been shown to be expressed by a subset of OPCs [23,24] and it is thought that these cells may operate as an early sensor of brain damage whereby they are activated by uracil nucleotides and cysteinyl leukotrienes which are increased in response to cerebral ischemia. In support of this, GPR17 positive cells are upregulated in response to cerebral ischemia and associated with oligodendrocyte differentiation [23].

The present study sought to determine whether the pools of oligodendrocytes and OPCs would be influenced by modest reductions in blood flow more akin to those occurring in the ageing brain. We utilised a mouse model of cerebral hypoperfusion induced by permanent bilateral carotid stenosis which we have previously shown to result in diffuse white matter pathology [12,25,26]. Importantly, these mice also exhibit impaired spatial working memory [12,27], providing a link between white matter disruption and cognitive decline. More recently, microarray analysis in mice subject to cerebral hypoperfusion has revealed increased expression of several genes involved in cell proliferation [25] which may underlie a potential white matter repair mechanism. We therefore also investigated the extent of OPC proliferation and differentiation and whether this was mediated by GPR17. In addition, ultrastructural analysis and myelin labelling were carried out to determine whether alterations to oligodendrocyte pools influenced myelin sheath thickness.

Materials and Methods

Ethics statement

All procedures were authorised under the Home Office approved Project Licenses, 'Pathophysiology of Alzheimer's disease: link to cerebrovascular disease' (licence number 60/3722) and 'Pathophysiology of vascular cognitive impairment and Alzheimer's disease' (licence number 60/4350) held by Prof. K. Horsburgh. The licences were approved by the University of Edinburgh's Ethical Review Committee and the Home Office, and adhered to regulations specified in the Animals (Scientific Procedures) Act (1986).

Animals and surgery

Adult male C57Bl/6J mice (aged 3–5 months old, 25–30 g) were obtained from Charles River Laboratories Inc, UK. Animals were subject to chronic cerebral hypoperfusion as previously described [25–28]. In brief, wire microcoils (0.18 mm internal diameter, Sawane Spring Co., Japan) were applied to both common carotid arteries under isoflurane anaesthesia (induced at 5%, and maintained at 1.2–1.6%). A 30 minute interval was left between left and right coil application. Sham-operated animals underwent identical procedures with the exception that coils were not placed around the arteries. Housing of animals and all procedures were carried out in pathogen-free animal units.

BrdU labelling

Animals from the 1 month cohort were given intraperitoneal injections (35 mg/kg body weight) of 5′-bromo-2′-deoxyuridine (BrdU; Fluka, UK) twice daily for the first 3 days following surgery to label proliferating cells during this period by an individual blinded to surgical group.

Laser speckle contrast imaging

An additional cohort of animals underwent measurement of cerebral blood flow using laser speckle flowmetry. Animals were anaesthetised with 5% isoflurane in oxygen for 1.5 minutes in an anaesthetic chamber. Animals were then transferred to a stereotaxic frame and their heads were fixed into position. Anaesthesia was maintained at 2–2.5% isoflurane via a nose cone and body temperature was monitored and regulated. An incision was made to expose the skull and the skin overlying the skull was reflected. The skull was moistened using saline and a small amount of water-based gel (37°C) was spread evenly onto the skull. A moorFLPI2 Speckle Contrast Imager (Moor Instruments, UK) was positioned 20 cm above the head. Image sequences were acquired at a resolution of 752×580 pixels and a frequency of 1 frames/second (20 ms/frame). Following stabilisation of perfusion readings, a 2 minute perfusion recording was carried out.

Raw speckle contrast sequences were analysed using moorFLPI2 Review software (v4.0). Regions of interest were consistent between each mouse and made 1 mm to −2 mm from Bregma with care taken to avoid any artefacts on the skull surface. Data were measured in blood perfusion units (PU) and calculated for each mouse as the percentage change relative to baseline (Figure S1).

Tissue preparation and immunohistochemistry

At 3 days or 28 days post-surgery, mice were deeply anaesthetised with 5% isoflurane and transcardially perfused with 20 ml 0.9% heparinised saline followed by 20 ml 4% paraformaldehyde (PFA) in 0.1% phosphate buffer (PB, pH 7.4). Following perfusion, the brains were removed and post-fixed in 4% PFA overnight. Brains were then transferred to PB and stored overnight at 4°C. The brains were cut along the midline and free-floating 50 μm sagittal sections were cut using a vibrating blade microtome (Hydrax V50, Zeiss, Germany). Sections were stored in cryoprotective medium (30% glycerol/30% ethylene glycol in PB) at −20°C until required. Different cohorts of animals were used due to the sensitivity of some antibodies to tissue fixation (n = 13 sham, 12 hypoperfused and n = 9 sham, 10 hypoperfused for 3 day studies; n = 10 sham, 11 hypoperfused and n = 9 sham, 9 hypoperfused for 1 month studies). Occasionally animals were excluded from analysis if there was an absence of cellular staining or the quality was deemed too poor to perform accurate analysis.

The following primary antibodies were used in this study: anti-BrdU (1:200, AB6326, Abcam, UK), anti-CC1 (APC 1:20, OP80, Calbiochem, USA), anti-GFAP (1:1000, Z0334, Dako UK), anti-GPR17 (1:200, 10136, Cayman Chemical, USA) anti-Iba1 (1:100, ab5076, Abcam UK), anti-MAG (1:100, sc-9543, Santa Cruz, USA) anti-NG2 (1:100, AB5320, Millipore, UK), anti-Olig2 (1:500, Ab9610, and 1:100, MABN50, both Millipore, UK), anti-PCNA (1:500 ab29, Abcam UK), anti-PDGFRα (1:100, 558774, BD Pharmingen UK), and anti-PDGFRβ (1:100, AF1042, R and D Systems, UK). Cy2, Cy3, DyLight 488 and Alexa Fluor 488 and 647 (all 1:200) conjugated secondary antibodies were purchased from Jackson ImmunoResearch Laboratories Inc (USA). Alexa Fluor 488 and 546 conjugated secondary antibodies (1:500) were purchased from Life Technologies Ltd (UK). Double labelling experiments were carried out to

confirm the cellular specificity of antibodies used for OPC and oligodendrocyte labelling. Non-specific labelling was blocked using 3% normal serum and sections were incubated in primary and secondary antibodies overnight at 4°C. Sections were mounted onto SuperFrost slides and mounted using Vectashield hard set mounting medium containing the nuclear stain 4′,6-diamidino-2-phenylindole (DAPI) (H-1500, Vector Laboratories, USA).

For BrdU labelling experiments, an additional antigen retrieval step was required. Following 3 washes in PBS, sections were incubated for 30 minutes in 2M HCl at 37°C to allow denaturation of DNA. Following this, sections were given three 5 minute washes in 0.1 M sodium borate buffer ($Na_2B_4O_7$, pH 8.5). For PCNA labelling, sections were retrieved in 10 mM citrate buffer for 30 minutes at 85°C and blocked using 10% normal serum and 0.5% bovine serum albumin.

Fluoromyelin staining was used to assess myelin integrity following hypoperfusion. Free-floating sections were washed in PBS and mounted onto slides. Following rehydration in PBS, sections were incubated in Fluoromyelin Green (1:200, Invitrogen) for 1 hour at room temperature. At the outset the conditions were optimised as recommended by the manufacturer. This protocol was determined to be optimal for studying myelin alterations in thick vibratome sections and is a slight modification of that suggested by the manufacturer for thin paraffin sections.

Confocal laser scanning microscopy and image analysis

Immunolabelled 50 μm sections were imaged using confocal laser scanning microscopy (Zeiss Axioskop LSM 510 or Zeiss LSM710, Zeiss, Germany). All images were acquired using a 20× objective (numerical aperture 0.75) representing an area of 460×460 μm. Images were obtained at a resolution of 1024×1024 pixels. Z-stacks of a minimum of 7 μm were acquired with a step size of 1 μm. The region of the corpus callosum, in sagittal sections, was imaged above the lateral ventricle at the stereotactic co-ordinates, lateral 2.40±0.1 mm, Bregma −1.5±0.1 mm.

Stereological cell counting was performed using ImageJ software (version 1.42q) (National Institutes of Health, USA). Cells were identified based on expression of the immunolabel(s) of interest co-localised with the nuclear stain (DAPI). Cells were manually identified and counted using the ImageJ Cell Counter plugin. To prevent over-counting, cells crossing the left and top sides of the region of interest were included, but any cells crossing the right or bottom boundaries were not counted. Images from the top of the Z-stack were excluded from analysis whilst counts from the bottom image from the stack were included. Cell counts are expressed as the percentage of sham controls or as the number of cells/0.01 mm^3.

To assess the intensity of GPR17 and fluoromyelin staining, sections were imaged using identical gain and offset settings on the confocal microscope which ensured a common threshold was set in the acquisition of all images. For GPR17 staining, individual $GPR17^+$ cells within the corpus callosum were manually outlined and the mean gray value measured and expressed as the average per animal. To assess the intensity of fluoromyelin staining, the corpus callosum was manually outlined and mean gray value measured. All intensity measurements were carried out in triplicate and values averaged. For analysis of MAG immunostaining, images were acquired using identical confocal settings and background subtraction was applied before calculating the percentage area of positive staining. All experiments and subsequent analysis were carried out blind to surgical condition.

Western blot analysis

In a separate cohort of mice after one month of hypoperfusion (n = 8) or a sham (n = 5) procedure, after decapitation, the brain was rapidly removed, the cerebellum discarded and the remaining brain frozen in liquid nitrogen. Myelin-enriched fractions were prepared by sucrose density centrifugation [29] and the total protein concentration was determined using Pierce BCA Protein Assay Kit (Thermo Fisher Scientific, UK). Proteins were separated by Bis-Tris 4–12% SDS-PAGE (NuPage® Novex®, Life Technologies) and transferred onto PVDF membrane (Immobilon-FL, Millipore). Immunobloting was performed using the Odyssey Infrared Imaging System (LiCor Biosciences, Lincoln, NE, USA). Membranes were blocked 1 hour at room temperature in Odyssey blocking buffer (diluted 1:1 with phosphate-buffered saline), washed in phosphate-buffered saline–Tween (phosphate-buffered saline with 0.1% Tween) and incubated over-night at 4°C with MBP (1:10.000, Millipore). After gentle washing, membranes were then incubated 1 hour at room temperature with GAPDH (1:14.000, Sigma) which was used as a loading control. Membranes were then incubated for 45 minutes with the appropriate fluorescent secondaries (1:3000, LiCor Biosciences). The western blots were analysed using the LiCOR Bioscience Odyssey system and software. The four MBP isoforms were analysed together and normalized to GAPDH.

Electron microscopy

To determine whether 3 days or 1 month of chronic cerebral hypoperfusion led to alterations in myelin sheath thickness in the corpus callosum, transmission electron microscopy was carried out.

Animals were transcardially perfused with 5% glutaraldehyde/4% paraformaldehyde, 3 days (n = 5 sham, 6 hypoperfused) or 28 days (n = 7 sham, 7 hypoperfused) after the onset of cerebral hypoperfusion. The brains were then cut into 1 mm thick sections and the corpus callosum manually dissected out. Corpus callosum samples were fixed in 3% glutaraldehyde in 0.1M sodium cacodylate buffer (pH 7.3) for 2 hours and then washed 3 times in the same buffer. Samples were then post-fixed in 1% osmium tetroxide in 0.1M sodium cacodylate. Following dehydration, sections were embedded in araldite resin. Samples were then cut from the midline into the corpus callosum and 60 nm ultrathin transverse sections were cut using a Reichert OMU4 ultramicrotome (Leica Microsystems (UK) Ltd, Milton Keynes) and stained in uranyl acetate and lead citrate. Sections were viewed using a Philips CM120 transmission electron microscope (FEI UK Ltd., Cambridge, England) and images taken at a magnification of 3500× using a Gatan CCD camera (Gatan UK, Oxon, England). To quantify changes in myelin sheath thickness, a lined grid of 0.95×0.95 μm^2 was overlaid onto each image using Image J software (v1.42q) and fibres were selected for analysis if their myelin sheath was intersected by a grid line. Using the freehand tool, the perimeters of each fibre and axon were manually traced and whole fibre area and axonal area were measured. These values were used to calculate corresponding fibre and axonal diameters. To calculate g-ratio, axonal diameter was divided by whole fibre diameter. For each animal a minimum of 137 fibres were analysed with the observer blind to surgical condition.

Statistical analysis

Data were analysed using Student's unpaired t-test or the Mann-Whitney U-test depending on parametric or non-parametric distribution. Statistical analysis was performed using GraphPad Prism 5 software (GraphPad Software, San Diego, USA). A

probability (p) value ≤ 0.05 was considered to be statistically significant.

Results

Decreased numbers of OPCs and mature oligodendrocytes during the early response to cerebral hypoperfusion

To assess the acute response of OPCs to chronic cerebral hypoperfusion, NG2 labelling was carried out and numbers of $NG2^+$ OPCs were counted. We determined that NG2 specifically labelled OPCs in the corpus callosum through colocalisation with the OPC marker PDGFRα (Figure S2A). In addition, $NG2^+$ cells lacked PDGFRβ expression, a marker of pericytes (Figure S2B). Two distinct populations of $NG2^+$ cells were identified: one population showed circular immunoreactivity around the nucleus and few processes, corresponding to 'early' stage OPCs, whilst the other were more intensely stained and displayed more extensive cellular processes, corresponding to 'late' stage OPCs (Figure 1A). Cell counting of both $NG2^+$ populations revealed that during the acute response to hypoperfusion, numbers of early $NG2^+$ cells were significantly decreased compared to sham controls ($p = 0.015$) (Figures 1B, S3A). Numbers of $NG2^+$ cells displaying late OPC morphology were unchanged after 3 days ($p = 0.532$) (Figure 1C).

The early effects of cerebral hypoperfusion on mature oligodendrocyte populations were then examined using CC1 immunolabelling (Figure 1D, Figure S3B). This revealed a significant decrease in oligodendrocyte number in the hypoperfused group compared to sham controls ($p = 0.027$) (Figure 1E). It has been reported that astrocytes may express the CC1 antigen [30], but in this study $CC1^+/GFAP^+$ double labelling determined that only 0.8% of $CC1^+$ cells were $GFAP^+$ in the corpus callosum (Figure S4A). Furthermore the numbers of astrocytes were unchanged after 1 month of cerebral hypoperfusion (Figures S4B-C). Together these results show that rapid alterations in OPC and oligodendrocyte populations occur in response to modest reductions in cerebral blood flow.

Restoration of the precursor pool and increased numbers of oligodendrocytes after long term cerebral hypoperfusion

The longer term responses of the oligodendrocyte pools to cerebral hypoperfusion were next investigated. $NG2^+$ labelled cells were counted and showed no differences in numbers of early ($p = 0.245$) or late ($p = 0.860$) $NG2^+$ cells between sham and hypoperfused groups (Figure 2A and 2B respectively). In contrast to the loss of mature oligodendrocytes observed after 3 days of hypoperfusion, $CC1^+$ labelling (Figures 2C, S3B) revealed a significant increase (19%) in the number of mature oligodendrocytes in the hypoperfused animals compared to sham operated animals ($p = 0.007$) (Figure 2D). Together these results indicate that in response to longer term cerebral hypoperfusion a replacement mechanism is acting to restore OPCs and in the case of mature oligodendrocytes, increase numbers of cells.

Proliferation and differentiation of OPCs in response to cerebral hypoperfusion

To characterise levels of proliferation in response to hypoperfusion, PCNA labelling was carried out to determine numbers of proliferating cells at 3 days and 1 month of hypoperfusion (Figure 3A). This showed that overall numbers of proliferating cells were not different between groups at either 3 days ($p = 0.20$) (Figure 3B) or 1 month ($p = 0.564$) (Figure 3C). We next sought to determine the extent of OPC proliferation and whether this contributed to the restoration of oligodendroglial pools following hypoperfusion. For technical reasons PCNA/NG2 double labelling could not be carried out therefore PCNA/Olig2 labelling experiments were carried out in 3 day and 1 month cohorts (Figure 3D). Whilst Olig2 is expressed throughout the oligodendrocyte lineage, only OPCs can proliferate and thus express PCNA. The number of $PCNA^+/Olig2^+$ cells were significantly decreased in 3 day hypoperfused animals compared to sham controls ($p = 0.02$) (Figure 3E) while no differences in proliferating OPCs were observed after 1 month of hypoperfusion ($p = 0.323$) (Figure 3F). Together these results show that whilst overall levels of proliferation were unchanged after 3 days of hypoperfusion, numbers of proliferating OPCs were decreased in hypoperfused animals compared to controls.

To further investigate the early proliferative responses to cerebral hypoperfusion, animals from the 1 month cohort received injections of BrdU for the first three days following surgery to label all proliferating cells within this period (Figure 3G). $BrdU^+$ cells were present in 2 of the 9 (22%) of the sham control group and in 5 out of 10 (50%) of the hypoperfused group (Figure 3H) although the difference between groups was not statistically significant ($p = 0.157$). BrdU and NG2 double labelling failed to demonstrate any proliferating OPCs (data not shown).

We next sought to determine whether $BrdU^+$ cells generated early in response to hypoperfusion had differentiated into mature oligodendrocytes and carried out $BrdU^+/CC1^+$ labelling (Figure 3I). This showed that $BrdU^+/CC1^+$ cells were present in 3 of the 10 (30%) 1 month hypoperfused mice but were completely absent in sham-operated controls (Figure 3J). Although the difference was not statistically significant ($p = 0.095$), the presence of these double labelled cells in a proportion of hypoperfused animals indicates that OPC differentiation has occurred in a subset of animals in response to reduced cerebral blood flow. CBF responses in individual mice may vary which may account for differences in the proliferative/differentiation responses. An indication of the individual CBF responses was investigated in different cohorts of mice to those used to assess pathology at 3 days and 1 month hypoperfusion (see Figure S1).

Decreased expression of GPR17 in response to cerebral hypoperfusion

To elucidate a possible mechanism involved in OPC differentiation in response to cerebral hypoperfusion, we analysed the expression of the G protein-coupled receptor GPR17 (Figures 4A, S3D). Previous studies have shown that in the intact brain GPR17 is expressed by premyelinating oligodendrocytes and a subset of OPCs, and receptor activation has been demonstrated to play a permissive role in OPC differentiation [22,23]. GPR17/NG2 double labelling could not be performed due to the antibodies being raised in the same species therefore we confirmed GPR17 expression by oligodendrocyte lineage cells using Olig2. This showed approximately 64% of $GPR17^+$ cells co-expressed Olig2 (Figure S5), which is in agreement with a previous report [23]. Numbers of $GPR17^+$ cells were not significantly different between groups at either time point examined (Figures 4B and 4C). We next assessed expression of the receptor, as indicated by the intensity of staining. This revealed a decrease in the GPR17 labelling intensity after 3 days in hypoperfused as compared to shams ($p = 0.007$) (Figure 4D). However, after 1 month of hypoperfusion there was no difference between groups ($p = 0.363$) (Figure 4E).

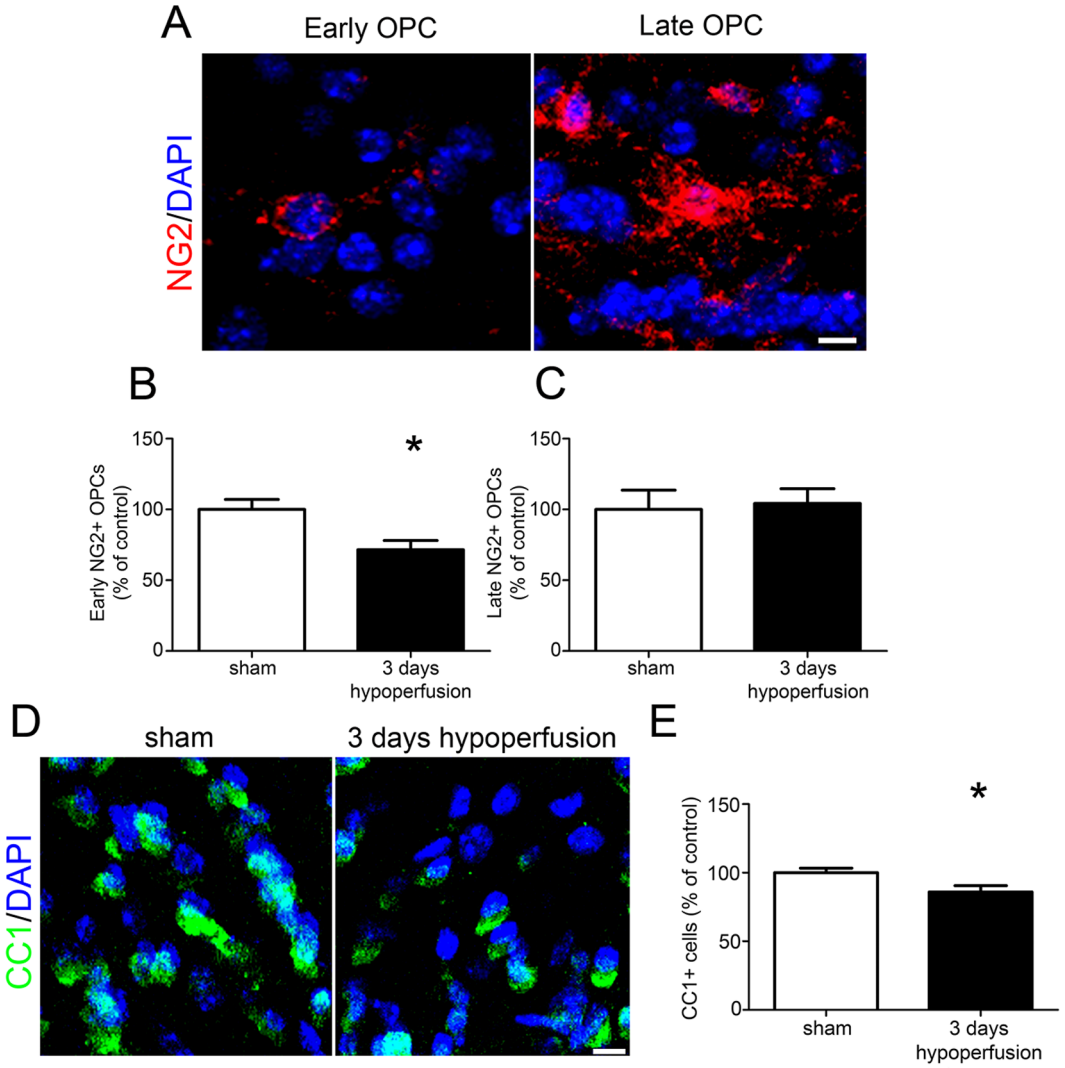

Figure 1. Reduced numbers of OPCs and mature oligodendrocytes after 3 days of chronic cerebral hypoperfusion. (A) Representative confocal images showing morphology of early and late NG2$^+$ OPCs in the corpus callosum. (B) A significant decrease in numbers of early NG2$^+$ OPCs was found in the corpus callosum after 3 days of chronic cerebral hypoperfusion. (C) No significant differences in numbers of late NG2$^+$ cells were observed after 3 days. (D) Representative confocal images of CC1$^+$ labelling of oligodendrocyte cell bodies in the corpus callosum. (E) A significant decrease in CC1$^+$ oligodendrocytes was found after 3 days of hypoperfusion. n = 13 sham, 12 hypoperfused for NG2 labelling experiments; n = 9 sham, 10 hypoperfused for CC1 labelling. Scale bars = 10 μm * $p<0.05$.
doi:10.1371/journal.pone.0087227.g001

Impairment of axon-glial integrity, increased microglia and absence of gross myelin alterations in response to cerebral hypoperfusion

To determine whether alterations in oligodendrocyte numbers may be paralleled by alterations in myelin density following cerebral hypoperfusion, myelin status was assessed using the fluorescent lipophilic dye fluoromyelin (Figure 5A). However, there were no significant differences in staining intensity following either 3 days of cerebral hypoperfusion ($p = 0.598$) or after 1 month of cerebral hypoperfusion ($p = 0.063$) (Figure 5B & C). Investigation of myelin-enriched extracts using Western blot analysis additionally indicated that there was no significant difference in MBP levels between sham and one month hypoperfused mice (Figure S6).

To further investigate the myelin integrity, electron microscopy was carried out and measurements of myelin sheath thickness relative to fibre diameter, i.e. g-ratio, were conducted in separate cohorts of 3 day and 1 month hypoperfused animals (Figure 5D). This revealed no significant difference in g-ratio values following both short and long term hypoperfusion compared to respective sham-operated controls (Figure 5E). As a note since the 3 days and 1 month cohorts underwent surgery and tissue processing at different times no statistical comparisons can be made between sham cohorts or the hypoperfused cohorts.

Despite an absence of gross myelin alterations, in our group we have consistently determined that cerebral hypoperfusion results in a disruption of axon-glial integrity [12,25,26] and thus sought to verify whether similar alterations occur in the white matter in this study. Axon-glial integrity was assessed by myelin associated glycoprotein (MAG), a key myelin protein involved in the maintenance of axon-glial integrity (Figure 6A). There was a reduction in the density of MAG staining in the corpus callosum after 3 days ($p = 0.008$) and 1 month ($p = 0.027$) of chronic cerebral hypoperfusion (Figures 6B and 6C).

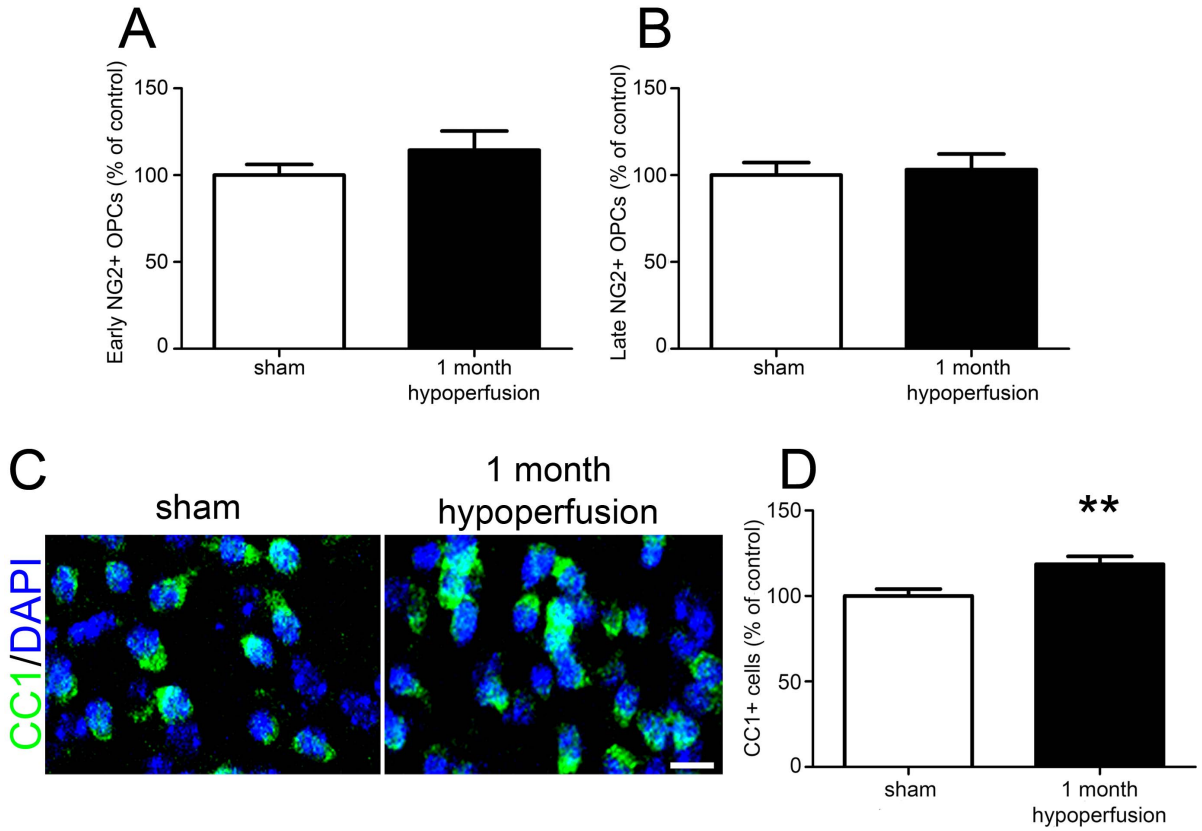

Figure 2. Restoration of the NG2$^+$ precursor pool and increased numbers of mature oligodendrocytes after 1 month of chronic cerebral hypoperfusion. (A) No significant differences in numbers of early or (B) late NG2$^+$ cells were observed after 1 month of cerebral hypoperfusion. (C) Representative confocal images of CC1$^+$ labelling of oligodendrocyte cell bodies in the corpus callosum. Scale bar = 10 μm. (D) A significant increase in CC1$^+$ oligodendrocytes in the corpus callosum was observed following 1 month of chronic cerebral hypoperfusion. n = 10 sham, 11 hypoperfused for NG2 and CC1 labelling. ** $p<0.01$.
doi:10.1371/journal.pone.0087227.g002

A pronounced microglial response as determined by Iba1 immunoreactivity has also been a robust finding in our model of hypoperfusion (Figure 6D). In support of this after 1 month of hypoperfusion, numbers of microglia were significantly increased compared to sham controls ($p = 0.0011$) (Figure 6E), whilst numbers of microglia were unchanged after 3 days of cerebral hypoperfusion ($p = 0.425$) (Figure 6F), consistent with earlier studies using this mouse model [12,28].

Taken together these data indicate that whilst gross myelin morphology remains intact and increased numbers of oligodendrocytes are observed following hypoperfusion, axon-glial integrity is impaired supporting our previous observations [25].

Discussion

Previous studies have demonstrated the susceptibility of oligodendrocytes to severe reductions in cerebral blood flow (>70% to that of baseline levels) with profound oligodendrocyte loss occurring early in response to the insult [6,17]. The present study additionally highlights the vulnerability of these oligodendroglial cells to more modest reductions in blood flow comparable to those observed in the ageing brain.

In the present study we investigated the pools of OPCs and mature oligodendrocytes. We observed two different populations of NG2$^+$ cells identified by differences in morphology. One population of NG2$^+$ cells showed circular reactivity around the nucleus and few processes, corresponding to 'early' stage OPCs, whilst the other population of cells was more intensely stained and more processed, corresponding to 'late' stage OPCs. Interestingly only the 'early' stage OPCs were affected by hypoperfusion. It is possible that these early OPCs have responded rapidly to hypoperfusion by extending more processes and have thus been classified as late OPCs. Mature oligodendrocytes were also reduced in response to hypoperfusion, highlighting the vulnerability of these glial cells to even modest reductions in cerebral blood flow. Although the mechanisms underlying this early oligodendroglial loss with hypoperfusion remain to be determined, these may involve damage to the oligodendrocytes and OPCs as a result of oxidative stress [31,32] or inflammation [33,34], both of which are known inducers of oligodendroglial damage and/or death (for review see [9,35]). In the present study, consistent with our previous work, we demonstrated a marked microglial response with hypoperfusion. Previously we have also shown alterations in indices of hypoxia [25] in white matter after hypoperfusion. Localised alterations in glutamate levels as a result of compromised blood flow could also contribute to the loss of oligodendrocytes and OPCs via NMDA receptor activation leading to intracellular Ca^{2+}-dependent injury to oligodendroglia [36,37]. However it should be noted that whilst we propose that the loss of CC1+ and NG2+ labelling of cells is an indicator of cell loss, a loss of cellular antigenicity could also account for the reduction in cellular staining.

With sustained hypoperfusion, marked alterations in oligodendroglial pools were observed. The OPC pool was restored and

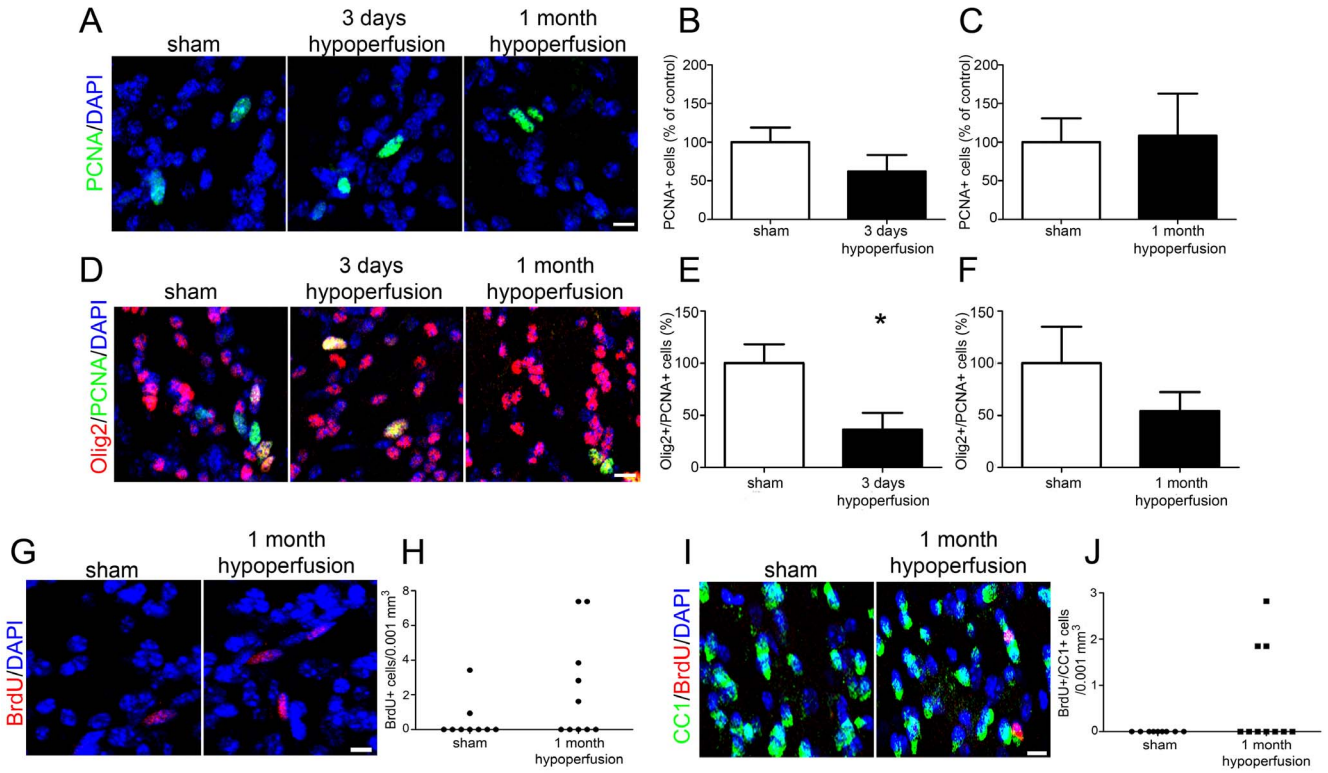

Figure 3. Low numbers of proliferating cells are observed in response to cerebral hypoperfusion however a proportion of newly generated cells differentiate into mature oligodendrocytes within 1 month of cerebral hypoperfusion. (A) Representative confocal images showing PCNA labelling of proliferating cells in the corpus callosum. (B) No significant differences in numbers of $PCNA^+$ cells were observed after 3 days or (C) 1 month of cerebral hypoperfusion. (D) Confocal images showing $Olig2^+/PCNA^+$ labelling of proliferating oligodendroglia in the corpus callosum. (E) Decreased numbers of $Olig2^+/PCNA^+$ cells were observed after 3 days of cerebral hypoperfusion. (F) No significant differences in numbers of $Olig2^+/PCNA^+$ cells were found after 1 month of hypoperfusion. (G) Representative confocal images showing BrdU labelled cells in the corpus callosum. (H) $BrdU^+$ cells were present in 2 out of 9 (22%) sham control animals but were observed in 5 out of 10 (50%) hypoperfused animals. (I) Representative confocal images showing $BrdU^+/CC1^+$ cells in the corpus callosum. (J) $CC1^+/BrdU^+$ double labelled cells were present in 3 out of 10 (30%) of the hypoperfused cohort but were completely absent from the sham control group. n = 13 sham, 11 hypoperfused for PCNA and Olig2 labelling at 3 days. One animal was excluded from analysis on the basis of poor cellular staining; n = 9 sham, 9 hypoperfused for PCNA/Olig2 and CC1/BrdU labelling at 1 month. Scale bars = 10 μm. * $p<0.05$.
doi:10.1371/journal.pone.0087227.g003

numbers of mature oligodendrocytes were increased when examined after 1 month hypoperfusion. This suggests that there is sufficient capacity with the adult brain to overcome the initial loss of oligodendrocyte pools. Similarly, in models of focal cerebral ischaemia when either blood flow is restored with reperfusion or in the peri-infarct region where there is sufficient collateral flow, increased numbers of OPCs are detectable [16]. In contrast, other studies of mouse cerebral hypoperfusion have shown that oligodendrocyte numbers remain reduced at one month of hypoperfusion [38,39]. There are notable differences between the model of cerebral hypoperfusion in our group compared to others [28,38,39]. Importantly we do not detect demyelination but instead a robust disruption of axon-glial integrity and a pronounced microglial response in white matter [12,25,26]. There may also be differences in the time course of progression of oligodendrocyte changes between our studies and others. The level of reduction in cerebral blood flow may be a critical factor which influences the extent of pathology and proliferation/differentiation response. We used laser speckle imaging and demonstrated that in our hands the reduction in CBF was approximately 36% that of baseline at 3 days and then restored to 22% that of shams at 1 month. These are slightly greater than the levels reported previously by Shibata et al. 2004 [28] where the maximal levels of CBF reduction as assessed by laser Doppler flowmetry were 30% although are consistent with more recent studies such as that by Duan et al. [40] who have reported reductions of 37% from that of baseline using Laser Speckle imaging. However, there are a number of other factors that may influence the outcome and differences in pathology in models between different laboratories including the anaesthetic used; the background strain of mice (influences differences in cerebrovasculature) and environment (pathogen status, temperature). Notably however, in these studies that report sustained reductions in oligodendrocyte numbers [38,39,41,42] the pools can be restored by either pharmacological intervention [39,41,42] or bone marrow cell treatment [38] indicating that there is restorative capacity of oligodendrocytes in the model. In a previous study we detected a marked increase in genes associated with cell proliferation in white matter in response to hypoperfusion [25] and as a consequence expected to observe marked increases in cell proliferation. However, assessment using the acute proliferation marker PCNA showed that overall levels of proliferation were unchanged with hypoperfusion but revealed that proliferation of $Olig2^+$ cells was decreased in 3 day hypoperfused animals compared to controls. It is important to note that whilst proliferation of OPCs was reduced after 3 days, there may be a proliferative response of other cells within the white matter although characterisation of this was beyond the scope of the current study.

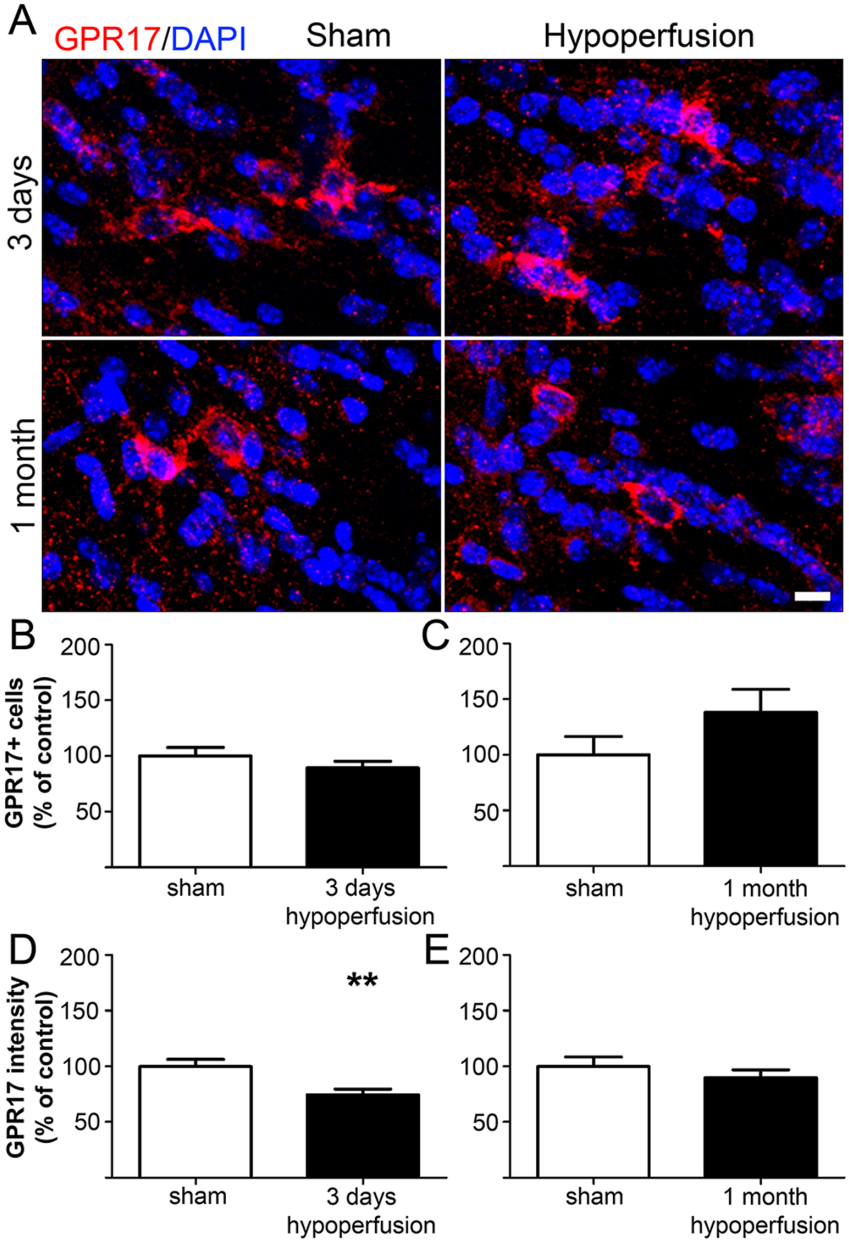

Figure 4. Chronic cerebral hypoperfusion does not alter numbers of GPR17-expressing cells. (A) Representative confocal images showing GPR17 labelling in the corpus callosum following 3 days and 1 month of hypoperfusion. Scale bar = 10 μm. (B) Numbers of GPR17$^+$ cells in the corpus callosum were unchanged after 3 days and (C) 1 month of cerebral hypoperfusion. (D) Intensity of GPR17 labelling was significantly decreased after 3 days of cerebral hypoperfusion. (E) No difference in GPR17 labelling intensity was observed after 1 month of cerebral hypoperfusion. n = 13 sham and 11 hypoperfused for 3 day analysis; n = 9 sham and 9 hypoperfused for 1 month analysis. ** $p<0.01$.
doi:10.1371/journal.pone.0087227.g004

To further characterise the early proliferative responses to cerebral hypoperfusion, BrdU incorporation was used to assess the total number of proliferating cells during the first 3 days after the onset of hypoperfusion. This revealed that proliferating cells were detectable in 50% of the hypoperfused cohort compared to 22% of sham operated animals suggesting a modest proliferative response early in response to hypoperfusion. However, this low level of proliferation would be insufficient to account for the restoration of the oligodendroglial pool. It is possible that the BrdU labelling protocol used in this study has not adequately labelled all proliferating cells and thus has underestimated the extent of proliferation. Although it has been reported that BrdU at 200 mg/kg body weight is a saturating dose and does not result in cytotoxicity [43], the dosage used in this study (70 mg/kg body weight/day) is within the standard range of 50–100 mg/kg reported in many studies. However, the use of only two injections per day coupled with the short bioavailability of BrdU may have been insufficient to label all proliferating cells within the injection period. In addition, a comprehensive characterisation of cell proliferation would require continuous administration of BrdU (for example in drinking water) and assessment of BrdU$^+$ cells at various time points.

The lack of convincing evidence of proliferation in response to cerebral hypoperfusion raises the question as to whether differen-

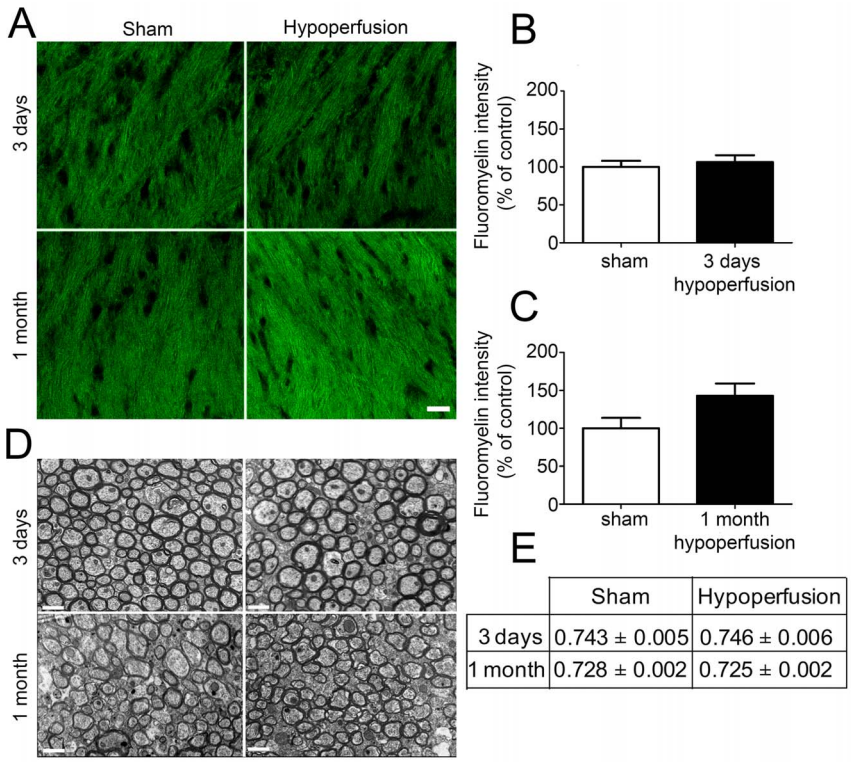

	Sham	Hypoperfusion
3 days	0.743 ± 0.005	0.746 ± 0.006
1 month	0.728 ± 0.002	0.725 ± 0.002

Figure 5. Alterations to numbers of oligodendrocytes as a result of chronic cerebral hypoperfusion does not impact on myelination of axons within the corpus callosum. (A) Representative confocal images showing fluoromyelin labelling in the corpus callosum after 3 days and 1 month of cerebral hypoperfusion. Scale bar = 20 μm (B) No significant difference in fluoromyelin intensity was observed after 3 days of chronic cerebral hypoperfusion. (C) Fluoromyelin intensity was not significantly different between groups after 1 month of cerebral hypoperfusion. n = 13 sham, 12 hypoperfused for 3 day analysis and n = 9 sham, 10 hypoperfused for 1 month analysis. (D) Representative electron micrographs showing myelinated fibres in the corpus callosum after 3 days and 1 month of cerebral hypoperfusion. Scale bars = 1 μm. (E) G-ratio values were unchanged following 3 days and 1 month of hypoperfusion compared to respective sham controls. n = 5 sham and 6 hypoperfused for 3 day analysis; n = 7 sham and 7 hypoperfused for 1 month analysis.
doi:10.1371/journal.pone.0087227.g005

tiation of pre-existing OPCs may contribute to the restoration of oligodendrocyte pools. Consistent with the hypothesis that glutamate and ATP may be involved in white matter disruption following cerebral hypoperfusion, there is growing evidence implicating these two neurotransmitters in the regulation of OPC proliferation and differentiation. *In vitro* studies have demonstrated that glutamate inhibits OPC proliferation [21] but promotes OPC differentiation via NMDA receptor activation [44]. Similarly it has been demonstrated that ATP and related derivatives also inhibit proliferation whilst promoting OPC differentiation [20]. Therefore it is possible that the low numbers of proliferating cells in this study may be due to extracellular ATP and glutamate acting to limit OPC proliferation whilst promoting differentiation. In the current study we have demonstrated that a small proportion of newly generated cells had differentiated into mature oligodendrocytes however this is unlikely to exclusively account for the significant increase in oligodendrocyte numbers observed after 1 month. It is possible that differentiation of pre-existing OPCs has also occurred to boost oligodendrocyte numbers in response to cerebral hypoperfusion. Interestingly, this is consistent with a study in a model of cerebral ischaemia which similarly showed repopulation of the oligodendrocyte pool in the absence of significant OPC proliferation [6].

To investigate a potential mechanism involved in differentiation of OPCs in response to hypoperfusion we examined the expression of GPR17, a novel dual uracil nucleotide and cysteinyl-leukotriene G protein-coupled receptor which has been implicated in mediating OPC responses to injury such as ischaemia [22]. It has previously been demonstrated that expression of GPR17 is upregulated in response to ischaemia and it has been suggested that receptor activation may act as a sensor of local damage [22–24]. In the current study, we have shown that numbers of GPR17-expressing cells were unchanged but expression of the receptor was decreased during the acute response to cerebral hypoperfusion. There is however conflicting evidence regarding the effects of receptor activation on OPC differentiation. Studies using transgenic mice have shown that receptor over-expression results in decreased myelination whereas knockout leads to increased myelination suggesting that GPR17 is a negative regulator of OPC differentiation [45]. In contrast, it has been shown *in vitro* that receptor agonism results in increased numbers of mature oligodendrocytes, implying that receptor activation promotes differentiation, whilst antagonism increases the proportion of OPCs [24]. Additionally it has also been demonstrated that when cultured OPCs are transferred to medium which promotes differentiation, GPR17 expression is increased [46]. Despite this apparently permissive role of GPR17 in OPC differentiation, it has also been reported that receptor expression may also increase the susceptibility of a cell to ATP-induced death [46]. Thus although GPR17 activation does not appear to mediate OPC responses to cerebral hypoperfusion at the time points examined, its downregulation after 3 days may represent an attempt to limit cell damage and/or death induced by hypoperfusion.

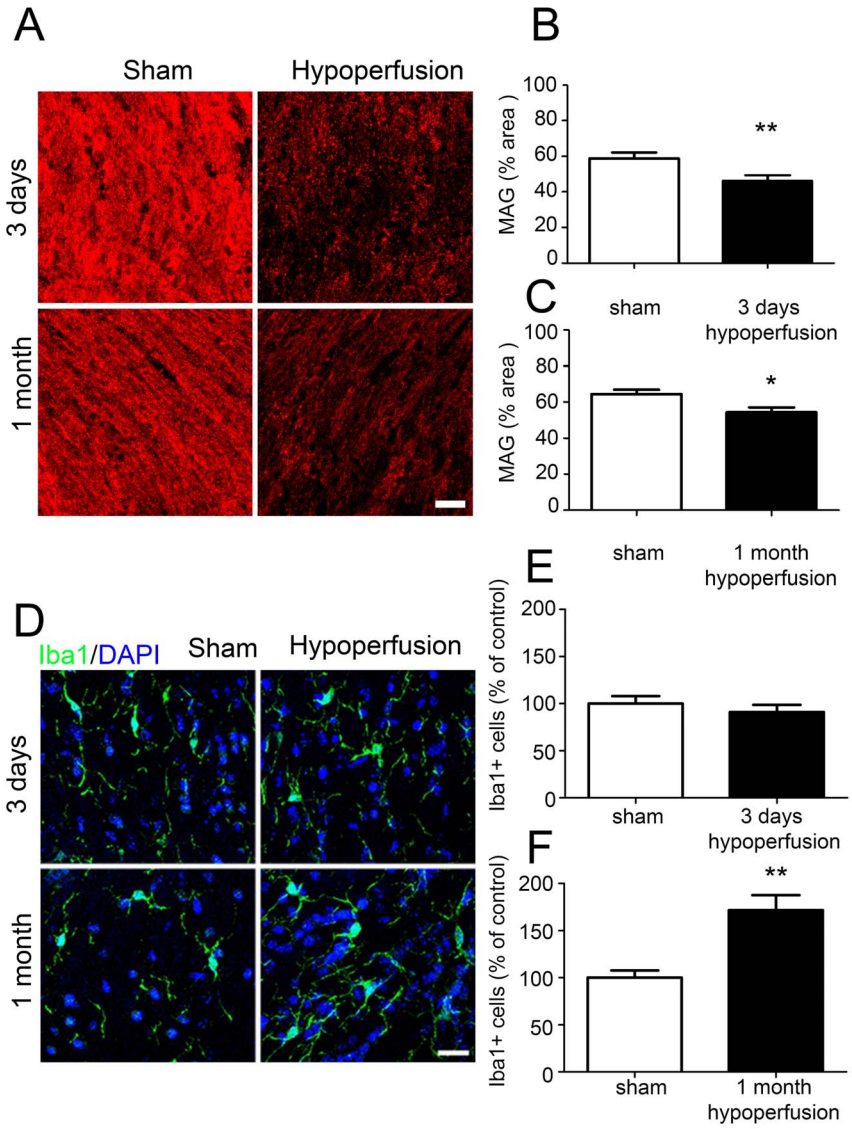

Figure 6. Axon-glial integrity is disrupted and increased numbers of microglia after cerebral hypoperfusion. (A) Representative confocal images showing MAG labelling in the corpus callosum following 3 days and 1 month of chronic cerebral hypoperfusion. Scale bar = 20 μm. (B) A significant decrease in the density of MAG labelling was observed following 3 days of cerebral hypoperfusion compared to sham controls. (C) Similarly, decreased density of MAG was also observed following 1 month of hypoperfusion. n = 12 sham, 12 hypoperfused for 3 day analysis. One animal was excluded due to a lack of positive MAG labelling; n = 9 sham, 8 hypoperfused for 1 month analysis. (D) Representative confocal images showing 1ba1 labelling 3 days and 1 month after the onset of cerebral hypoperfusion. Scale bar = 10 μm. (E) Numbers of microglia were unchanged following 3 days of cerebral hypoperfusion. (F) Following 1 month of cerebral hypoperfusion, a significant increase in microglial number was observed compared to sham controls. n = 13 sham, 12 hypoperfused for 3 day analysis; n = 9 sham, 10 hypoperfused for 1 month analysis.
doi:10.1371/journal.pone.0087227.g006

Myelinated axons in the corpus callosum were examined at the ultrastructural level to determine whether alterations to oligodendrocyte numbers had an impact on myelin sheaths. We observed no significant differences in g-ratio, an index of myelin sheath thickness, between sham and 3 day hypoperfused mice despite hypoperfusion inducing around a 15% reduction in mature oligodendrocytes at this time point. Furthermore there were no differences in myelin levels as assessed by fluoromyelin-labelling of myelin in the corpus callosum or MBP levels measured in myelin-enriched extracts. Limitations of these approaches may have precluded detection of myelin alterations after hypoperfusion. In the present study, fluoromyelin staining was conducted in thick sections using a slightly modified protocol to that of previously published work which did detect alterations in myelin in the hypoperfusion model [38,41]. Thus, differences in fluoromyelin staining methods might explain the different outcomes. Additionally, the present study assessed MBP alterations in myelin-enriched fractions [29] prepared from both white matter and grey matter. Arguably there may have been a dilutional effect of the grey matter on the measurement of MBP levels since this model has been shown to exhibit predominantly a white matter pathology without robust grey matter pathology within 1 month after the surgery [12,27,28]. However, this finding (loss of oligodendrocytes and absence of myelin changes), is consistent with a recent study which used diphtheria toxin to specifically ablate oligodendrocyte numbers by approximately 26% and reported that myelin was

preserved despite this extensive oligodendrocyte loss [47]. This lack of effect on myelination despite profound alterations in oligodendrocyte pools is also consistent with previous studies by our group which have determined that there are no gross alterations to the protein levels of myelin basic protein as assessed by immunohistochemistry [25]. Instead, in this model, hypoperfusion results in disruption of MAG and breakdown of axon-glial integrity associated with disruption of the paranodal septate junctions [25]. The current study used an antibody against the CC1 protein which labels oligodendrocyte cell bodies but not processes, and as a result cannot reliably distinguish between myelinating and non-myelinating oligodendrocytes. One possible explanation for our findings is that in response to cerebral hypoperfusion, a non-myelinating population of $CC1^+$ oligodendrocytes are lost and thus no disruption to myelin has been observed. Another possibility is that neighbouring oligodendrocytes may compensate for oligodendrocyte loss by extending processes and 'filling in' non-myelinated areas [48]. We also observed that g-ratio was similarly unchanged following 1 month of hypoperfusion and so it remains to be determined whether increased numbers of oligodendrocytes observed at this time point are surplus to requirements. Overall these findings suggest that even in the presence of cerebral hypoperfusion, the CNS can tolerate significant alterations to mature oligodendrocyte pools without any apparent detriment to myelin thickness or density.

Thus in conclusion this study provides further support that oligodendrocytes are vulnerable to modest blood flow reductions and evidence supporting their regenerative capacity. This turnover of the pool of oligodendrocytes appears to occur in the absence of changes in myelination but it would be interesting to investigate in future studies whether there are any functional consequences of these changes within the white matter.

Supporting Information

Figure S1 Reduced cerebral blood flow in hypoperfused animals. Cerebral blood flow was measured using laser speckle flowmetry prior to surgery (baseline) and at 3 days and 1 month following surgery to assess the extent of hypoperfusion at the times white matter alterations were investigated. (A) Representative images showing speckle images at baseline, 3 days and 1 month for a sham and hypoperfused mouse. Images show the average of 100 frames. Baseline CBF was not significantly different ($p<0.05$) between groups (1130±36 perfusion units in shams vs 1072±24 perfusion units in hypoperfused group). (B&C) After 3 days and 1 month, CBF was significantly decreased in hypoperfused compared to sham animals to ($p<0.001$ and $p<0.005$ respectively). Data are calculated for each mouse as the percentage change relative to baseline. (B) Cerebral blood flow was decreased by approximately 36% to that of shams following 3 days of cerebral hypoperfusion. (C) Following 1 month of hypoperfusion, CBF values had recovered to approximately 22% of sham levels. Data is shown for each mouse, n = 8 sham, 6 hypoperfused.
(TIF)

Figure S2 NG2 is a specific marker of OPCs. NG2 and PDGFRα labelling confirmed the specificity of NG2 as an OPC marker in the corpus callosum. (A) NG2 and PDGFRα co-labelled OPCs in the corpus callosum. Scale bar = 10 μm. (B) Confocal images showing representative NG2 and PDGFRβ labelling. No $PDGFR\beta^+$ labelling of pericytes was observed in the corpus callosum and only occasional $PDGFR\beta^+$ labelling was observed in the cortex. No $NG2^+/PDGFR\beta^+$ cells were observed in either region. Scale bar = 20 μm.
(TIF)

Figure S3 Low magnification images of NG2, CC1, Olig2 and GPR17 labelling. (A) Low magnification confocal images showing $NG2^+$ labelling of OPCs in the corpus callosum (CC). (B) Confocal images showing $CC1^+$ labelling of mature oligodendrocytes in the corpus callosum. (C) Confocal images showing $Olig2^+$ labelling of oligodendroglia in the corpus callosum. (D) Confocal images showing $GPR17^+$ labelling in the corpus callosum. Scale bars = 50 μm. CTx = Cortex, CC = corpus callosum, CPu = caudate putamen.
(TIF)

Figure S4 Astrocytes are not labelled with CC1 and numbers are unchanged following 1 month of cerebral hypoperfusion. It has been reported that a subpopulation of astrocytes can express the CC1 (APC) antigen, therefore CC1 and GFAP double labelling was carried out to determine numbers of $CC1^+$ astrocytes. (A) Representative confocal images showing $CC1^+/GFAP^+$ double labelling in the corpus callosum (CC). Scale bar = 50 μm, inset scale bar = 10 μm. Cell counts of numbers of double labelled cells revealed approximately 0.8% of $CC1^+$ cells expressed GFAP thus confirming the high specificity of CC1 as a marker of mature oligodendrocytes. (B) Representative confocal images showing $GFAP^+$ labelling of astrocytes in the corpus callosum (CC). Scale bar = 50 μm. (C) Numbers of $GFAP^+$ astrocytes are unchanged following 1 month of chronic cerebral hypoperfusion. CTx = Cortex, CC = corpus callosum, CPu = caudate putamen.
(TIF)

Figure S5 GPR17 is expressed by oligodendroglia and a small number of microglia. (A) Representative confocal images showing $GPR17^+/Olig2^+$ double labelling in the corpus callosum. Arrows indicate double labelled cells. (B) Representative confocal images showing $GPR17^+/Iba1^+$ labelling in the corpus callosum. (C) Cell counting revealed approximately 64.4±3.33% of $GPR17^+$ cells express Olig2 in the corpus callosum. Only 8.29±0.75% of $GPR17^+$ cells co-expressed Iba1. Scale bars = 50 μm, inset scale bars = 10© μm. CTx = Cortex, CC = corpus callosum, CPu = caudate putamen.
(TIF)

Figure S6 MBP levels are unchanged following 1 month of cerebral hypoperfusion. (A) Representative Western blot from myelin enriched extracts showing the different MBP isoforms (25–16 kDa) and GAPDH, the later used as a loading control. (B) Analysis of fluorescent intensity relative to GAPDH showed no significant changes in MBP levels after 1 month of cerebral hypoperfusion. n = 5 sham, n = 8 hypoperfused.
(TIF)

Acknowledgments

We would like to thank the Euan MacDonald Centre for the use of confocal facilities, and Julia Edgar and Maj-lis McCulloch for their input and advice regarding electron microscopy studies.

Author Contributions

Conceived and designed the experiments: KH JM. Performed the experiments: JM MR JF PH YM MM. Analyzed the data: JM JF KH YM. Wrote the paper: JM KH.

References

1. Nave KA (2010) Myelination and support of axonal integrity by glia. Nature 468: 244–252.
2. Rivers LE, Young KM, Rizzi M, Jamen F, Psachoulia K, et al. (2008) PDGFRA/NG2 glia generate myelinating oligodendrocytes and piriform projection neurons in adult mice. Nature Neuroscience 11: 1392–1401.
3. Tomimoto H, Ihara M, Wakita H, Ohtani R, Lin JX, et al. (2003) Chronic cerebral hypoperfusion induces white matter lesions and loss of oligodendroglia with DNA fragmentation in the rat. Acta Neuropathology 106: 527–534.
4. Valeriani V, Dewar D, McCulloch J (2000) Quantitative assessment of ischemic pathology in axons, oligodendrocytes, and neurons: attenuation of damage after transient ischemia. Journal of Cerebral Blood Flow and Metabolism 20: 765–771.
5. Pantoni L, Garcia JH, Gutierrez JA (1996) Cerebral white matter is highly vulnerable to ischemia. Stroke 27: 1641–1646; discussion 1647.
6. McIver SR, Muccigrosso M, Gonzales ER, Lee JM, Roberts MS, et al. (2010) Oligodendrocyte degeneration and recovery after focal cerebral ischemia. Neuroscience 169: 1364–1375.
7. Lyons SA, Kettenmann H (1998) Oligodendrocytes and microglia are selectively vulnerable to combined hypoxia and hypoglycemia injury in vitro. Journal of Cerebral Blood Flow and Metabolism 18: 521–530.
8. McDonald JW, Levine JM, Qu Y (1998) Multiple classes of the oligodendrocyte lineage are highly vulnerable to excitotoxicity. Neuroreport 9: 2757–2762.
9. Merrill JE, Scolding NJ (1999) Mechanisms of damage to myelin and oligodendrocytes and their relevance to disease. Neuropathology and Applied Neurobiology 25: 435–458.
10. Head D, Buckner RL, Shimony JS, Williams LE, Akbudak E, et al. (2004) Differential vulnerability of anterior white matter in nondemented aging with minimal acceleration in dementia of the Alzheimer type: evidence from diffusion tensor imaging. Cerebral Cortex 14: 410–423.
11. Kohama SG, Rosene DL, Sherman LS (2011) Age-related changes in human and non-human primate white matter: from myelination disturbances to cognitive decline. Age DOI 10.1007/s11357-011-9357-7.
12. Coltman R, Spain A, Tsenkina Y, Fowler JH, Smith J, et al. (2011) Selective white matter pathology induces a specific impairment in spatial working memory. Neurobiology of Aging 32: 2324 e2327–2312.
13. Desai MK, Mastrangelo MA, Ryan DA, Sudol KL, Narrow WC, et al. (2010) Early oligodendrocyte/myelin pathology in Alzheimer's disease mice constitutes a novel therapeutic target. American Journal of Pathology 177: 1422–1435.
14. Aboul-Enein F, Rauschka H, Kornek B, Stadelmann C, Stefferl A, et al. (2003) Preferential loss of myelin-associated glycoprotein reflects hypoxia-like white matter damage in stroke and inflammatory brain diseases. Journal of Neuropathology and Experimental Neurology 62: 25–33.
15. Zaidi AU, Bessert DA, Ong JE, Xu H, Barks JD, et al. (2004) New oligodendrocytes are generated after neonatal hypoxic-ischemic brain injury in rodents. Glia 46: 380–390.
16. Tanaka K, Nogawa S, Ito D, Suzuki S, Dembo T, et al. (2001) Activation of NG2-positive oligodendrocyte progenitor cells during post-ischemic reperfusion in the rat brain. Neuroreport 12: 2169–2174.
17. Tanaka K, Nogawa S, Suzuki S, Dembo T, Kosakai A (2003) Upregulation of oligodendrocyte progenitor cells associated with restoration of mature oligodendrocytes and myelination in peri-infarct area in the rat brain. Brain Research 989: 172–179.
18. Simpson JE, Fernando MS, Clark L, Ince PG, Matthews F, et al. (2007) White matter lesions in an unselected cohort of the elderly: astrocytic, microglial and oligodendrocyte precursor cell responses. Neuropathology and Applied Neurobiology 33: 410–419.
19. Back SA, Kroenke CD, Sherman LS, Lawrence G, Gong X, et al. (2011) White matter lesions defined by diffusion tensor imaging in older adults. Annals of Neurology 70: 465–476.
20. Agresti C, Meomartini ME, Amadio S, Ambrosini E, Volonte C, et al. (2005) ATP regulates oligodendrocyte progenitor migration, proliferation, and differentiation: involvement of metabotropic P2 receptors. Brain Research Reviews 48: 157–165.
21. Yuan X, Eisen AM, McBain CJ, Gallo V (1998) A role for glutamate and its receptors in the regulation of oligodendrocyte development in cerebellar tissue slices. Development 125: 2901–2914.
22. Ciana P, Fumagalli M, Trincavelli ML, Verderio C, Rosa P, et al. (2006) The orphan receptor GPR17 identified as a new dual uracil nucleotides/cysteinyl-leukotrienes receptor. The EMBO Journal 25: 4615–4627.
23. Lecca D, Trincavelli ML, Gelosa P, Sironi L, Ciana P, et al. (2008) The recently identified P2Y-like receptor GPR17 is a sensor of brain damage and a new target for brain repair. PLoS One 3: e3579.
24. Boda E, Vigano F, Rosa P, Fumagalli M, Labat-Gest V, et al. (2011) The GPR17 receptor in NG2 expressing cells: Focus on in vivocell maturation and participation in acute trauma and chronic damage. Glia 59: 1958–1973.
25. Reimer MM, McQueen J, Searcy L, Scullion G, Zonta B, et al. (2011) Rapid disruption of axon-glial integrity in response to mild cerebral hypoperfusion. Journal of Neuroscience 31: 18185–18194.
26. Holland PR, Bastin ME, Jansen MA, Merrifield GD, Coltman RB, et al. (2011) MRI is a sensitive marker of subtle white matter pathology in hypoperfused mice. Neurobiology of Aging 32: 2325.e2321–e2326.
27. Shibata M, Yamasaki N, Miyakawa T, Kalaria RN, Fujita Y, et al. (2007) Selective impairment of working memory in a mouse model of chronic cerebral hypoperfusion. Stroke 38: 2826–2832.
28. Shibata M, Ohtani R, Ihara M, Tomimoto H (2004) White matter lesions and glial activation in a novel mouse model of chronic cerebral hypoperfusion. Stroke 35: 2598–2603.
29. Yool DA, Klugmann M, McLaughlin M, Vouyiouklis DA, Dimou L, et al. (2001) Myelin proteolipid proteins promote the interaction of oligodendrocytes and axons. J Neurosci Res 63: 151–164.
30. Bhat RV, Axt KJ, Fosnaugh JS, Smith KJ, Johnson KA, et al. (1996) Expression of the APC tumor suppressor protein in oligodendroglia. Glia 17: 169–174.
31. Back SA, Gan X, Li Y, Rosenberg PA, Volpe JJ (1998) Maturation-dependent vulnerability of oligodendrocytes to oxidative stress-induced death caused by glutathione depletion. Journal of Neuroscience 18: 6241–6253.
32. Husain J, Juurlink BH (1995) Oligodendroglial precursor cell susceptibility to hypoxia is related to poor ability to cope with reactive oxygen species. Brain Research 698: 86–94.
33. Mabuchi T, Kitagawa K, Ohtsuki T, Kuwabara K, Yagita Y, et al. (2000) Contribution of microglia/macrophages to expansion of infarction and response of oligodendrocytes after focal cerebral ischemia in rats. Stroke 31: 1735–1743.
34. Deng Y, Lu J, Sivakumar V, Ling EA, Kaur C (2008) Amoeboid microglia in the periventricular white matter induce oligodendrocyte damage through expression of proinflammatory cytokines via MAP kinase signaling pathway in hypoxic neonatal rats. Brain Pathology 18: 387–400.
35. McTigue DM, Tripathi RB (2008) The life, death, and replacement of oligodendrocytes in the adult CNS. Journal of Neurochemistry 107: 1–19.
36. Alix JJ, Fern R (2009) Glutamate receptor-mediated ischemic injury of premyelinated central axons. Annals of Neurology 66: 682–693.
37. Stys PK, Lipton SA (2007) White matter NMDA receptors: an unexpected new therapeutic target? Trends in Pharmacological Sciences 28: 561–566.
38. Fujita Y, Ihara M, Ushiki T, Hirai H, Kizaka-Kondoh S, et al. (2010) Early protective effect of bone marrow mononuclear cells against ischemic white matter damage through augmentation of cerebral blood flow. Stroke; a journal of cerebral circulation 41: 2938–2943.
39. Maki T, Ihara M, Fujita Y, Nambu T, Miyashita K, et al. (2011) Angiogenic and vasoprotective effects of adrenomedullin on prevention of cognitive decline after chronic cerebral hypoperfusion in mice. Stroke; a journal of cerebral circulation 42: 1122–1128.
40. Duan W, Ran H, Zhou Z, He Q, Zheng J (2012) Adenosine A2A receptor deficiency up-regulates cystatin F expression in white matter lesions induced by chronic cerebral hypoperfusion. PLoS One 7: e52566.
41. Miyamoto N, Maki T, Pham LD, Hayakawa K, Seo JH, et al. (2013) Oxidative Stress Interferes With White Matter Renewal After Prolonged Cerebral Hypoperfusion in Mice. Stroke.
42. Miyamoto N, Pham LD, Hayakawa K, Matsuzaki T, Seo JH, et al. (2013) Age-Related Decline in Oligodendrogenesis Retards White Matter Repair in Mice. Stroke.
43. Taupin P (2007) BrdU immunohistochemistry for studying adult neurogenesis: paradigms, pitfalls, limitations, and validation. Brain Res Rev 53: 198–214.
44. Cavaliere F, Urra O, Alberdi E, Matute C (2012) Oligodendrocyte differentiation from adult multipotent stem cells is modulated by glutamate. Cell Death and Disease 3: e268.
45. Chen Y, Wu H, Wang S, Koito H, Li J, et al. (2009) The oligodendrocyte-specific G protein-coupled receptor GPR17 is a cell-intrinsic timer of myelination. Nature Neuroscience 12: 1398–1406.
46. Ceruti S, Vigano F, Boda E, Ferrario S, Magni G, et al. (2011) Expression of the new P2Y-like receptor GPR17 during oligodendrocyte precursor cell maturation regulates sensitivity to ATP-induced death. Glia 59: 363–378.
47. Oluich LJ, Stratton JA, Lulu Xing Y, Ng SW, Cate HS, et al. (2012) Targeted ablation of oligodendrocytes induces axonal pathology independent of overt demyelination. Journal of Neuroscience 32: 8317–8330.
48. Richardson WD, Young KM, Tripathi RB, McKenzie I (2011) NG2-glia as multipotent neural stem cells: fact or fantasy? Neuron 70: 661–673.

Neurobiology of Disease

Rapid Disruption of Axon–Glial Integrity in Response to Mild Cerebral Hypoperfusion

Michell M. Reimer,[1,3] Jamie McQueen,[1,3] Luke Searcy,[1,2] Gillian Scullion,[1] Barbara Zonta,[1] Anne Desmazieres,[1] Philip R. Holland,[1,3] Jessica Smith,[1] Catherine Gliddon,[1] Emma R. Wood,[2] Pawel Herzyk,[4] Peter J. Brophy,[1] James McCulloch,[2,3] and Karen Horsburgh[1,3]

[1]University of Edinburgh, Centre for Neuroregeneration, Edinburgh EH16 4SB, United Kingdom, [2]University of Edinburgh, Centre for Cognitive and Neural Systems, Edinburgh EH8 9JZ, United Kingdom, [3]University of Edinburgh, Centre for Cognitive Ageing and Cognitive Epidemiology, Edinburgh EH8 9JZ, United Kingdom, and [4]University of Glasgow, Institute of Molecular, Cell and Systems Biology College of Medical, Veterinary and Life Sciences, Glasgow G12 8QQ, United Kingdom

Myelinated axons have a distinct protein architecture essential for action potential propagation, neuronal communication, and maintaining cognitive function. Damage to myelinated axons, associated with cerebral hypoperfusion, contributes to age-related cognitive decline. We sought to determine early alterations in the protein architecture of myelinated axons and potential mechanisms after hypoperfusion. Using a mouse model of hypoperfusion, we assessed changes in proteins critical to the maintenance of paranodes, nodes of Ranvier, axon–glial integrity, axons, and myelin by confocal laser scanning microscopy. As early as 3 d after hypoperfusion, the paranodal septate-like junctions were damaged. This was marked by a progressive reduction of paranodal Neurofascin signal and a loss of septate-like junctions. Concurrent with paranodal disruption, there was a significant increase in nodal length, identified by Nav1.6 staining, with hypoperfusion. Disruption of axon–glial integrity was also determined after hypoperfusion by changes in the spatial distribution of myelin-associated glycoprotein staining. These nodal/paranodal changes were more pronounced after 1 month of hypoperfusion. In contrast, the nodal anchoring proteins AnkyrinG and Neurofascin 186 were unchanged and there were no overt changes in axonal and myelin integrity with hypoperfusion. A microarray analysis of white matter samples indicated that there were significant alterations in 129 genes. Subsequent analysis indicated alterations in biological pathways, including inflammatory responses, cytokine-cytokine receptor interactions, blood vessel development, and cell proliferation processes. Our results demonstrate that hypoperfusion leads to a rapid disruption of key proteins critical to the stability of the axon–glial connection that is mediated by a diversity of molecular events.

Introduction

The integrity of the brain's white matter, comprised mainly of myelinated axons, is critical in regulating efficient neuronal communication and maintaining cognitive function (Nave, 2010). Myelination of axons, by oligodendrocytes, determines the localization of key proteins along the axon and segregates the axonal membrane into defined regions: the node of Ranvier, paranode, juxtaparanode, and internode (Rios et al., 2003; Susuki and Rasband, 2008). In the adult brain, the nodes of Ranvier located at defined points along the axolemma are critical for action potential propagation. They are comprised of voltage-gated sodium channels that are clustered at a high density within a diffusion barrier of septate-like junctions. These paranodal septate-like junctions, consisting of glial Neurofascin (Nfasc)155, axonal contactin, and contactin-associated protein (Caspr), are critical to the maintenance of axon–glial junctions at the paranodes. A dynamic relationship exists between axons and glia, in addition to highly coordinated signaling with vascular components (endothelial cells, pericytes) that comprise the oligovascular niche (Arai and Lo, 2009), which, if disrupted, could impede neuronal communication and cognitive abilities.

With advancing age, there is a general decline in white matter integrity associated with cognitive decline (Bartzokis et al., 2004; Bastin et al., 2009). Although there is evidence that the protein architecture of myelinated axons may be altered at nodal regions in the aging brain (Lasiene et al., 2009), as yet the underlying molecular changes that occur early are not known. Cerebral hypoperfusion is suggested to contribute to the development of white matter changes in the aging brain (Fernando et al., 2006). In response to severe hypoperfusion as a result of stroke, axon–glial integrity is impaired, as demonstrated by a loss of myelin-associated glycoprotein (MAG) (Waxman, 2006), a protein

Received Sept. 28, 2011; revised Oct. 28, 2011; accepted Nov. 2, 2011.

Author contributions: M.M.R., L.S., and K.H. designed research; M.M.R., J.McQu, L.S., G.S., P.R.H., J.S., and C.G. performed research; B.Z., A.D., and P.B. contributed unpublished reagents/analytic tools; M.M.R., J.McQ., L.S., E.R.W., P.H., J.McC. and K.H. analyzed data; M.M.R. and K.H. wrote the paper.

This work was supported by the Disconnected Mind program (supported by Age, UK and Alzheimer's Research UK). We gratefully acknowledge the University of Edinburgh Centre for Cognitive Ageing and Cognitive Epidemiology (part of the cross council Lifelong Health and Wellbeing Initiative).

Correspondence should be addressed to Dr. Karen Horsburgh, Centre for Neuroregeneration, The Medical School, University of Edinburgh, Chancellor's Building, 49 Little France Crescent, Edinburgh EH16 4SB, United Kingdom. E-mail: Karen.Horsburgh@ed.ac.uk.

J. Smith's present address: Alzheimer's Society, Devon House, London E1W 1LB, United Kingdom.

DOI:10.1523/JNEUROSCI.4936-11.2011

 0270-6474/11/3118185-10$15.00/0

important in the maintenance of the axon–glial connection (Quarles, 2007; Schnaar and Lopez, 2009). Glutamate excitotoxicity has also been shown to cause paranodal myelin splitting and retraction (Fu et al., 2009). Disruption of the protein architecture of myelinated axons is often associated with demyelinating diseases. In multiple sclerosis, paranodal disruption of Nfasc155 and Caspr leads to dispersion of $Na_v1.6$ and Nfasc186 proteins along the axon (Howell et al., 2006; Waxman, 2006) and impaired nerve function (Quarles, 2007).

Using a mouse model of chronic cerebral hypoperfusion (Shibata et al., 2004), which mimics the modest, sustained reductions in blood flow of the aging brain, we previously demonstrated that hypoperfusion results in damage to white matter at the cellular level (Coltman et al., 2011) and *in vivo* (Holland et al., 2011). We hypothesized that hypoperfusion would cause alterations in axon–glial integrity associated with a disruption in key proteins responsible for anchoring nodal proteins and paranodal junctions. To test this, we undertook a systematic analysis of the integrity of key proteins at the paranodal and nodal regions in response to hypoperfusion. To define the complex alterations in gene expression and biological pathways that may contribute to axon–glial damage, microarray analysis was conducted in white matter-enriched tissue. Our results indicate that diverse molecular pathways are altered with hypoperfusion.

Materials and Methods

Animals. Male C57BL/6J mice (25–30 g, ~3–4 months old) were obtained from Charles River. All procedures were authorized under the Home Office approved project license number 60/3722 title "Pathophysiology of Alzheimer's disease: link to cerebrovascular disease" held by Dr. K. Horsburgh. This license was approved by the University of Edinburgh's Ethical Review Committee on 4 June 2007 and the Home Office on 30 July 2007, is valid until 30 July 2012, and adhered to regulations specified in the Animals (Scientific Procedures) Act (1986).

Chronic cerebral hypoperfusion. Chronic cerebral hypoperfusion was induced by applying microcoils (0.18 mm internal diameter; Sawane Spring Co.) to both common carotid arteries as previously described (Shibata et al., 2004; Coltman et al., 2011) under isoflurane anesthesia. There was a period of 30 min between the insertion of each coil. Sham-operated animals underwent an identical surgical approach except that microcoils were not applied to the common carotid arteries. The temperature of the mice was maintained between 36.5°C and 37.5°C. The recovery of the mice was monitored closely, and the weight of the mice, whether they were eating and drinking, and any signs of overt neurological dysfunction (e.g., circling, rolling, hunching) were recorded.

Tissue preparation and immunohistochemistry. At either 3 d or 1 month after surgery, mice were deeply anesthetized with 5% isoflurane and transcardially perfused with 20 ml of 0.9% heparinized PBS and then 20 ml of 4% paraformaldehyde in 0.1% phosphate buffer. After perfusion, brains were removed and postfixed either in 4% PFA overnight (for nodal and internodal structures) or for 30 min (for Nfasc186 immunolabeling or with subsequent Bouins fixation for Nfasc155 immunolabeling). Brains were cut along the midline and floating sagittal sections (50 μm thickness) were produced with a vibrating blade microtome (Hydrax V50; Zeiss). Sections were collected and stored in cryoprotective medium (30% glycerol/30% ethylene glycol in phosphate buffer) and stored at −20°C until use. Adjacent sections were stained with hematoxylin and eosin (H&E) stain to determine the presence of ischemic neuronal perikaryal damage. Any animals exhibiting ischemic damage were excluded from the study.

The antibodies used in this study were as follows: $Na_v1.6$ (1:200, AB5580; Millipore), MAG (1:100, L20, sc-9543; Santa Cruz Biotechnology), myelin basic protein (MBP; 1:100, MAB386; Millipore), SMI312R (1:100; Covance), Caspr (1:100, clone K65/35; UC Davies NIH NeuroMab), Nfasc155 (NFF3, 1:1000) (Tait et al., 2000), Nfasc186 (MNF2, 1:200) (Tait et al., 2000), Neurofascin common epitope (1:1000, AB15188; Millipore), AnkyrinG (H-215, sc-28561; Santa Cruz Biotechnology), human/mouse active caspase-3 (1:100, AF835; R & D Systems). Secondary Cy2, 3, and 5 antibodies were purchased from Jackson ImmunoResearch Laboratories. All antibodies were incubated overnight at 4°C in PBS, pH 7.4, with 0.1% Triton X-100.

Analysis of immunohistochemistry. Immunolabeled 50 μm vibratome sections were analyzed using a laser scanning confocal microscope (Zeiss Axioskope LSM 510). All images were acquired with a 63× oil-immersion objective (numerical aperture, 1.4), a pinhole of 1 Airy unit, and a 1024 × 1024 pixel resolution. The corresponding Nyquist settings, 3.1× zoom and 0.13 μm *z*-steps, were used to allow image deconvolution (Huygens Professional Deconvolution Software; SVI) for nodal counts, length measurements, and colocalization assessment. All length measurements and counts were performed in an image stack spanning 10 μm using ImageJ MBI 1.43 s. The observer was always blinded to the surgical procedure.

Sodium channel cluster ($Na_v1.6$) length was assessed after 3 d hypoperfusion ($n = 9$ sham; $n = 8$ hypoperfusion) and 1 month hypoperfusion ($n = 10$ sham; $n = 6$ hypoperfusion). The first 40 nodes in the acquired 10 μm confocal stack that were not directly in contact with the border of the stack were analyzed to exclude only partially imaged nodes of Ranvier. The regions of the corpus callosum, internal capsule, and optic tract in sagittal sections were imaged at the stereotactic coordinates, lateral 2.40 ± 0.1 mm, according to Franklin and Paxinos (1997). The identity of nodes of Ranvier was confirmed by Caspr double-labeling. AnkyrinG and Nfasc186 cluster length was analyzed accordingly. AnkyrinG was assessed after 3 d ($n = 9$ sham; $n = 8$ hypoperfusion) and 1 month ($n = 9$ sham; $n = 10$ hypoperfusion) in the corpus callosum. Neurofascin186 was assessed after 3 d ($n = 6$ sham; $n = 6$ hypoperfusion) and 1 month ($n = 6$ sham; $n = 4$ hypoperfusion) in the corpus callosum. Different cohorts needed to be used due to differences in fixation methods. All animals with ischemic neuronal perikaryal damage or infarcts confirmed by H&E staining were excluded from analysis (12%).

Colocalization of paranodal proteins was assessed using Caspr and Neurofascin/Nfasc155 double-immunolabeling. The tissue was post-fixed using Bouins fixative for Nfasc155 (Sigma Aldrich). The corpus callosum of animals after 3 d of hypoperfusion ($n = 5$ sham; $n = 5$ hypoperfusion) and 1 month hypoperfusion ($n = 6$ sham; $n = 4$ hypoperfusion) was imaged. To identify paranodal pairs, paired Caspr-positive rectangular clusters (paranodes), separated by a small void of labeling (indicating the node of Ranvier), were analyzed regarding their Nfasc155 colabeling. If both labels (Caspr and Nfasc155) were completely overlapping in a paranodal pair, the node was defined as intact. If Nfasc155 labeling was absent on one or more sides of a Caspr-positive paranodal pair, the paranode was defined as disrupted. Overall, after 3 d of hypoperfusion, 129 paranodal pairs in the sham group and 138 in the hypoperfused group and after 1 month 185 paranodal pairs in the sham group and 129 in the hypoperfused group were analyzed. For Caspr and Neurofascin, common epitope labeling colocalization analysis was performed (Rickman et al., 2007) using ImageJ 1.43 (NIH) and Manders' coefficients determined.

Fluorescent intensity of MAG, MBP, and SMI312R immunohistochemistry was measured on single optical confocal sections, spanning 47 × 47 μm, of the corpus callosum, internal capsule, and optic tract after 3 d of hypoperfusion ($n = 10$ sham; $n = 8$ hypoperfusion) and 1 month of hypoperfusion ($n = 10$ sham; $n = 7$ hypoperfusion) using ImageJ 1.43 (NIH). Activated caspase-3 immunolabeling was assessed using a Leica DMR fluorescence microscope. All activated caspase-3-positive cells in a 50 μm thick sagittal section in the entire corpus callosum, optic tract, and internal capsule were counted.

Number of nodes of Ranvier. The number of the nodes of Ranvier was determined on the same sections as the voltage-gated sodium channel cluster measurements. A 47 × 47 × 5 μm^3 confocal stack per region was analyzed. All nodes included in the first optical section and/or contacting the left or upper edge of the stack were excluded; all nodes contacting the last and/or right and lower edge of the stack were included.

TEM of optic nerves. Animals were transcardially perfused with 5% glutaraldehyde/4% paraformaldehyde after 1 month hypoperfusion. Optic nerves were removed, samples were fixed in 3% glutaraldehyde in 0.1

M sodium cacodylate buffer, pH 7.3, for 2 h, then washed in three 10 min changes of 0.1 M sodium cacodylate. Specimens were then postfixed in 1% osmium tetroxide in 0.1 M sodium cacodylate. After dehydration, samples were embedded in Araldite resin. Ultrathin sections (60 nm thick) were cut on a Reichert OMU4 ultramicrotome (Leica Microsystems), stained in uranyl acetate and lead citrate, then viewed in a Philips CM120 transmission electron microscope (FEI). Images were taken with an Orius CCD camera (Gatan). Paranodes in longitudinal sections of optic nerves were analyzed. The presence or absence of paranodal septate-like junctions were assessed in 37 paranodes of sham and 35 paranodes of hypoperfused animals ($n = 3$ sham; $n = 3$ hypoperfusion). The micrographs were assessed by two observers who were blinded to the surgical procedure. The optic nerve was studied for the ease of identification of sufficient numbers of nodal and paranodal structures, which is precluded in other regions, such as the corpus callosum and internal capsule, and is known to be damaged in response to hypoperfusion (Coltman et al., 2011).

White matter micropunch. Seventy-two hours after hypoperfusion or sham surgery, mice ($n = 12$/group) were deeply anesthetized with isoflurane and perfused with 0.9% PBS. Brains were excised and placed in ice-cold PBS. Brains were subsequently sectioned with a vibratome to obtain two 1 mm coronal sections containing the genu and body of the corpus callosum. Sections were placed on glass slides and flash frozen on dry ice. White matter microsamples were collected via micropunch from subthawed sections using a 0.5 mm blunt-end needle attached to an air-filled syringe under a dissecting microscope. Micropunches of the corpus callosum were collected and aspirated into microcentrifuge tubes and stored at −80°C until RNA extraction.

RNA extraction. RNA was extracted from white matter micropunches using an RNeasy Lipid Tissue Mini Kit (Qiagen) according to the manufacturer's instructions. RNA concentrations were determined using a Nanodrop (Thermo Scientific).

Microarray analysis. Microarray RNA was pooled from 12 animals per cohort in groups of three, resulting in four pooled samples per cohort. RNA quality was confirmed using an RNA BioAnalyzer 2100 (Agilent). cDNA preparation, the microarray assay, and primary analysis was performed in the Sir Henry Wellcome Functional Genomics Facility at the University of Glasgow using standard Affymetrix protocols. Briefly, samples were hybridized to GeneChip Mouse Exon 1.0 ST arrays (Affymetrix) representing >44,000 genes using the fluidic station 400. Raw data were obtained and quality control was assessed using the GeneChip Command Console Software and the Expression console (Affymetrix).

Raw data were then normalized using GC-content by the Robust Multichip Average method within Genomics Suite (Partek) using a selection of probes corresponding to the core annotation level, resulting in 23,332 transcripts. Transcripts lacking gene symbol annotation were filtered out and only transcripts with full annotations (16,711) were statistically analyzed.

The log2 transformation of normalized signal intensities of annotated transcripts were analyzed with Student's t test. To control for false positives, a p value cutoff of 0.001 corresponding to a false discovery rate <0.11 (Benjamini and Hochberg, 1995) was used. Significantly altered genes were uploaded to the WebGestalt Gene Set Analysis Toolkit version 2 (http://bioinfo.vanderbilt.edu/webgestalt, Vanderbilt University) for enrichment analysis.

Results

Paranodal breakdown with hypoperfusion

To test whether chronic cerebral hypoperfusion would cause alterations in proteins essential for the integrity of the paranodal junctions, we analyzed two key proteins (Caspr and Nfasc155) that are contained within the paranodal septate-like junctions. Caspr is located at the axonal paranode, and Nfasc155 is contained at the opposing paranodal loops of the myelin sheath. These proteins function as a diffusion barrier for the nodal $Na_v1.6$ sodium channels and are essential for the integrity of nodes of Ranvier. Sections were double-immunolabeled with the axonal Caspr and the glial Nfasc155 proteins and the number of disrupted paranodes was assessed in the corpus callosum (Fig. 1*A*). In response to hypoperfusion, there was a significant reduction in the number of paranodes labeled with both Nfasc155 and Caspr, due to a marked reduction of Nfasc155 immunolabeling. After 3 d of hypoperfusion, 21% of the paranodal pairs were affected compared with 9% in the sham group; after 1 month, 55% displayed a loss of the glial Nfasc155 protein compared with 7% in the sham group (Fig. 1*D*). To confirm that there was a loss of colocalization of Caspr and NFasc155, sections were double-immunolabeled with the axonal Caspr and panNeurofascin (labeling glial Nfasc155 and axonal Nfasc186), and colocalization was determined within the paranodes (Fig. 1*B*). A significant reduction in colocalization of Caspr and panNfasc within the paranodes was determined at both 3 d and 1 month after hypoperfusion (Fig. 1*E*). These data suggest a progressive breakdown of the paranodal composition with hypoperfusion.

To further determine whether the loss of Caspr/Nfasc double-immunolabeling indicates paranodal disruption, we performed ultrastructural analysis by EM on longitudinal optic nerve sections (Fig. 1*C*). EM images of paranodes showed a significant loss of septate-like junctions of paranodal loops in hypoperfused samples compared with sham controls (Fig. 1*F*).

Increased voltage-gated sodium channel cluster length with hypoperfusion

Breakdown of paranodal septate-like junctions could lead to changes in the structural organization of the nodes of Ranvier, which depend on a complex interplay between axons and glia. To determine this, we delineated nodal regions by double-labeling sections with antibodies to voltage-gated sodium channel ($Na_v1.6$) and Caspr, an integral component of paranodal junctions. Voltage-gated sodium channel ($Na_v1.6$) clusters are normally bounded by the paranodal protein Caspr and this was observed in the sham group (Fig. 2*A*). However, in response to hypoperfusion, after 3 d and 1 month, the distribution of the $Na_v1.6$ channels was markedly altered compared with shams. In sham-controls, $Na_v1.6$ staining is confined to the nodes of Ranvier and does not exceed beyond the localization of the paranodal barrier, as outlined by the protein Caspr. In contrast, in response to hypoperfusion, overlap between the $Na_v1.6$ and Caspr staining was observed (Fig. 2*A*). To quantify the extent and progression of these changes, we measured the length of the $Na_v1.6$ clusters in three white matter tracts (corpus callosum, internal capsule, and optic tract) after 3 d and 1 month of hypoperfusion (Fig. 2*B*). We found that there was a significant increase in the length of the $Na_v1.6$ domain after 3 d hypoperfusion in the corpus callosum and internal capsule, which was exacerbated with a longer duration of hypoperfusion at 1 month. At this later time, the length of the $Na_v1.6$ channels was also significantly increased in the optic tract after hypoperfusion (Fig. 2*B*).

Number of nodes does not change after hypoperfusion

We next determined whether the number of nodes of Ranvier is changed in response to hypoperfusion. Analysis of a $47 \times 47 \times 5$ μm^3 confocal stack of the corpus callosum (Fig. 2*C*), internal capsule, and optic tract by stereologically counting the number of nodes of Ranvier for both time points revealed that their number was not altered in response to hypoperfusion (Fig. 2*D*). This indicates that chronic cerebral hypoperfusion does not lead to a loss in the number of nodes of Ranvier but a disruption of the distribution of $Na_v1.6$ normally contained within the nodal region.

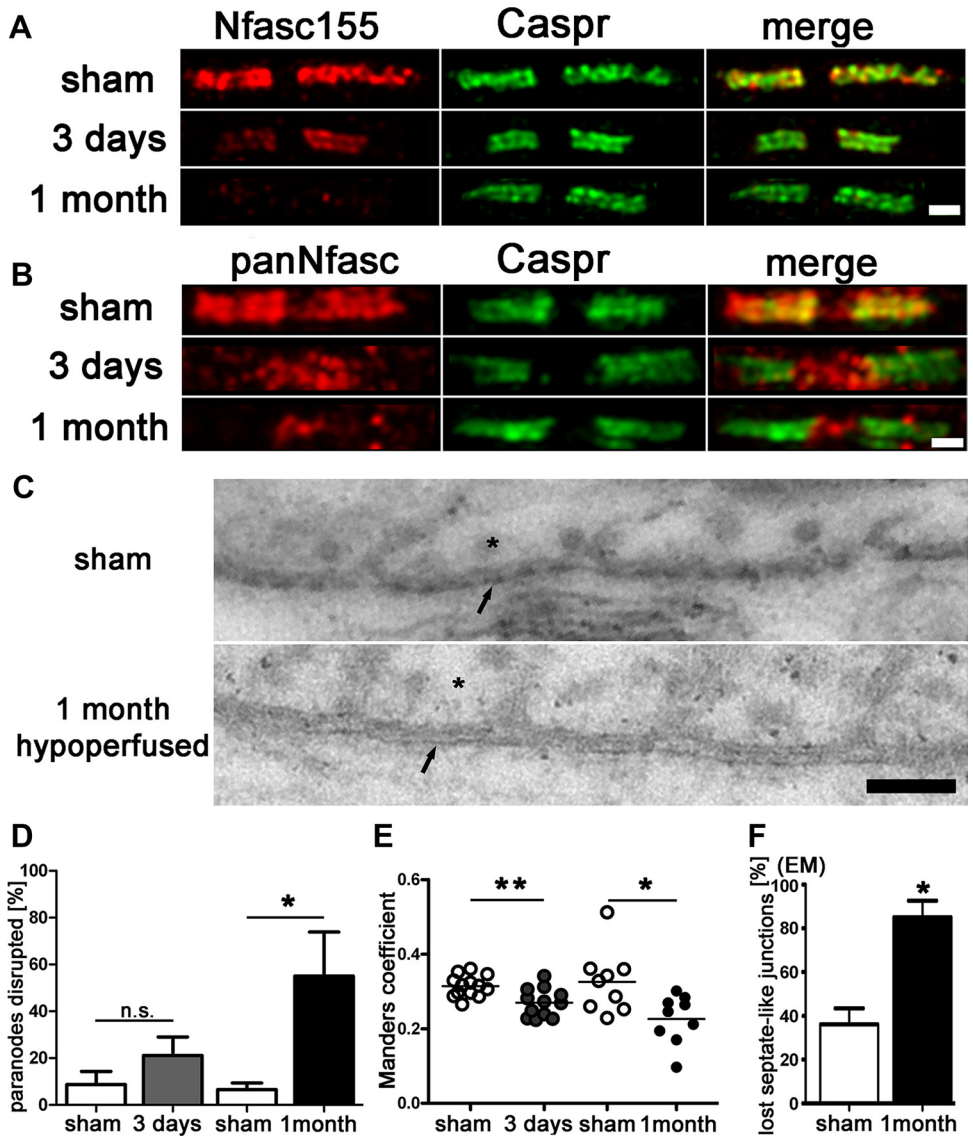

Figure 1. Paranodal disruption occurs early in response to hypoperfusion in the corpus callosum. ***A***, ***B***, Colocalization of axonal Caspr and glial Neurofascin protein indicates intact septate-like junctions at the paranodes in the sham group. In response to hypoperfusion, at both 3 d and 1 month, there is a selective loss of Neurofascin colocalization with Caspr, which is indicative of a disruption of the paranodes. Scale bar, 1 μm. ***C***, Electron micrographs show paranodal disruption in response to hypoperfusion in the optic nerve. Arrows indicate axonal membrane at the paranodal region; asterisks indicate paranodal loop. Disruption of septate-like junctions is indicated by loss of transverse bands. Scale bars, 0.1 μm. ***D***, There is a nonsignificant increase in the number of paranodes disrupted at 3 d hypoperfusion ($n = 5$) compared with shams ($n = 5$), which is significant at 1 month after hypoperfusion ($n = 4$) compared with shams ($n = 6$). Analysis was conducted in the corpus callosum. $^*p < 0.05$ (unpaired *t* test, two-tailed). ***E***, The overlap coefficient after Manders, which is insensitive to differences in signal intensities between the two channels, shows significant loss in colocalization after 3 d and after 1 month of hypoperfusion (3 d sham: $n = 13$, hypoperfusion: $n = 12$; 1 month sham: $n = 9$, hypoperfusion: $n = 9$). Analysis was conducted in the corpus callosum. $^*p < 0.05$, $^{**}p < 0.005$ (unpaired *t* test, two-tailed). ***F***, A significant increase in paranodes without septate-like junctions was observed after 1 month of hypoperfusion. $^*p < 0.05$ (unpaired *t* test, two-tailed).

Nodal anchoring proteins remain unaltered after hypoperfusion

At the node of Ranvier, the scaffolding protein AnkyrinG interacts with Nfasc186 and $Na_v1.6$ channels. This interaction is proposed to be involved in maintenance of the nodal $Na_v1.6$ complex (Susuki and Rasband, 2008). Nfasc186 connects the complex to the extracellular matrix and AnkyrinG via βIV-spectrin to the underlying cytoskeleton. Therefore, we assessed changes in the nodal distribution of these proteins. Surprisingly, in response to hypoperfusion, at either 3 d or 1 month, AnkyrinG and Nfasc186 show no change in localization (Fig. 3*A*,*B*). Furthermore, the length of the AnkyrinG and Nfasc186 domains after 3 d or 1 month of hypoperfusion were not significantly different to shams, i.e., there was no lateral spreading of these protein domains along the axon (Fig. 3*C*).

Internodal axon–glial alterations after hypoperfusion

The axon–glial connection at the internode between nodes of Ranvier consists of the glial cell membrane glycoprotein MAG and its axonal binding partners. As the paranodal axon–glial integrity appeared to be compromised due to hypoperfusion, we investigated whether the internodal axon–glial connection is similarly affected. We analyzed the spatial distribution of the glial MAG protein in response to hypoperfusion and found it to be markedly changed compared with the sham group. A discontinuous granular accumulation of the MAG labeling in the hypoper-

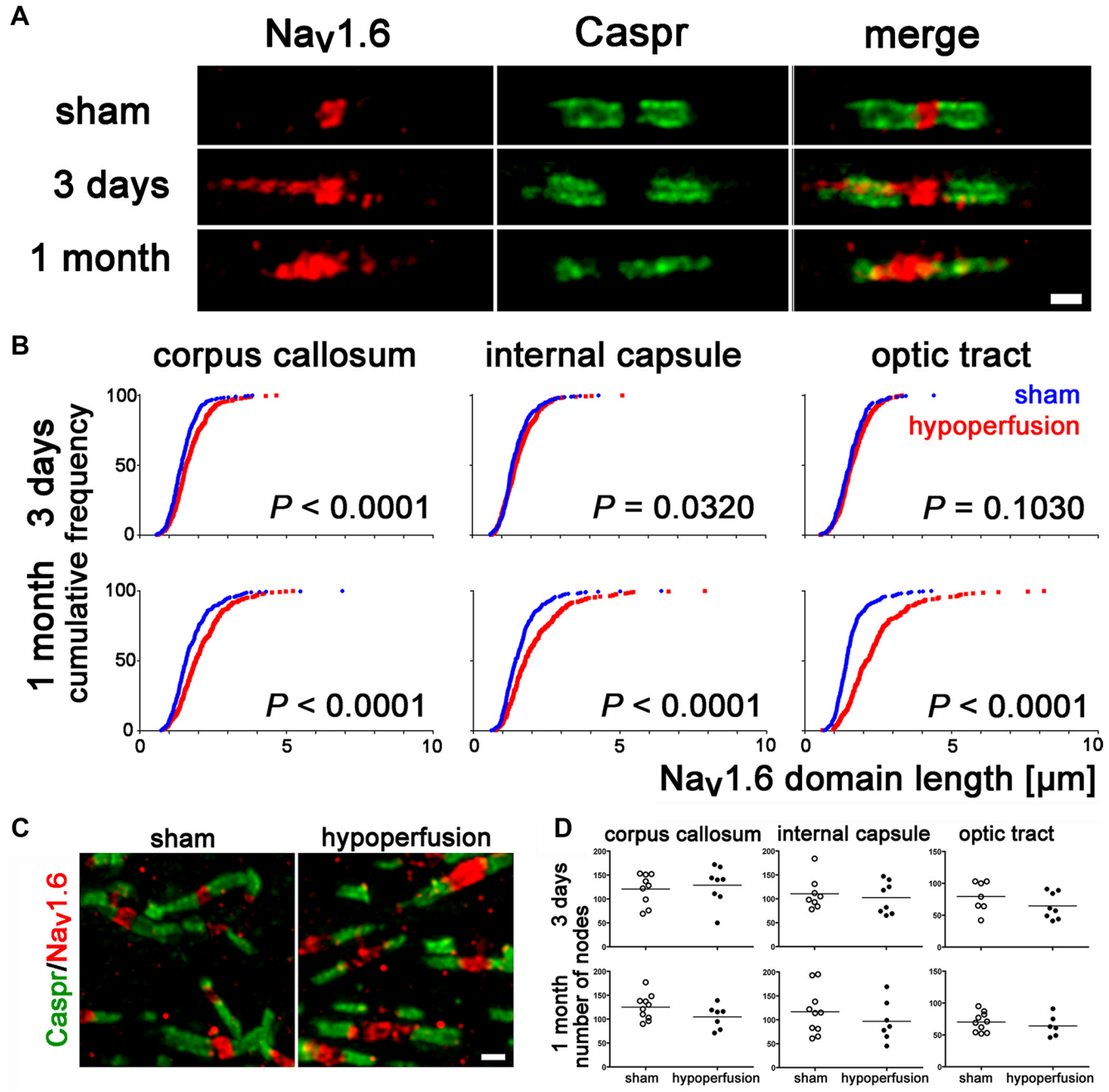

Figure 2. Voltage-gated sodium channel distribution is rapidly disrupted by hypoperfusion. ***A***, $Na_v1.6$ sodium channels, which outline the node of Ranvier, are normally bounded by the paranodal protein Caspr, as shown in the sham. In response to hypoperfusion, after 3 d and 1 month, the distribution of the $Na_v1.6$ sodium channels is markedly altered and laterally spreads along the axon (corpus callosum). Scale bar, 1 μm. ***B***, There is a significant increase in the length of the $Na_v1.6$ clusters after 3 d of hypoperfusion in the corpus callosum and, after 1 month, in the internal capsule and optic tract. Forty nodes per animal were analyzed and these 240–400 nodes are plotted as cumulative frequency distribution, tabulated as relative frequencies as percentage (two-sample Kolmogorov–Smirnov test). Number of nodes of Ranvier remains unchanged after 3 d or 1 month of hypoperfusion. ***C***, Confocal stack of nodes of Ranvier in the corpus callosum, double-labeled with Nav1.6 and Caspr. Left, Sham; right, 1 month of hypoperfusion. Scale bar, 1 μm. ***D***, Numbers of nodes of Ranvier are not altered in response to hypoperfusion. After 3 d and after 1 month, the number of $Na_v1.6$ immunopositive nodes was not changed between the sham and hypoperfused groups. Analysis was conducted by confocal laser microscopy in the corpus callosum, internal capsule, and optic tract in a $47 \times 47 \times 5$ μm^3 confocal stack (Mann–Whitney, two-tailed).

fused group was observed (Fig. 4*A*). To quantify these changes, we determined the fluorescent intensity of single optical confocal sections in the same white matter regions that displayed a breakdown in paranodal integrity, and found a significant reduction in the intensity of MAG staining at both 3 d and at 1 month of hypoperfusion compared with shams (Fig. 4*B*). These results build on and extend our previous findings in which MAG was shown to be disrupted in response to 1 month of hypoperfusion (Coltman et al., 2011). Together, these findings suggest that the internodal axon–glial connection is compromised due to chronic cerebral hypoperfusion.

Similarly, we assessed the spatial distribution and measured the intensity of the MBP, which is located in the compact myelin sheath, in single optical confocal sections. However, we found

that neither the spatial distribution nor the fluorescent intensity of MBP was changed in response to hypoperfusion after 3 d or 1 month compared with shams (Fig. 4*A*,*B*).

In addition, we assessed whether the underlying axons, which would contain the binding partners for the MAG protein, show obvious morphological changes with hypoperfusion. The axons were labeled using the panaxonal neurofilament marker SMI312R and measured in the same way as the myelin on single optical confocal sections. There was no evidence that there were either structural changes or differences in the fluorescent intensity in response to hypoperfusion compared with shams (Fig. 4).

No evidence of increased apoptosis with hypoperfusion

To analyze the extent of apoptosis in our model, we counted activated caspase-3-positive cells in white matter regions after 3 d and 1 month of hypoperfusion (Fig. 5). No significant increase in numbers of apoptotic cells were determined in any of the regions studied or at any time point.

Multiple molecular events in white matter associated with hypoperfusion

To investigate potential molecular events in response to hypoperfusion that may contribute to the axon–glial damage, we undertook a microarray study in white matter-enriched tissue at 3 d posthypoperfusion, a time when we detected early changes. Of the 16,711 fully annotated genes, 129 were found to be regulated differently within the white matter-enriched samples in response to hypoperfusion at $p < 0.001$. Hypoperfusion is associated with alterations in multiple biological processes. Enrichment analysis of the 129 regulated genes presented in Table 1 demonstrates the multiple processes regulated in response to hypoperfusion. In particular, genes associated with inflammatory responses (Table 1), such as those represented by the annotations Jak–STAT signaling pathway (seven genes) and cytokine–cytokine receptor interaction (eight genes), which included *Stat3*, *Il2rg*, *Osmr*, and *Tnfrsf1a*, were found to be regulated. Cardiovascular development, represented by the functional annotations angiogenesis (nine genes) and blood vessel development (10 genes) and including the genes *Angpt2*, *Vegfa*, *Serpine1*, and *Dll4*, were also altered. Cell proliferation processes were altered as represented by regulation of cell proliferation (15 genes) and included *Cdh5*, *Adm*, *Igfb3*, and *Cdkn1a*. Other highlighted processes were anatomical structure formation/morphogenesis and cell adhesion.

Hypoperfusion is a complex and multifactorial process, as demonstrated by the number of biological processes listed in Table 1. These affect genes involved in cell death and plasticity across multiple cell types even within white matter-enriched samples. The exact mechanism leading to the nodal changes observed remains to be established, but the complexity of action of the molecules involved would indicate that no single molecular event is responsible.

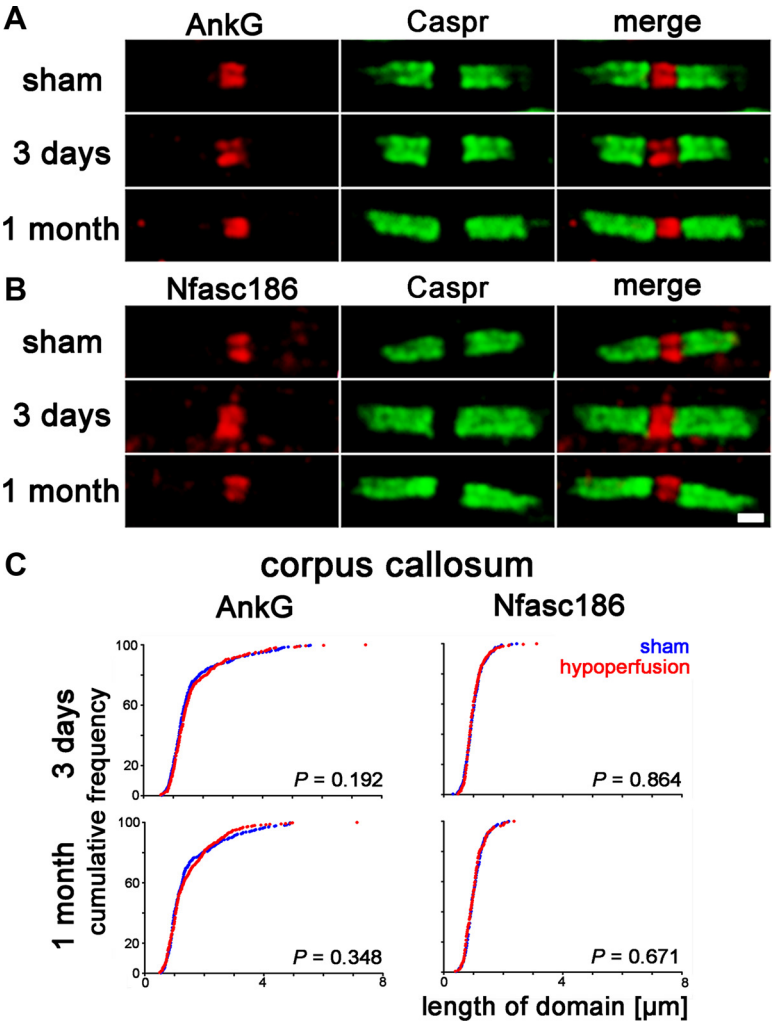

Figure 3. AnkyrinG and Neurofascin186 distribution remains unchanged with hypoperfusion. ***A***, Axonal AnkyrinG remains within the node of Ranvier in response to hypoperfusion. ***B***, The spatial distribution of Neurofascin186, which connects nodal proteins to the extracellular matrix, does not change. Scale bar, 1 μm. ***C***, There is no significant increase in the length of the AnkyrinG or Neurofascin186 domains after 3 d or 1 month of hypoperfusion in the corpus callosum. Forty nodes per animal were analyzed and these 160–400 nodes are plotted as cumulative frequency (two-sample Kolmogorov–Smirnov test).

Discussion

Our results demonstrate that within days of cerebral hypoperfusion, there is a rapid and selective disruption of key proteins within the paranodal axon–glial junctions, which are critical to the stability and function of myelinated axons. Furthermore, in the early response to hypoperfusion, there are several biological pathways altered (notably inflammatory, vascular development, and cell adhesion) that could contribute to the axon–glial damage.

These results are relevant to age-related changes in white matter to which cerebral hypoperfusion is suggested to contribute. Although there is some evidence that the protein architecture may be altered at nodal regions in the aging brain (Lasiene et al., 2009), specific protein changes have yet to be identified. The present study identifies key changes in paranodal and nodal proteins in response to cerebral hypoperfu-

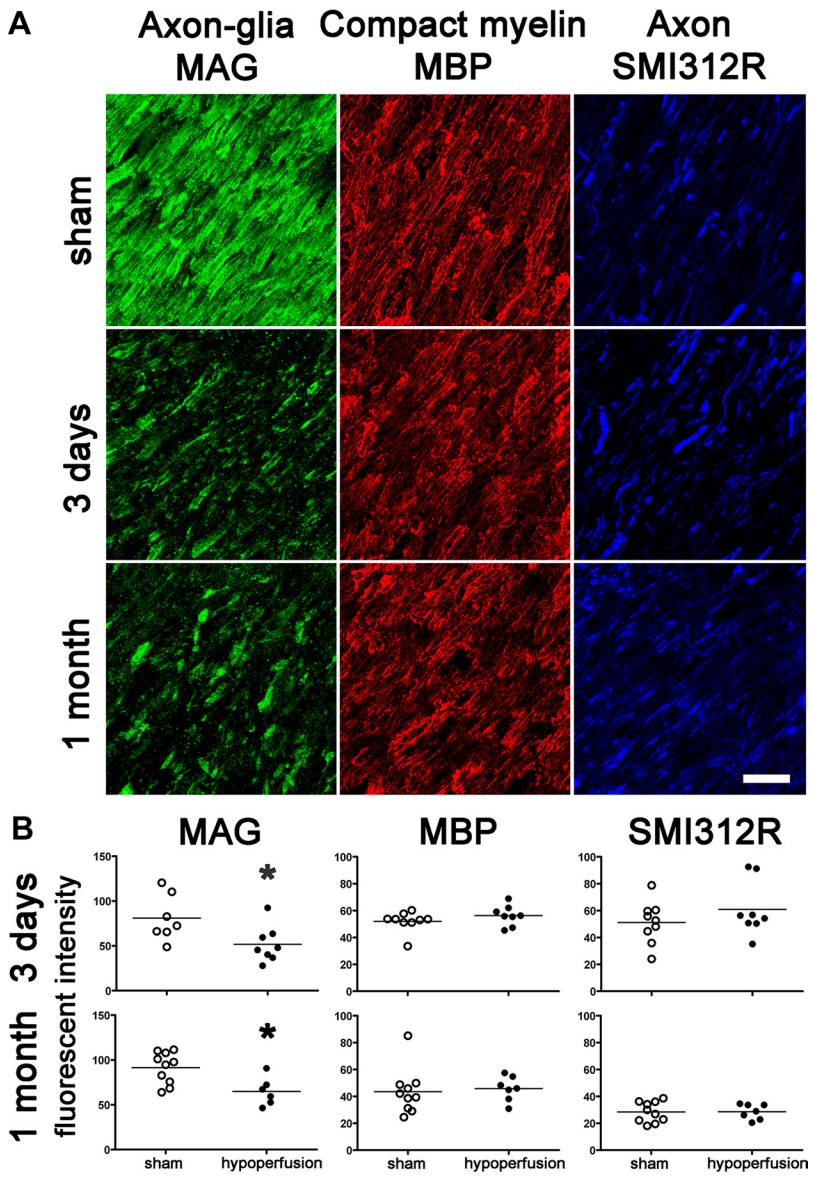

Figure 4. Axon–glial integrity is disrupted, whereas myelin and axonal integrity remains intact. ***A***, Disruption of axon–glial integrity was defined as reduced and discontinuous granular accumulation of the MAG staining in response to hypoperfusion compared with shams. In contrast, the integrity of the myelin sheath (assessed by MBP) and integrity of axons (assessed by SMI312R) remains intact at 3 d and at 1 month. Scale bar, 10 μm. ***B***, Measurement of the fluorescent intensity of MAG, MBP, and SMI312R staining was conducted by confocal laser microscopy in the corpus callosum, internal capsule, and optic tract in sham and hypoperfused groups at 3 d (sham, $n = 9$; hypoperfused, $n = 8$) and 1 month (sham, $n = 10$; hypoperfused, $n = 7$). There was a significant reduction in the intensity of MAG staining at both 3 d and at 1 month hypoperfusion compared with shams. There were no alterations in MBP and SMI312R immunostaining in response to hypoperfusion at any time studied. *$p < 0.05$ (Mann–Whitney, two-tailed).

sion. Normally, Nfasc155 is located at the paranodal loops and is known to form the paranodal septate-like junctions with the axonal protein Caspr and contactin. The stability of these proteins is critical to maintain nodal structure. We determined a disruption of the paranodes occurs in response to hypoperfusion, with a loss of the glial protein Nfasc155 at the paranode concomitant with a loss of septate-like junctions. This selective damage to paranodal integrity was also associated with a compromised nodal structure, as demonstrated by an increase in $Na_v1.6$ channel cluster length. This increase in nodal length was dependent on the white matter tract examined. The corpus callosum and internal capsule appeared particularly susceptible early in response to hypoperfusion, with a significant increase in nodal length, detectable within 3 d, while the optic tract remained unaffected. After 1 month of hypoperfusion, the effect appeared to be progressive and alterations within the optic tract were subsequently determined. One explanation for this observation is regional differences of blood supply due to the cerebrovascular architecture and increased energy demand of myelinated fibers during even modest hypoxia (Dorr et al., 2007; Trapp and Stys, 2009). In addition to vascular alterations, dynamic distribution of blood and turnover of oligodendrocytes might result in the differences of progression between the analyzed white matter tracts.

Consistent with changes at the paranodes, there was a marked and rapid disruption of the axon–glial connection at the internodal region of myelinated axons in response to hypoperfusion. MAG plays an important role in signaling and maintenance of the axon–glial connection and the myelin sheath (for review, see Quarles, 2007; Schnaar and Lopez, 2009). The cellular distribution of glial MAG protein was disrupted in response to hypoperfusion and determined to accumulate in discontinuous granular staining. Interestingly, the protein level of MAG was not altered after 1 month of chronic cerebral hypoperfusion. This suggests that the observed changes could be a result of protein misdistribution rather than a loss of protein. A preferential loss of MAG in hypoxia-like white matter damage after stroke, multiple sclerosis, and other inflammatory brain diseases has been previously described (Aboul-Enein et al., 2003). A link between myelin-associated glycoprotein disruption and paranodal integrity has been shown in mice deficient in both MAG and myelin galactolipids, which display impaired maintenance of nodes of Ranvier (Marcus et al., 2002).

At the node of Ranvier, the scaffolding protein AnkyrinG interacts with Nfasc186 and $Na_v1.6$ channels, and this interaction is proposed to be involved in maintenance of the nodal $Na_v1.6$ complex (Susuki and Rasband, 2008). Nfasc186 connects the complex to the extracellular matrix and AnkyrinG via βIV-spectrin to the underlying cytoskeleton. Thus, it was surprising to determine in the present study that alterations in $Na_v1.6$ were not accompanied by alterations in Nfasc186 and the anchoring protein AnkyrinG. The lack of changes in AnkyrinG and Nfasc186 despite alterations in Nav1.6 channels might indicate a dissociation of Nav1.6 channels from the AnkyrinG/Nfasc186 complex. There are a number of mechanisms by which voltage-gated sodium channels could dissociate from its AnkyrinG scaffolding. Previously, it has been demonstrated that phosphorylation of the Ankyrin-binding motif of $Na_v1.2$

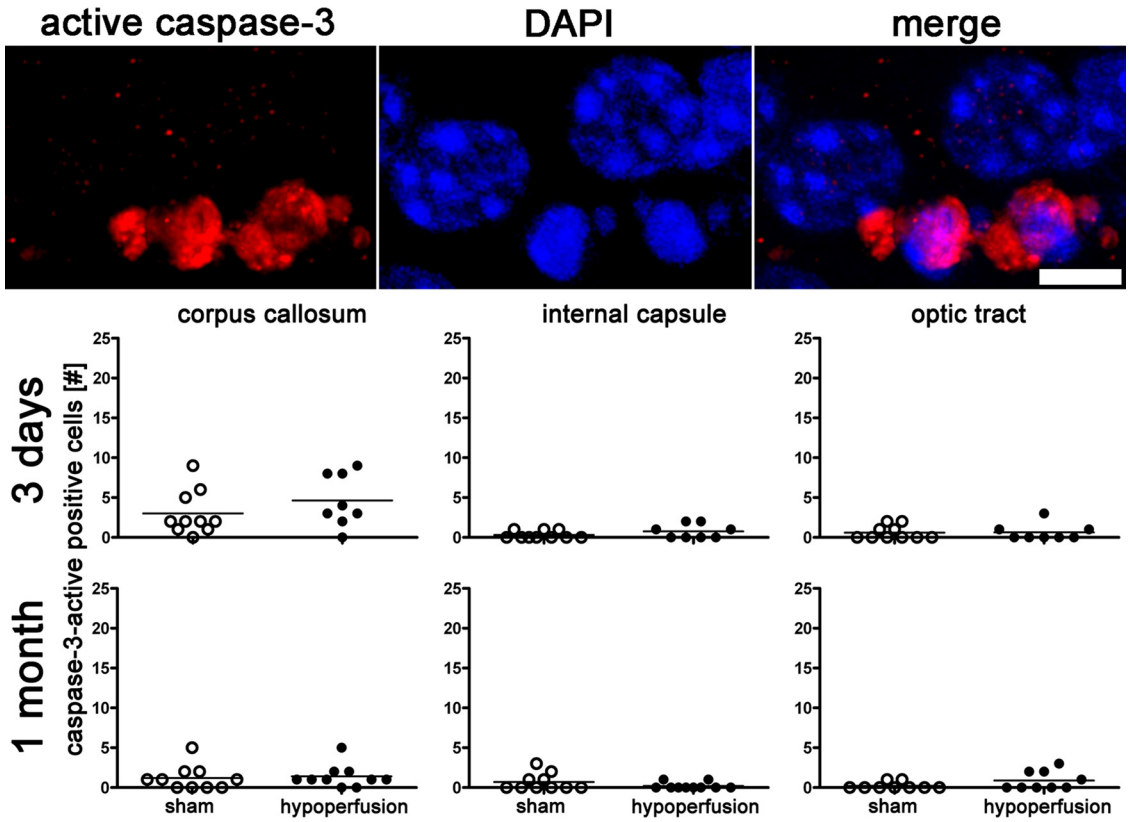

Figure 5. Increased apoptosis does not occur after 3 d or 1 month of chronic cerebral hypoperfusion. The number of active caspase-3-positive cells in the corpus callosum, internal capsule, and optic tract is not increased in response to hypoperfusion. Colocalization of active caspase-3 with DAPI is shown. *$p < 0.05$ (Mann–Whitney, two-tailed).

Table 1. Microarray analysis of enriched white matter from the corpus callosum indicates multiple pathways involved in the response to hypoperfusion

Database	Biological process	Observed	Expected	*p* value
GO	Regulation of cell proliferation	15	3.66	0.001
GO	Angiogenesis	9	1.23	0.001
KEGG	Jak–STAT signaling pathway	7	1.06	0.0027
KEGG	Complement and coagulation cascades	5	0.54	0.0029
GO	Organ development	28	12.89	0.0037
GO	Blood vessel morphogenesis	9	1.7	0.0037
GO	Blood vessel development	10	2.07	0.0037
GO	Vasculature development	10	2.11	0.0037
GO	Anatomical structure formation/ morphogenesis	12	2.88	0.0037
KEGG	Cytokine–cytokine receptor interaction	8	1.79	0.0039
GO	Cell adhesion	14	4.34	0.0048
GO	Cell proliferation	15	4.99	0.0048
GO	Anatomical structure development	32	16.39	0.0048
KEGG	Acute myeloid leukemia	4	0.42	0.0058

Genes ($n = 129$) altered ($p < 0.001$) were uploaded to WebGestalt enrichment analysis based on Gene Ontology (GO) and Kyoto Encyclopedia of Genes and Genomes (KEGG) pathways. Biological processes [adjusted $p < 0.01$ (Benjamini and Hochberg, 1995)] from both Gene Ontology and Kyoto Encyclopedia of Genes and Genomes databases, along with the observed and expected number of molecules represented for each category, are listed.

channels via protein kinase CK2 regulates the sodium channel interaction with Ankyrins (Bréchet et al., 2008). Alternatively, calpain-mediated proteolysis of the voltage-gated sodium channel α-subunit has been described for Nav1.2 (von Reyn et al., 2009). Similar events to $Na_v1.6$ at the nodes of Ranvier could explain the dissociation of sodium channels from nodal AnkyrinG.

Additionally, we did not detect axonal damage nor demyelination in response to hypoperfusion, which is in agreement with our previous studies using cellular pathology and MRI approaches (Holland et al., 2011).The observation that AnkyrinG and Neurofascin186 are unaltered after hypoperfusion supports the absence of detectable alteration of the underlying axonal cytoskeleton. This is in contrast to more severe models of cerebral ischemia where myelin/axonal pathology is evident, [such as focal cerebral ischemia (Yam et al., 2000) and global cerebral ischemia (Jiwa et al., 2010)] in which blood flow is severely reduced (70%), and axonal and neuronal perikaryal damage occur within hours to days of the initial blood flow reduction. In the present study, hypoperfusion induced by carotid stenosis is associated with modest reductions in blood flow (<30%) within the first 24 h, and recovers gradually over weeks and is reduced by 10–20% compared with baseline (Shibata et al., 2004). This is more akin to changes that occur in the normal aging brain, where blood flow reductions are modest (~20%) and sustained over years. The myelin sheath and underlying axon do not appear to be changed in our model of hypoperfusion but instead there is rapid axon–glial disruption. Western blot analysis revealed that there was no change in the levels of the proteins studied (MBP, SMI312, MAG, Nfasc155, and $Na_v1.6$; our unpublished observations), providing further support that the hypoperfusion causes disruption of the cellular distribution and coupling of axon–glial proteins. Several mechanisms of damage, including excitotoxicity and caspase activation, have been suggested (Craner et al., 2004; Fu et al., 2009) to lead to axonal degeneration in models of severe ischemia. Since we found no evidence of axonal injury or caspase-3-labeled oligodendrocytes at the times studied (Fig. 5) in our model, alternative mechanisms may contribute to the axon–glial disruption.

Vascular brain injury has been shown to cause white matter deterioration and response of the oligodendrocyte lineage in a

human cohort (Back et al., 2011). This highlights the link between vascular disturbances and changes in white matter integrity. Furthermore, dynamic communication between endothelial cells and oligodendrocytes is suggested to maintain their homeostasis and the integrity of white matter (Arai and Lo, 2009). This current view of an oligovascular niche suggests a highly coordinated exchange mediated by a diversity of signaling molecules between cerebral blood vessels and oligodendrocytes (Arai and Lo, 2009). Thus, it is likely that not one molecular event can explain the axon–glial damage in response to hypoperfusion. Indeed, within our microarray analysis of white matter-enriched tissue from the corpus callosum, we determined significant alterations in a number of genes and biological processes in response to hypoperfusion, including inflammatory, vascular, and cell-adhesion pathways. Each of these may contribute to the degenerative processes. The extent of their participation in axon–glial disruption requires intensive future studies.

It is well recognized that axon–glial integrity is critical to maintenance of cognitive function (Nave, 2010). Previously, we demonstrated that selective disruption of white matter integrity in response to hypoperfusion results in impairment of spatial working memory (Coltman et al., 2011). Although these distinct changes to the protein architecture at a subcellular level might appear subtle, they might be sufficient to explain the previously described cognitive dysfunction. In development, conduction velocities are significantly increased with clustering of $Na_v1.6$ sodium channels at the node of Ranvier (Rasband et al., 1999) and disrupted paranodes lead to changes in electrophysiological measurements (Susuki et al., 2007). Disruption of nodal structures would be expected to result in changes in action potential propagation and thus could lead to functionally impaired connections between different brain regions.

We propose that the axon–glial connection at the paranodes and internodes in white matter tracts are rapidly disrupted in response to hypoperfusion relevant to the aging brain. The onset of this disruption is fast, which may indicate a narrow window of opportunity to prevent damage from occurring. However, in future studies, it will be important to determine whether this damage is reversible. In our model, the underlying axon remains intact, as does the compact myelin in the myelin sheaths. Although it is not clear whether long-term axonal degeneration and myelin sheath loss occurs with progressive hypoperfusion, there is emerging evidence that it leads to neuronal cell loss (Nishio et al., 2010). The complexity of the molecular mechanisms elicited by hypoperfusion suggests that there is no single molecular target. However, stabilizing the axon–glial connection at the early onset of disruption to myelinated axons could be crucial to prevent further degenerative processes and cognitive impairment.

Notes

Supplemental material for this article is available at http://www.cnr.ed.ac.uk/Research/horsburgh.html. Supplemental Table 1: Genes regulated by hypoperfusion in white matter-enriched microsamples. This material has not been peer reviewed.

References

Aboul-Enein F, Rauschka H, Kornek B, Stadelmann C, Stefferl A, Brück W, Lucchinetti C, Schmidbauer M, Jellinger K, Lassmann H (2003) Preferential loss of myelin-associated glycoprotein reflects hypoxia-like white matter damage in stroke and inflammatory brain diseases. J Neuropathol Exp Neurol 62:25–33.

Arai K, Lo EH (2009) An oligovascular niche: cerebral endothelial cells promote the survival and proliferation of oligodendrocyte precursor cells. J Neurosci 29:4351–4355.

Back SA, Kroenke CD, Sherman LS, Lawrence G, Gong X, Taber EN, Sonnen JA, Larson EB, Montine TJ (2011) White matter lesions defined by diffusion tensor imaging in older adults. Ann Neurol 70:465–476.

Bartzokis G, Sultzer D, Lu PH, Nuechterlein KH, Mintz J, Cummings JL (2004) Heterogeneous age-related breakdown of white matter structural integrity: implications for cortical "disconnection" in aging and Alzheimer's disease. Neurobiol Aging 25:843–851.

Bastin ME, Clayden JD, Pattie A, Gerrish IF, Wardlaw JM, Deary IJ (2009) Diffusion tensor and magnetization transfer MRI measurements of periventricular white matter hyperintensities in old age. Neurobiol Aging 30:125–136.

Benjamini Y, Hochberg Y (1995) Controlling the false discovery rate: a practical and powerful approach to multiple testing. J R Stat Soc B 57:289–300.

Bréchet A, Fache MP, Brachet A, Ferracci G, Baude A, Irondelle M, Pereira S, Leterrier C, Dargent B (2008) Protein kinase CK2 contributes to the organization of sodium channels in axonal membranes by regulating their interactions with ankyrin G. J Cell Biol 183:1101–1114.

Coltman R, Spain A, Tsenkina Y, Fowler JH, Smith J, Scullion G, Allerhand M, Scott F, Kalaria RN, Ihara M, Daumas S, Deary IJ, Wood E, McCulloch J, Horsburgh K (2011) Selective white matter pathology induces a specific impairment in spatial working memory. Neurobiol Aging 32:2324.e7–2324.e12.

Craner MJ, Hains BC, Lo AC, Black JA, Waxman SG (2004) Co-localization of sodium channel Nav1.6 and the sodium-calcium exchanger at sites of axonal injury in the spinal cord in EAE. Brain 127:294–303.

Dorr A, Sled JG, Kabani N (2007) Three-dimensional cerebral vasculature of the CBA mouse brain: a magnetic resonance imaging and micro computed tomography study. Neuroimage 35:1409–1423.

Fernando MS, Simpson JE, Matthews F, Brayne C, Lewis CE, Barber R, Kalaria RN, Forster G, Esteves F, Wharton SB, Shaw PJ, O'Brien JT, Ince PG (2006) White matter lesions in an unselected cohort of the elderly: molecular pathology suggests origin from chronic hypoperfusion injury. Stroke 37:1391–1398.

Franklin K, Paxinos G (1997) The mouse brain in stereotaxic coordinates. San Diego: Academic Press.

Fu Y, Sun W, Shi Y, Shi R, Cheng JX (2009) Glutamate excitotoxicity inflicts paranodal myelin splitting and retraction. PLoS One 4:e6705.

Holland PR, Bastin ME, Jansen MA, Merrifield GD, Coltman RB, Scott F, Nowers H, Khallout K, Marshall I, Wardlaw JM, Deary IJ, McCulloch J, Horsburgh K (2011) MRI is a sensitive marker of subtle white matter pathology in hypoperfused mice. Neurobiol Aging 32:2325.e1–2325.e6.

Howell OW, Palser A, Polito A, Melrose S, Zonta B, Scheiermann C, Vora AJ, Brophy PJ, Reynolds R (2006) Disruption of neurofascin localization reveals early changes preceding demyelination and remyelination in multiple sclerosis. Brain 129:3173–3185.

Jiwa NS, Garrard P, Hainsworth AH (2010) Experimental models of vascular dementia and vascular cognitive impairment: a systematic review. J Neurochem 115:814–828.

Lasiene J, Matsui A, Sawa Y, Wong F, Horner PJ (2009) Age-related myelin dynamics revealed by increased oligodendrogenesis and short internodes. Aging Cell 8:201–213.

Marcus J, Dupree JL, Popko B (2002) Myelin-associated glycoprotein and myelin galactolipids stabilize developing axo-glial interactions. J Cell Biol 156:567–577.

Nave KA (2010) Myelination and support of axonal integrity by glia. Nature 468:244–252.

Nishio K, Ihara M, Yamasaki N, Kalaria RN, Maki T, Fujita Y, Ito H, Oishi N, Fukuyama H, Miyakawa T, Takahashi R, Tomimoto H (2010) A mouse model characterizing features of vascular dementia with hippocampal atrophy. Stroke 41:1278–1284.

Quarles RH (2007) Myelin-associated glycoprotein (MAG): past, present and beyond. J Neurochem 100:1431–1448.

Rasband MN, Peles E, Trimmer JS, Levinson SR, Lux SE, Shrager P (1999) Dependence of nodal sodium channel clustering on paranodal axoglial contact in the developing CNS. J Neurosci 19:7516–7528.

Rickman C, Medine CN, Bergmann A, Duncan RR (2007) Functionally and spatially distinct modes of munc18-syntaxin 1 interaction. J Biol Chem 282:12097–12103.

Rios JC, Rubin M, St Martin M, Downey RT, Einheber S, Rosenbluth J, Levinson SR, Bhat M, Salzer JL (2003) Paranodal interactions regulate expression of sodium channel subtypes and provide a diffusion barrier for the node of Ranvier. J Neurosci 23:7001–7011.

Schnaar RL, Lopez PH (2009) Myelin-associated glycoprotein and its axonal receptors. J Neurosci Res 87:3267–3276.

Shibata M, Ohtani R, Ihara M, Tomimoto H (2004) White matter lesions and glial activation in a novel mouse model of chronic cerebral hypoperfusion. Stroke 35:2598–2603.

Susuki K, Rasband MN (2008) Molecular mechanisms of node of Ranvier formation. Curr Opin Cell Biol 20:616–623.

Susuki K, Baba H, Tohyama K, Kanai K, Kuwabara S, Hirata K, Furukawa K, Furukawa K, Rasband MN, Yuki N (2007) Gangliosides contribute to stability of paranodal junctions and ion channel clusters in myelinated nerve fibers. Glia 55:746–757.

Tait S, Gunn-Moore F, Collinson JM, Huang J, Lubetzki C, Pedraza L, Sherman DL, Colman DR, Brophy PJ (2000) An oligodendrocyte cell adhesion molecule at the site of assembly of the paranodal axo-glial junction. J Cell Biol 150:657–666.

Trapp BD, Stys PK (2009) Virtual hypoxia and chronic necrosis of demyelinated axons in multiple sclerosis. Lancet Neurol 8:280–291.

von Reyn CR, Spaethling JM, Mesfin MN, Ma M, Neumar RW, Smith DH, Siman R, Meaney DF (2009) Calpain mediates proteolysis of the voltage-gated sodium channel alpha-subunit. J Neurosci 29:10350–10356.

Waxman SG (2006) Axonal conduction and injury in multiple sclerosis: the role of sodium channels. Nat Rev Neurosci 7:932–941.

Yam PS, Dunn LT, Graham DI, Dewar D, McCulloch J (2000) NMDA receptor blockade fails to alter axonal injury in focal cerebral ischemia. J Cereb Blood Flow Metab 20:772–779.